
Molecular and functional characterization of pathways
relevant to metastasis and cancer therapy in circulating tumor
cells of breast and prostate cancer patients

Dissertation

zur Erlangung der Würde des Doktors der Naturwissenschaften der Fakultät für
Mathematik, Informatik und Naturwissenschaften,
Fachbereich Biologie der Universität Hamburg

vorgelegt von

Claudia Koch

aus Paderborn, Deutschland

Hamburg, den 12.11.2021

Vorsitzende der Prüfungskommission:	Prof. Dr. rer. nat. Julia Kehr
1. Gutachter:	Prof. Dr. med. Klaus Pantel
2. Gutacherin:	Prof. Dr. rer. nat. Sigrun Reumann
Datum der Disputation:	08.07.2022

I Table of Contents

I.	Table of Contents	I
II.	Abstract	IV
III.	Zusammenfassung.....	VII
1.	Introduction	1
1.1.	Cancer	1
1.1.1.	Breast Cancer	2
1.1.2.	Prostate Cancer	3
1.1.2.1.	Prostate Cancer and the Androgen Axis	5
1.2.	Circulating Tumor Cells (CTCs) as Liquid Biopsy.....	8
1.2.1.	Biology of CTCs in Cancer Metastasis	9
1.2.2.	CTC Enrichment and Detection	12
1.2.3.	CTC Identification and Characterization	14
1.2.4.	Functional Analysis of CTCs	16
1.2.5.	Clinical Relevance of CTCs	17
2.	Aims of this Thesis	20
3.	Results	22
3.1.	Pre-Analytical and Analytical Variables of Label-Independent Enrichment and Automated Detection of Circulating Tumor Cells in Cancer Patients	23
3.2.	Evaluation of Microfluidic Ceiling Designs for the Capture of Circulating Tumor Cells on a Microarray Platform	41
3.3.	Proficiency Testing to Assess Technical Performance for CTC-processing and Detection Methods in CANCER-ID	50
3.4.	Characterization of Circulating Breast Cancer Cells with Tumorigenic and Metastatic Capacity	61
3.5.	In situ Detection and Quantification of AR-V7, AR-FL, PSA, and KRAS Point Mutations in Circulating Tumor Cells.....	83

3.6.	Detection of Androgen Receptor Variant (ARV7) mRNA Levels in EpCAM-enriched CTC Fractions for Monitoring Response to Androgen Targeting Therapies.....	94
4.	Discussion	117
4.1.	Improving the Enrichment of CTCs.....	117
4.1.1.	Impact of Pre-Analytical and Analytical Variables on CTC Enumeration.....	118
4.1.2.	Influence of Cancer Entity and Clinical Setting on CTC Enrichment.....	120
4.1.3.	Intra- and Inter-Laboratory Comparability of CTC Enumeration	122
4.2.	Development of a Model for Functional CTC Analysis.....	125
4.2.1.	Luminal CTC-Derived Cell Lines	125
4.2.2.	Metastatic Potential of CTC-ITB-01.....	126
4.2.3.	Cancer Stem Cell Pathways in CTC-ITB-01.....	127
4.2.4.	CTC-Derived Cell Lines as Surrogate Model for CTCs and Tumor Tissue	130
4.3.	Characterization of CTCs for Therapy Relevant Gene Expression.....	132
4.3.1.	Label-Dependent and Label-Independent ARV7 Detection	133
4.3.2.	Intensity and Localization of ARV7 expression in prostate cancer patient CTCs.....	135
5.	Conclusion and Outlook.....	138
6.	Literature and References	140
7.	Declaration of Contribution	153
7.1.	Pre-Analytical and Analytical Variables of Label-Independent Enrichment and Automated Detection of Circulating Tumor Cells in Cancer Patients.....	153
7.2.	Evaluation of Microfluidic Ceiling Designs for the Capture of Circulating Tumor Cells on a Microarray Platform	154
7.3.	Proficiency Testing to Assess Technical Performance for CTC-processing and Detection Methods in CANCER-ID.....	155
7.4.	Characterization of Circulating Breast Cancer Cells with Tumorigenic and Metastatic Capacity	156
7.5.	In situ Detection and Quantification of AR-V7, AR-FL, PSA, and KRAS Point Mutations in Circulating Tumor Cells.....	157

7.6.	Detection of Androgen Receptor Variant (ARV7) mRNA Levels in EpCAM-enriched CTC Fractions for Monitoring Response to Androgen Targeting Therapies.....	158
8.	Abbreviations.....	159
9.	Supplementary Data.....	165
10.	Acknowledgement.....	166
11.	Curriculum Vitae	169
12.	Publications and Presentations	171
13.	Eidesstattliche Erklärung	175

II Abstract

Traditional tissue biopsies and classical imaging techniques (e.g. radiology) have dominated the field of cancer patient management and shaped our understanding of tumorigenesis, metastasis, treatment response, and therapy resistance. In recent years, the analysis of circulating tumor cells (CTCs) as a non-invasive liquid biopsy has gained momentum. CTC enumeration has become a valuable prognostic marker for patient survival as well as a surrogate biomarker to assess treatment response for multiple cancer entities. Molecular characterization of CTCs has furthermore broadened our understanding of intra-tumor heterogeneity and its effect on treatment response and prognosis. Collectively, CTC research has opened a path towards real-time personalized medicine for cancer patients.

A major hurdle of CTC research is the rarity with which these cells can be found in the bloodstream. Improving CTC enumeration and detection therefore remain of paramount importance in the field. In this thesis, extensive efforts were made towards optimization and analytical validation of a promising label-independent CTC enrichment approach. CTC capture was increased 4.7-fold as demonstrated by direct comparison in paired breast cancer patient samples. Overall, two separate robust protocols allowing for the capture of un-fixed (EDTA) or preserved (TransFix®) single CTCs and CTC clusters were developed and their proficiency was corroborated on a mixed cancer patient collective. Also, compatibility with standard downstream molecular analysis and semi-automated sample evaluation were demonstrated. In a separate step, this enrichment technology was paired with a novel, innovative microfluidic device which immobilizes inoculated CTC populations within a microfluidic chamber. Near full CTC capture efficiency was achieved following improvement of the chip design. Also high retained cell viability (>90%) and compatibility with downstream molecular analysis approaches was shown. Finally, in an effort to assess intra- and inter-technology performance, multiple CTC enrichment platforms were compared across internationally renowned partner laboratories. Both label-dependent and label-independent technologies were assessed using well characterized EpCAM^{low} and EpCAM^{high} lung cancer cell lines. Vast differences in capture efficiency as well as performance variability were shown for the five different enrichment technologies tested, underlining the relevance of this multi-center technical benchmarking. The established international platform to assess technical validity will remain in operation via the European Liquid Biopsy Society (ELBS) consortium.

The formation of distant metastasis marks the transition from localized to systemic disease for cancer patients and is accompanied by a significant decrease in patient survival. Despite substantial advances in the field of cancer research, the underlying mechanisms of blood-borne dissemination remain largely unknown. Circulating tumor cells (CTC), and especially functional CTC models, hold the potential to provide insight into the fundamental requirements of tumor cells within the process of haematogeneous spread. In this thesis, we describe the establishment and in-depth molecular and functional characterization of an estrogen-receptor positive (ER⁺) CTC-derived permanent cell line (CTC-ITB-01). CTC-ITB-01 was isolated from a metastatic ER⁺ breast cancer patient following the development of resistance towards endocrine therapy. High genetic concordance was demonstrated between the established cell line and the original CTCs present at time point of blood draw, strongly indicating CTC-ITB-01's descent of from a subpopulations of these tumor cells. The CTC cell line was classified as epithelial-like and expresses stem cell markers such as ALDH1 and NUMB. In line with this, CTC-ITB-01 displayed tumorigenic and metastatic capacities in mice and adequately mirrored the metastatic tropism of ER⁺ breast cancer patients. Overall, CTC-ITB-01 represents a valuable new model to study CTC biology and allow for testing of drug efficacy in ER⁺ breast cancer.

As a form of surrogate material for tumor tissue, CTCs can reflect the emergence of tumor cell clones resistant to specific drugs and support the identification of innate or acquired resistance. The timely detection and optimal management of such therapy resistance may save valuable time for the patient and stratify them for alternative therapeutic branches. In this thesis, two assays were developed to detect *ARV7*, an established biomarker for resistance towards secondary hormone therapy in prostate cancer. Both assays were thoroughly technically validated and demonstrated clinical feasibility with prostate cancer patient samples. (a) A highly sensitive and specific qPCR assay based on the only FDA-approved technology for enrichment of prostate cancer CTCs was developed for detection of *ARV7* and *keratin-19* mRNA. This assay showed sensitivity down to a single *ARV7*-positive cell even after 24h of sample storage and high level of robustness for samples containing ≥ 5 CTCs. (b) *In situ* detection of *ARV7*, *PSA* and *AR-FL* transcripts, combined with immunocytochemical staining of pan-keratin and CD45 protein levels provided valuable insight into inter-, and intra-patient heterogeneity of *ARV7* and keratin expression in prostate cancer patient CTCs. Absolute quantification of *ARV7* expression was possible while cellular integrity is maintained. This approach is combinable with various CTC enrichment platforms. Label-independent CTC enrichment resulted in the identification of keratin-low *ARV7*⁺ CTC populations that probably has

undergone an epithelial-mesenchymal transition and would have surely been missed by label-dependent technologies. In summary, this thesis provides valuable tools and novel insights into CTC biology to answer pressing questions on the clinical and biological relevance of *ARV7*⁺, as well as keratin-low, CTC subpopulations in prostate cancer.

III Zusammenfassung

Klassische Gewebsbiopsien und bildgebende Verfahren (z.B. Radiologie) haben die Behandlung von Krebspatienten, sowie unser Verständnis der Karzinogenese, Metastasierung, des Ansprechens auf sowie der Resistenz gegenüber Therapeutika maßgeblich bestimmt. Innerhalb der letzten Jahre hat die Untersuchung zirkulierender Tumorzellen (CTCs) als Form der nicht-invasiven Flüssigbiopsie zunehmend wissenschaftliches und klinisches Interesse geweckt. Die Enumeration zirkulierender Tumorzellen ist ein wertvoller prognostischer Marker für das Überleben von Krebspatienten, sowie ein Surrogatmarker für das Therapieansprechen in mehreren Krebsentitäten. Die molekulare Charakterisierung von CTCs hat unser Verständnis der intra-Tumor Heterogenität und deren Einfluss auf Therapieansprechen und Prognose zudem entscheidend erweitert. Die Forschung an CTCs eröffnet einen Weg in Richtung personalisierter Medizin für Krebspatienten.

Eines der größten Hindernisse der CTC-Analyse ist die Seltenheit mit der diese Zellen in der Blutbahn vorliegen. Die Anzahl detektierbarer CTCs zu maximieren stellt daher weiterhin ein höchst relevantes Ziel dieses Forschungsfeldes dar. Innerhalb dieser Arbeit wurden weitreichende Anstrengungen unternommen um ein vielversprechendes, größenbasiertes CTC Anreicherungsverfahren zu optimieren und analytisch zu validieren. Die Anzahl detektierter CTCs konnte erfolgreich um das 4,7-fache erhöht werden. Dies wurde im direkten Vergleich gepaarter Patientenproben metastatischer Brustkrebspatientinnen nachgewiesen. Es wurden zudem zwei robuste Protokolle entwickelt, welche die Detektion unfixierter (EDTA) sowie fixierter (TransFix®) Einzelzellen und sogenannter CTC-Cluster (CTC-Gruppen/Aggregate) ermöglichen. Die Leistungsfähigkeit dieser Protokolle wurde anhand einer gemischten Krebspatientenkohorte bestätigt. Des Weiteren wurde die Vereinbarkeit der entwickelten Protokolle mit gängigen molekularen Analyseverfahren, sowie mit einem semi-automatisierten Nachweisverfahren demonstriert. In einem weiteren Schritt wurde die untersuchte Anreicherungs-methode mit einem neuen, innovativen mikrofluidischen System verbunden, welches markierte CTC Populationen innerhalb einer mikrofluidischen Kammer immobilisiert. Durch Anpassung der Chip Struktur konnte eine fast vollständige CTC Anreicherungs-effizienz erreicht werden. Die angereicherten CTCs zeigten darüberhinaus einen hohen Anteil an Viabilität (>90%) und waren molekularen Analyseverfahren zugänglich. Um die intra- und inter-technologischen Abweichungen in der Leistungsfähigkeit ausgewählter CTC Anreicherungsverfahren zu prüfen, wurden in einem letzten Schritt internationale Ringstudien aufgesetzt. Fünf unterschiedliche Anreicherungsverfahren wurden in unterschiedlichen

renomierten Laboren verglichen und auf die Effizienz Ihrer Anreicherung EpCAM^{niedriger} und EpCAM^{hoher} Tumorzelllinien geprüft. Die Studie wies große Unterschiede in der Anreicherungs-effizienz und Messungsvariabilität der untersuchten Methoden auf, welches die Relevanz multizentrischer technischer Vergleichsstudien unterstreicht. Die in dieser Studie etablierte internationale Plattform zur Beurteilung technischer Validität wird ihre Aktivität über das gegründete European Liquid Biopsy Society (ELBS) Konsortium weiterführen.

Die Bildung von Fernmetastasen markiert den Übergang einer lokalen zu einer systemischen Krebserkrankung und wird von einem entscheidenden Abfall der Überlebenswahrscheinlichkeit begleitet. Trotz substanziellem Fortschritt im Bereich der Krebsforschung sind die zugrundeliegenden Mechanismen der Dissemination von Tumorzellen immer noch weitestgehend unbekannt. CTCs und funktionelle CTC-Modelle im speziellen, haben das Potential weitreichende Einblicke in die grundlegenden Bedingungen und Voraussetzungen der blutbasierten Streuung zu ermöglichen. In dieser Arbeit wird die Etablierung und weitreichende molekulare sowie funktionelle Charakterisierung einer neuen, permanenten Estrogenrezeptor-positiven (ER⁺) CTC Zelllinie (CTC-ITB-01) beschrieben. CTC-ITB-01 wurde aus der Blutprobe einer ER⁺, metastatischen Brustkrebspatientin gewonnen. Die hohe genetische Übereinstimmung zwischen CTC-ITB-01 und den zur Zeit der Blutentnahme vorliegenden CTCs der Patientin, weisen stark auf eine Abstammung der CTC-Zelllinie von einer Subpopulation dieser CTCs hin. CTC-ITB-01 vereint primär epitheliale Protein- und mRNA- Expressionsmuster mit der Expression von Krebsstammzell-assoziierten Proteinen, wie ALDH1 und NUMB. Die kanzerogene und metastatische Kapazität der CTC-Zelllinie wurde in Mausexperimenten bestätigt. Im Mausmodell zeigte sich ebenfalls, dass CTC-ITB-01 den metastatischen Tropismus ER positiven Brustkrebses widerspiegelt und zur Effizienztestung neuer Therapeutika herangezogen werden könnte. Zusammenfassend stellt CTC-ITB-01 ein wertvolles funktionelles Model zur Untersuchung der biologischen Charakteristika zirkulierender Tumorzellen dar.

Als Surrogat für Tumorgewebe können CTCs das Aufkommen resistenter Tumorzellklone sowie die Existenz innerter oder erworbener Resistenz gegenüber spezifischer Therapeutika anzeigen. Die zeitnahe Identifikation einer Therapieresistenz und die darauf angepasste Behandlung des Patienten kann entscheidend für den Verlauf der Erkrankung werden. In dieser Arbeit wurden zwei Methoden entwickelt um die Transkription von ARV7 (Androgenrezeptor Splice-Variante 7), einem etablierten Biomarker für Resistenz gegenüber sekundärer Hormontherapie im Prostatakarzinom, nachzuweisen. Beide Methoden wurden umfassend technisch validiert und auf

Ihre Übertragbarkeit auf klinische Patientenproben hin untersucht. (a) Basierend auf der CTC Anreicherung mittels des einzigen von der Amerikanischen Food and Drug Association (FDA) für das Prostatakarzinom zugelassenen Technologie (CellSearch®), wurde ein hochsensitiver qPCR Ansatz entwickelt um *ARV7* und *keratin-19* mRNA in CTCs zu detektieren. Mittels dieser Methode konnten *ARV7* Transkripte aus einer einzelnen CTC, selbst nach 24 Stunden der Probenlagerung, nachgewiesen werden. Bei Blutproben mit ≥ 5 CTCs war *ARV7* höchst robust und zuverlässig detektierbar. (b) Der *in-situ* Nachweis von *ARV7*, *PSA*, und *AR-FL* (vollständiger Androgenrezeptor) Transkripten, kombiniert mit der immunozytochemischen Färbung von Keratinen und CD45, ermöglicht wertvolle Einblicke in die Heterogenität der *ARV7*- und Keratin-expression innerhalb und zwischen Prostatakarzinompatienten. Die Methode erlaubt darüber hinaus eine absolute Quantifizierung von *ARV7* Transkripten bei gleichzeitiger Bewahrung der zellulären Integrität. Diese Nachweismethode ist mit einem breiten Spektrum an CTC Anreicherungsverfahren kombinierbar. Die größenabhängige CTC Anreicherung identifizierte eine *ARV7*-positive CTC Subpopulation mit niedriger Keratin Expression, welche höchstwahrscheinlich von anderen Marker-abhängigen Technologien nicht detektiert worden wäre. Zusammenfassend stellt diese Arbeit daher wertvolle Methoden, sowie neue Erkenntnisse der CTC Biologie, zur Verfügung um offene Fragen hinsichtlich der biologischen und klinischen Relevanz von *ARV7*⁺ und Keratin^{niedrigen} CTC Subpopulationen im Prostatakarzinom zu beantworten.

1. Introduction

1.1. Cancer

Cancer remains the second leading cause of death worldwide with 9.56 million cancer-related deaths being reported in 2017 [1]. Cancer is a blanket term for a plethora of diseases caused by abnormal and uncontrolled cell division. These neoplasms may derive from practically any bodily cell type and are classified according to their cell of origin. Malignant solid tumors stemming from epithelial cells, so called carcinomas, represent the majority of diagnosed cancers and are responsible for most cancer-related deaths [2]. The most common carcinoma entities worldwide are breast and lung cancer, followed colorectal and prostate cancer [2].

The underlying mechanisms causing deregulation of the cell cycle machinery and uncontrolled proliferation within a specific tissue vary across tumor types. While age represents a universal risk factor for most cancers, other causes such as radiation, viruses, hereditary genetic background and lifestyle choices (smoking, alcohol consumption, obesity, etc.) are associated at higher levels with specific tumor entities [3]. Apart from differences in cancer causes, tumor cell morphology, underlying molecular mechanisms, drivers of tumor progression, as well as efficient treatment regimens may vary drastically between cancer entities [4]. Six biological capabilities, the so called “hallmarks of cancer” have been postulated to be critical in the development of human tumors. These comprise of sustaining proliferative signaling, evading growth suppression, resisting cell death, enabling replicative immortality, inducing angiogenesis, and activating invasion and metastasis [5]. As soon as a tumor has formed, reliable and early diagnosis is crucial to improve patient survival [6]. Early on in the disease, curative therapy approaches may remain available. These treatments aim at reducing tumor mass or eradicating the malignant tissue entirely. Curative therapy options include surgical tumor tissue removal, radiation, targeted monoclonal antibodies, and chemotherapy. The importance of early cancer detection is underscored by the fact that 90% of cancer related deaths are caused by the formation of distant metastases and not by growth of the primary tumor [7]. Therapeutic options in late disease stages are frequently ineffective, merely prolonging life instead of enabling complete recovery. Despite ongoing attempts at improving therapy, patients diagnosed in the metastatic setting show significantly lower survival rates across most cancer entities [8-11].

1.1.1. Breast Cancer

Breast cancer (BC) remains the most common cancer type in women. More than 530.000 new BC patients were diagnosed in Europe alone in 2020 [2]. For about 141.000 women the disease had a lethal outcome in the same year [2]. While breast cancer incidence has increased over the last decades, mortality has overall slightly declined across Europe, most likely due to improved screening techniques and novel treatment regimens [12-14]. A multitude of risk factors for the development of BC have been identified, the most prominent including age, family history of breast cancer, socioeconomic factors, genetic predisposition (e.g. *BRCA1* and *BRCA2* mutations), hormonal/reproductive events (menarche, pregnancy, breastfeeding, menopause), but also life style choices (obesity, alcohol consumption, physical activity, etc.) [15].

Breast cancer screening has become common practice in Western Europe and the United States. Women routinely undergo physical breast examinations during their yearly visit with their gynecologist and are encouraged by clinicians to perform regular self-examination of the breast and surrounding lymph nodes in order to seek medical attention if a suspicious lump becomes palpable. In addition, bi-annual or annual mammography is performed in women above the age of 50 (and even younger if risk factors are known). While other methods such as magnetic resonance imaging (MRI) and ultrasound of the breast prove useful in disease staging and management, mammography is the current gold standard for breast imaging. The benefit of mammography screening, especially in lower age groups (between 40-49 years of age), has been controversially debated [16, 17]. However, it represents one of the most important advances in the early detection of non-palpable tumor masses and remains the mainstay of BC detection [18].

BC is classified according to the Union Internationale Contre le Cancer (UICC) guidelines into stages 0-IV based on TNM (Tumor, Node, Metastasis) criteria [18, 19]. The malignant nature of an identified lesion is usually confirmed via tissue biopsy (punch biopsy). The latter provides valuable additional information on morphological classification, histological grade and molecular subtype of the tumor [18]. All three are important prognostic and predictive factors for therapeutic choices [18, 20, 21]. BC is a biologically heterogeneous disease and its distinct molecular subtypes (Luminal A, Luminal B, HER2-positive, Basal-like and Claudin-low) show significant differences in their incidence, responsiveness to therapy, risk factors and prognosis [18, 22-24]. Molecular subtyping is most frequently performed by surrogate markers in histopathology although analysis of gene expression signatures (e.g. PAM50 classifier) remain more detailed [18]. The pathological classification is based

on immunohistochemical (IHC) staining of 4 relevant target proteins, the estrogen receptor (ER), progesterone receptor (PR), amplification of human-epithelial-growth-factor-receptor 2 (HER2/ERBB2), and Ki-67 as a marker of cell proliferation. The approximated frequency and identifiers of the 4 major subtypes are summarized in Table 1 below.

Table 1: Molecular subtypes as defined by histopathology [20, 24]

Molecular Subtype	Frequency	Receptor Status	Ki67	Additional markers	Prognosis
Luminal A	50-60%	HR+(ER+/- and/or PR+/-) & ERBB2-	low	K8/18+	Good
Luminal B	15-20%	HR+(ER+/- and/or PR+/-) & ERBB2+/-	high	K8/18+	Intermediate
ERBB2 positive	10-15%	HR- (ER- and PR-) /ERBB2+	high	TP53 mutation common	Intermediate
Triple-negative	15-20%	HR- (ER- and PR-) /ERBB2-	high	K5/6+ EGFR+	Poor

In conclusion, BC is clinically and biologically heterogeneous and the benefit of specific therapeutic options may vary according to a multitude of factors including the molecular subtype of the tumor and the disease stage [18, 25]. While molecular analysis into BC biology have generated a vast wealth of knowledge and thus advanced the understanding of this tumor entity, novel insights as well as refinements to current paradigms are constantly being added.

1.1.2. Prostate Cancer

In Europe, prostate cancer (PC) is the most common cancer type in men with over 470,000 new cases diagnosed in 2020 [26]. In the same year, PC accounted for approximately 108,000 deaths in Europe alone [26]. While the etiology of PC remains somewhat inconclusive, well established risk factors such as age, ethnicity and family history of the disease have been identified [27, 28].

In contrast to other cancer types, PC screening has become accessible to, and well accepted by large parts of the European public. This ensures that the vast majority of patients are diagnosed at early disease stages, resulting in high survival rates [29]. The most frequently used biomarker to

detect and monitor PC is prostate specific antigen (PSA), a protein secreted by the epithelial cells of the prostate gland. PSA is measured in blood serum and is often elevated in the presence of PC, but also in the presence of other conditions such as prostatitis or benign prostatic hyperplasia. Broadly speaking, serum PSA levels above 4.0 ng/ml are considered elevated. However, due to the unspecific nature of this screening approach, initial results need to be confirmed by additional sequential tests [30]. When indicated, tissue biopsy is performed to determine whether PC is in fact the cause of the elevated PSA levels. Transrectal ultrasound guided prostate (TRUS) biopsy is currently the most commonly applied biopsy procedure, although transperineal biopsy has demonstrated higher detection rates of clinically significant PC with fewer adverse effects [31]. PC is a multifocal disease, about 80% of prostate cancers contain >1 disease focus [32]. To increase chances of detecting the tumor(s), multiple biopsy cores (average of 12-14) are taken during TRUS using a fine needle. These tissue samples are subsequently analyzed and staged/graded by a pathologist. Apart from the UICCs staging according to TNM criteria, PC is also assigned a Gleason grade (6-10) (Table 2). Both parameters together describe the growth, spread and location of the tumor and are combined with PSA values to help determine optimal therapy regiments [30].

Table 2: Meaning of the Gleason grade. The Gleason score is determined by pathologists according to the sum of the two most common patterns of cell growth determined across multiple tissue biopsies [33, 34].

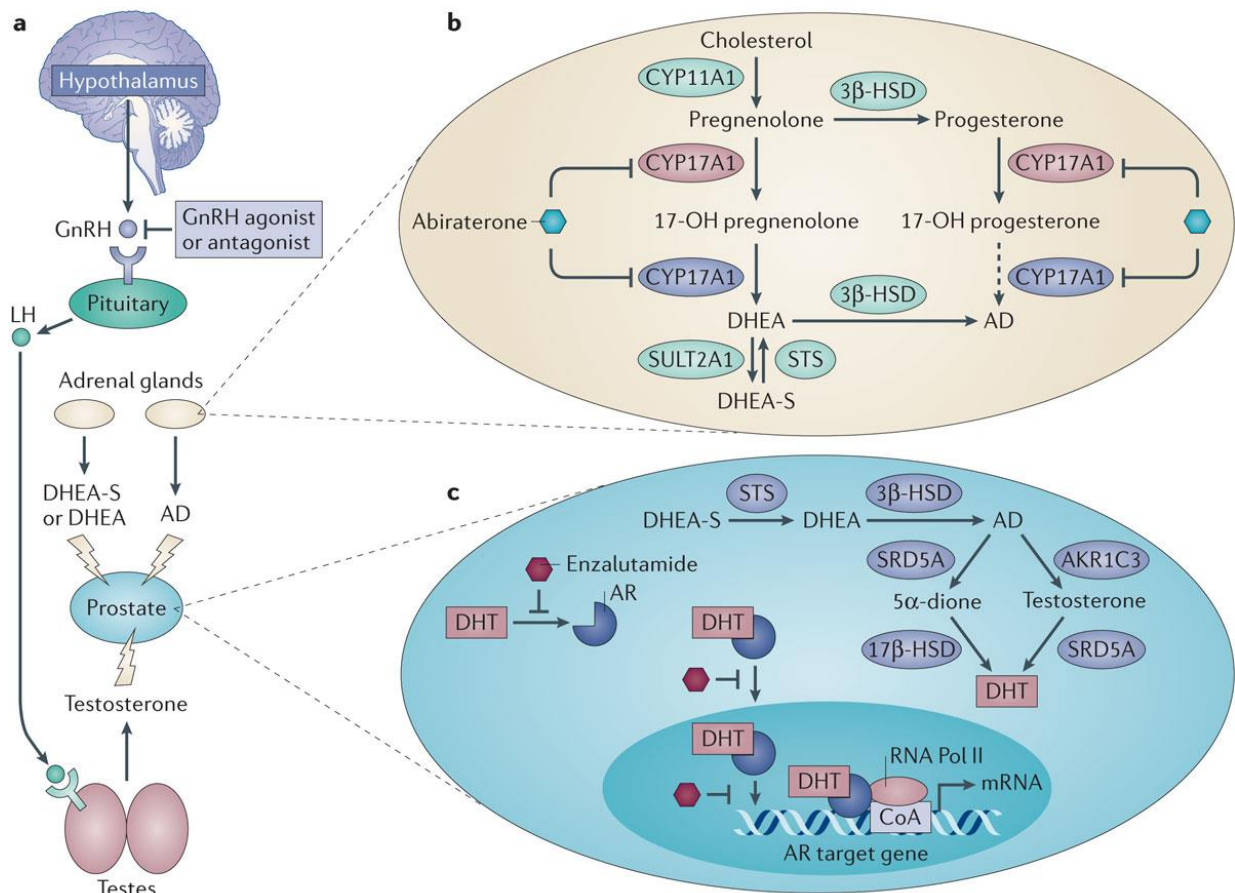
Gleason score	Grade Group	Meaning
6 (3+3)	1	Tumor cells show similar morphology to regular prostate cells. The tumor is likely to show slow growth, if any.
7 (3+4)	2	Tumor cells still appear well differentiated. The cancer will most likely grow slowly.
7 (4+3)	3	Cancer cells are moderately differentiated, resulting in moderate outgrowth.
8 (4+4)	4	Tumor cells display increasing de-differentiation. The morphology is abnormal. The tumor may grow at a moderate or high pace.
9 or 10 (4+5, 5+4, or 5+5)	5	The vast majority of cells are highly de-differentiated, resulting in abnormal morphology. The tumor is most likely to grow at a rapid pace.

In most cases PC represents a relatively slow progressing cancer. Therefore, while incidence is high, many cases of PC remain subclinical and are managed by active surveillance, requiring no further medical intervention. In fact, the indolent disease course combined with the low specificity of PSA as a biomarker has raised concerns of over diagnosing and over treating this cancer type [35]. The European clinical practice guidelines for PC therefore discourage testing for prostate cancer in asymptomatic men above the age of 70 years [30]. When diagnosed in a localized stage, treatment options for localized PC (LPC) are plentiful and consist of active surveillance, brachytherapy, radical prostatectomy, radiotherapy and neoadjuvant androgen deprivation therapy (ADT) [30]. While these curative approaches are successful in containing the disease for the majority of LPC cases, a subset of patients develop aggressive PC subtypes that defy current therapeutic options. Survival rates for this patient cohort decrease significantly from 99% to around 30% [29]. In the metastatic setting, the defining factor for the choice of therapy remains tumor responsiveness to hormones, primarily androgen-dependency. In hormone naïve metastatic prostate cancer (mPC), ADT is either initiated or continued [30]. Androgen-independent tumor growth is termed castration-resistant prostate cancer (CRPC) and represents the aggressive final mPC stage. The treatment landscape for CRPC has significantly broadened in the last decade and includes chemotherapy (e.g. docetaxel, cabazitaxel), as well as secondary hormone therapy (abiraterone, enzalutamide), monoclonal antibodies (denosumab), and immunotherapy (sipuleucel-T) as first and second line therapeutic options for these patients [30].

1.1.2.1. Prostate Cancer and the Androgen Axis

Upon development, PC, similar to BC, is initially hormone dependent, meaning its growth and survival is dominated by androgens activating the androgen receptor (AR) [36]. The AR belongs to the steroid hormone group of nuclear transcription factors. In brief, AR ligands such as testosterone and 5 α -dihydrotestosterone (DHT) enter the prostate cell and activate the AR in the cells cytoplasm. The AR subsequently translocates to the nucleus, dimerizes and binds to the DNAs androgen-response-elements (AREs) where it initiates transcription of genes involved in differentiation, secretion (e.g. PSA), migration and survival [37-39]. Thus, as the main driver of tumor initiation and progression in PC, the AR represents the primary therapeutic target in management of high-risk LPC and advanced PC stages.

Androgen synthesis is governed by the hypothalamic-pituitary-testicular axis (Figure 1a). Therefore, first line androgen deprivation therapy (ADT) commonly involves chemical castration through gonatropin-releasing hormone (GnRH) agonists or antagonists [40]. While patients initially respond well to first line ADT, resulting in disease regression, it is generally not curative and a majority of patients acquire resistance and progress to lethal metastatic castration-resistant PC [41]. Originally, it was assumed that the AR-pathway plays a subordinate role in CRPC. For years chemotherapy (docetaxel) therefore represented the only approved treatment option for CRPC. However, studies have strongly indicated that the AR axis is reactivated in CRPC and that both residual androgens, as well as the AR itself remain crucial drivers even in this lethal disease stage [42-44]. These novel insights have led to the development of so called secondary hormone therapies for advanced PC. These agents (abiraterone, enzalutamide) target the AR-pathway and have significantly improved survival of CRPC patients [45-47]. While abiraterone inhibits androgen biosynthesis by blocking CYP17A1 in the testis and adrenal glands (Figure 1b), enzalutamide is a potent AR antagonist, inhibiting the AR ligand binding domain within the prostate (Figure 1c). Despite the initial effectiveness of these novel therapeutics, neither of them increase survival longer than a few months on average [45-49]. Inherent and acquired resistance to second generation hormone therapies remain a major clinical challenge and identifying mechanisms that allow restored AR signaling, AR bypass and complete AR independence are of critical importance. Currently, the resistance mechanism studied most in-depth in the realm of secondary hormone therapy is the expression of AR-splice variants, first and foremost the androgen-receptor splice variant 7 (ARV7). The expression of ARV7 mRNA and ARV7 protein in circulating tumor cells (CTCs) has been associated with resistance towards secondary hormone therapies [50, 51]. This splice variants lacks the ligand binding domain of the androgen receptor, thus conferring ligand-independent constitutional transcriptional activity [52, 53]. Through this absence of the ligand binding domain, it is assumed that ARV7 is no longer responsive to either enzalutamide (as the drug targets the ARs ligand binding domain) or abiraterone (as ligand levels are no longer of critical importance). Furthermore, ARV7 has been associated with the repression of known tumor suppressor genes in CRPC, providing additional insight into the functional role of ARV7 in disease recurrence [54]. Despite the described link between ARV7 expression and resistance, a multitude of open questions remain and further studies will be necessary to shed more light into the detailed functional role of ARV7, its relationship with the full-length AR, and the required level of ARV7 expression in PC.



Nature Reviews | Cancer

Figure 1: Androgen signaling cascade and targets of secondary hormone therapy (taken from [42]). (A) Gonadotropin-releasing hormone (GnRH) and luteinizing hormone (LH) are released from the hypothalamus and pituitary gland respectively and induce testosterone secretion from the Leydig cells of the testis. This in turn affects the prostate. GnRH agonists or antagonists reduce LH production, resulting in a decline of serum testosterone to castrate levels. The androgens dehydroepiandrosterone sulfate (DHEA-S), DHEA, and androstenedione (AD) are produced and secreted by the adrenal glands, also influencing the prostate. **(B)** The enzyme CYP17A1 (cytochrome-P450 family 17 A polypeptide 1) executes two critical reactions (red and blue) within the *de novo* synthesis of adrenal androgens. Both are inhibited by abiraterone. The dashed arrow indicates a weak effect. **(C)** Within the prostate, incoming androgens are converted to dihydrotestosterone (DHT), which binds to the androgen receptor (AR), thus initiating translocation to the nucleus, homodimerization, and subsequent binding to AR-response elements of the DNA. Together with co-activators (CoA), and RNA-polymerase II (RNA Pol II) this leads to activation or repression of AR-target genes. Enzalutamide inhibits AR activation by blocking the AR binding site.

1.2. Circulating Tumor Cells (CTCs) as Liquid Biopsy

Cancer diagnosis, as well as cancer management (e.g. the choice of treatment) is most commonly determined by analysis of tissue biopsies combined with certain imaging technologies (e.g. CT, MRI or PET scan). The bulk of current knowledge on cancer development, therapeutic targets and mechanisms of resistance towards therapy has been derived from clinical tumor tissue samples and through animal models. Unfortunately, invasive tissue biopsies can be associated with adverse effects for the patient and are therefore not sequentially repeated during disease progression or treatment course in routine clinical practice [55]. This limits their capacity to provide real-time information on the ever changing landscape of tumor evolution and tumor heterogeneity within the patient. Furthermore, selected tumor entities do not lend themselves well to traditional biopsy procedures (e.g. brain tumors), thus preventing more detailed insight into the development of these cancers.

Luckily, other unique sources of tumor material exist. Solid tumors of epithelial origin (carcinomas) actively and/or passively shed tumor cells from the main tumor mass into the bloodstream. These so called circulating tumor cells (CTCs) can stem from the primary tumor and/or existing metastatic sites [56]. While it is difficult to determine the exact amount of CTCs in the blood at any given time, mathematical models based on animal studies indicate that for each Gramm of detectable tumor mass, millions of CTCs enter the circulation on a daily basis [57, 58]. This CTC shed appears to be continuous and independent of circadian rhythm [59]. The approach of utilizing CTCs to answer urgent questions in clinical patient care in form of a “liquid biopsy” was coined in 2010 [60]. Since then the term of liquid biopsy has been extended to include the analysis of circulating nucleic acids (e.g. ctDNA, miRNA), extracellular vesicles (e.g. exosomes), and others (e.g. platelets) in blood or other bodily fluids such as cerebral spinal fluid (CSF) or urine [61-63]. Blood based liquid biopsies possess unique advantages over traditional biopsy procedures. They are accessible through a minimally invasive standard blood draw which allows for repeated sampling. Additionally, liquid biopsies are not limited to the site of tissue removal. They can therefore encompass cells originating from the primary tumor but also from existing metastases and thus provide a more holistic view of the disease status as well as tumor heterogeneity [64]. While CTC-analysis does not aspire to completely replace tissue biopsy, it has enormous potential to provide valuable and multifaceted additional information for the clinical management of cancer and personalized cancer care (Figure 2).

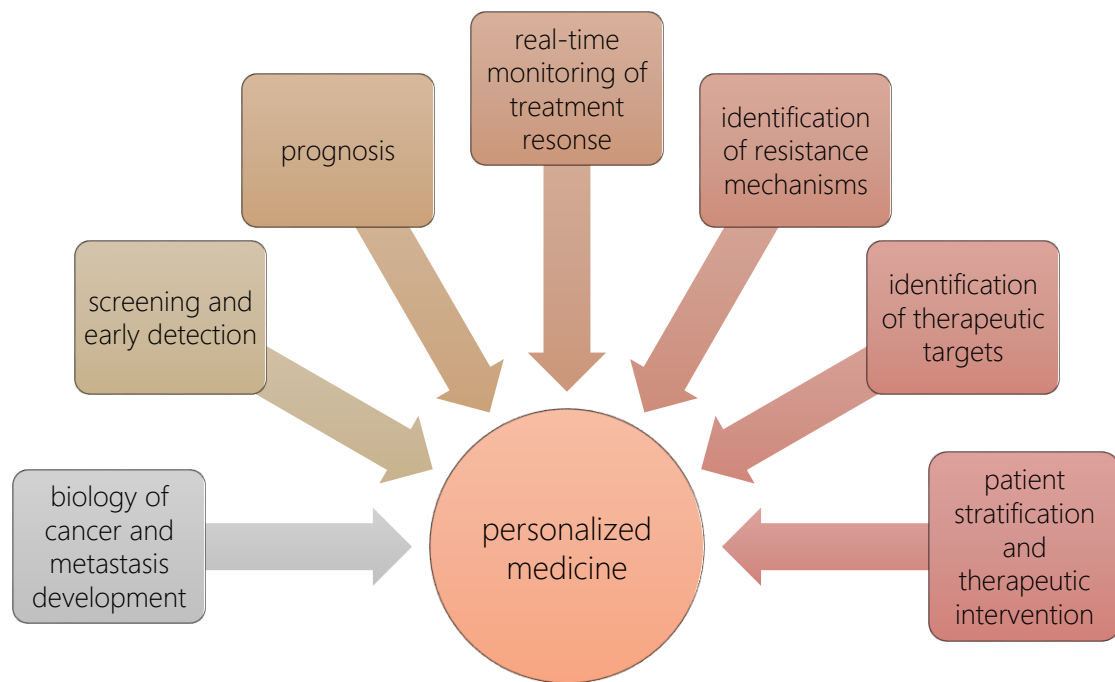


Figure 2: Potential contributions of CTC analysis towards personalized cancer care.

1.2.1. Biology of CTCs in Cancer Metastasis

A localized, primary tumor that has not ruptured the structural barriers of its surrounding tissue or invaded the adjacent blood or lymphatic system is called *carcinoma in situ* (CIS). The formation of metastatic lesions represents the defining step in the transition from localized towards systemic disease and is associated with a sharp decline of overall survival for most cancer patients [11]. Originally, it was assumed that tumor cell spread throughout the body was associated with late disease stages. In recent years this paradigm has shifted, as experimental and clinical observations increasingly indicate that tumor cells can detach from the tumor mass as early as primary tumor formation [65–68]. While locoregional spread most commonly occurs via the lymphatic system to the nearest lymph nodes [69], colonialization of distant tissues is primarily driven by hematogenous dissemination [70, 71]. Detecting and analyzing the cells in circulation at early disease stages could therefore provide an important strategy to monitor and ideally prevent the formation of overt metastasis.

In healthy physiological tissues and solid tumors, cells are closely attached to one another (cell-cell adhesion) and the surrounding extracellular matrix (ECM). This connection is driven by adhesion molecules such as integrins, cadherins (e.g. E-cadherin) and the epithelial cell adhesion molecule (EpCAM). The morphological result is a cobble stone-like appearance of the tissue. Cellular disaggregation and transition from an immobile to a mobile state is complex and involves a multitude of structural changes. While the mechanisms underlying the acquisition of motility are still not fully understood, a leading hypothesis postulates that tumor cells are required to undergo epithelial to mesenchymal transition (EMT) to gain invasive capacity [72, 73]. EMT is an essential and highly coordinated physiological program that is activated during embryogenesis and wound healing [72]. Briefly, during EMT epithelial cells de-differentiate, reverting to a more mesenchymal, highly plastic phenotype. In carcinomas, EMT is triggered by a plethora of different signals stemming mostly from the surrounding tumor stroma [74-76]. The tumor microenvironment directly impacts selected signaling cascades of the tumor cells such as the Wnt, TGF β and Notch pathways, amongst others [75, 77]. Additionally, a host of growth factors, cytokines, and inflammatory signals has been associated with initiating the EMT program [77, 78]. The expression of specific EMT-associated transcription factors (TFs) such as SNAIL, TWIST, ZEB and SLUG as well as other epigenetic and post-transcriptional regulators subsequently drives EMT [75, 79, 80]. In combination, these factors initiate the downregulation of epithelial adhesion molecules (e.g. EpCAM and E-Cadherin), the upregulation of mesenchymal markers (e.g. N-Cadherin and Vimentin), and the reorganization of the cytoskeleton, thus modifying shape and deformability of the cell. The latter is achieved through a shift in keratin expression resulting in a loss of cellular polarity. In addition, increased secretion of proteolytic enzymes such as matrix metalloproteases (MMPs), result in the degradation of the ECM and further facilitate invasiveness [81, 82]. Gaining motility and detaching from the surrounding tissue represents the first step of the metastatic cascade. Usually, the loss of cell-cell or cell-ECM connectivity results in a specialized form of cell death termed anoikis [83]. This regulatory response to anchorage-independent growth stimuli is essential in multicellular organisms and guarantees tissue homeostasis. Overcoming anoikis is therefore one of the hallmarks of metastasis formation [84].

Once tumor cells have gained motility, they need to traverse the surrounding tissue and endothelium to infiltrate the bloodstream in order to spread. This process can be actively mediated by invadopodia and macrophage-dependent transendothelial migration [85]. It can also take place passively, through permeable vasculature resulting from hasty angiogenesis in rapidly growing

tumors [86]. In this setting, the growing tumor mass presses through endothelial gaps into the bloodstream. There, tumor cells are “ripped” from the bulk of the tumor by shear forces and the velocity of the blood flow. Independent of whether CTCs enter the blood actively or passively, the environment within the vasculature is harsh. While the tumor microenvironment (TME) is frequently immunosuppressed [87, 88], CTCs in the bloodstream are subject to attack from the immune system. Additionally, biomechanical aspects such as hemodynamic shear forces, collision with blood cells, and constraints of the vessel architecture negatively impact CTC survival [89, 90]. This is reflected by a short half-life of CTCs within the bloodstream of around 1-2.5 hours [91] as well as the high frequency of fragmented or apoptotic CTCs found in the blood [92]. One mechanism by which CTCs attempt to circumvent these adverse effects involves the recruitment of platelets [93-95]. Mouse models have shown that platelet-induced mechanical protection and shielding from natural killer cell mediated lysis within the bloodstream significantly promotes metastatic proficiency [96]. Furthermore platelets induce pro-survival genes inhibiting apoptosis and anoikis [97].

To exit from the vasculature and enter into the surrounding tissue at a distant site, it is crucial for CTCs to first attach to the endothelium. Favorable blood flow profiles are required to allow for successful arrest and extravasation [98]. Additionally, platelets have been implicated in facilitating the adhesion of CTCs to the vascular endothelium by generating a thrombus that allows CTCs to attach and spread at the vessel wall [93, 99]. Once the tumor cell has entered the surrounding tissue, it is believed to revert to a more epithelial state involving a program called mesenchymal to epithelial transition (MET) [56]. This assumption is supported by studies that demonstrate an inability of mesenchymal tumor cells to form solid metastasis [100]. Similarly to EMT, MET is a critical cellular program required at various stages of morphogenesis and organogenesis [101]. While mesenchymal and epithelial cells represent both ends of the phenotypic spectrum, recent research indicates, that they are not static cellular phenotypes [102]. Tumor cells can display high levels of phenotypic plasticity and are able to not only switch between both extremes but also to find balance in-between [72, 102, 103].

Outgrowth represents the final step of the metastatic cascade. In order to establish a novel tumor lesion, tumor cells must survive in their novel microenvironment and, more importantly, retain the ability to proliferate. It is now well established that outgrowth can take place very quickly or slowly, depending on the tumor type. CTCs that have exited the blood flow and entered a novel niche, are called disseminated tumor cells (DTCs). DTCs are able to lie in a dormant state, arresting their cell cycle in G^0/G^1 phase for years, prior to initiating growth and developing into micro- or

macrometastasis [100, 104]. In fact, micrometastasis (DTC clusters) have been detected in up to 30% of bone marrow aspirates from primary BC patients at time of diagnosis [104]. However, in a 10 year follow-up, only 50% of these micro- develop into macrometastasis [104]. The factors triggering proliferation after dormancy remain poorly understood. However, multiple studies demonstrate that DTCs are able to cause tumor recurrence many years after primary diagnosis [104-107].

1.2.2. CTC Enrichment and Detection

The greatest obstacle when trying to analyze CTCs is their rarity compared to the high background of healthy blood cells within a standard blood sample. It is estimated that 1 CTC can be found within the backdrop of 10^8 - 10^9 normal blood cells [56, 108]. Enriching these rare cells to a ratio of 1 CTC in 10^2 - 10^3 blood cells is technically challenging and requires highly sensitive and specific methods [56]. To this day, more than 50 different platforms and assays have been developed for this purpose [109, 110]. These enrichment approaches can be classified into two groups, label-dependent and label-independent enrichment, although a combination of both is also practicable. Label-dependent enrichment is primarily based on biological properties, while label-independent enrichment predominantly makes use of physical features of tumor cells as indicated in Figure 3 [109].

The majority of label-dependent enrichment technologies rely on protein-based detection of CTCs via specific antibodies, so called positive selection (Figure 3). Tumor cells are captured by antibodies against certain antigens on their cell surface. Antibodies are usually coupled with magnetic beads, allowing for separation along a magnetic field (e.g. CellSearch®, AdnaTest®, MACS®, Isoflux®), or bound to microchips leading to immobilization on a specific surface (e.g. CellCollector™, CTCapture chip) [56, 111]. The most wide-spread cell surface protein targeted in this context is EpCAM [112]. EpCAM-based positive selection is used in a multitude of different *in vitro* and *in vivo* enrichment approaches [56], including the current “gold-standard” of CTC detection, the CellSearch® system [113]. In addition to positive selection, label-dependent enrichment technologies also make use of negative selection (Figure 3), targeting leucocyte markers (e.g. CD45) and depleting the leucocyte background, leading to indirect CTC enrichment (e.g. MACS®, EasySep®). Some technologies combine both selection approaches (e.g. CTC-iChip) [114].

While EpCAM-based positive selection is widely used and accepted, limitations to this approach exist. For one, EpCAM expression is specific for epithelial cells, not tumor cells. This

necessitates further validation steps to ensure the captured cells are in fact of tumor origin. Additionally, not all epithelial tumor cells express EpCAM at significant levels to ensure capture [115]. In fact, some tumor entities, such as non-small-cell lung cancer (NSCLC) and melanoma are known to express EpCAM at very low or non-detectable levels [116, 117]. Additionally, even tumors with traditionally high EpCAM expression can undergo EMT, downregulating their epithelial protein profile and evading detection [103]. Label-independent CTC enrichment technologies therefore base their assays on physical properties (Figure 3) such as cell size and/or rigidity (e.g. Parsortix®, VyCAP), cell density (Ficoll®), migratory capability (VitaAssay™), or centrifugal forces (ClearCell®) [56, 118]. In theory these technologies are more flexible as to the CTC populations they are able to enrich due to the fact that they do not focus solely on epithelial markers.

In summary, which technology is best suited for CTC enrichment is highly dependent on the investigated cancer entity as well as the CTC subpopulation of interest. Unfortunately, to this day, none of the established assays (apart from the CellSearch® system) are standardized and clinically validated to a level that grants them approval by regulatory agencies. This significantly hampers their use in routine clinical practice, limiting them primarily to the research setting for the time being. Extensive collective efforts need to be undertaken by the CTC field to ensure that (a) researchers can rely on and directly access in depth information on device performance, and (b) CTC enrichment protocols are externally validated to ensure robustness and comparability. This will be necessary to enable researchers and clinicians alike to make informed decisions on enrichment technologies for their research project and allow for as un-biased and reliable results as possible.

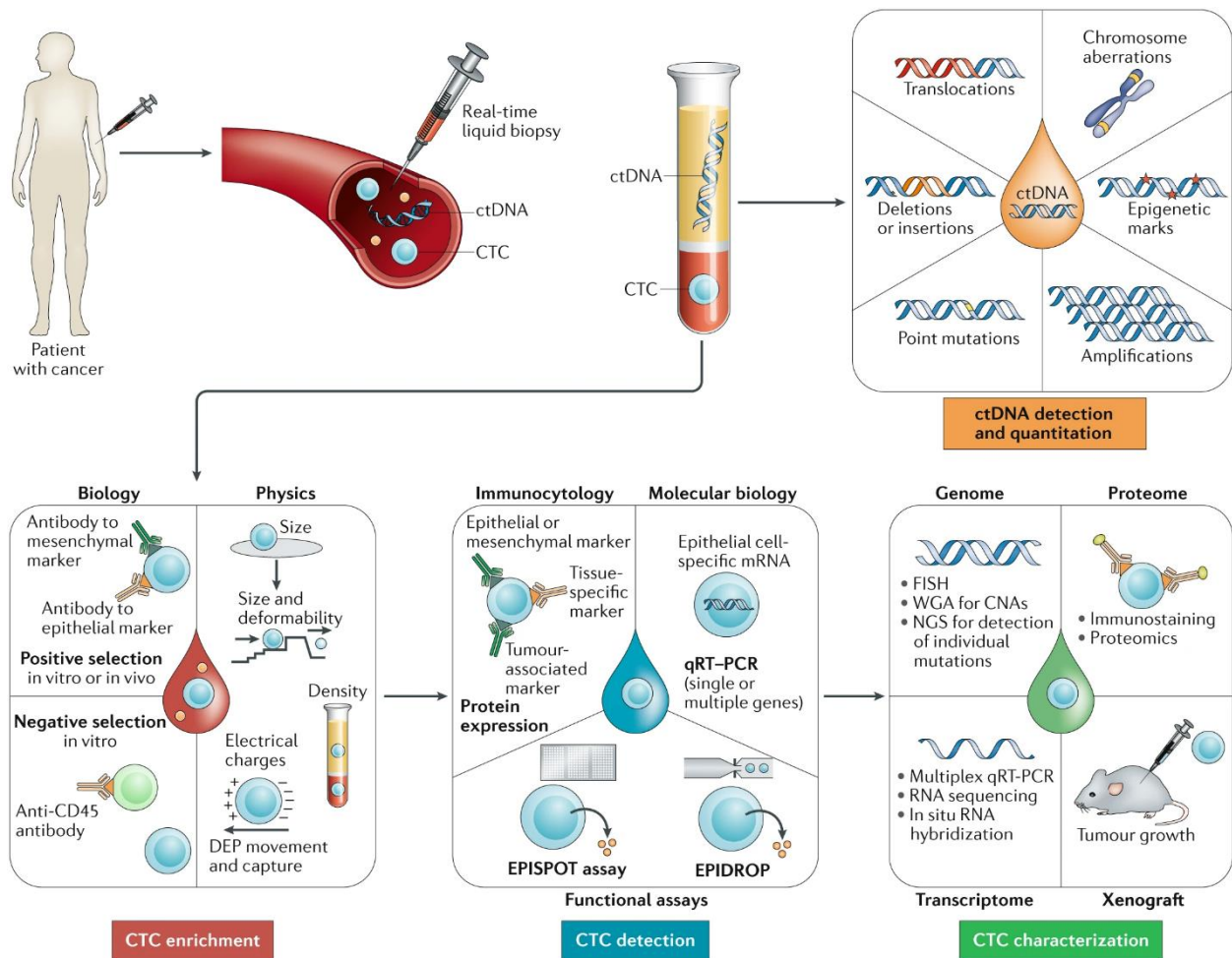


Figure 3: CTC and ctDNA enrichment, detection, and potential downstream analysis (taken from [119]). A cancer patient's blood draw can be separated into two main sample fractions. The plasma fraction contains circulating nuclear acids (ctDNA, ctRNA), while the cellular fraction contains circulating tumor cells (CTCs), peripheral blood mononuclear cells (PBMCs), immune cells, and circulating endothelial cells (CECs) amongst others. Isolated nuclear acids are mainly used for DNA analysis of mutations, translocations and deletions but also amplifications and epigenetic modifications (upper right square). CTCs within the cellular blood fraction can be further enriched to ensure higher purity and easier downstream analysis. Enrichment can be based on biological or physical CTC properties (lower left square). Subsequently, CTCs are detected by immunocytological, molecular or functional assays (lower middle square). CTC analysis can provide information on genomic, proteomic, and transcriptomic changes of the patient's tumor cells. Additionally, functional studies via mouse models (xenografts) or CTC cell lines are possible (lower right square).

1.2.3. CTC Identification and Characterization

Depending on the technology used for CTC enrichment, different assays can be applied for subsequent identification and further characterization of the potential tumor cells isolated.

The most common identification approach is the visualization of protein expression by staining of the enriched cell fraction using labelled antibodies (Figure 3). This can either be done in liquid (Parsortix®, Flow-Cytometry, DEPArray®), bound to magnetic or microchip surfaces (CellSearch®, CellCollector™) or on glass slides (RareCyte®). Some devices such as the CellTracks Analyzer® and DEPArray® allow for semi-automated visualization of CTCs, giving the user an image gallery from which to confirm putative CTCs. However, the majority of stainings are still performed on traditional glass slides and manually checked via fluorescence microscopes or by microscope based analyzing systems (RareCyte®, CytoTrack™). A CTC is most commonly defined as an intact, round or oval cell of at least 4µm diameter containing a nucleus (DAPI⁺) that is EpCAM and/or keratin positive and negative for the leucocyte marker CD45. This firmly established CTC definition has been predominantly derived from studies using the highly standardized and validated CellSearch® system [120]. Pan-keratin antibodies are frequently applied for CTC identification. These antibody cocktails detect a multitude of epithelial keratins such as K8, K18, and K19. Furthermore, the exclusion panel can be extended to incorporate additional blood cell markers such as CD66b (granulocytes), CD68 (macrophages), and others, if required. Most devices (e.g. CellSearch®, DEPArray®) and fluorescence microscopes provide at least one additional fluorescence channel that can be filled with a freely chosen marker to further characterize the identified tumor cells [113]. It is often used to detect therapy relevant markers such as HER2, ER, PSMA, and AR or EMT-associated markers such as N-cadherin and vimentin [113, 121]. The latter allows for the detection of CTCs showing intermediate EMT phenotypes [102, 122].

Another approach to CTC identification and molecular characterization is genomic analysis (Figure 3). This can be performed on a single cell level or on pooled cell lysates. Methods such as fluorescence *in situ* hybridization (FISH) can identify genomic aberrations including amplifications and deletions, thus reliably identifying tumor cells on a single cell level. In parallel they provide therapy relevant information such as *HER2* amplification in BC [123]. Multiplex PCR and qPCR based assays are also used to identify expression of certain tumor associated genes and/or mutations, confirming the tumor origin of the enriched cell fraction [50, 124-126]. These approaches are most commonly based on the analysis of pooled cell lysates and therefore do not allow for conclusions regarding tumor cell heterogeneity. However, elaborate workflows allowing single cell multiplex transcript analysis have been recently published [125]. Tumor associated markers that are often utilized to identify CTCs via PCR-based methods include *EpCAM*, *K19*, and *HER2* [50, 125, 126]. Furthermore, stem cell markers such as *ALDH1* and EMT-associated markers (*TWIST1*, *Akt2*) have

been applied [121, 125, 126]. Finally, microarrays and especially sequencing methods are gaining increased traction as they are becoming more affordable, sensitive and reliable [127, 128]. Selected companies provide whole genome as well as whole exome sequencing services on a single cell level (e.g. Silicon Biosystems). These approaches provide a wealth of information including copy number aberration (CNA) profiles, specific mutations, and translocations.

More functional assays such as the EPithelial Immuno SPOT technology (EPISPOT) rely on biological traits of live tumor cells to identify CTCs [129]. The EPISPOT assay detects the secretion of specific proteins by CTCs, such as Keratin 19, PSA, FGF2 and others. CTCs are kept in short term culture following enrichment and secreted proteins are detected via specific fluorescently labelled antibodies [129, 130]. More in depth information on functional CTC analysis is given in the following chapter.

1.2.4. Functional Analysis of CTCs

The predominant functional assays when analyzing CTCs consist of *in vitro* approaches such as CTC-derived cell line models and *in vivo* approaches, focusing primarily on mouse models. Work from these angles has provided much of the temporary knowledge on the processes of tumor cell dissemination and blood-borne metastasis [131].

Due to the difficulty of *ex vivo* CTC culture, most *in vitro* studies focus on short term culture [130, 132]. Naturally, this brief time window significantly limits experimental possibilities and thereby hampers the accrual of more complex knowledge on CTC biology. Traditional CTC isolation technologies have relied primarily on negative depletion of background leucocytes and red blood cells by density gradient or FACS-sorting. These approaches employ rather harsh sample processing conditions, thus potentially decreasing the already low number of viable CTCs. Multiple CTC-enrichment technologies have catered to this issue by developing work-flows and protocols to enrich viable CTCs for culturing purposes (Parsortix®, DEPArray®, ClearCell®FX, EPISPOT). Despite these recent advances, the generation of permanent CTC-derived cell lines remains extremely rare. To date, only very few long-term CTC-derived cell lines have been successfully described, most of which have subsequently been injected into immunocompromised mice for further analysis [133-137]. These patient derived xenograft (PDX) models have been used to demonstrate and analyze tumorigenic capacity [135, 138, 139], identify CTC subpopulations with increased metastatic

capability [134, 138], and have been able to predict therapy response as well as drug susceptibility [133, 140].

PDX and CTC-derived eXplant (CDX) models have also been developed with freshly isolated CTC fractions, circumventing CTC culture [141-143]. Here, it could be shown, that the CDX models originating from small cell lung cancer (SCLC) or non small lung cancer (NSCLC) patients mirrored the response of the patient of origin to chemotherapy [141, 144].

In addition to mouse models, zebrafish embryos have recently been presented as a valuable functional model to evaluate aspects of the metastatic cascade, such as cell arrest, adhesion and extravasion [98]. The quick development, cheap maintenance and near transparency of zebrafish embryos (allowing for live *in vivo* imaging) pose some advantages of this system compared to costly and ethically more challenging mouse models.

Overall, there is an urgent need for the accrual of additional, permanent, and stable CTC-derived cell lines for a vast range of tumor types to ensure that further insight can be gained into the biological properties required by tumor cells for successful dissemination and metastasis formation. Apart from CDX models, CTC-derived cell lines represent the only access to patient-derived surrogate material that have the capacity to accurately portray tumor cells within the process of blood-borne dissemination and allow for extensive functional analysis in parallel.

1.2.5. Clinical Relevance of CTCs

As indicated in Figure 2: **Potential contributions of CTC analysis towards personalized cancer care**, the clinical applications of liquid biopsy in general, and CTCs specifically, are broad [145]. To date, most clinical studies involving CTCs focus on their use for advanced cancer patients due to the overall higher CTC prevalence in late disease stages. In the metastatic setting, the independent prognostic value of CTC enumeration has been firmly established for multiple cancer types in large phase II and phase III clinical trials using the FDA-approved CellSearch® system [113, 146-148]. In these studies a cut-off of ≥ 5 CTCs [146, 147, 149], and ≥ 3 CTCs [148] per 7.5 ml of whole blood was significantly associated with decreased progression free (PFS) and overall survival (OS). In metastatic breast cancer patients, CTC count of ≥ 5 CTCs at baseline and before cycle 2 of chemotherapy represented a highly independent and prognostic marker of PFS and OS compared to serum tumor markers [150]. In the same study, detection of ≥ 1 CTC using the CellSearch® system was associated

with decreased PFS but not OS in this patient group [150]. The firm evidence indicating prognostic stratification via CTC count in metastatic breast cancer has led to inclusion of CTC enumeration into the 2018 American Joint Committee on Cancer's breast cancer staging system as cM0(i+). For metastatic prostate cancer (mPC) patients receiving systemic therapy, strong evidence supports the use of CTC enumeration as a surrogate marker for survival in clinical trials [151], a step that would significantly accelerate decision making, thus saving both valuable time for the patients and financial assets for the trial organizers.

In addition to prognosis, liquid biopsies have demonstrated potential to detect clinical relapse in advance of standard imaging procedures [152, 153]. Following curative resection of the primary tumor or first line systemic therapy, occult cancer cells can linger undetected at the site of the primary tumor and/or in form of initial distant metastasis. These tumor cells either remain in a state of dormancy for extended time periods prior to initiating outgrowth, or quickly or aggressively drive disease recurrence. Identifying minimal residual disease (MRD) in patients in the absence of clinical indicators could drastically improve patient survival allowing treatment to be administered swiftly, thus, targeting a smaller tumor burden. For breast cancer, the detection of CTCs after 2 to 5 years after initial adjuvant therapy posed a strong and independent marker of relapse risk [154, 155]. Molecular characterization of detected CTCs could provide additional important information on the properties of the remaining tumor cells. These traits may differ significantly from the initial tumor biopsy, thus impacting the choice of treatment for these patients. For primary breast cancer, for example, HER2 overexpression in micrometastasis of the bone has been found to increase to 60% from only 20% in the primary tumor [156]. In line with these results, HER2 status has been shown to differ in up to 30% of cases between the primary tumor, distant metastasis and the CTCs in circulation [157]. These shifts in protein expression or mutation patterns potentially originate from selection and evolution of the tumor cells by the altered environment of the new metastatic niche and/or under therapeutic pressure. They are usually not assessed by additional tissue biopsies.

In advanced cancer patients under systemic therapy, sequential CTC enumeration has been shown to provide early and reliable prognostic information, allowing for real-time monitoring of treatment response [158-161]. In CRPC patients receiving chemotherapy, conversions from favourable (<5 CTC/7.5ml of blood) to unfavourable (≥ 5 CTC/7.5ml of blood) CTC status (or vice versa) under chemotherapy or secondary hormone therapy with abiraterone mirrored disease outcome and decreased or improved prognosis, respectively [147, 162]. For metastatic breast cancer, the increase of CTC counts from baseline to cycle 2 of first line chemotherapy with or without

targeted therapy have been shown to be an early predictive marker of poor PFS as OS, thus indicating their suitability to monitor treatment benefit [150]. Additional clinical studies, such as the phase III DETECT III study (NCT01619111) are currently underway and will provide further insight into the value of CTCs as an early predictive marker of treatment response.

The identification of therapeutic targets, as well as intrinsic and acquired resistance toward therapeutic options can be supported by CTC characterization. First promising results have been published in this realm for prostate cancer. In PC, second generation hormone therapy (enzalutamide, abiraterone) displays reduced efficacy in patients harboring the constitutively active androgen receptor (AR) splice variant 7 (*ARV7*) [50, 163, 164]. *ARV7* mRNA detection on CTCs of prostate cancer patients was highly predictive of resistance towards secondary hormone therapy, but not taxane-based chemo therapy [165], and prognostic for PFS and OS in this cohort [50]. Detection of nuclear *ARV7* protein via immunochemistry has recently been approved as a predictive biomarker for treatment selection [51].

2. Aims of this Thesis

Despite the established clinical relevance of circulating tumor cells (CTCs) as a new diagnostic tool in the context of “liquid biopsies”, little is known about their biological characteristics due to their very low concentration in peripheral blood. To foster understanding of the biology of tumor cell dissemination in cancer patients it therefore becomes necessary to improve the detection and characterization of CTCs as well as address the scarcity of functional models. A particular focus of this thesis lies on hormone dependent cancer types, such as breast and prostate cancer. For both tumor types, blood based metastasis represents a crucial mode of dissemination. Additionally, both BC and PC commonly metastasize to the bone, indicating similarities in metastasis tropism [166]. This thesis can be subdivided into three specific aims:

Aim 1: Improving the enrichment of CTCs: The first aim focused on improving the enrichment of CTCs, mainly in breast cancer patients. The greatest obstacle when trying to analyze CTCs remains their rarity compared to the background of healthy blood cells. While difficult, detection and identification are crucial prerequisites for all further downstream analyses. Therefore, the goal of this aim was to perform in-depth assessment of technological platforms allowing for more specialized detection of a broad range of CTC subpopulations. Furthermore, it was aspired to develop protocols ensuring optimal device performance and CTC yield. Additionally, within the European IML consortium CANCER-ID, it was attempted to identify inter- and intra-laboratory deviations in the output of different technologies, compare their efficiency, and develop standard operating procedure (SOPs) to allow for enhanced comparability of study results.

Aim 2: Developing a model for functional CTC analysis: The second aim focused on the functional analysis of a novel, permanent breast cancer CTC cell line, first cultivated at the Institute of Tumor Biology. Permanent cell lines generated from patient derived CTCs are notoriously difficult to obtain yet offer enormous potential to gain insight into various aspects of cancer research including blood borne dissemination, metastasis formation, and resistance mechanisms towards therapy. The goal of this project was to perform an in depth *in vitro* and *in vivo* characterization of this new CTC cell line model.

Aim 3: Characterizing CTCs for therapy relevant gene expression: Translating our understanding of CTC biology into a treatment benefit for cancer patients represents one of the highest goals of CTC research. The ARV7 splice variant of the androgen receptor has been shown

to decrease therapy response towards abiraterone and enzalutamide in mPC [50]. The final aim of this thesis was therefore to provide novel insight into *ARV7* mediated resistance to secondary hormone therapy in PC patients. Detecting predictive markers that have the potential of guiding therapy choice in the clinic is a promising application of liquid biopsies. By developing sensitive and specific assays to identify *ARV7* on CTCs from PC patients it was attempted to provide sophisticated tools to answer urgent biological questions in the realm of *ARV7* mediated resistance. These methods could in future be included into clinical trials.

In summary, the objective of this PhD thesis is the comparison and improvement of different technologies for CTC identification and the subsequent molecular characterization of isolated tumor cells. The results of this thesis provide insights into the biology of tumor cell dissemination and metastasis. They furthermore strengthen the relevance of CTCs analysis as an important diagnostic tool in personalized cancer medicine by establishing new biomarkers (e.g., *ARV7* in prostate cancer) that can be used to stratify patients with respect to personalized therapy, and by allowing real-time insight into treatment response of individual patients over time.






3. Results

The results generated within this thesis have been published in form of the following manuscripts in peer-reviewed scientific journals. The manuscripts are arranged according to their appearance within the thesis, not according to publication date. Publications 3.1. to 3.3. were generated within the first project mentioned in the aims of this thesis. Publication 3.4. contains the results of the second project and publications 3.5. and 3.6. summarize the results of the third project. My specific contribution to each published manuscript is detailed under section 6 of this thesis “Declaration of Contribution”.

- 3.1. Pre-Analytical and Analytical Variables of Label-Independent Enrichment and Automated Detection of Circulating Tumor Cells in Cancer Patients - *Cancers (2020)*
- 3.2. Evaluation of Microfluidic Ceiling Designs for the Capture of Circulating Tumor Cells on a Microarray Platform - *Advanced Biosystems (2019)*
- 3.3. Proficiency Testing to Assess Technical Performance for CTC-Processing and Detection Methods in CANCER-ID – *Clinical Chemistry (2021)*
- 3.4. Characterization of Circulating Breast Cancer Cells with Tumorigenic and Metastatic Capacity – *EMBO Molecular Medicine (2020)*
- 3.5. In situ Detection and Quantification of AR-V7, AR-FL, PSA, and KRAS Point Mutations in Circulating Tumor Cells – *Clinical Chemistry (2018)*
- 3.6. Detection of Androgen Receptor Variant (ARV7) mRNA Levels in EpCAM-enriched CTC Fractions for Monitoring Response to Androgen Targeting Therapies – *Cells (2019)*

Article

Pre-Analytical and Analytical Variables of Label-Independent Enrichment and Automated Detection of Circulating Tumor Cells in Cancer Patients

Claudia Koch ¹, Simon A. Joosse ^{1,†} , Svenja Schneegans ^{1,†} , Okka J. W. Wilken ^{1,†},
Melanie Janning ^{1,2} , Desiree Loreth ¹, Volkmar Müller ³, Katharina Prieske ³,
Malgorzata Banys-Paluchowski ^{4,5}, Ludwig J. Horst ¹, Sonja Loges ^{1,2}, Sven Peine ⁶,
Harriet Wikman ¹ , Tobias M. Gorges ¹ and Klaus Pantel ^{1,*} 

¹ Department of Tumor Biology, Center of Experimental Medicine, University Medical Center Hamburg-Eppendorf, 20246 Hamburg, Germany; c.koch@uke.de (C.K.); s.joosse@uke.de (S.A.J.); s.schneegans@uke.de (S.S.); okka.wilken@stud.uni-goettingen.de (O.J.W.W.); m.janning@uke.de (M.J.); d.loreth@uke.de (D.L.); ludwig-j.horst@outlook.de (L.J.H.); sonjaloges@me.com (S.L.); h.wikman@uke.de (H.W.); t.gorges@uke.de (T.M.G.)

² Department of Oncology, Hematology and Bone Marrow Transplantation with section Pneumology, Hubertus Wald Tumorzentrum, University Comprehensive Cancer Center Hamburg, University Medical Center Hamburg-Eppendorf, 20246 Hamburg, Germany

³ Department of Gynecology and Gynecologic Oncology, University Medical Center Hamburg-Eppendorf, 20246 Hamburg, Germany; v.mueller@uke.de (V.M.); k.prieske@uke.de (K.P.)

⁴ Department of Gynecology, Asklepios Clinic Barmbek, 22307 Hamburg, Germany; maggiebanys@yahoo.de

⁵ Department of Gynecology and Obstetrics, Marienkrankenhaus Hamburg, 22087 Hamburg, Germany

⁶ Department of Transfusion Medicine, University Medical Center Hamburg-Eppendorf, 20246 Hamburg, Germany; s.peine@uke.de

* Correspondence: pantel@uke.de; Tel.: +49-40-741053503; Fax: +49-40-7410-55379

† These authors contributed equally to this work.

Received: 6 January 2020; Accepted: 11 February 2020; Published: 13 February 2020



Abstract: Circulating tumor cells (CTCs) are promising tools for risk prediction and the monitoring of response to therapy in cancer patients. Within the EU/IMI CANCER-ID consortium, we validated CTC enrichment systems for future inclusion into clinical trials. Due to the known heterogeneity of markers expressed on CTCs, we tested the Parsortix[®] system (ANGLE plc) which enables label-independent CTC enrichment from whole blood based on increased size and deformability of these tumor cells compared to leukocytes. We performed extensive comparisons both with spiked-in blood models (i.e., MDA-MB-468 tumor cell line cells spiked at very low concentration into blood from healthy donors) and validated the protocol on actual clinical samples from breast, lung, and gastrointestinal cancer patients to define optimal conditions for CTC enrichment. Multiple parameters including cassette gap, separation pressure, and cell fixatives were compared in parallel. Also, the compatibility of blood collection tubes with whole genome amplification of isolated tumor cells was demonstrated and we furthermore established a workflow for semi-automated CTC detection using a quantitative cell imager. The established workflow will contribute to supporting the use of size-based CTC enrichment platforms in clinical trials testing the clinical validity and utility of CTCs for personalized medicine.

Keywords: circulating tumor cells; CTC; enrichment; Parsortix; cancer metastasis

1. Introduction

Solid tumors are able to actively or passively shed tumor cells into the blood at times as early as primary tumor formation [1]. A subset of these circulating tumor cells (CTCs) harbors the potential to extravasate from the circulation and colonize distant organs. As 90% of cancer-related deaths are caused by distant metastasis, the presence and relevance of CTCs in the bloodstream has been intensively investigated over the past 10 years. CTCs have been shown to correlate significantly with the probability of metastatic relapse in various carcinomas [2]. These studies demonstrate that the capability of a tumor to release malignant cells into the blood presents a specific risk for the development of metastasis. In addition to CTC enumeration, the characterization of these rare cells holds great promise as they harbor valuable information on the patient's current tumor profile and could therefore function as "liquid biopsy" [3,4].

The greatest challenge when detecting CTCs is their extremely low concentration in peripheral blood. A single CTC can be present in a background of approximately 10^8 – 10^9 blood cells, explaining why technical hurdles have limited the analysis of these cells in the past. Thus, to unlock the full potential of CTC research, extremely sensitive and specific enrichment methods have to be applied. Currently, more than 50 distinct CTC detection systems are available on the market or under development in different laboratories all over the world [5,6]. However, the FDA-cleared CellSearch® system remains the "gold-standard" for capture of CTCs in a standardized and validated manner [7–12]. Due to its dependency on the epithelial cell adhesion molecule (EpCAM), this system is limited to EpCAM positive tumor cells with primarily epithelial phenotypes [13]. While this applies to most carcinoma cells, metastatic outspread is often associated with the transition of epithelial-like tumor cells into a more mesenchymal state (epithelial to mesenchymal transition, EMT), indicated by loss or downregulation of EpCAM expression [14,15]. Mesenchymal CTCs have been associated with greater invasiveness, chemo-resistance, and lower overall survival rates for patients [16–18]. Hence, the establishment of additional, non-EpCAM-based assays is of high importance.

Although new EpCAM-independent CTC technologies have already shown promising results [5], standardized protocols for most approaches are still lacking. The CANCER ID consortium (www.cancer-id.eu), funded by the European Innovative Medicine Initiative (IMI), aimed to close this gap and validate innovative CTC detection approaches for future clinical trials. This standardization of novel technologies and workflows is much needed to increase the acceptance of CTCs as biomarkers in the clinic.

The Parsortix® system (ANGLE plc)-a size-based enrichment device - has been introduced to the CTC field and shown promising results across multiple tumor entities [19–24]. In addition to enumeration, the device has demonstrated its capabilities in isolating rare CTC clusters [24,25] and preserving cell viability following CTC enrichment [19,26]. When first introduced to the market, several individual research groups using this device applied different pre-analytical conditions (e.g., blood tubes for sample collection) as well as distinct separation protocols for CTC enrichment, making direct comparison of the Parsortix® system performance across those research groups and studies very difficult.

Here, we conducted extensive spiking experiments to establish tumor cell capture rates using various pre-analytical and analytical conditions in spike-in model experiments and cross-validated the results by the analysis of peripheral blood samples from patients with different forms of cancer (breast, lung, and gastrointestinal). The complete workflow was tested for its compatibility with whole genome amplification (WGA) and molecular characterization of the amplified tumor cells. Finally, we additionally established a workflow for semi-automated CTC detection using the XCyto® 10 quantitative cell imager. The established standardized workflows enable the enrichment of viable or fixed CTCs and open the avenue for precise enumeration and downstream analysis of patient-derived CTCs.

2. Materials and Methods

2.1. Cell Lines and Culture

The breast cancer derived cell lines MDA-MB-468 and MCF-7 acquired from ATCC (ATCC, Manassas, VA, USA), were chosen for analysis. Cells were cultured in cell culture flasks under standard conditions in humidified incubators at 37 °C with 10% CO₂. Medium (Gibco-Life Technologies, Darmstadt, Germany) was employed as recommended by ATCC and fortified with 10% fetal bovine serum (Gibco-Life Technologies, Darmstadt, Germany, 1% L-glutamine (Gibco-Life Technologies, Darmstadt, Germany) and 1% penicillin/streptomycin (Gibco-Life Technologies, Darmstadt, Germany). Cell passaging was performed at 70% confluency. This study was approved by the local ethical review board under numbers PV3779 and PV5392.

2.2. Spiking of Healthy Donor Blood with Cell Line Cells

Cell line cells were prepared for spiking experiments by washing with 1 × PBS (Gibco-Life Technologies, Darmstadt, Germany) and incubating with 0.25% trypsin-EDTA (Gibco-Life Technologies, Darmstadt, Germany) for 5 min at 37 °C prior to resuspending in culture medium. The cell suspension was centrifuged at 190× g for 5 min after which the supernatant was discarded and the cells were resuspended in fresh culture medium. The cells were spread to a petri dish filled with medium, manually counted and picked under a light microscope. Defined cell counts of 50 MDA-MB-468 cells were added to blood samples from 55 healthy donors (HD). Subsequently, tubes containing ethylenediaminetetraacetic acid (EDTA) were used to collect 7.5 mL of whole blood from healthy volunteers. Following blood spiking, the Ficoll density-gradient-based Leucosep™ pre-enrichment (Greiner Bio One, Kremsmünster, Austria) was used to separate peripheral mononuclear cells (PBMCs) from whole blood according to the manufacturer's instructions for selected spike experiments.

2.3. Blood Sample Collection and Processing

Patient blood samples were acquired in accordance to the World Medical Association Declaration of Helsinki and the guidelines for experimentation with humans by the Chambers of Physicians of the State of Hamburg ("Hamburger Ärztekammer"). All participants gave written informed consent prior to blood donation (Ethics Nr. PV3779 and PV5392). Blood was drawn directly into standard EDTA vacutainers, CellSave® Preservative tubes (Menarini Silicon Biosystems, Florence, Italy), Circulating Tumour Cell TransFix/EDTA Vacuum Blood Collection Tubes (CTC-TVT tubes, CYTOMARK, Buckingham, UK), or Streck Cell-free DNA BCT tubes (Streck, La Vista, Nebraska, USA), respectively. EDTA blood was processed within 2 h of sample collection by the Parsortix® system (ANGLE plc, Guildford, UK) and fixed blood within 24 h. In total, samples from 61 patients were analyzed in this study, including 48 metastatic breast cancer (mBC) as well as 6 metastatic non-small-cell lung cancer (mNSLC), 1 metastatic small-cell lung cancer (mSCLC), and 6 metastatic gastrointestinal (mGIC) cancer patients.

2.4. Tumor Cell Enrichment by the Parsortix® System

The Parsortix® system (ANGLE plc, Guildford, UK) is a benchtop microfluidic device designed for the size-based capture of rare cells from whole blood [19]. The blood sample is passed through an enclosed disposable cassette with a controlled liquid flow. The cassettes contain a stepped structure, gradually narrowing in diameter until reaching a final gap of 6.5 µm or 10 µm, respectively. The separation principle is based on the assumption that most tumor cells are larger in size and more rigid than normal, healthy blood cells [27]. These cells of interest are therefore retained by the critical gap of the separation cassette while all smaller cells continue to flow through the cassette and into a waste container. Following separation, the liquid flow through the cassette is reversed and the captured

tumor cells are flushed out. Cells were directly harvested into cytopsin funnels, centrifuged onto a glass slide (190× g, 3 min), dried overnight, and stored at −80 °C until further processing.

2.5. Immunocytochemistry

Tumor cells isolated with the Parsortix® system were identified via immunocytochemistry. Dried cytopsin slides were brought to room temperature (RT) and fixed with 2% PFA (Sigma Aldrich, Steinheim, Germany) for 10 min. The samples were washed with 0.5 mL of 1x-PBS prior to permeabilization with 0.1% Triton X 100/PBS (Sigma Aldrich, Steinheim, Germany) for 10 min. Following two additional wash steps, 10% AB-serum/PBS (BioRad, Rüdigheim, Germany) was applied for blocking (20 min). Directly Alexa Fluor 488 conjugated pan-keratin (AE1/AE3-eBioscience; C11-CellSignaling) and APC labelled CD45 (clone REA747-Miltenyi Biotec) antibodies were incubated for 60 min, followed by 5 min of DAPI-incubation (1 µg/mL). Subsequently, cytopsin were covered with Prolong Gold Antifade Reagent (Thermo Fisher Scientific, Dreieich, Germany), sealed with a cover slip and examined by fluorescence microscopy (Axioplan2, Zeiss). Keratin-positive, DAPI-positive, CD45-negative cells with intact morphology were defined as tumor cells.

2.6. Measurement of Cell Size

MDA-MB-468 cell culture cells were trypsinized and resuspended in medium. The cell suspension was transferred to a glass slide via cytocentrifuge (190× g, 3 min). The resulting cytopsin were left to dry overnight and stained with fluorescently labelled antibodies for pan-keratin and DAPI, as described above. Subsequently, 50 of the fluorescently labelled cells were photographed. The cell diameter was determined using the AxioVision LE64 microscope software (Zeiss) measurement tool and utilizing the borders of cytokeratin expression. An average was calculated from 50 separate cell measurements.

2.7. Whole Genome Amplification and DNA Quality Control

In order to test the feasibility of downstream genomic analyses, the complete workflow was tested for its compatibility with whole genome amplification (WGA) and molecular characterization of the genomic material. In brief, breast cancer cell line cells (MDA-MB-468) were transferred into EDTA or Transfix® preserved healthy donor blood and processed by standard protocol (Parsortix® system separation–99 mbar, cytopsin and standard ICC). Subsequently, 10 single MDA-MB-468 and 5 background leukocytes were manually picked from the glass slides for each blood tube type and processed by WGA using the Ampli1™ WGA kit (Menarini Silicon Biosystems, Florence, Italy) according to the manufacturer's instructions. 5 µg of gDNA were utilized as internal positive WGA control. Negative controls consisted of H₂O. The quality of the amplified DNA was assessed by multiplex PCR producing 96, 108–166, 299, and 614 bp fragments from target sites in the *GAPDH* gene using the Ampli1™ QC Kit (Menarini Silicon Biosystems, Florence, Italy). To visualize PCR products, they were mixed with DNA Gel loading dye (6x) (Thermo Fisher Scientific, Dreieich, Germany) and applied to 1.2% agarose gels containing GelRed® Nucleic Acid Gel Stain (Biotum, Fremont, CA, USA) at 1 µL per mL of agarose gel. The Quick-Load® 100 bp DNA Ladder (New England Biolabs, Frankfurt am Main, Germany) was used as a size standard. PCR fragments were visualized using the Gene Genius bioimaging system (Syngene, Bangalore, India).

2.8. Image Analysis Using the XCyto 10 Platform

Immunocytochemistry-stained cytopsin containing PBMCs (300 000), spiked with 1000 MCF-7 cells, were imaged using the XCyto® 10 Quantitative Cell Imager (ChemoMetec, Lillerød Denmark). XCyto® 10 is a high sensitivity image cytometer for suspended and adherent cells with a CCD 2.8 MP camera, four LEDs and 9 emission filters. A program was developed for semi-automatic detection of CTCs. First the slides were scanned with the XCyto® 10 at 4× magnification. Acquisition times were 100 ms (milli seconds) for DAPI, and 500 ms for both Alexa Fluor 488 and APC fluorophores. The corresponding excitation light sources/emission filters were LED405/430-475

nm, LED488/513–555 nm, and LED635/665–676 nm, respectively. Within the XcytoView software, the “Xcyto 2-Sample 15-A v1” slide type was chosen for imaging as well as the 4× objective and the “Adherent, User defined–Fluorescence Mask” method for cell nucleus identification. The default analysis setup settings were applied except for a threshold intensity of 10,000 of the DAPI input channel, and a max area of 900 μm^2 .

The distinction of pan-keratin positive tumor cells against the background of CD45-positive PBMCs was established by plotting APC intensities of single cells against their corresponding intensity in the Alexa Fluor 488 channel. The data was visualized by application of bi-exponential scaling. Separation of both populations was achieved by gating the cells with high 488 nm signal and low 660 nm signal. The gating was set so that weakly positive cells were identified as well, and therefore some false positive cells were also included. Therefore, this pre-selection produced a gallery of potential CTCs which were then analyzed further by re-imaging at 20× magnification to manually exclude false positive hits. The same gating protocol was then reapplied to images of patient samples with identical staining and image acquisition parameters. The automated imaging set-up for CTC detection can be adjusted retrospectively, to further improve the gating parameters, making it an easily adaptable and time-saving tool for screening, e.g., large numbers of patient samples.

2.9. Statistics

Statistical analyses were performed using R version 3.6.1 (R Foundation for Statistical Computing) and In-Silico Online, version 2.1.2 [28]. Tumor cell recovery of spiking experiments of the three investigated fixed factors cassette gap (6.5 or 10 μm), separation pressure (23 or 99 mbar), and blood sample types (CellSave, EDTA, or Ficoll) were tested using a general linear model including interactions. Dependency of cassette gap (6.5 or 10 μm) on the recovery of CTCs in patient samples was tested by general linear modeling in Poisson distribution, using patient as within factor. McNemar’s exact test, Cohen’s kappa, and Kendall’s tau were employed to assess agreement between cassette gaps in CTC positive samples, as well as to assess agreement in detected CTCs using manual and automated (XCyto 10) screening. Difference between median cell counts was assessed by Wilcoxon signed rank test. A binomial test was employed to test which cassette gap outperformed the other.

3. Results

3.1. Tumor Cell Recovery of Different Cassette Gaps in Spiking Experiments

Within the last years, ANGLE introduced a novel separation cassette with a decreased critical gap of 6.5 μm compared to the originally designed 10 μm . These cassettes could therefore theoretically allow the isolation of additional CTC populations with a smaller diameter. To test the performance of the 6.5 μm gap size cassettes in comparison to the original 10 μm gap size cassettes, we conducted extensive spiking experiments using the breast cancer cell line MDA-MB-468. MDA-MB-468 has a mean cell diameter of 13.5 μm ($s = 2.03$), with a measured range of 8.71–19.68 μm (Table S1). We focused on CTC capture rates for the different cassette gap sizes (6.5 μm and 10 μm), in 3 different blood sample types (EDTA, Ficoll, and CellSave®) and two separation pressures (23 mbar and 99 mbar) to allow a comprehensive overview (Table 1). Healthy donor (HD) blood collected in EDTA or CellSave® tubes was spiked with a standard amount of 50 MDA-MB-468 cells. Samples drawn into EDTA were either directly processed or their PBMC fraction was pre-enriched via density gradient centrifugation (Ficoll) prior to separation with the Parsortix® system. All conditions were tested in triplicate or more ($n \geq 3$). Mean recoveries as well as standard deviations (s) are indicated in Table 1. Detailed results of the spike-in experiments are listed in Table S2. Overall, the cassettes with the 6.5 μm gap size led to a clear increase in the proportion of harvested tumor cells for each blood processing type and separation pressure (Table 1, Figure 1). This was confirmed in a generalized linear fixed-effects model (GLM) analysis showing that independent of protocol and blood sample type, a mean of 15.9% higher recovery was achieved with the cassettes with 6.5 μm gap size compared to 10 μm (Figure 1).

Apart from recovery, a more efficient priming of 6.5 μm gap sized cassettes was observed, leading to an optimized blood flow within the separation cassette compared to the 10 μm version (Figure S1A). This increase in recovery comes at the cost of higher white blood cell (WBC) background (Figure S1B) and increased separation times (Table S2).

Table 1. Mean tumor cell recovery rates determined from spike experiments using MDA-MB-468 tumor cell line cells. Recovery percentages and standard deviation (s) for each cassette type, blood processing type and separation pressure are indicated.

Cassette Gap	Protocol	Blood Processing and Tube Type					
		EDTA		Ficoll		CellSave	
		Recovery [%]	s [%]	Recovery [%]	s [%]	Recovery [%]	s [%]
10 μm	23 mbar	34	6.9	27.3	8.1	12.7	1.2
	99 mbar	16	2.0	10.7	6.1	2.7	1.2
6.5 μm	23 mbar	68.7	5.0	45.3	4.2	29.3	15.1
	99 mbar	60.7	10.1	24.7	5.0	16.7	3.1

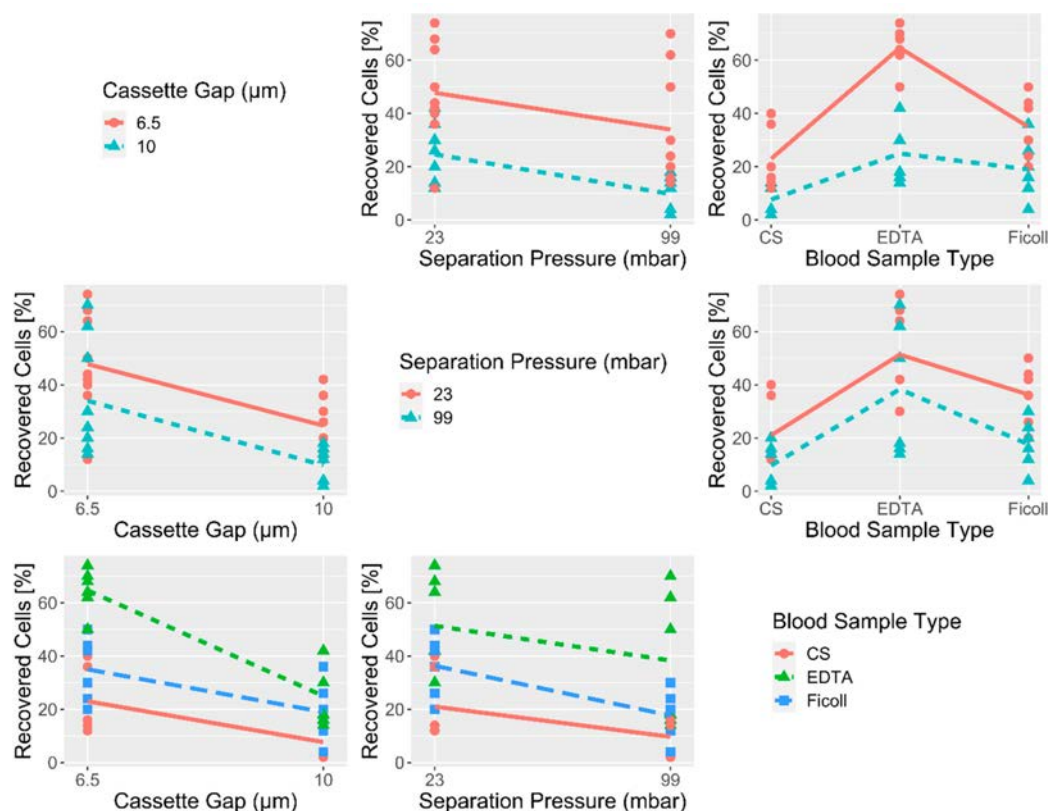


Figure 1. Visualization of initial spike experiment results. Correlation matrix showing the recovery of tumor cells under the different experimental conditions of the cassette gap (6.5 μm and 10 μm), separation pressure (23 mbar and 99 mbar), and the blood sample type (CellSave[®]-CS, EDTA and Ficoll).

The 23 mbar (lower pressure) separation protocol allowed for higher tumor cell recovery than applying a greater separation pressure of 99 mbar (Figure 1), resulting in a mean increase of recovery of 10.8% for the lower pressure protocol, as calculated by GLM analysis. The most dramatic influence was detected when comparing different blood collection tubes. Here, EDTA outperformed Ficoll pre-enriched and CellSave[®] fixed samples, showing an average 40.8% increase in recovery compared to CellSave[®] fixed cells, independent of the cassette type and separation protocol used. Combining

EDTA blood tubes with the 6.5 μm gap sized cassette further increases the mean recovery with an additional 24.3%, independent of the chosen protocol.

While the lower separation pressure (23 mbar) resulted in increased recoveries compared to the higher pressure (99 mbar) separation, it doubled the mean sample running time (Table S2). Therefore, although performing better, the 23 mbar protocol was abandoned for standard 7.5 mL whole-blood samples to allow for better sample turnover.

3.2. Analysis of Blood Samples from Breast Cancer Patients with Different Cassette Gaps

To confirm the increase of CTC capture with the 6.5 μm gap sized cassette in cancer patient samples, we analyzed 43 blood samples from 37 mBC patients progressing under their current therapy. 6 patients were monitored on a second visit. Disease progression in this cohort was clinically assessed by CT-scan or MRI. An overview of the clinical parameters of this patient cohort is given in Table S3. Matched 7.5 mL EDTA samples from each patient were processed with the 6.5 μm and the 10 μm gap sized cassettes. Overall, 32.4% (12/37 patients) of patients in our cohort were positive for ≥ 1 CTC and 13.5% (5/37 patients) for ≥ 5 CTCs when combining both measurements (6.5 μm and 10 μm runs) (Table S3). Overall positivity rates for ≥ 1 CTC remained comparably high at 32.6% when focusing on total blood samples analyzed (14/43 samples); however, the percentage of finding ≥ 5 CTCs increased to 20.9% (9/43 samples). A moderate agreement of CTC status (positive/negative) within samples between the two cassette gap sizes was assessed by Cohen's kappa test (kappa = 0.57, 95% CI: (0.28, 0.86), $p = 0.0018$). Additionally, using a McNemar's exact test, no detectable change in the CTC status (positive/negative) was determined by both cassettes within a sample ($p = 0.13$). Agreement between CTC counts across the complete sample cohort (37 patients, 43 samples) was moderate between the two cassette sizes (Kendall's tau test: tau = 0.65, $p = 2.4 \times 10^{-6}$). However, the majority of measurements were CTC-negative for both samples (29/43 samples), which significantly influenced these results.

Looking more closely at the positive samples, 13/14 had ≥ 1 CTC detectable using the 6.5 μm gap sized cassette (92.9%) and 8/14 with the 10 μm gap sized cassette (57.1%). CTC counts with established prognostic relevance in mBC (≥ 5 CTCs) were detected in 7/14 samples (range: 1–28 CTCs) with the smaller separation gap (50%) compared to 2/14 samples (range: 1–6 CTCs) with the original, larger gap (14.3%). Only a weak agreement in CTC count was discerned within the positive samples between the two chip sizes (Kendall's tau test: tau = 0.51, $p = 0.023$). Across all samples, a total of 99 CTCs were detected using the 6.5 μm versus a total of 21 CTCs with the 10 μm gap sized cassette, marking a 4.7-fold increase in CTC numbers using the smaller cassette diameter (Table S3). An exact binomial test performed on this data, resulted in a 92.9% probability of the smaller cassette gap recovering higher CTC counts than the larger cassette gap (95% CI: (0.70, 1.00), $p = 0.0009$). Finally, we performed a Wilcoxon signed rank test with continuity correction to test whether the median CTC count of the samples were equal with both cassette types. The median CTC counts between the 6.5 μm and 10 μm gap sized cassette differed ($V = 102.5$, $p = 0.0018$), as visualized in the corresponding box plots (Figure 2A). Conclusively, our data indicates that, while both cassette types show a moderate correlation in the CTC-positive and CTC-negative results they generate for each sample, the 6.5 μm gap sized cassette captures substantially higher CTC numbers in mBC patients, confirming its superiority for CTC analysis.

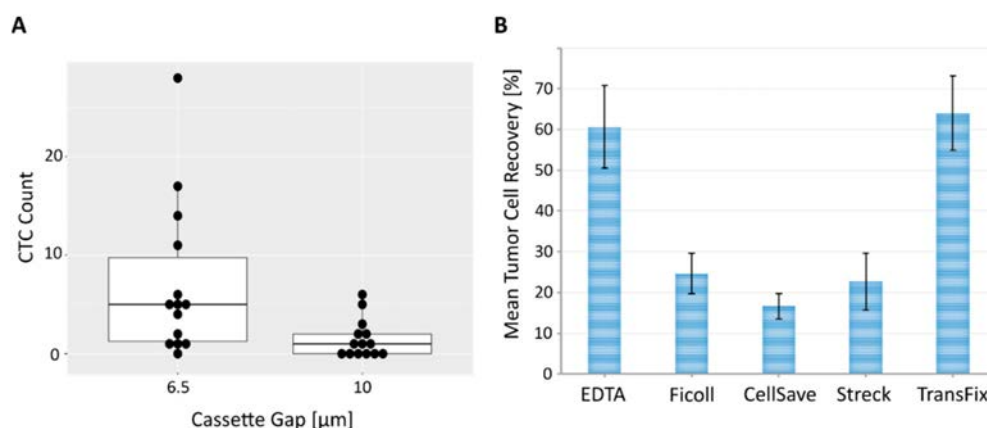


Figure 2. Performance comparison between 6.5 µm and 10 µm cassette gap as well as different blood sample types. (A) Box plot demonstrating distribution of CTC counts within the 14 CTC positive mBC patients detected in our cohort. Matched blood samples that showed ≥ 1 CTC in either the 6.5 µm or 10 µm gap sized cassettes are depicted. Each dot represents a single patient. (B) Mean tumor cell recovery [%] calculated from spike experiments using MDA-MB-468 breast cancer cell line cells for different blood sample types. Cell line cells were spiked into healthy donor blood, processed via the Parsortix[®] system (6.5 µm gap sized cassette, 99 mbar separation pressure) and subsequent cytopsin and ICC staining. Depending on the sample type, blood was either processed directly (EDTA), immediately pre-enriched via density gradient centrifugation (Ficoll) or fixed for 24 h (CellSave[®], Streck[®], TransFix[®]) prior to separation with the Parsortix[®] system. Recovery rates for each blood sample condition are indicated with standard deviation (black bars).

3.3. Effect of Blood Collection Tube on Tumor Cell Enrichment

Standard EDTA tubes are well suited when analyzing fresh samples that can be processed within 2–3 h following blood draw. However, clinical routine does not always allow such short processing time frames. Additionally, shipping of samples across sites for clinical studies requires some form of cell fixation to allow optimal sample processing. The CellSave[®] preservation tube (CS) tested initially did not yield high recovery rates in combination with the Parsortix[®] system (16.7%, $s = 3.1$, S99F separation protocol). Therefore, we extended our analysis to additional blood tubes, including Streck Cell-free DNA BCT tubes (Streck, La Vista, Nebraska, USA), which should technically allow the isolation of ctDNA and CTCs from the same tube [20], and Circulating Tumour Cell TransFix/EDTA Vacuum Blood Collection Tubes (CTC-TVT) by CYTOMARK (Buckingham, UK). Additional spiking experiments (50 MDA-MB-468 cells, S99F separation protocol, $n = 3$) resulted in a mean recovery of 21.5% ($s = 6.2$) for Streck[®] tubes and 64% ($s = 9.2$) for TransFix[®] stabilized blood (Table 2). Across all measured spike conditions, blood from EDTA and TransFix[®] tubes therefore resulted in the best tumor cell recoveries (Figure 2B). We furthermore tested an additional separation protocol for EDTA samples using a medium separation pressure of 50 mbar (S50F). While this protocol did not significantly increase recovery (65.7%, $s = 6.5$) compared to the 99 mbar protocol (60.7%, $s = 10.1$), it did improve the morphological intactness of unfixed tumor cells as well as of the leukocyte background. Detailed results for all blood tube types are listed in Table S2.

Table 2. Mean tumor cell recovery rates determined from spike experiments (using MDA-MB-468 tumor cell line cells) for 6.5 µm cassette gap and various additional blood sample fixatives. Recovery percentages and standard deviation (s) for each blood processing type and tube are indicated.

Cassette Gap	Protocol	Mean Recovery [%]				
		EDTA	Ficoll	CellSave	Streck	TransFix
6.5 µm	99 mbar	60.7	24.7	16.7	22.7	64.0
	s [%]	10.1	5.0	3.1	7.0	9.2

3.4. Validation of Optimized Protocol on Blood Samples from Cancer Patients

To allow for a direct comparison of all blood tube types analyzed in prior spike experiments (EDTA, CellSave[®], Streck[®], and TransFix[®]), and to compare the 99 mbar and 50 mbar EDTA separation protocols in clinical samples, blood was drawn in parallel from 6 metastatic non-small-cell lung cancer, 1 metastatic small-cell lung cancer, and 6 metastatic gastrointestinal cancer patients into all blood tube types and analyzed via the Parsortix[®] system. Clinical data for this patient collective is detailed in Table S4.

The highest rates of finding ≥ 1 CTC in patients were reached at 46.2% (6/13 patients) for blood collected into the Streck[®] and TransFix[®] tubes (Figure 3A). This was followed by CellSave[®] fixed and EDTA blood (processed by the 50 mbar separation protocol) at 30.8% CTC-positivity (4/13 patients). Unfixed EDTA samples processed by a high separation pressure of 99 mbar rendered the lowest CTC positivity rates with 15.4% (2 out of 13 patients). While the overall percentage of CTC-positive patient cases were equal for Streck[®] and TransFix[®] fixed, as well as for CellSave[®] fixed and EDTA blood (50 mbar separation), the total amount of CTCs detected via immunocytochemistry (ICC) was considerably higher in TransFix[®] samples (Figure 3B, Table S5). Also, EDTA (50 mbar separation) and TransFix[®] samples resulted in the highest total amount of CTC clusters compared to the other tube types and separation protocols (Figure 3B, Table S5). CTC clusters were defined as ≥ 2 CTCs closely attached to one another. Representative ICC staining images of tumor cells detected using the different blood tubes and separation protocols are depicted in Figure 3C. Cell morphology of tumor cells and leucocytes remained intact following enrichment and analysis with our protocols. However, leucocyte nuclei appeared slightly enlarged or “puffy” when blood was treated with CellSave[®] or Streck[®] fixatives (Figure 3C). This effect was not detected in EDTA or TransFix[®] blood samples (Figure 3C). Additionally, staining and therefore fluorescence signal intensity varied across tube types, especially for the leukocyte background. Heterogeneous staining intensity of leukocytes is demonstrated for an EDTA and Streck fixed patient sample in Figure 3C. Overall best and most homogeneous ICC staining performance was achieved using TransFix[®] preserved blood (Figure 3C).

In conclusion, TransFix[®] preservation tubes proved optimal in combination with Parsortix[®] separation and subsequent ICC staining on cytospins, resulting in high overall positivity rates of 46.2% (Figure 3A) and highest total CTC counts detected (Figure 3B). Furthermore, these tubes guarantee intact tumor cell morphology (Figure 3C) and enable detection of CTC clusters (Table S5).

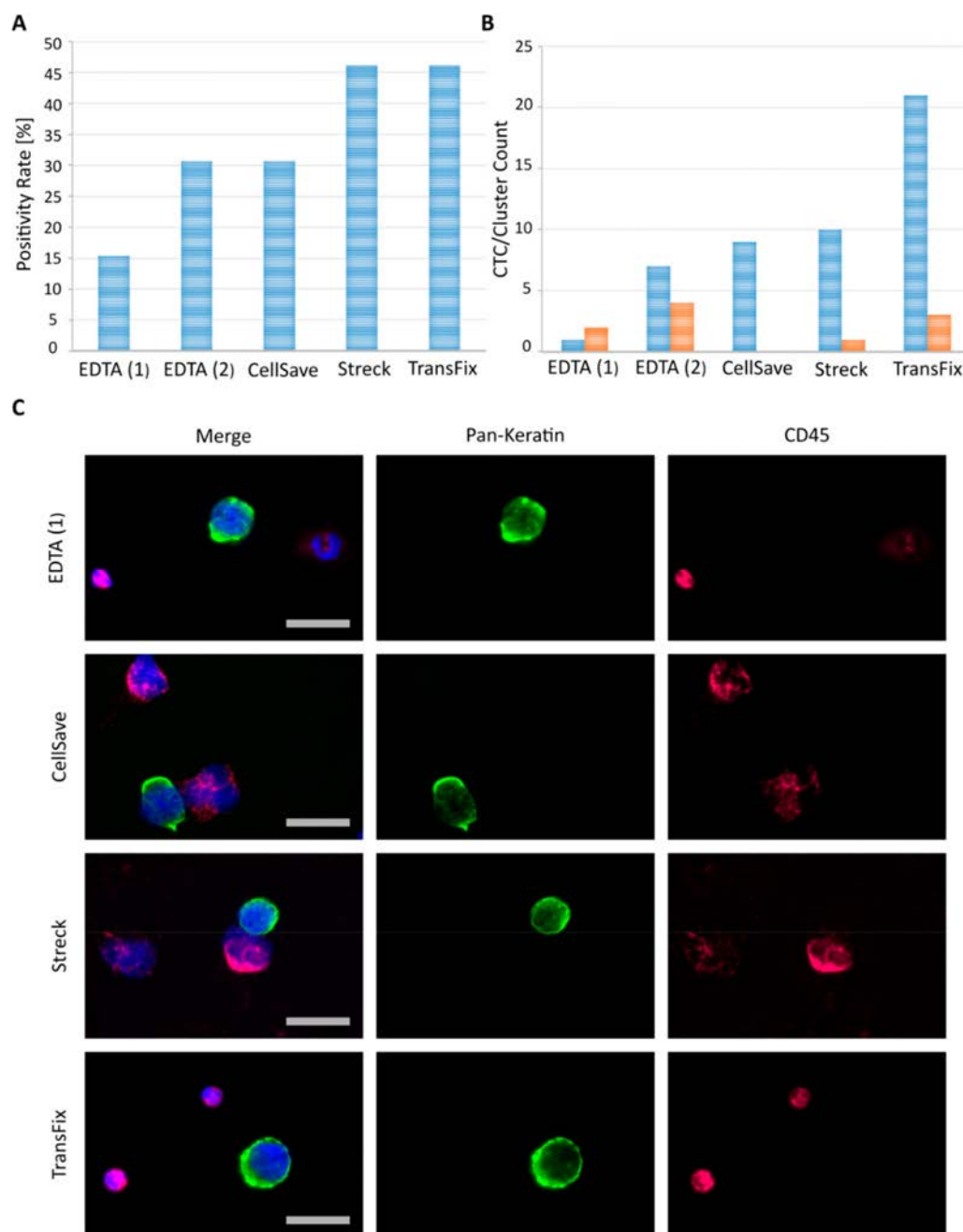


Figure 3. Comparison of blood collection tubes in clinical patient samples drawn and processed in parallel. EDTA (1) indicates samples were processed by the 99 mbar separation protocol, while EDTA (2) samples were run using the reduced 50 mbar Parsortix® protocol. Fixed samples were stored for 24 h following blood draw and separated using the high pressure Parsortix® protocol (99 mbar). All samples were subsequently cytopspun and stained by fluorescent antibodies against and DAPI (blue). (A) Percentage of CTC-positive patients (defined as ≥ 1 CTC per 7.5 mL of blood) across the 14 cancer patients tested. (B) Blue bars: Overall single CTC count detected in the 14 cancer patients tested in parallel for each collection tube. Orange bars: Amount of CTC clusters (≥ 2 directly attached CTCs) detected in the 14 cancer patients tested in parallel for each collection tube. (C) Representative CTC and leukocyte images from selected index patients within our cohort. Images were taken manually with a standard fluorescence microscope at 40 \times magnification. Size bars equal 20 μ m.

3.5. Downstream Molecular Analysis of Single Tumor Cells Following Enrichment

Molecular analysis on a genomic level represents a key tool allowing further in-depth characterization of CTCs following their successful detection. While a multitude of different methods are available and routinely applied (e.g., next generation sequencing, ddPCR, microarrays), in most cases, pre-amplification of genomic material is necessary to enable conclusive and robust results. This is especially true when focusing on single tumor cells with an initial DNA content of a few picograms. The most prevalent method of increasing DNA quantity for subsequent molecular analysis is currently whole genome amplification (WGA).

To test the feasibility and efficiency of successful WGA following Parsortix® separation and subsequent ICC staining on cytopins, additional spiking experiments were conducted. Because patient derived CTCs can be genetically heterogeneous [29], we spiked blood from healthy donors with MDA-MB-468 tumor cell line cells, fixed with either Transfix® preservative or in standard EDTA tubes to have identical starting material in all experiments and control for other confounding factors. Next, cell separation was performed using the Parsortix® system (99 mbar protocol). Following ICC staining, 10 single tumor cell line cells and 5 leukocytes were picked from glass slides by micromanipulation and processed by WGA (Ampli1™ WGA kit, Menarini Silicon Biosystems). Amplified cells were subsequently subjected to DNA quality control (Ampli1™ QC kit, Menarini Silicon Biosystems) and analyzed via gel electrophoresis. High DNA integrity was defined as ≥ 3 GAPDH amplification products detected in quality control, while medium DNA integrity was defined as ≥ 2 GAPDH amplification products. WGA was successful in generating high DNA integrity for 80% (12/15 single cells, ≥ 3 GAPDH amplification products) of the single cells picked from EDTA as well as from TransFix® preserved blood (Figure S2). For TransFix®, an additional medium quality sample was generated (1/15 single cells; ≥ 2 GAPDH amplification products), leading to an overall success rate of 87% (13/15 single cells). In total, highest achievable DNA quality (4/4 GAPDH amplification products) was seen for 73% (11/15 single cells) of single cells picked from TransFix® and 46% (7 out of 15 single cells) of single cells from EDTA blood (Figure S2).

In conclusion these results indicate that both EDTA and TransFix® blood tubes are suitable not only for enrichment of CTCs via the Parsortix® system, but also allow for the robust amplification of single cell DNA at excellent quality for subsequent molecular analysis.

3.6. Compatibility with an Automated CTC Screening Device

Manual evaluation of CTC counts remains user-dependent and time-consuming. To further improve the comparability of results generated with the Parsortix® protocols defined in this study, we additionally established a workflow for semi-automated CTC detection using the XCyto® 10 quantitative cell imager (ChemoMetec). For this, a gating protocol was established using blood from healthy donors spiked with MCF-7 tumor cell line cells to distinguish tumor cells (pan-keratin^{high}/CD45^{low}) and surrounding leukocyte background (pan-keratin^{low}/CD45^{high}) according to their respective Alexa Fluor 488 and APC signal intensities (Figure 4A,B). The same gating was then applied on patient samples processed through the Parsortix® device. Cell counts identified by this gating were subsequently compared with the results of manual screening by fluorescence microscope.

In total, a set of 27 blood samples originating from 16 mBC patients was evaluated (Figure 4C,D). Samples of the analyzed cohort consisted of blood collected for the prior comparison of 6.5 μ m and 10 μ m cassette gaps (Table S3), as well as 18 additional blood samples from 10 mBC patients (mBC_38 to mBC_48) collected and processed solely by the 6.5 μ m cassette gap (clinical data in Table S3). Both microscopes had comparable results with respect to image resolution and signal intensities in the different fluorescence channels (Figure 4E,F). 48.1% (13/27) of patient samples were found to be negative for CTCs using both screening approaches (Table S6). By manual screening, 44.4% (12/27) samples were found to be CTC-positive (Table 3). With the exception of two additional patient samples, these same samples were also identified to harbor CTCs after imaging with the XCyto® 10 (48.1%, 14/27). Of these 14 CTC-positive patient samples, 97 CTCs were identified in total by using the automated settings,

in comparison to 98 CTCs from manual screening (Table 3). For the majority of samples (74.1%, 20/27) equal CTC levels were detected with both screening approaches (Table 3 and Table S6). This was underlined by the result of a Wilcoxon signed rank test with continuity correction, indicating that the median CTC count of the samples were equal with both evaluation approaches ($V = 14.5$, $p = 1$). Furthermore, a very strong agreement in CTC count was discerned within the total 27 samples between the two screening methods (Kendall's tau test: $\tau = 0.917$, $p = 2.22 \times 10^{-16}$). When focusing on CTC-positive cases only, manual screening outperformed semi-automated screening in 21.4% (3/14) of samples analyzed. Vice-versa, in 28.6% (4/14) of CTC-positive samples analyzed, semi-automated screening outperformed manual screening (Table 3). However, differences were mostly confined to a small number of cells (range Δ : 1–4 cells). In line with this, a very strong agreement in CTC count was observable within the CTC-positive samples between the two screening methods (Kendall's tau test: $\tau = 0.902$, $p = 3.79 \times 10^{-5}$).

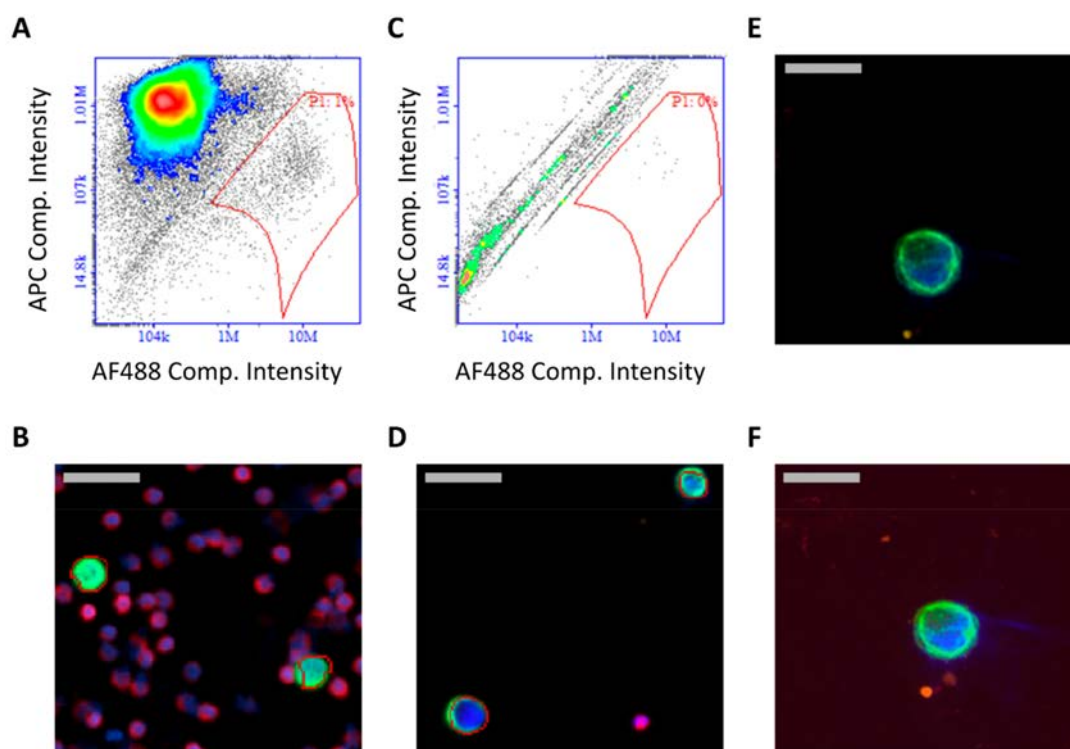


Figure 4. Semi-automated CTC evaluation using the XCyto® 10 imaging system. (A) Image of the plot used for setting up a suitable gating to distinguish tumor cells from PBMCs. APC intensities (CD45 on leukocytes) of individual cells are plotted against their intensities in the Alexa Fluor 488 (pan-keratin on MCF-7 cells) channel. Cells with low CD45 (APC) and high pan-keratin (Alexa Fluor 488) signals were considered as tumor cells. Gate P1 was chosen so that a maximal separation of tumor cells from PBMCs was achieved. (B) Overlay of the P1 gate with a section of the original image. Cell nuclei were visualized with DAPI (blue), tumor cell marker pan-keratin- Alexa Fluor 488 was used (green) and CD45-APC (red) as a negative selection marker for PBMCs. Grey scale bar represents 40 μm . (C) Exemplary image of the gating from a patient sample. Cells with low APC- and high Alexa Fluor 488 signals were considered as potential CTCs in gate P1. (D) Overlay of positive hits of the P1 gate with a section from the original image. Grey scale bar represents 40 μm . (E) CTC from patient sample no. 13 imaged with 2 different settings. Above: CTC imaged with 40 \times objective of Axioplan2 (Zeiss) microscope. Grey scale bar represents 20 μm . (F) The same cell was imaged with XCyto® 10 (20 \times objective). Grey scale bar represents 20 μm .

Table 3. Summary of CTC-positive mBC patient samples and their corresponding CTC counts analyzed by either manual or XCyto[®] 10-based semi-automated screening. Cases in which one approach yielded higher CTC counts are marked in bold. The evaluation contains CTC-positive samples from prior analysis (Table S3) as well as 6 additional CTC-positive mBC samples (Table S3, Sheet 2). In the cases of “re-evaluated” samples (1) indicates samples processed via the 6.5 μ m cassette gap and (2) samples that were separated via the 10 μ m gap size. The 6 additional blood samples were solely processed using the narrow 6.5 μ m cassette gap. All samples were drawn in EDTA.

Sample No. (CTC pos.)	Sample ID	CTC Count (Manual Screening)	CTC Count (XCyto10 Screening)
1	mBCa_15 (1)	14	13
2	mBCa_15 (2)	6	6
3	mBCa_22 (1)	1	2
4	mBCa_22 (2)	0	1
5	mBCa_26 (1)	5	5
6	mBCa_27 (1)	4	4
7	mBCa_27 (2)	0	1
8	mBCa_29 (1)	14	17
9	mBC_38	2	2
10	mBC_39	1	1
11	mBC_40	42	38
12	mBC_41	1	1
13	mBC_42	7	5
14	mBC_43	1	1
Total CTC count detected		98	97

4. Discussion

The Parsortix[®] system is a flexible platform which can allow some user-defined modification of various parameters in addition to cassette gap size (6.5 μ m and 10 μ m), including blood sample type and separation pressures. This allows for a versatile applicability of the device while in parallel complicating the determination of standardized protocols. In depth systematic comparisons are therefore warranted in order to ensure optimal device performance. In this study, we extensively evaluated a multitude of different parameters influencing the tumor cell capture efficiency of the Parsortix[®] system and established optimized enrichment protocols ensuring robust performance.

Beginning with extensive spiking experiments mimicking clinical blood samples, we could show that the 6.5 μ m cassette gap dramatically improves the amount of captured tumor cells in comparison to the 10 μ m cassette gap (Table 1, Figure 1). The breast cancer cell line used for these initial experiments (MDA-MB-468) displayed an average cell diameter of 13.5 μ m ($s = 2.03$), with a measured range of 8.71–19.68 μ m (Table S1). Its diameter therefore lends itself to enrichment with both cassette gap sizes while its size distribution mirrors the morphological heterogeneity commonly seen between tumor cells [30,31]. In EDTA samples, which showed the highest overall mean recovery rates in these initial spiking experiments, an increase from 34% ($s = 6.9$) to 68.7% ($s = 5.0$) of mean recovery was demonstrated when using the 6.5 μ m cassette gap instead of the 10 μ m gap (Table 1). The results of our spiking experiments were validated on 43 blood samples of a cohort of 37 mBCa patients. Analyzing parallel blood draws via the Parsortix[®] system, subsequent cytospin and ICC staining corroborated the superiority of the 6.5 μ m cassette gap (Figure 2A), indicating a significant improvement compared to the 10 μ m cassette gap used in prior studies [19,20]. We would therefore recommend the 6.5 μ m cassette gap size for future Parsortix[®] system studies.

Drawing blood into standard EDTA vacutainers is cost efficient and well suited for direct processing of fresh clinical samples within a few hours. However, this is not practical in clinical settings of large multi-center trials which usually require shipments over 24–96 h from the clinical site to the central laboratory. Therefore, we additionally tested various commercially available blood fixatives for their tumor cell recovery performance in combination with the Parsortix[®] system. In spike experiments,

TransFix® preservation tubes showed overall best mean recovery rates, similarly high to EDTA spiked blood samples, while CellSave® and Streck® fixed blood performed less well (Table 2, Figure 2B). TransFix® preservation tubes are designed to stabilize blood for up to 5 days, offering a wide window for sample processing. In clinical samples drawn and analyzed in parallel for the different sample types, combining TransFix® preserved blood with Parsortix® enrichment (6.5 µm, 99 mbar) resulted in acceptable CTC positivity rates of 46.2% across patients and the highest overall CTC count (Table S5, Figure 3A,B). The fixatives outperformed EDTA blood in clinical samples when looking at total single CTC counts (Figure 3B). This discrepancy to the results of our spike experiments could be rooted in higher fragility of patient CTCs compared to cultured tumor cell line cells. In contrast to cell lines, CTCs are influenced by a multitude of adverse factors (e.g., therapy, disease stage, blood passage etc.) which could lead to the observed benefit when using stabilizing reagents. However, the EDTA and lower pressure separation (50 mbar) protocol did result in the highest amount of CTC clusters detected in clinical samples (Table S5, Figure 3B), thereby shifting the reasoning somewhat in favor of an EDTA-based approach compared to fixatives such as CellSave®. Both EDTA and TransFix® samples delivered intact, high quality cells, as demonstrated by quality control of whole genome amplification performed on single cell basis (Figure S2). In conclusion, we would suggest one of two protocols, depending on the research question posed as well as the logistics of the study in question. Fresh EDTA blood and 50 mbar separation represent the best option when cell viability is of highest importance (e.g., for subsequent attempts at cell culture or RNA analysis [19,32]). For morphological characterizations using ICC and subsequent molecular analysis based on DNA, samples preserved in TransFix® (99 mbar separation) lead to the highest CTC yield and offer the possibility of prolonged sample shipment and extended processing windows.

A common point of criticism for novel CTC enrichment platforms is the necessity of manual instead of automated tumor cell calling. This manual sample evaluation is time consuming and limits comparability across different laboratory sites and clinical centers. Additionally, defining standardized staining protocols and evaluation criteria is necessary to allow for direct CTC comparison across sites. To address these issues, the feasibility of combining a new semi-automated CTC screening device, the XCyto® 10 quantitative cell imager, with Parsortix®-based CTC enrichment was evaluated in this study. The high concordance of CTC-positive patients and the total number of identified CTCs between both semi-automated XCyto® 10 based and traditional manual identification demonstrated the suitability of the XCyto® 10 imaging platform for CTC screening purposes (Table 3). Automated sample scanning time using the XCyto® 10 was faster (appr. 10 min per slide) compared to manual scanning (appr. 20 min per slide), resulting in an image gallery of potential CTCs (“hits”) displayed for the user in a similar manner to the CellSearch®. Being able to reapply a standardized set of gating parameters to a whole set of patients within a study cohort has the potential to increase reproducibility and furthermore to reduce bias from individual image analysis.

While the workflow resulting from this study stems from extensive experiments, some limitations require mentioning. The main limitation is that switching to the 6.5 µm gap sized cassette increased processing time and white blood cell background (Table S2, Figure S1). Sample processing time can be managed by using a high separation pressure of 99 mbar. Average processing times of 2 h for a complete EDTA (50 mbar) and 1.5 h for a TransFix sample (99 mbar) were deemed acceptable for sufficient sample turnover. White blood cell background has been shown to lie at 200–800 nucleated cells per mL of processed blood when using the 6.5 µm gap sized cassette [33]. This is known to be donor dependent [20], yet translates to an at least 10^5 fold depletion of white blood cells [33]. In combination with our approach to CTC visualization, comprised of cytopsin and subsequent ICC staining, this background leukocyte level is of no hindrance. Single CTCs detected on the cytopsin can easily be picked via micromanipulation for subsequent molecular characterization. Additionally, this approach allows for sample storage and does not necessitate direct staining and evaluation (such as in cassette enumeration would), thereby circumventing long processing times and increasing comparability between samples. Another point of criticism might be the limited patient collective

processed in this study as well as the mixed tumor entities of our cohort. This point is somewhat compensated by the fact that the entities tested (mNSCLC and mGIC) are known to be difficult for CTC enrichment [13,34,35]. A positivity rate of 46.2% in these patients therefore speaks to the value of our established workflow. Additionally, establishing protocols that demonstrate superiority across multiple tumor entities increase credibility and translational value of the tested method.

This study represents an extensive attempt at optimizing the performance for size-based CTC enrichment via the Parsortix® system. How well the workflow established in this study performs across additional tumor entities will need to be further evaluated in large clinical studies, similar to those performed for the FDA-cleared CellSearch® system [7–9,36–38]. However, we believe that the protocols established here represent a valuable first step towards methodological standardization of this promising CTC enrichment platform and show a clear path for inclusion into future clinical trials.

5. Conclusions

Extensive examinations of pre-analytical and analytical variables using the label-independent Parsortix® system were performed in this study. Initial experimental results with spiked tumor cell line cells were cross-validated with clinical cancer patient samples and resulted in the identification of robust workflows for CTC detection utilizing this enrichment platform.

Depending on the nature of further downstream analysis, a combination of either EDTA blood samples with medium separation pressure or TransFix® preservative tubes with high separation pressure lead to optimal CTC detection from whole blood. Intact tumor cell morphology was maintained, as confirmed via immunocytochemical staining for both workflows. Furthermore, whole genome amplification on a single cell basis, a prerequisite for multiple downstream analyses, was highly efficient. Therefore, the established standardized workflows enable the enrichment of viable or fixed CTCs and allow for precise enumeration and successful downstream analysis of patient-derived CTCs.

Supplementary Materials: The following are available online at <http://www.mdpi.com/2072-6694/12/2/442/s1>, Figure S1: Cassette priming and white blood cell (WBC) count, Figure S2: Efficiency of whole genome amplification (WGA) and results of DNA quality control on single cells processed with our optimized protocols. MDA-MB-468 cells were spiked into EDTA or TransFix® blood and processed via Parsortix® (6.5 µm cassette, 99 mbar). Subsequently, cells were stained, manually picked and DNA amplified using the Ampli1™ WGA kit (Menarini Silicon Biosystems). 10 single tumor cell line cells (1–10) and 5 leukocytes (L1–L5) were processed per blood tube type. gDNA was applied as positive (+) and H₂O as negative (–) control. Following amplification, DNA was subjected to quality control using the Ampli1™ QC Kit (Menarini Silicon Biosystems) and visualized via agarose gel electrophoresis, Table S1: Cell diameters measured for MDA-MB-468 breast cancer cell line cells. Average and standard deviation was assessed from 50 separate cell measurements, Table S2: Detailed recovery results using MDA-MB-468 cells spiked into different blood sample types and processed with various experimental Parsortix™ conditions. Each measurement was carried out in triplicates and absolute as well as averaged values (including s = standard deviation) are indicated. Additionally, average processing time is noted, Table S3: Information on mBC patients providing blood samples for the Parsortix™ cassette gap comparison and the testing of semi-automated evaluation using the XCyto 10 platform. (Sheet1) Absolute CTC counts detected for the 37 mBC patients enrolled in this study are indicated. Each patient donated matched EDTA blood samples at blood draw to allow for direct comparison of 6.5 µm and 10 µm cassette gap performance. A second sample set was collected for 6 mBCa patients. (Sheet2) Basic clinical patient data available for our analyzed mBC cohort including additional patients for comparison of manual vs. semi-automated sample screening. Abbreviations include: pos–positive, neg–negative, and nA–not available, Table S4: Clinical information on the mixed cancer patient collective analyzed for blood tube comparison (n = 13). Clinical samples were obtained from 6 metastatic non-small-cell lung cancer (mNSCLC), 1 metastatic small-cell lung cancer (mSCLC) and 6 metastatic gastrointestinal cancer (mGIC) patients, Table S5: Detailed recovery results for 13 clinical cancer patient samples drawn in parallel into different blood tubes and processed with the 6.5 µm cassette gap via the Parsortix™ system. Clinical samples were obtained from metastatic non-small-cell lung cancer (mNSCLC), small-cell lung cancer (SCLC) and metastatic gastrointestinal cancer (mGIC) patients. In cases in which CTCs were found, results are presented as (x/y), x = total number of single CTCs, y = total number of CTC clusters detected, Table S6: Number of CTCs in blood samples from metastatic breast cancer patients detected by manual screening and by the automated XCyto 10 platform.

Author Contributions: Conception and design: K.P., T.M.G., C.K.; Development and methodology: C.K., T.G.; Acquisition of data: C.K., O.J.W.W., S.S., L.J.H.; Analysis and interpretation of data: C.K., S.A.J., K.P.; Administrative, technical, or material support: S.A.J., M.J., S.L., M.B.-P., V.M., K.P., S.P., S.S., H.W., K.P., D.L.; Study supervision: K.P., T.M.G.; Writing, review, and/or revision of the manuscript: C.K., K.P., S.A.J., S.S.; Final approval: All authors. All authors have read and agreed to the published version of the manuscript.

Funding: Klaus Pantel received funding from the European Union-EFPIA Innovative Medicines Initiative grant CANCER-ID (Grant no. 115749), the ERC Advanced Investigator Grant INJURMET (Nr. 834974), and from an unrestricted grant of ANGLE plc (Guildford, UK). This project received funding from the European Union's Horizon 2020 research and innovation program under Marie Skłodowska-Curie grant agreement No 765492.

Acknowledgments: The authors acknowledge Antje Andreas and Cornelia Coith from the University Medical Center Hamburg-Eppendorf for technical assistance.

Conflicts of Interest: Klaus Pantel has ongoing patent applications related to circulating tumor cells; his institution received research funding from European Federation of Pharmaceutical Industries and Associations (EFPIA) partners (Angle, Menarini, Agena and Servier) of the CANCER-ID programm (www.cancer-id.eu) of the European Union-EFPIA Innovative Medicines Initiative. Sonja Loges is the recipient of a Heisenberg-Professorship from the DFG (LO-1863/6-1). Sonja Loges and Melanie Janning receive funding from the Margarethe-Clemens Stiftung. The remaining authors declare no conflict of interest.

References

1. Kang, Y.; Pantel, K. Tumor cell dissemination: emerging biological insights from animal models and cancer patients. *Cancer Cell* **2013**, *23*, 573–581. [[CrossRef](#)] [[PubMed](#)]
2. Alix-Panabieres, C.; Pantel, K. Clinical Applications of Circulating Tumor Cells and Circulating Tumor DNA as Liquid Biopsy. *Cancer Discov.* **2016**, *6*, 479–491. [[CrossRef](#)] [[PubMed](#)]
3. Pantel, K.; Alix-Panabieres, C. Liquid biopsy and minimal residual disease - latest advances and implications for cure. *Nat. Rev. Clin. Oncol.* **2019**, *16*, 409–424. [[CrossRef](#)] [[PubMed](#)]
4. Keller, L.; Pantel, K. Unravelling tumour heterogeneity by single-cell profiling of circulating tumour cells. *Nat. Rev. Cancer* **2019**, *19*, 553–567. [[CrossRef](#)]
5. Alix-Panabieres, C.; Pantel, K. Challenges in circulating tumour cell research. *Nat. Rev. Cancer* **2014**, *14*, 623–631. [[CrossRef](#)]
6. Joosse, S.A.; Gorges, T.M.; Pantel, K. Biology, detection, and clinical implications of circulating tumor cells. *EMBO Mol. Med.* **2015**, *7*, 1–11. [[CrossRef](#)]
7. Cohen, S.J.; Punt, C.J.; Iannotti, N.; Saidman, B.H.; Sabbath, K.D.; Gabrail, N.Y.; Picus, J.; Morse, M.; Mitchell, E.; Miller, M.C.; et al. Relationship of circulating tumor cells to tumor response, progression-free survival, and overall survival in patients with metastatic colorectal cancer. *J. Clin. Oncol.* **2008**, *26*, 3213–3221. [[CrossRef](#)]
8. Cristofanilli, M.; Budd, G.T.; Ellis, M.J.; Stopeck, A.; Matera, J.; Miller, M.C.; Reuben, J.M.; Doyle, G.V.; Allard, W.J.; Terstappen, L.W.; et al. Circulating tumor cells, disease progression, and survival in metastatic breast cancer. *N. Engl. J. Med.* **2004**, *351*, 781–791. [[CrossRef](#)]
9. De Bono, J.S.; Scher, H.I.; Montgomery, R.B.; Parker, C.; Miller, M.C.; Tissing, H.; Doyle, G.V.; Terstappen, L.W.; Pienta, K.J.; Raghavan, D. Circulating tumor cells predict survival benefit from treatment in metastatic castration-resistant prostate cancer. *Clin. Cancer Res.* **2008**, *14*, 6302–6309. [[CrossRef](#)]
10. Riethdorf, S.; Fritsche, H.; Muller, V.; Rau, T.; Schindlbeck, C.; Rack, B.; Janni, W.; Coith, C.; Beck, K.; Janicke, F.; et al. Detection of circulating tumor cells in peripheral blood of patients with metastatic breast cancer: a validation study of the CellSearch system. *Clin. Cancer Res.* **2007**, *13*, 920–928. [[CrossRef](#)]
11. Miller, M.C.; Doyle, G.V.; Terstappen, L.W. Significance of Circulating Tumor Cells Detected by the CellSearch System in Patients with Metastatic Breast Colorectal and Prostate Cancer. *J. Oncol.* **2010**, *2010*, e617421. [[CrossRef](#)]
12. Scher, H.I.; Jia, X.Y.; de Bono, J.S.; Fleisher, M.; Pienta, K.J.; Raghavan, D.; Heller, G. Circulating tumour cells as prognostic markers in progressive, castration-resistant prostate cancer: a reanalysis of IMMC38 trial data. *Lancet Oncol.* **2009**, *10*, 233–239. [[CrossRef](#)]
13. Riethdorf, S.; O'Flaherty, L.; Hille, C.; Pantel, K. Clinical applications of the CellSearch platform in cancer patients. *Adv. Drug Deliv. Rev.* **2018**, *125*, 102–121. [[CrossRef](#)]
14. Tam, W.L.; Weinberg, R.A. The epigenetics of epithelial-mesenchymal plasticity in cancer. *Nat. Med.* **2013**, *19*, 1438–1449. [[CrossRef](#)]
15. Gorges, T.M.; Tinhofer, I.; Drosch, M.; Rose, L.; Zollner, T.M.; Krahn, T.; von Ahsen, O. Circulating tumour cells escape from EpCAM-based detection due to epithelial-to-mesenchymal transition. *BMC Cancer* **2012**, *12*, e178. [[CrossRef](#)]

16. Yu, M.; Bardia, A.; Wittner, B.S.; Stott, S.L.; Smas, M.E.; Ting, D.T.; Isakoff, S.J.; Ciciliano, J.C.; Wells, M.N.; Shah, A.M.; et al. Circulating breast tumor cells exhibit dynamic changes in epithelial and mesenchymal composition. *Science* **2013**, *339*, 580–584. [\[CrossRef\]](#)
17. Yokobori, T.; Iinuma, H.; Shimamura, T.; Imoto, S.; Sugimachi, K.; Ishii, H.; Iwatsuki, M.; Ota, D.; Ohkuma, M.; Iwaya, T.; et al. Platin3 Is a Novel Marker for Circulating Tumor Cells Undergoing the Epithelial-Mesenchymal Transition and Is Associated with Colorectal Cancer Prognosis. *Cancer Res.* **2013**, *73*, 2059–2069. [\[CrossRef\]](#)
18. Mego, M.; Mani, S.A.; Lee, B.N.; Li, C.; Evans, K.W.; Cohen, E.N.; Gao, H.; Jackson, S.A.; Giordano, A.; Hortobagyi, G.N.; et al. Expression of epithelial-mesenchymal transition-inducing transcription factors in primary breast cancer: The effect of neoadjuvant therapy. *Int. J. Cancer* **2012**, *130*, 808–816. [\[CrossRef\]](#)
19. Hvichia, G.E.; Parveen, Z.; Wagner, C.; Janning, M.; Quidde, J.; Stein, A.; Muller, V.; Loges, S.; Neves, R.P.; Stoecklein, N.H.; et al. A novel microfluidic platform for size and deformability based separation and the subsequent molecular characterization of viable circulating tumor cells. *Int. J. Cancer* **2016**, *138*, 2894–2904. [\[CrossRef\]](#)
20. Chudziak, J.; Burt, D.J.; Mohan, S.; Rothwell, D.G.; Mesquita, B.; Antonello, J.; Dalby, S.; Ayub, M.; Priest, L.; Carter, L.; et al. Clinical evaluation of a novel microfluidic device for epitope-independent enrichment of circulating tumour cells in patients with small cell lung cancer. *Analyst* **2016**, *141*, 669–678. [\[CrossRef\]](#)
21. Xu, L.; Mao, X.; Imrali, A.; Syed, F.; Mutsvangwa, K.; Berney, D.; Cathcart, P.; Hines, J.; Shamash, J.; Lu, Y.J. Optimization and Evaluation of a Novel Size Based Circulating Tumor Cell Isolation System. *PLoS ONE* **2015**, *10*, e0138032. [\[CrossRef\]](#)
22. Gorges, K.; Wiltfang, L.; Gorges, T.M.; Sartori, A.; Hildebrandt, L.; Keller, L.; Volkmer, B.; Peine, S.; Babayan, A.; Moll, I.; et al. Intra-Patient Heterogeneity of Circulating Tumor Cells and Circulating Tumor DNA in Blood of Melanoma Patients. *Cancers (Basel)* **2019**, *11*, 1685. [\[CrossRef\]](#)
23. El-Heliebi, A.; Hille, C.; Laxman, N.; Svedlund, J.; Haudum, C.; Ercan, E.; Kroneis, T.; Chen, S.; Smolle, M.; Rossmann, C.; et al. In Situ Detection and Quantification of AR-V7, AR-FL, PSA, and KRAS Point Mutations in Circulating Tumor Cells. *Clin. Chem.* **2018**, *64*, 536–546. [\[CrossRef\]](#)
24. Janning, M.; Kobus, F.; Babayan, A.; Wikman, H.; Velthaus, J.L.; Bergmann, S.; Schatz, S.; Falk, M.; Berger, L.A.; Bottcher, L.M.; et al. Determination of PD-L1 Expression in Circulating Tumor Cells of NSCLC Patients and Correlation with Response to PD-1/PD-L1 Inhibitors. *Cancers (Basel)* **2019**, *11*, 835. [\[CrossRef\]](#)
25. Gkoutela, S.; Castro-Giner, F.; Szczerba, B.M.; Vetter, M.; Landin, J.; Scherrer, R.; Krol, I.; Scheidmann, M.C.; Beisel, C.; Stirnimann, C.U.; et al. Circulating Tumor Cell Clustering Shapes DNA Methylation to Enable Metastasis Seeding. *Cell* **2019**, *176*, 98–112. [\[CrossRef\]](#)
26. Franken, A.; Driemel, C.; Behrens, B.; Meier-Stiege, F.; Endris, V.; Stenzinger, A.; Niederacher, D.; Fischer, J.C.; Stoecklein, N.H.; Ruckhaeberle, E.; et al. Label-Free Enrichment and Molecular Characterization of Viable Circulating Tumor Cells from Diagnostic Leukapheresis Products. *Clin. Chem.* **2019**, *65*, 549–558. [\[CrossRef\]](#)
27. Chen, L.; Bode, A.M.; Dong, Z. Circulating Tumor Cells: Moving Biological Insights into Detection. *Theranostics* **2017**, *7*, 2606–2619. [\[CrossRef\]](#)
28. Joosse, S.A. In-Silico Online (version 2.1.2). Available online: <http://in-silico.online> (accessed on 10 August 2019).
29. Joosse, S.A.; Pantel, K. Genetic traits for hematogeneous tumor cell dissemination in cancer patients. *Cancer Metastasis Rev.* **2016**, *35*, 41–48. [\[CrossRef\]](#)
30. Park, S.; Ang, R.R.; Duffy, S.P.; Bazov, J.; Chi, K.N.; Black, P.C.; Ma, H. Morphological differences between circulating tumor cells from prostate cancer patients and cultured prostate cancer cells. *PLoS ONE* **2014**, *9*, e85264. [\[CrossRef\]](#)
31. Follain, G.; Osmani, N.; Azevedo, A.S.; Allio, G.; Mercier, L.; Karreman, M.A.; Solecki, G.; Garcia Leon, M.J.; Lefebvre, O.; Fekonja, N.; et al. Hemodynamic Forces Tune the Arrest, Adhesion, and Extravasation of Circulating Tumor Cells. *Dev. Cell* **2018**, *45*, 33–52. [\[CrossRef\]](#)
32. Gorges, T.M.; Kuske, A.; Rock, K.; Mauermann, O.; Muller, V.; Peine, S.; Verpoort, K.; Novosadova, V.; Kubista, M.; Riethdorf, S.; et al. Accession of Tumor Heterogeneity by Multiplex Transcriptome Profiling of Single Circulating Tumor Cells. *Clin. Chem.* **2016**, *62*, 1504–1515. [\[CrossRef\]](#)
33. Miller, M.C.; Robinson, P.S.; Wagner, C.; O'Shannessy, D.J. The Parsortix Cell Separation System-A versatile liquid biopsy platform. *Cytometry A* **2018**, *93*, 1234–1239. [\[CrossRef\]](#)
34. O'Flaherty, L.; Wikman, H.; Pantel, K. Biology and clinical significance of circulating tumor cell subpopulations in lung cancer. *Transl. Lung Cancer Res.* **2017**, *6*, 431–443. [\[CrossRef\]](#)

35. Lindsay, C.R.; Blackhall, F.H.; Carmel, A.; Fernandez-Gutierrez, F.; Gazzaniga, P.; Groen, H.J.M.; Hiltermann, T.J.N.; Krebs, M.G.; Loges, S.; Lopez-Lopez, R.; et al. EPAC-lung: pooled analysis of circulating tumour cells in advanced non-small cell lung cancer. *Eur. J. Cancer* **2019**, *117*, 60–68. [[CrossRef](#)]
36. Tibbe, A.G.; Miller, M.C.; Terstappen, L.W. Statistical considerations for enumeration of circulating tumor cells. *Cytometry A* **2007**, *71*, 154–162. [[CrossRef](#)]
37. Martin, M.; Garcia-Saenz, J.A.; Maestro De las Casas, M.L.; Vidaurreta, M.; Puente, J.; Veganzones, S.; Rodriguez-Lajusticia, L.; De la Orden, V.; Oliva, B.; De la Torre, J.C.; et al. Circulating tumor cells in metastatic breast cancer: timing of blood extraction for analysis. *Anticancer Res.* **2009**, *29*, 4185–4187.
38. Allard, W.J.; Matera, J.; Miller, M.C.; Repollet, M.; Connelly, M.C.; Rao, C.; Tibbe, A.G.; Uhr, J.W.; Terstappen, L.W. Tumor cells circulate in the peripheral blood of all major carcinomas but not in healthy subjects or patients with nonmalignant diseases. *Clin. Cancer Res.* **2004**, *10*, 6897–6904. [[CrossRef](#)]



© 2020 by the authors. Licensee MDPI, Basel, Switzerland. This article is an open access article distributed under the terms and conditions of the Creative Commons Attribution (CC BY) license (<http://creativecommons.org/licenses/by/4.0/>).

Evaluation of Microfluidic Ceiling Designs for the Capture of Circulating Tumor Cells on a Microarray Platform

Hui-Yu Liu, Claudia Koch, Anna Haller, Simon A. Joosse, Ravi Kumar, Michael J. Vellekoop, Ludwig J. Horst, Laura Keller, Anna Babayan, Antonio Virgilio Failla, Jana Jensen, Sven Peine, Franz Keplinger, Harald Fuchs, Klaus Pantel,* and Michael Hirtz*

The capture of circulating tumor cells (CTCs) is still a challenging application for microfluidic chips, as these cells are rare and hidden in a huge background of blood cells. Here, different microfluidic ceiling designs in regard to their capture efficiency for CTCs in model experiments and more realistic conditions of blood samples spiked with a clinically relevant amount of tumor cells are evaluated. An optimized design for the capture platform that allows highly efficient recovery of CTCs from size-based pre-enriched samples under realistic conditions is obtained. Furthermore, the viability of captured tumor cells as well as single cell recovery for downstream genomic analysis is demonstrated. Additionally, the authors' findings underline the importance of evaluating rational design rules for microfluidic devices based on theoretical models by application-specific experiments.

a metastatic lesion.^[2–9] The detection of CTCs in patient blood is associated with reduced overall survival (OS) in various cancer types.^[10–12]

Currently, cancer is primarily diagnosed by tissue biopsy, an invasive procedure that can lead to side effects such as bleeding and infection and is not feasible in all tissues (e.g., brain). Additionally, information gained by biopsy is limited to the site of tissue removal and furthermore cannot mirror the ever changing landscape of tumor evolution within a single patient. Blood-based analysis of CTCs could therefore function as a minimal invasive “liquid biopsy,” allowing repeated sampling, a more holistic overview on disease development, and additional insights into the biology of metastasis formation.^[13,14]

When analyzing CTCs, the main hurdle is the rarity of these cells in the background of millions of blood cells (≈ 1 CTC in 10^8 blood cells).^[15] To overcome this limitation, a multitude of assays have been and are currently under development.^[3,16] However, so far only the CellSearch system (Menarini Silicon Biosystems, Italy) has gained approval for use in specific cancer

1. Introduction

Cancer remains the second most common cause of death worldwide.^[1] As 90% of cancer-related deaths are caused by the formation of distant metastasis, understanding and preventing this decisive step of disease progression will be crucial for treatment improvement. Circulating tumor cells (CTCs) are cells released into the blood from the primary tumor and/or

H.-Y. Liu, Dr. R. Kumar, Prof. H. Fuchs, Dr. M. Hirtz
Institute of Nanotechnology (INT) and Karlsruhe Nano
Micro Facility (KNMF)
Karlsruhe Institute of Technology (KIT)
76344 Eggenstein-Leopoldshafen, Germany
E-mail: michael.hirtz@kit.edu

C. Koch, Dr. S. A. Joosse, L. J. Horst, Dr. L. Keller, Dr. A. Babayan,
J. Jensen, Prof. K. Pantel
Department of Tumor Biology
University Medical Center Hamburg-Eppendorf
20246 Hamburg, Germany
E-mail: pantel@uke.de


Dr. A. Haller, Prof. F. Keplinger
Institute of Sensor and Actuator Systems
TU Wien

1040 Vienna, Austria
Prof. M. J. Vellekoop
Institute for Microsensors
Microactuators and Microsystems (IMSAS)
Microsystems Center Bremen MCB
University of Bremen
28359 Bremen, Germany

Dr. A. V. Failla
Microscopy Imaging Facility (UMIF)
University Medical Center Hamburg-Eppendorf
20246 Hamburg, Germany

Dr. S. Peine
Department of Transfusion Medicine
University Medical Center Hamburg-Eppendorf
20246 Hamburg, Germany

Prof. H. Fuchs
Physical Institute and Center for Nanotechnology (CeNTech)
University of Münster
48149 Münster, Germany

 The ORCID identification number(s) for the author(s) of this article can be found under <https://doi.org/10.1002/adbi.201900162>.

© 2019 The Authors. Published by WILEY-VCH Verlag GmbH & Co. KGaA, Weinheim. This is an open access article under the terms of the Creative Commons Attribution License, which permits use, distribution and reproduction in any medium, provided the original work is properly

DOI: 10.1002/adbi.201900162
cited.

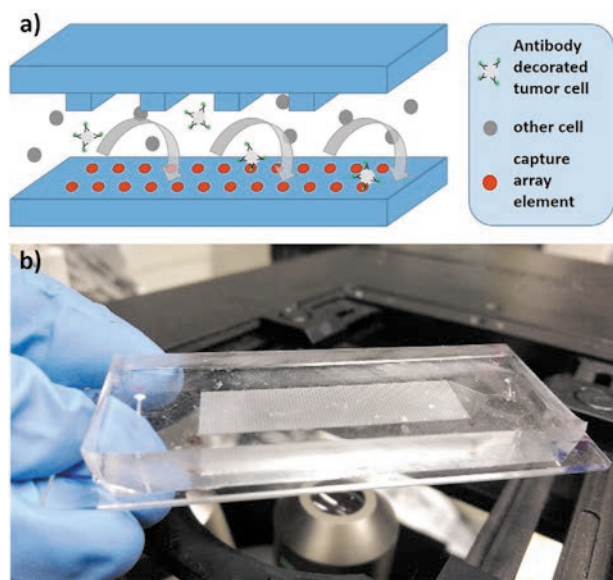


Figure 1. The CTC capture chip. a) Scheme of the capture principle. Antibody sensitized CTCs are captured on a microarray at the channel bottom, while other cells can pass the microfluidic chip. Structures in the channel ceiling ensure frequent contacts of cells with the microarray by inducing transverse flows. b) Photograph of a real microfluidic chip on an inverted microscope.

entities by the American Food and Drug Administration (FDA). While this system has been extensively validated, its limitation lies in the dependence of its CTC capture on EpCAM epithelial cell adhesion molecule (EpCAM).^[17] While EpCAM is expressed on most epithelial tissues and therefore carcinoma cells, a growing amount of evidence is indicating that tumor cells undergo transition to a more mesenchymal state when initiating the metastatic cascade.^[18,19] These cells downregulate epithelial markers such as EpCAM and therefore would most likely not be detected by the CellSearch system. This necessitates the development of promising and highly sensitive EpCAM-independent CTC detection platforms in order to isolate these highly aggressive CTC subtypes.

Recently, we developed a different approach in microfluidic CTC capture, based on a microfluidic encapsulated microarray.^[20] Here, the CTC-containing samples are incubated with an antibody targeting the desired surface marker and then introduced into a microfluidic chip with a herringbone structured ceiling (Figure 1). The ceiling structure disrupts laminar streamlines and, thereby, enhances the number of cellular interactions with the reactive micropattern, comprising the specific binding sites for the CTCs. Thus, CTCs are immobilized on the array, while healthy cells leave the microfluidic chip on the outlet. The microarray within the microfluidic channel was printed via polymer pen lithography (PPL).^[21] This technique combines aspects of microcontact printing and dip-pen nanolithography (DPN)^[22] in a hybrid way and allows large area (several cm²) patterning,^[23] especially for sensitive, bioactive molecules in gradients^[24,25] and in a multiplexed fashion.^[26–29] This allows also easy integration into microfluidic systems as we demonstrated for the above-mentioned application of CTC capture^[20] and mast cell screening.^[30] recently. In the application of these microarrays for CTC capture, the design of the microfluidic chip

chamber ceiling is key to disrupt laminar streamlines in order to get CTCs into contact with the specific binding sites on the microarray. Structuring the channel ceiling with a staggered herringbone (SHB) design has proven to be an effective method to increase the number of cell–surface contacts. Originally, SHBs were proposed as a chaotic mixer for microchannels by Strook et al.^[31] They showed that SHB mixers generate transverse flows that induce a stirring within the microchannel. These microvortices lead to stretching and folding of fluid volumes over the channel's cross section. Thereby, the diffusion length is reduced and, hence, mixing is significantly accelerated.

Stott et al. were among the first to apply the SHB mixer design to the isolation of CTCs.^[32] Since then, SHBs have been utilized frequently for CTC capture.

The initial SHB design has been proposed and optimized for mixing purposes. For the purpose of capturing CTCs the aim is not mixing but transporting cells to a binding surface. On that account, Forbes et al. developed a computational model and a theoretical framework to optimize the geometry of the SHB design.^[33] Recently, Lynn et al. have optimized the design of the SHB mixer for biosensing purposes as well, focusing on analyte transfer to the surface opposite the SHB grooves.^[34,35] Considering the importance and benefits of theoretical and simulation results in the design process of microfluidics,^[36] we set out to implement and compare these propositions in practice.

In the present work, we evaluate our chip platform with different SHB structures as suggested in the literature. As different herringbone structures are theoretically proposed for maximum efficiency of analyte delivery to active channel surface, we compare three different setups: design HA is the SHB design that we utilized in a previous publication,^[20] design HB implements the suggestions of Forbes et al.,^[33] and design HC follows the design rules that Lynn et al.^[34,35] proposed. Additionally, the capture efficiency of a channel with smooth walls is included in the comparison.

2. Results and Discussions

2.1. The Chip Platform

In order to assess the influence of the different SHB structures in the chip ceiling (Figure 2) on the capture efficiency of the chip platform, three different designs were produced (Table 1, called ceiling type HA, HB, HC) and compared with each other as well as an unstructured microfluidic channel. The herringbone is composed of a series of chevrons with a long and a short groove. The short groove covers one third of the symmetry width w_{hb} and the long groove covers the remaining two thirds. The angle between grooves θ_{hb} is 90° and the angle with the channel wall θ_c is 45°.

Each chevron is w_{hb} wide and placed side by side to cover the complete channel width w_c . Grooves are w_g wide, h_g high and separated with a pitch Λ . The height of the smooth part of the channel is h_c . The shape of the SHBs is varied as a function of the axial position in the microchannel. After N_g chevrons per part-cycle, they are staggered by an offset δ_g .

Publications by Forbes et al. and Lynn et al. on geometrical optimization of the SHB design provide design guidelines to enhance

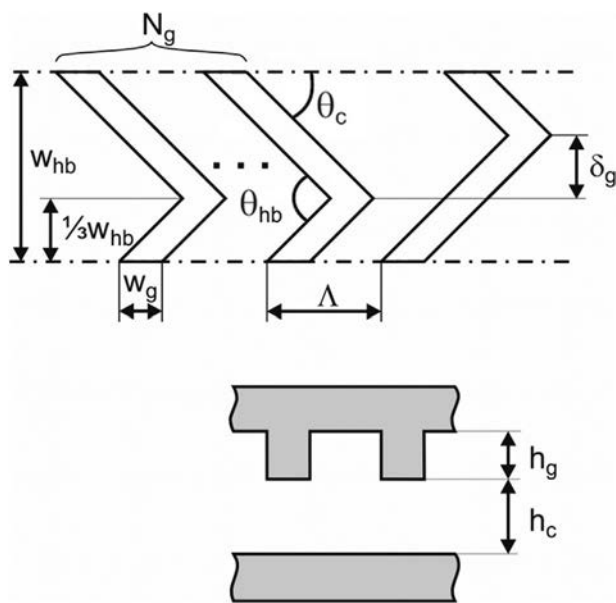


Figure 2. Scheme of chip ceilings. Schematic of a staggered herringbone design, illustrating the geometrical parameters: channel height h_c , groove height h_g , groove width w_g , groove pitch Λ , symmetry width w_{HB} , number of chevrons per part-cycle N_g and offset per cycle δ_g .

the number of particle–surface interactions in SHBs.^[33–35] However, the results published by these two groups contradict each other in the following parameters: groove width w_g , groove height h_g , and symmetry width w_{HB} . Nevertheless, they agree that the groove pitch Λ has little or no effect on capture efficiency.

Forbes et al. focus on the groove-to-channel relative hydraulic resistance and suggest that SHBs with wide and deep grooves enhance the number of interactions at the surface opposite to the SHBs.^[33] Consequently, the geometrical parameters, labeled HB in Table 1, were chosen.

Lynn et al. conclude that the ratio h_g/h_c is one of the most important design parameters and should be in the region of $1.2 < h_g/h_c$.^[34,35] As the channel height is 50 μm , the groove height was chosen to be 75 μm , resulting in $h_g/h_c = 1.5$. The geometrical parameters following these suggestions are given in Table 1, labeled HC.

To find the optimal SHB structure for CTCs capture purposes, the designs HB and HC were fabricated and their capture efficiency was evaluated experimentally. Additionally,

Table 1. Design parameters of the staggered herringbone ceiling.

Geometrical parameter	HA [μm] ^{a)}	HB [μm] ^{b)}	HC [μm] ^{c)}
Channel height h_c	50	50	50
Groove height h_g	50	150	75
Groove width w_g	100	125	50
Groove pitch Λ	100	200	100
Symmetry width w_{HB}	300	500	150
Offset per cycle δ_g	100	500	150

^{a)}As used in our previous publication^[20]; ^{b)}Following design rules by Forbes et al.^[33]; ^{c)}Following design rules by Lynn et al.^[34,35]

the SHB design that was utilized in a previous publication by our group, labeled HA, and a smooth channel with height $h_c = 150 \mu\text{m}$ were included in the comparison.

All designs have the following parameters in common: complete channel width $w_c = 9600 \mu\text{m}$, number of grooves per part-cycle $N_g = 5$, angle of herringbone $\theta_{hb} = 90^\circ$ and the angle with channel wall $\theta_c = 45^\circ$.

2.2. Performance in Tumor Cell Capture

To compare the performance of the different ceiling types for the microarray chip platform, trials with different concentrations of cancer cell line cells were performed. Mixtures of 100 and 10000 biotinylated cancer cells (MCF-7) and 10^4 to 10^6 non-biotinylated cancer cells were tested on the different microfluidic chips (different pattern pitches and chamber designs). A streptavidin-patterned chip surface with an array feature pitch of 50 μm combined with the SHB design type HC showed the highest capture rate among the different tested combinations (Figure 3c and Table S1, Supporting Information).

Statistical analyses showed that both the ceiling type ($p = 0.0015$) and pattern structure ($p < 0.0001$) had a significant impact on the capture rate, with a possible interaction between the two ($p = 0.0089$), cell suspension concentration was also significantly correlated to the capturing rate ($p = 0.044$), but not as strong and was therefore not further considered. Pairwise analyses indicated that ceiling type HB was outperformed by HA with 29.8% (95% CI: [10.1, 49.4], $p = 0.0019$) and HC with 30.8% (95% CI: [9.2, 52.3], $p = 0.0034$), whereas the smooth ceiling type was not highly statistically different compared to the other three ($p > 0.005$). The pattern structure of 50 μm showed a 25.2% better mean capturing than the 25 μm (95% CI: [11.0, 39.5], $p = 0.0006$) and a 28% better capturing than the homogeneous pattern structure (95% CI: [13.1, 42.9], $p = 0.0003$). Interaction effects between the ceiling type and pattern structure confirmed that 60% higher mean recovery rates could be achieved with the 50 μm herringbone HA and HC compared to the smooth type or HB ($p < 0.005$). No statistically significant difference in the mean rate of capture was detected between ceiling types HA and HC at the same pattern structure.

Based on these results, a pattern pitch of 50 μm was chosen (as here the overall highest recovery performance was found) for subsequent experiments to allow more in-depth comparison across the different chip designs under “mock” blood sample conditions. Here, 100 cancer cell line cells (MCF-7) were spiked into blood samples of healthy donors (containing around 5×10^9 cells mL^{-1}). As described previously,^[20] these “mock” blood samples were subjected to a size-based pre-enrichment by the Parsortix system. This workflow allows for removal of a large fraction of healthy white blood cells and erythrocyte background by size exclusion.^[37] After pre-enrichment, the remaining cells (1500–6000 dependent on donor)^[38,39] were sensitized by biotinylated-anti-EpCAM antibodies and pumped into the respective chip. Following additional staining with fluorescently labeled antibodies (secondary anti-mouse, DAPI, CD45), the tumor cells bound on the chip surface were manually counted with an upright fluorescence microscope.

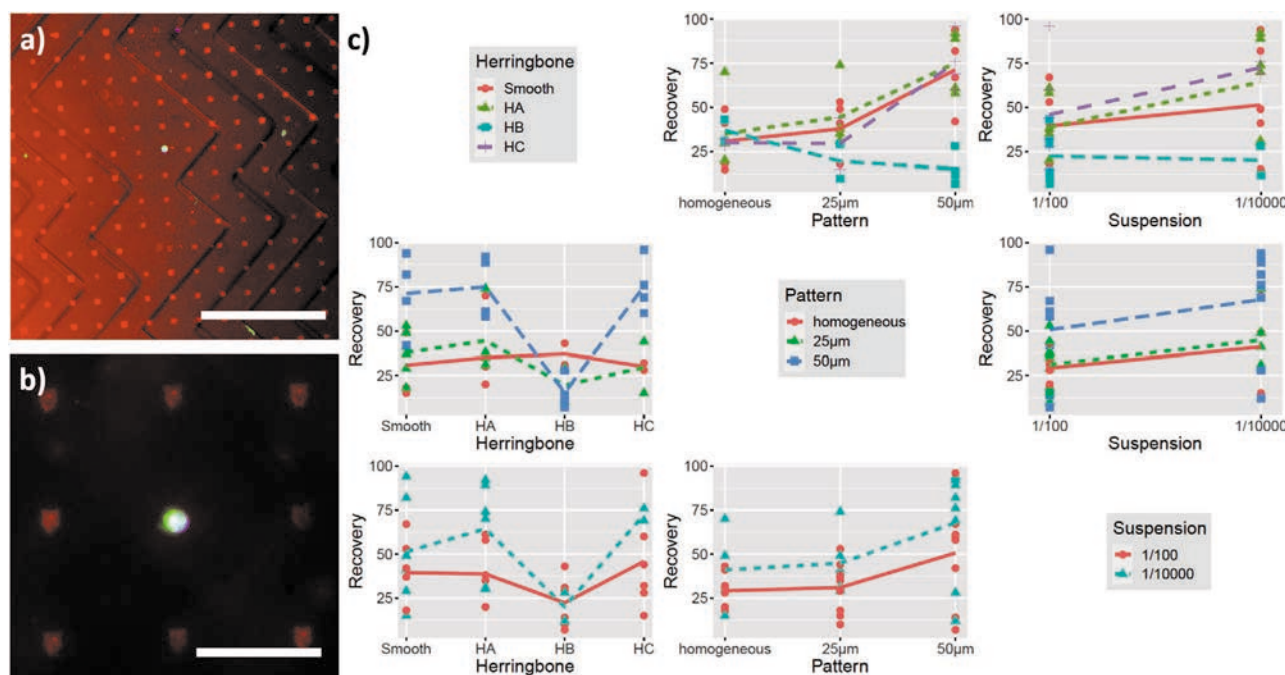


Figure 3. Captured cells on a microarray and correlation matrix of examined chip and pattern designs. a) Single captured CTC on a microarray. The translucent herringbone ceiling structure is visible. Scale bar equals 250 μm. b) Close-up of the cell. Note the low background of other cells and the co-localization of microarray pattern with the captured CTC. Scale bar equals 50 μm. c) Correlation matrix showing the recovery of tumor cells under the different experimental conditions of the ceiling type (Herringbone, top row), pattern design (Pattern, center row), and the cell suspension concentration (Suspension, bottom row).

Representative images of stained tumor cells captured on the streptavidin dots of the chip are shown in Figure 3a,b. As median recovery for the different ceiling types, 10% for smooth, 13% for type HA, 3% for type HB, and 38% for type HC, respectively, were obtained (Figure 4). The standard deviations (SD) measured here represent an accumulation of the SD of both the pre-enrichment via Parsortix, and the actual chip processing. The SD of the HC chip appears to be higher than in the other chips which is most likely due to the fact that more cells can be detected with this compared to the other chip types (e.g., HB). It is natural for the variation in recovery to decrease the closer the recovery is to zero. Since the recovery obtained with the HC chip among the different experiments is normally distributed, the results remain highly trustworthy. Nonetheless, we will strive to further improve the reproducibility in future experiments. Statistical analysis shows a significant difference in the mean recovery rate between the ceiling types ($p = 0.0006$). Type HC outperformed the smooth type with 30.3% (95% CI: [11.8, 48.7], $p = 0.0025$), type HA with 22.9% (95% CI: [4.5, 41.4], $p = 0.015$), and type HB with 34.6% (95% CI: [16.1, 53.1], $p = 0.0009$). No statistically significant difference was detected between type HA and HB ($p = 0.35$), HA and smooth ($p = 0.70$), and HB and smooth ($p = 0.92$). Taken together, the HC type (designed as suggested by the Lynn et al. rules for maximization of the number of surface interactions)^[34,35] shows the overall best recovery performance and significantly improves on our previously used^[20] HA type and the HB type (based on the alternative design rules suggested by Forbes et al.).^[33] Current standard approaches used downstream of the Parsortix system, such as the classical ICC staining on cytopins

(pan-cytokeratin, CD45, and DAPI) reach an average recovery of $(32 \pm 4)\%$ using MCF-7 cells and the same Parsortix separation protocol (Table S2, Supporting Information). Of note, a broader

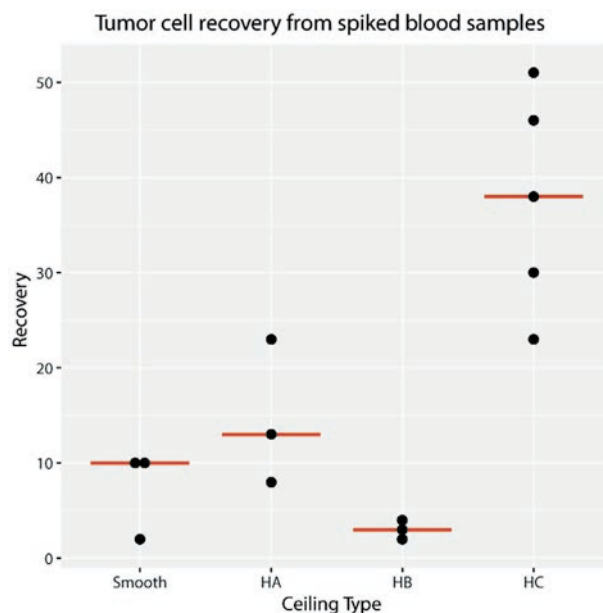


Figure 4. Capture efficiency in spiked blood samples. Ceiling type HC (median recovery 38%) outperforms the other ceiling types significantly. No statistically significant differences were detected between the smooth ceiling (median recovery 10%) and ceiling types HA (median recovery 13%) and HB (median recovery 3%).

discussion and comparison of different CTC isolation systems can be found in the literature.^[3,40,41] Factoring in these losses in the upstream processing and assuming that the Parsortix separation is the main point these occur (neglecting the contribution of the cytospin process), the HC system would have a (theoretical) recovery of 118% (excess of 100% probably reflecting the neglected losses during cytospin that cannot easily be deconvoluted). This estimation shows that the HC system has a virtually full recovery of cells obtained in the upstream process.

Sample purity represents a crucial factor of CTC isolation techniques. However, it is most relevant when no further discrimination between target cells (CTCs) and cellular background (e.g., leucocytes) takes place and when samples are furthermore subjected to bulk analysis. In our case, potential target cells on the chip are fluorescently stained using established CTC markers as well as leucocyte exclusion markers allowing apt differentiation between both cellular populations. The microarray features themselves provide a strong reference to distinguish targets and unspecific background by co-localization of targets with the array features (Figure S1, Supporting Information). Furthermore, analysis of CTCs identified on the chip is based on single cell isolation and not bulk analysis, therefore circumventing the need for even higher purity in samples. Overall, leukocyte background remained under 500 nucleated cells for all blood samples tested (data not shown). Sample pre-enrichment via Parsortix was shown to result in a residual count of 200–800 nucleated cells per mL of processed blood,^[38] translating to 1500–6000 nucleated cells post size-based enrichment of a standard 7.5 mL EDTA blood tube. This leukocyte background is known to be donor dependent.^[39] Considering these numbers, our chip achieves a minimal further sample purification of threefold and maximum additional sample purification of over 12-fold.

2.3. Cell Viability following Tumor Cell Capture

Although progress has been made during recent years, culturing CTCs from patient blood *ex vivo* remains challenging to this day. So far only very few CTC-derived cell lines could successfully be established,^[42–44] limiting the functional understanding of these cells. The viability of captured tumor cells following enrichment or isolation represents a vital prerequisite for successful transient or permanent culture. A cell viability of 99% was demonstrated for cells separated by the Parsortix system in earlier studies^[37,45] indicating that processing of samples using this technology has a negligible effect on cell viability. For this reason, in this study, we focused on assessing the impact of chip processing in itself on cell viability. To test the viability of cells passed through our chip, we sensitized breast cancer cell line cells (MDA-MB-468) with biotinylated-anti-EpCAM antibodies and captured them on the streptavidin surface according to standard protocol. Subsequently, dead cells were stained directly within the chip using 0.4% trypan blue. Cells were screened and images were taken in bright field (Figure 5). The vast majority of MDA-MB-468 cells captured on the chip remained viable showing no evident trypan blue staining. In total, around 10% of dead and 90% of viable cells were detected. Combined with the possibility of removing the

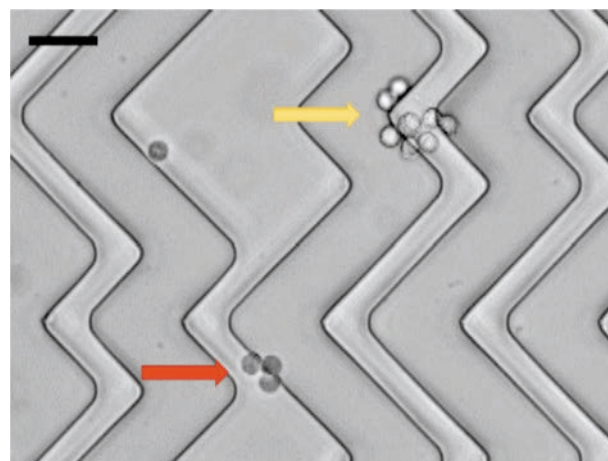


Figure 5. Viability staining of captured cancer cell line cells. Exemplary image of MDA-MB-468 cells taken in bright field, following capture on the chip. An image containing trypan blue stained cells was chosen, while representing the minority, to demonstrate staining efficiency. The herringbone structure of the microfluidic chamber is visible as grey waves. Black scale bar represents 50 μm . Viable cells indicated by yellow arrow and dead cells stained by trypan blue indicated by red arrow.

PDMS microfluidic chamber and placing the glass slide containing the immobilized tumor cells directly into a petri dish for culture, this promising result of 90% viable tumor cells following enrichment with the chip, suggests good starting conditions for future CTC culture.

2.4. Feasibility of the Workflow for Downstream Genomic Analysis of Single Tumor Cells

In order to test the compatibility of our chip workflow with downstream molecular single cell analysis, tumor cell line cells (MCF-7 and SK-MEL-28 cell line cells) were spiked into a background of peripheral blood mononuclear cells (PBMCs), captured on the chip, stained with immunofluorescent markers, and picked by micromanipulation for subsequent whole genome amplification (WGA). As negative control for the WGA, PBS pipetted from the same chip was used, whereas human reference DNA was employed as positive control. Ten MCF-7 and 10 SK-MEL-28 single cells were used for WGA of which 50% (5/10) of the genomes could be successfully amplified at highest quality (4/4 bands) for each cell line, as determined by a multiplex PCR against four different fragments of the human *GAPDH* gene (Figure S2, Supporting Information). An additional single SK-MEL-28 cell showed 1/4 quality control bands, indicating sufficient DNA quality for PCR or Sanger sequencing applications. These results demonstrate compatibility of the CTC chip isolation workflow with micromanipulation and WGA of cells of interest for downstream applications.

3. Conclusion

In this study, we investigated the influence of ceiling structure and target cell concentration on the capture efficiency of

our CTC capture platform based on microarrays. Trialing different design rules, we were able to greatly enhance the capture rate in comparison to our previous design. Compared to other tandem systems such as pre-enrichment by Parsortix and detection via staining on cytopins, our system is performing on a competitive level. Additionally, when the cell loss during pre-enrichment is factored in to enable comparison to other microfluidic chips described in the literature working not as tandem device,^[32,46–49] this chip platform is estimated to have a near full recovery. To further allow the chip platform to unfold its unique potential, necessary pre-enrichment steps will need to be addressed and refined in future studies. Furthermore, the chip platform is suitable for live cell capture, as demonstrated by a 90% viability of captured cells. These could potentially be used for cell culture and further downstream genomic analysis. Microfluidic systems have been shown to outperform the “gold standard” CellSearch device on multiple occasions.^[50–56] However, it is important to keep in mind, that most of these platforms utilize additional or alternative markers for CTC isolation^[50–52] or work with antibody cocktails,^[53,54] thereby complicating the direct comparison of both approaches. At this point in time, we chose EpCAM as a target for CTC capture on our chip in order to demonstrate the feasibility of our workflow using a well-established marker and to allow for future direct comparison to the CellSearch. While we demonstrate capturing by EpCAM, it should be noted that the design allows free exchange of used antibody without need for other changes in setup or operations, thus allowing virtual free choice of target marker. Overall, the optimized chip platform is a very promising tool enabling future studies on CTCs and other potential diagnostic applications.

4. Experimental Section

Microarray Printing: The microarray was printed according to the procedures published previously.^[20] Briefly, the polydimethylsiloxane (PDMS, ABCR, Karlsruhe, Germany) stamps were prepared from silicon master (50 μm and 100 μm pitch) which was previously fabricated by photolithography and chemical etching process. The PDMS stamps were treated with oxygen plasma (0.2 mbar, 100 W, 10 sccm O_2 , 2 min, ATTO system, Diener electronics, Germany) before inking to render the surface hydrophilic. The stamps were spin coated (3000 rpm, 30 s) for homogenous coating with the ink of biotin-4-fluorescein (Sigma-Aldrich, Germany). The stamp was first glued with two component epoxy resin adhesive (UHU, Germany) to a microscopic glass slide, then the whole glass slide was glued to the bar of a custom made holder and rested for 2 min to dry. The stamp holder was then attached to the NLP2000 system (Nanolnk Inc., USA) that offers a piezo-driven stage, able to perform micro-printing. As substrate, the microscopy glass slides (Menzel Gläser, Germany) were sonicated for 10 min each in chloroform, isopropanol, and deionized water. The cleaned microscopy slides were then immersed in a solution of 3% bovine serum albumin (BSA, Sigma-Aldrich, Germany) in phosphate buffered saline (PBS, Sigma-Aldrich, Germany) overnight. The slides were then dipped ten times in ultrapure water (18.2 M Ωcm) to remove the extra BSA and subsequently dried with nitrogen. After this, the BSA-coated substrates were ready to use for the microarray printing. The plasma-cleaned PDMS stamp of area 10 \times 10 mm² was levelled^[29] and contacted once to the substrate for printing patterns having 50 μm distance between ink dots. Then the stamp was moved by 10 mm and contacted again to obtain a large area biotin dots pattern next to the already printed area. This process of printing was repeated four times, resulting in a total

area of 40 \times 10 mm². Printing was done at 50–70% relative humidity and dwell time of 1–10 s. The biotin-4-fluorescein micropatterns were then immediately immobilized by a UV lamp (365 nm, Technotray CU, Heraeus, Germany) for 15 min after printing (bleaching the fluorescein and in the process photochemically binding it to the BSA) and stored at room temperature until use.

Fabrication of the Staggered Herringbone Chip: The microfluidic chips were fabricated in a three-step process. Initially, a mold was produced, that exhibits the inverse of the microfluidic channel including the SHB structure, by photolithographically patterning two layers of a negative photoresist (SU-8, MicroChem, USA) on a silicon wafer. A 50 μm thick layer of SU-8 was spin coated, followed by a soft bake. This layer was exposed to form the negative of the channel without grooves. After post exposure bake and before developing the photoresist, a second layer of SU-8 was spin coated and soft baked. Depending on the design, the rotational speed was altered to reach the groove height. The SU-8 was then exposed to form the negative of the herringbone-shaped channel ceiling. Following another post exposure bake, the pattern was developed. Finished master templates can be reused for replica molding without any noticeable degradation in performance.

In the second step, PDMS prepolymer and its curing agent (Sylgard, 184, Dow Corning, USA) were mixed at 10:1 weight ratio, degassed, and casted to replicate the molding template. After curing on a hot plate (70 $^{\circ}\text{C}$, 4 h), the PDMS replica was carefully released from the mold. Fluidic inlet and outlet ports were punched with a syringe needle.

In the third step, the SHB chip was bonded onto the microarray glass slide by oxygen plasma treatment to form a microfluidic flow chamber. An additional PDMS layer was placed onto the micropattern to protect it during plasma exposure. Finally, tubings (material: PEEK, outer diameter ϕ = 790 μm , inner diameter ϕ = 250 μm , Lab-Smith, USA) were fitted into the punched fluid connector holes to finish the microfluidic chip featuring a direct syringe interface (see Figure 1b for a photograph of a completed chip). The smooth channel comparison chips were produced by attaching a commercially available smooth channel with height h_c = 150 μm (sticky-Slide I 0.1 Luer, ibidi, Germany) onto a microarray glass.

Preparation and Connection of Microfluidic Chips: The connection procedure for the SHB chips was performed according to the procedures published previously.^[20] The ibidi chips (with unstructured channel) were prepared as follows: To provide a steady flow, a 1 mL syringe (BD Bioscience, USA) in a syringe pump (NE-1002X, Fisher Scientific, USA) was directly inserted into the inlet port of an ibidi chip and the outlet port was connected to a tube by a male Luer lock connector (ibidi, Germany) for waste collection. In order to rinse the whole chamber and to block unspecific protein binding at the channel walls before use, 100 μL of PBS with 1% w/v BSA (Sigma-Aldrich, Germany) and 1% v/v Tween20 (Fluka Analytical, Germany) was pumped into the chip and incubated for 15 min. Then the entire solution in the chamber was replaced with 200 μL of cy3 labeled streptavidin in PBS (0.5% v/v). The binding of streptavidin on the biotin patterns was allowed for 20 min. Finally, the chip was flushed with 500 μL PBS to remove excess streptavidin and rendered ready to use.

Standard Cell Culture: MCF-7, MDA-MB-468 breast cancer cell line cells, and SKMEL28 melanoma cell line cells, were cultured in Dulbecco's modified Eagle's medium (Life Technologies, Germany) supplemented with 10% calf bovine serum (Sigma-Aldrich, Germany), 1% L-glutamine (Gibco—Life Technologies, USA), and 1% penicillin/streptomycin (Gibco—Life Technologies, USA) under standard cell culture conditions (37 $^{\circ}\text{C}$ and 5% CO_2).

Preparation of Cell Culture Cells for Chip Experiments: 1 \times 10⁵ MCF-7 cells were sensitized with 0.5 $\mu\text{g mL}^{-1}$ of biotinylated-anti-EpCAM antibody (VU-1D9, Abcam, UK) in a shaker (Eppendorf Thermomixer Comfort, Hamburg, Germany) revolving at 300 rpm at 37 $^{\circ}\text{C}$ for 40 min. The biotinylated cells were then washed with PBS to remove unbound antibody. 100 biotinylated MCF-7 cells were manually counted and mixed with \approx 10000 (based on cell concentration) untreated MCF-7 cells as negative controls in a total volume of 300 μL of pre-warmed 0.1% BSA in PBS buffer (37 $^{\circ}\text{C}$). This mixture was used to test and

compare the recovery of different microfluidic chip designs. For manual spiking, 10 μL of cell culture cell suspension were applied to a petri dish containing 1 \times PBS. The petri dish was then placed under a light microscope and focused on in 5 \times or 10 \times magnification. Using a 10 μL Eppendorf pipette, single cells were manually pipetted into the pipette tip and transferred to the respective background cell solution.

Preparation of “Mock” Blood Samples for Chip Experiments: 7.5 mL of whole blood was collected from healthy donors in accordance to the World Medical Association Declaration of Helsinki and the guidelines for experimentation with human materials by the Chambers of Physicians of the State of Hamburg (“Hamburger Ärztekammer”). Blood was spiked with 100 manually counted MCF-7 cells to mimic clinical cancer patient samples. Manually spiked cells were handled as mentioned above. These “mock” blood samples were pre-enriched using the size-based Parsortix system (ANGLE plc) before applying our microfluidic chip assay. The function and handling of the Parsortix system has been described in detail in prior publications.^[37] The total amount of cells remaining following Parsortix enrichment was between 1500 and 6000 dependent on donor.^[38,39] Cells were harvested into a 1.5 mL reaction tube and centrifuged at 500 \times g, for 5 min to replace the PBS with pre-warmed 0.1% BSA in PBS buffer (37 $^{\circ}\text{C}$). The pre-enriched cells were then incubated with 0.5 $\mu\text{g mL}^{-1}$ of biotinylated-anti-EpCAM antibody (VU-1D9, Abcam, UK) in a shaker (Eppendorf Thermomixer Comfort, Hamburg, Germany) revolving at 300 rpm at 37 $^{\circ}\text{C}$ for 40 min. Following antibody incubation, the cells were centrifuged at 500 \times g, for 5 min to remove excess antibody and subsequently re-suspended in 200 μL of 0.1% BSA/PBS (37 $^{\circ}\text{C}$). The sensitized pre-enriched cell fraction was then pumped into different microfluidic chip designs.

Capture and Staining of Tumor Cells on the Chip: The process of running the microfluidic chip has been described in detail in our prior publication.^[20] In brief, the sensitized cells were pipetted into a 1 mL syringe (BD Bioscience, USA) which was connected to the device. A syringe pump passes the cells into the chip with a steady flow rate of 20 $\mu\text{L min}^{-1}$. During this time, the chips were placed on a hot plate (Heidolph MR Hei-Tec, Schwabach, Germany) set to 37 $^{\circ}\text{C}$. After a 15 min of incubation, the captured cells were fixed with 0.5% paraformaldehyde for 15 min and stained with DAPI (1:1000, Sigma-Aldrich, Germany) and a secondary fluorescently labeled antibody (anti-mouse Alexa488-fluorophore 1:200, Abcam) for 30 min. Finally, chips were flushed with PBS (500 μL , 50 $\mu\text{L min}^{-1}$) and transferred to microscopy for readout.

Readout of the Chips and Analysis: The entire chip area containing the immobilized tumor cells was manually scanned with a 10 \times objective on an upright fluorescence microscope (Eclipse 80i, Nikon Instruments Europe B.V., Germany) and the number of stained tumor cells bound to streptavidin dots was obtained by manual counting.

Viability Assessment of Captured Tumor Cells: Viability of tumor cells captured by the chip was assessed by trypan blue staining. Trypan blue is an azo dye that is only able to enter through the cell membrane of dead cells, staining them in a dark blue color, while live cells remain unstained. The blue color was visible by standard light microscopy. 1×10^6 MDA-MB-468 cells (without leucocyte background) were processed through the chip according to standard protocol in a HC-type chip. A temperature of 37 $^{\circ}\text{C}$ was strictly maintained for the entire duration of the chip run and all used fluids. Following an incubation period of 15 min, 80 μL of 0.4% trypan blue (Sigma-Aldrich, Germany) were passed through the chip at a flow rate of 1.2 mL h^{-1} . Subsequently, excess dye was washed out with 500 μL of PBS and the chip was analyzed by bright-field microscopy (Axiovert 200M, Zeiss, Germany). Random areas of the chip were selected for imaging (Software: Axiovision 4.8.2) and to assess the number of dead cells in relation to viable cells.

Single Cell Manipulation and Downstream Analyses: In order to test the efficiency of the proposed system for downstream genomic analyses, the complete workflow was tested for its compatibility with WGA and molecular characterization of the genomic material. In brief, breast cancer cell line MCF-7 and melanoma cell line SK-MEL-28 cells were transferred into a background of 60000 PBMCs and sensitized with biotinylated-anti-EpCAM antibody (VU-1D9, Abcam, UK) or the

combination of biotinylated MCAM (REA773, Miltenyi, Germany) and NG2 (EP1, Miltenyi, Germany) antibodies, respectively. Next, the enrichment and staining of tumor cells was performed in a HC-type chip as described above. MCF-7 cells were stained with pan-keratin antibody coupled to Alexa 488 (clone AE1/AE3, eBioSciences, USA), and SK-MEL-28 cells were stained with anti-MCAM (clone 541-10B2, Miltenyi, Germany) and anti-NG2 (LMH2, Novus Biological, USA) antibodies both coupled to PhycoErythrin. In both cases DAPI nuclear staining was performed. The chips were opened by removing the microfluidic chamber from the printed slide by cutting the PDMS layer with a scalpel. Single tumor cells ($n = 10$ for each cell line) were isolated from the pattern by micromanipulation, individually transferred into 0.2 mL PCR tubes and immediately frozen at -80°C . Next, WGA was performed using the Ampli1 WGA kit (Menarini Silicon Biosystems, Italy) according to the manufacturer's recommendations. The quality of the amplified DNA was assessed by multiplex PCR producing 96, 108–166, 299, and 614 bp fragments from target sites in the *GAPDH* gene using the Ampli1 QC Kit (Menarini Silicon Biosystems, Italy). PCR products were analyzed in a 1.2% agarose TAE ethidium bromide stained gel.

Statistical Analysis: Statistical analyses were performed in R.^[57] ANOVA followed by Tukey's pairwise analyses were employed to test the capture efficiency of the different ceiling type structures and patterns under the two different cell concentration conditions, as well as to test the recovery of spiking experiments using the different SHB structures. p -values of ≤ 0.005 were considered statistically significant as recommended by novel statistical guidelines.^[58]

Supporting Information

Supporting Information is available from the Wiley Online Library or from the author.

Acknowledgements

H.-Y.L., C.K., and A.H. contributed equally to this work. The authors thank Prof. Andrew C. Cato (ITG, KIT) for access to his lab and fruitful discussions. This work was partly carried out with the support of the Karlsruhe Nano Micro Facility (KNMF, www.knmf.kit.edu), a Helmholtz Research Infrastructure at Karlsruhe Institute of Technology (KIT, www.kit.edu) and supported by the European Research Council (ERC) in a proof of concept grant.

Conflict of Interest

H.F., K.P., and M.H. have applied for a patent regarding the microarray capture platform (WO 2016/128125 A1).

Keywords

breast cancer, circulating tumor cells, microfluidics, polymer pen lithography, staggered herringbone design

Received: July 25, 2019

Revised: November 26, 2019

Published online: December 23, 2019

[1] WHO cancer fact sheet, <http://www.who.int/news-room/fact-sheets/detail/cancer> (accessed: November, 2019).

[2] C. Chaffer, R. Weinberg, *Science* **2011**, 331, 1559.

- [3] S. A. Joosse, T. M. Gorges, K. Pantel, *EMBO Mol. Med.* **2015**, *7*, 1.
- [4] S. Riethdorf, V. Müller, S. Loibl, V. Nekljudova, K. Weber, J. Huober, T. Fehm, I. Schrader, J. Hilfrich, F. Holms, H. Tesch, C. Schem, G. Von Minckwitz, M. Untch, K. Pantel, *Clin. Cancer Res.* **2017**, *23*, 5384.
- [5] F.-C. Bidard, S. Michiels, S. Riethdorf, V. Mueller, L. J. Esserman, A. Lucci, B. Naume, J. Horiguchi, R. Gisbert-Criado, S. Sleijfer, M. Toi, J. A. Garcia-Saenz, A. Hartkopf, D. Generali, F. Rothé, J. Smerage, L. Muinelo-Romay, J. Stebbing, P. Viens, M. J. M. Magbanua, C. S. Hall, O. Engebraaten, D. Takata, J. Vidal-Martínez, W. Onstenk, N. Fujisawa, E. Diaz-Rubio, F.-A. Taran, M. R. Cappelletti, M. Ignatiadis, et al., *JNCI, J. Natl. Cancer Inst.* **2018**, *110*, 560.
- [6] F.-C. Bidard, D. J. Peeters, T. Fehm, F. Nolé, R. Gisbert-Criado, D. Mavroudis, S. Grisanti, D. Generali, J. A. Garcia-Saenz, J. Stebbing, C. Caldas, P. Gazzaniga, L. Manso, R. Zamarchi, A. F. de Lascoiti, L. De Mattos-Arruda, M. Ignatiadis, R. Lebofsky, S. J. van Laere, F. Meier-Stiegen, M.-T. Sandri, J. Vidal-Martínez, E. Politaki, F. Consoli, A. Bottini, E. Diaz-Rubio, J. Krell, S.-J. Dawson, C. Raimondi, A. Rutten, et al., *Lancet Oncol.* **2014**, *15*, 406.
- [7] H. I. Scher, G. Heller, A. Molina, G. Attard, D. C. Danila, X. Jia, W. Peng, S. K. Sandhu, D. Olmos, R. Riisnaes, R. McCormack, T. Burzykowski, T. Kheoh, M. Fleisher, M. Buyse, J. S. de Bono, *J. Clin. Oncol.* **2015**, *33*, 1348.
- [8] H. I. Scher, R. P. Graf, N. A. Schreiber, B. McLaughlin, D. Lu, J. Louw, D. C. Danila, L. Dugan, A. Johnson, G. Heller, M. Fleisher, R. Dittamore, *Eur. Urol.* **2017**, *71*, 874.
- [9] M. G. Krebs, R. Sloane, L. Priest, L. Lancashire, J.-M. Hou, A. Greystoke, T. H. Ward, R. Ferraldeschi, A. Hughes, G. Clack, M. Ranson, C. Dive, F. H. Blackhall, *J. Clin. Oncol.* **2011**, *29*, 1556.
- [10] M. Cristofanilli, G. Budd, N. Engl. J. Med. **2004**, *351*, 781.
- [11] S. J. Cohen, C. J. A. Punt, N. Iannotti, B. H. Saidman, K. D. Sabbath, N. Y. Gabrail, J. Picus, M. Morse, E. Mitchell, M. C. Miller, G. V. Doyle, H. Tissing, L. W. M. M. Terstappen, N. J. Meropol, *J. Clin. Oncol.* **2008**, *26*, 3213.
- [12] J. S. De Bono, H. I. Scher, R. B. Montgomery, C. Parker, M. C. Miller, H. Tissing, G. V. Doyle, L. W. M. M. Terstappen, K. J. Pienta, D. Raghavan, *Clin. Cancer Res.* **2008**, *14*, 6302.
- [13] C. Alix-Panabières, K. Pantel, *Cancer Discovery* **2016**, *6*, 479.
- [14] A. Bardelli, K. Pantel, *Cancer Cell* **2017**, *31*, 172.
- [15] C. Alix-Panabières, K. Pantel, *Nat. Rev. Cancer* **2014**, *14*, 623.
- [16] C. Alix-Panabières, K. Pantel, *Lab Chip* **2014**, *14*, 57.
- [17] S. Riethdorf, L. O'Flaherty, C. Hille, K. Pantel, *Adv. Drug Delivery Rev.* **2018**, *125*, 102.
- [18] C. Alix-Panabières, S. Mader, K. Pantel, *J. Mol. Med.* **2017**, *95*, 133.
- [19] C. L. Chaffer, B. P. San Juan, E. Lim, R. A. Weinberg, *Cancer Metastasis Rev.* **2016**, *35*, 645.
- [20] F. Brinkmann, M. Hirtz, A. Haller, T. M. Gorges, M. J. Vellekoop, S. Riethdorf, V. Müller, K. Pantel, H. Fuchs, *Sci. Rep.* **2015**, *5*, 15342.
- [21] F. Huo, Z. Zheng, G. Zheng, L. R. Giam, H. Zhang, C. A. Mirkin, *Science* **2008**, *321*, 1658.
- [22] R. D. Piner, J. Zhu, F. Xu, S. Hong, C. A. Mirkin, *Science* **1999**, *283*, 661.
- [23] D. J. Eichelsdoerfer, X. Liao, M. D. Cabezas, W. Morris, B. Radha, K. A. Brown, L. R. Giam, A. B. Braunschweig, C. A. Mirkin, *Nat. Protoc.* **2013**, *8*, 2548.
- [24] L. R. Giam, M. D. Massich, L. Hao, L. Shin Wong, C. C. Mader, C. A. Mirkin, *Proc. Natl. Acad. Sci. USA* **2012**, *109*, 4377.
- [25] R. Kumar, A. Urtizberea, S. Ghosh, U. Bog, Q. Rainer, S. Lenhert, H. Fuchs, M. Hirtz, *Langmuir* **2017**, *33*, 8739.
- [26] Z. Zheng, W. L. Daniel, L. R. Giam, F. Huo, A. J. Senesi, G. Zheng, C. A. Mirkin, *Angew. Chem., Int. Ed.* **2009**, *48*, 7626.
- [27] F. Brinkmann, M. Hirtz, A. M. Greiner, M. Weschenfelder, B. Waterkotte, M. Bastmeyer, H. Fuchs, *Small* **2013**, *9*, 3265.
- [28] G. Arrabito, H. Schroeder, K. Schröder, C. Filips, U. Marggraf, C. Dopp, M. Venkatachalapathy, L. Dehmelt, P. I. H. Bastiaens, A. Neyer, C. M. Niemeyer, *Small* **2014**, *10*, 2870.
- [29] R. Kumar, S. Weigel, R. Meyer, C. M. Niemeyer, H. Fuchs, M. Hirtz, *Chem. Commun.* **2016**, *52*, 12310.
- [30] R. Kumar, A. Bonicelli, S. Sekula-Neuner, A. C. B. Cato, M. Hirtz, H. Fuchs, *Small* **2016**, *12*, 5330.
- [31] A. D. Stroock, S. K. W. Dertinger, A. Ajdari, I. Mezic, H. A. Stone, G. M. Whitesides, *Science* **2002**, *295*, 647.
- [32] S. L. Stott, C. Hsu, D. I. Tsukrov, M. Yu, D. T. Miyamoto, B. A. Waltman, S. M. Rothenberg, A. M. Shah, M. E. Smas, G. K. Korir, F. P. Floyd, A. J. Gilman, J. B. Lord, D. Winokur, S. Springer, D. Irimia, S. Nagrath, L. V. Sequist, R. J. Lee, K. J. Isselbacher, S. Maheswaran, D. A. Haber, M. Toner, *Proc. Natl. Acad. Sci. USA* **2010**, *107*, 18392.
- [33] T. P. Forbes, J. G. Kralj, *Lab Chip* **2012**, *12*, 2634.
- [34] N. S. Lynn, J. Homola, *Anal. Chem.* **2015**, *87*, 5516.
- [35] N. S. Lynn, M. Bocková, P. Adam, J. Homola, *Anal. Chem.* **2015**, *87*, 5524.
- [36] A. Grimmer, X. Chen, M. Hamidović, W. Haselmayr, C. L. Ren, R. Wille, *RSC Adv.* **2018**, *8*, 34733.
- [37] G. E. E. Hvichia, Z. Parveen, C. Wagner, M. Janning, J. Quidde, A. Stein, V. Müller, S. Loges, R. P. L. Neves, N. H. H. Stoecklein, H. Wikman, S. Riethdorf, K. Pantel, T. M. T. M. Gorges, *Int. J. Cancer* **2016**, *138*, 2894.
- [38] M. C. Miller, P. S. Robinson, C. Wagner, D. J. O'Shannessy, *Cytometry, Part A* **2018**, *93*, 1234.
- [39] J. Chudziak, D. J. Burt, S. Mohan, D. G. Rothwell, B. Mesquita, J. Antonello, S. Dalby, M. Ayub, L. Priest, L. Carter, M. G. Krebs, F. Blackhall, C. Dive, G. Brady, *Analyst* **2016**, *141*, 669.
- [40] Z. Shen, A. Wu, X. Chen, *Chem. Soc. Rev.* **2017**, *46*, 2038.
- [41] N. H. Stoecklein, J. C. Fischer, D. Niederacher, L. W. M. M. Terstappen, *Expert Rev. Mol. Diagn.* **2016**, *16*, 147.
- [42] L. Cayrefourcq, T. Mazard, S. Joosse, J. Solassol, J. Ramos, E. Assenat, U. Schumacher, V. Costes, T. Maudelonde, K. Pantel, C. Alix-Panabières, *Cancer Res.* **2015**, *75*, 892.
- [43] Y. Su, T. J. Pogash, T. D. Nguyen, J. Russo, *Cancer Med.* **2016**, *5*, 558.
- [44] M. Yu, A. Bardia, N. Aceto, F. Bersani, M. W. Madden, M. C. Donaldson, R. Desai, H. Zhu, V. Comaills, Z. Zheng, B. S. Wittner, P. Stojanov, E. Brachtel, D. Sgroi, R. Kapur, T. Shioda, D. T. Ting, S. Ramaswamy, G. Getz, A. J. Iafrate, C. Benes, M. Toner, S. Maheswaran, D. A. Haber, *Science* **2014**, *345*, 216.
- [45] A. Franken, C. Driemel, B. Behrens, F. Meier-Stiegen, V. Endris, A. Stenzinger, D. Niederacher, J. C. Fischer, N. H. Stoecklein, E. Ruckhaeberle, T. Fehm, H. Neubauer, *Clin. Chem.* **2019**, *65*, 549.
- [46] S. Wang, K. Liu, J. Liu, Z. T.-F. Yu, X. Xu, L. Zhao, T. Lee, E. K. Lee, J. Reiss, Y.-K. Lee, L. W. K. Chung, J. Huang, M. Rettig, D. Seligson, K. N. Duraiswamy, C. K.-F. Shen, H.-R. Tseng, *Angew. Chem., Int. Ed.* **2011**, *50*, 3084.
- [47] H. J. Yoon, T. H. Kim, Z. Zhang, E. Azizi, T. M. Pham, C. Paoletti, J. Lin, N. Ramnath, M. S. Wicha, D. F. Hayes, D. M. Simeone, S. Nagrath, *Nat. Nanotechnol.* **2013**, *8*, 735.
- [48] W. Sheng, O. O. Ogunwobi, T. Chen, J. Zhang, T. J. George, C. Liu, Z. H. Fan, *Lab Chip* **2014**, *14*, 89.
- [49] Y. Song, Y. Shi, M. Huang, W. Wang, Y. Wang, J. Cheng, Z. Lei, Z. Zhu, C. Yang, *Angew. Chem., Int. Ed.* **2019**, *58*, 2236.
- [50] B. J. Kirby, M. Jodari, M. S. Loftus, G. Gakhar, E. D. Pratt, C. Chanel-Vos, J. P. Gleghorn, S. M. Santana, H. Liu, J. P. Smith, V. N. Navarro, S. T. Tagawa, N. H. Bander, D. M. Nanus, P. Giannakakou, *PLoS One* **2012**, *7*, e35976.
- [51] K. Yoneda, T. Kuwata, Y. Chikaishi, M. Mori, M. Kanayama, M. Takenaka, S. Oka, A. Hirai, N. Imanishi, K. Kuroda, Y. Ichiki, T. Ohnaga, F. Tanaka, *Cancer Sci.* **2019**, *110*, 726.
- [52] J. Jiang, H. Zhao, W. Shu, J. Tian, Y. Huang, Y. Song, R. Wang, E. Li, D. Slamon, D. Hou, X. Du, L. Zhang, Y. Chen, Q. Wang, *Sci. Rep.* **2017**, *7*, 42612.
- [53] C. V. Pecot, F. Z. Bischoff, J. A. Mayer, K. L. Wong, T. Pham, J. Bottsford-Miller, R. L. Stone, Y. G. Lin, P. Jaladurgam, J. W. Roh,

- B. W. Goodman, W. M. Merritt, T. J. Pircher, S. D. Mikolajczyk, A. M. Nick, J. Celestino, C. Eng, L. M. Ellis, M. T. Deavers, A. K. Sood, *Cancer Discovery* **2011**, 1, 580.
- [54] D. Issadore, J. Chung, H. Shao, M. Liong, A. A. Ghazani, C. M. Castro, R. Weissleder, H. Lee, *Sci. Transl. Med.* **2012**, 4, 141ra92.
- [55] E. Ozkumur, A. M. Shah, J. C. Ciciliano, B. L. Emmink, D. T. Miyamoto, E. Brachtel, M. Yu, P.-I. Chen, B. Morgan, J. Trautwein, A. Kimura, S. Sengupta, S. L. Stott, N. M. Karabacak, T. A. Barber, J. R. Walsh, K. Smith, P. S. Spuhler, J. P. Sullivan, R. J. Lee, D. T. Ting, X. Luo, A. T. Shaw, A. Bardia, L. V. Sequist, D. N. Louis, S. Maheswaran, R. Kapur, D. A. Haber, M. Toner, *Sci. Transl. Med.* **2013**, 5, 179ra47.
- [56] S. Ribeiro-Samy, M. I. Oliveira, T. Pereira-Veiga, L. Muinelo-Romay, S. Carvalho, J. Gaspar, P. P. Freitas, R. López-López, C. Costa, L. Diéguez, *Sci. Rep.* **2019**, 9, 8032.
- [57] R. C. Team, R: A language and environment for statistical computing, <https://www.r-project.org> (accessed: November 2019).
- [58] D. J. Benjamin, J. O. Berger, M. Johannesson, B. A. Nosek, E.-J. Wagenmakers, R. Berk, K. A. Bollen, B. Brembs, L. Brown, C. Camerer, D. Cesarini, C. D. Chambers, M. Clyde, T. D. Cook, P. De Boeck, Z. Dienes, A. Dreber, K. Easwaran, C. Efferson, E. Fehr, F. Fidler, A. P. Field, M. Forster, E. I. George, R. Gonzalez, S. Goodman, E. Green, D. P. Green, A. G. Greenwald, J. D. Hadfield, et al., *Nat. Hum. Behav.* **2018**, 2, 6.

Proficiency Testing to Assess Technical Performance for CTC-Processing and Detection Methods in CANCER-ID

Rui P.L. Neves,^{a,†} Wim Ammerlaan,^{b,†} Kiki C. Andree,^c Sebastian Bender,^d Laure Cayrefourcq,^e Christiane Driemel,^a Claudia Koch,^f Merlin Verena Luetke-Eversloh,^d Marianne Oulhen,^g Elisabetta Rossi,^{h,i} Catherine Alix-Panabières,^e Fay Betsou,^b Françoise Farace,^g Sabine Riethdorf,^f Thomas Schlange,^d Harriet Wikman,^f Rita Zamarchi,ⁱ Klaus Pantel,^f Leon W.M.M. Terstappen,^c and Nikolas H. Stoecklein,^{a,*} for the CANCER-ID Consortium

BACKGROUND: Multiple technologies are available for detection of circulating tumor cells (CTCs), but standards to evaluate their technical performance are still lacking. This limits the applicability of CTC analysis in clinic routine. Therefore, in the context of the CANCER-ID consortium, we established a platform to assess technical validity of CTC detection methods in a European multi-center setting using non-small cell lung cancer (NSCLC) as a model.

METHODS: We characterized multiple NSCLC cell lines to define cellular models distinct in their phenotype and molecular characteristics. Standardized tumor-cell-bearing blood samples were prepared at a central laboratory and sent to multiple European laboratories for processing according to standard operating procedures. The data were submitted via an online tool and centrally evaluated. Five CTC-enrichment technologies were tested.

RESULTS: We could identify 2 cytokeratin expressing cell lines with distinct levels of EpCAM expression: NCI-H441 (EpCAM^{high}, CK^{pos}) and NCI-H1563 (EpCAM^{low}, CK^{pos}). Both spiked tumor cell lines were detected by all technologies except for the CellSearch system that failed to enrich EpCAM^{low} NCI-H1563 cells. Mean recovery rates ranged between 49% and 75% for NCI-H411 and 32% and 76% for NCI-H1563 and significant differences were observed between the tested methods.

CONCLUSIONS: This multi-national proficiency testing of CTC-enrichment technologies has importance in the establishment of guidelines for clinically applicable (pre)analytical workflows and the definition of minimal performance qualification requirements prior to clinical validation of technologies. It will remain in operation beyond the funding period of CANCER-ID in the context of the European Liquid Biopsy Society (ELBS).

Introduction

Circulating tumor cells (CTCs) are cancer cells that have entered the blood stream and can become detectable in the peripheral blood. CTCs have become of high interest since they can provide direct access to systemic cancer hallmarks with the potential to develop superior assays for detection, analysis, and treating systemic cancer (1–4). When compared to other circulating biomarkers, the clear advantage of CTCs is that they can provide cancer-related information on the DNA, RNA, and protein levels, which might be used for more rational treatment decisions.

Since CTC concentration in blood is extremely low and cancer specific markers are lacking, their enrichment and detection remains very challenging (5). In addressing these challenges, several platforms have been established to enrich and detect CTCs in blood samples. According to their underlying principle, current CTC-

^aDepartment of General, Visceral and Paediatric Surgery, University Hospital and Medical Faculty of the Heinrich-Heine University Düsseldorf, Düsseldorf, Germany; ^bIntegrated BioBank of Luxembourg, Dudelange, Luxembourg; ^cDepartment of Medical Cell BioPhysics, University of Twente, Enschede, The Netherlands; ^dBayer AG, Biomarker Research, Wuppertal, Germany; ^eLaboratory of Rare Human Circulating Cells, University Medical Centre of Montpellier, Montpellier, France; ^fInstitute of Tumor Biology, University Medical Center Hamburg-Eppendorf, Hamburg, Germany; ^gGustave Roussy, Université Paris-Saclay, "Circulating Tumor Cells" Translational Platform, CNRS UMS3655-INERM US23 AMMICA, Villejuif, France; ^hDepartment of Surgery, Oncology

and Gastroenterology, University of Padova, Padua, Italy; ⁱVeneto Institute of Oncology IOV-IRCCS, Padua, Italy.

*Address correspondence to this author at: Department of General, Visceral and Pediatric Surgery, University Hospital of the Heinrich-Heine University Düsseldorf, Moorenstr. 5, 40225 Düsseldorf, Germany. Fax 0049-2118104494; e-mail nikolas.stoecklein@uni-duesseldorf.de.

[†]These authors contributed equally to the work.

Received May 28, 2020; accepted November 12, 2020.

DOI: 10.1093/clinchem/hvaa322

enrichment methods can be divided into 2 groups: one targets biological properties of CTCs (marker dependent) and the other their biophysical characteristics (marker independent) (6, 7). The prevailing strategy for the first group is immuno-magnetic enrichment via conjugated antibodies directed against EpCAM, a membrane-protein widely expressed in different cancer types (8). This first strategy avoids the loss of deformable CTCs with small sizes. The second group utilizes differences in size, deformability, or electric properties to capture CTCs. This could be advantageous if cells do not express typical epithelial markers such as EpCAM [e.g., due to epithelial-to-mesenchymal transition (EMT)] (9). EpCAM-based enrichment is also employed in the CellSearch[®] system. This system is FDA-cleared for CTC analysis in metastatic breast, prostate, and colorectal cancers (10, 11). However, the prognostic significance of CTCs detected by CellSearch has been demonstrated for several cancer entities (12), including non-small cell lung cancer (NSCLC) (13). Since the introduction of the CellSearch[®] system around 15 years ago, more than 40 CTC-detection systems have become commercially available. In view of the promises for therapy prediction in personalized medicine, the global forecasts for the CTC market have been very optimistic with compound annual growth rates of up to 23% to attain an expected global market value of around 28 billion USD by the end of 2023 (14). In light of these developments, it is surprising that for almost all available CTC-technologies (with the exception of the CellSearch[®] system) large multicenter trials to show clinical validity have been missing, a fundamental requirement for more complex trials testing predictive value or even their routine clinical use. An obvious reason for this is the associated costs, which are difficult to cover for small and medium sized enterprises (SMEs) or academic groups, from which most technologies emerged.

However, an essential step for each CTC-detection method on the way to demonstrate clinical utility is to establish first its technical validity. This is already a complex, time consuming, and expensive task that appears challenging for most technology developers. This dilemma and the wish to support current and future CTC-technology developers triggered the idea to establish a sustainable proficiency testing platform to benchmark technical performance for CTC-detection methods and to allow for independent comparison of different technologies. The proficiency testing platform was developed within the frame of the Innovative Medicines Initiative (IMI) consortium CANCER-ID (15), which aims to test standard operating procedures (SOPs) for preanalytical sample handling and detection of CTCs in NSCLC as a blood-based biomarker. The increasing number of treatment options for patients

with NSCLC has created a need for biomarkers to stratify patients and/or to monitor patient's response. In this context, CTCs could be a valuable source of tumor material fulfilling this need; however, detection of NSCLC CTCs remains a major challenge due to their rarity and their potential phenotypical heterogeneity. Here, we present the first results of this proficiency testing platform for CTC enrichment/isolation/detection technologies. As quality control materials, we used NSCLC cell lines spiked blood.

Materials and Methods

PREPARATION AND SHIPPING OF SPIKED SAMPLES

Blood collection and preparation of spiked samples were done at Integrated Biobank of Luxembourg (IBBL). On the day of spiking, blood was collected from 1 healthy donor under informed consent "CNER: 201107/02" version 1.3 and following amendments (approved by the local Luxembourg ethic committee) directly into the blood collection tubes (BCTs) indicated in the SOPs of the different technology providers: CellSearch[®] and VyCAP Microsieves required CellSave Preservative Tubes (Menarini), Siemens and Parsortix[®] used CTC TransFix EDTA tubes (Cytomark), and RareCyte used AccuCyte[®] BCT (RareCyte). NCI-H441 and NCI-H1563 cell lines in culture (Supplemental Methods) were harvested following standard treatment with trypsin, and quantified and evaluated for their viability and cell size using the Cell Counter CASY (OLS). Subsequently cells were stabilized with the fixation solution from the BCT required by the respective SOP, diluted to 15000 cells/mL and stained with Hoechst 33342 nuclear marker (Thermo Scientific). For the RareCyte spike in tests, cells were stained with 0.5 nmol/L Syto-83 (Thermo Fisher Scientific) because of possible interference of Hoechst with the downstream analysis. Two to 3 drops of 2 μ L of stained cell suspension were placed unto a 1% BSA/PBS precoated microscope slide. Stained nuclei were counted by fluorescence microscopy, and if in the range of 50 to 100 cells in total, flushed into the collected blood with 200 μ L PBS. On the same day, the spiked blood samples were shipped to the participants' sites by overnight shipment via courier. Shipping conditions were according to the provided SOPs: the CellSave ensures sample stability for 4 days at a temperature range of 15°–30°C; the TransFix ensures sample stability for 5 days at a temperature range of 18°–25°C and required special room temperature isothermal packaging. The AccuCyte[®] BCTs have a maximum processing delay of 3 days and require a transport temperature range of 20°–25°C. This procedure was repeated twice using blood from a different donor each time, with 1-week intervals, resulting in 3 enumerations with blood from 3 different

Proficiency Testing of CTC Detection Methods

donors, per platform per cell line per site. All the participant sites were informed in advance of the shipping dates.

ENRICHMENT OF CTCs AND REPORT OF RESULTS

Five methods for CTC-enrichment were tested: the CellSearch[®] system (Menarini Silicon Biosystems); VyCAP Microsieves (VyCAP); Siemens filtration unit (Siemens; prototype is not for sale); Parsortix[®] (ANGLE); and RareCyte platform (RareCyte) (Table 1), using

consensus SOPs (Supplemental Methods). For all technologies, detection of spiked cells after enrichment was based on immunofluorescence staining and fluorescent microscope imaging (Supplemental Methods). Results were reported using an online questionnaire made available to the sites in the secured web-based reporting tool within the Biospecimen Proficiency Testing Programme of Integrated BioBank of Luxembourg (IBBL) (16) (Supplemental Methods, Supplemental Fig. 1).

Table 1. Main characteristics of the technologies tested.

Characteristics provided by the manufacturers					
Technology	Siemens	Parsortix [®]	VyCAP	CellSearch [®]	RareCyte
Enrichment principle	Filtration	Filtration	Filtration	Immunomagnetic	Density
Enrichment criterion	Size >8 µm	Size >6.5 µm	Size >5 µm	EpCAM positivity	Density < 1.1 g/mL
Detection principle	Fluorescence microscopy	Fluorescence microscopy	Fluorescence microscopy	Fluorescence microscopy	Fluorescence microscopy
Staining method	Automated	Manual	Manual	Automated	Automated
Detection system	User-provided microscope	User-provided microscope	User-provided microscope	Integrated microscope (Cell Tracks)	Integrated microscope (CyteFinder)
CTC identification modus	Manual	Manual	Manual	Semi-automated	Semi-automated
Reagents	Provided in SOP	Provided in SOP	Provided in SOP	Provided as an IVD assay	Provided as a kit
CTC definition	DAPI ^{pos} , CK(A53-B/A2+UCD/PR10.11) ^{pos} , CD45(9.4) ^{neg} , CD66b(G10F5) ^{neg}	DAPI ^{pos} , CK(EP1628Y+EP1580Y) ^{pos} , CD45(5B1) ^{neg}	DAPI ^{pos} , CK(C11+ AE1/AE3) ^{pos} , CD45(HI30) ^{neg}	DAPI ^{pos} , CK ^{pos} , CD45 ^{neg}	SYTOX Orange ^{pos} , CK/EpCAM ^{pos} , CD45(HI30) ^{neg}
Type of tube (sample volume)	TransFix TVT-09-50-45 (9 mL)	TransFix TVT-09-01 (9 mL)	CellSave (10 mL)	CellSave (10 mL)	AccuCyte BCT (9 mL)
Blood volume used on assay	9 mL	9 mL	10 mL	7.5 mL	7.5 mL
Parallel processing of samples	Yes	No	Yes	Yes	Yes
Throughput	20 samples/week	15 samples/week	50 samples/week	40 samples/week	15 samples/week
Characteristics assessed by the users					
Technology	Siemens	Parsortix [®]	VyCAP	CellSearch	RareCyte
Level of automation ^{ab} (enrichment)	3-4	2-4	2	4-5	2
Hands-on time needed ^{bc} (enrichment/staining)	20-45 min	20-45 min	20-60 min	20-30 min	105 min
Level of automation ^{ab} (identification)	1	1	1 - 2	3 - 4	4
Hands-on time needed ^{bc} (identification)	30 - 60 min	15 - 60 min	15-20 min	10 - 40 min	45 min
Total time until results ^{bc}	5 - 6 h	2 - 3.5 h	1.5 - 2 h	3 - 3.5 h	1.5 days

^aLevel of automation was graded from 1 (bad) to 5 (very good). ^bThe values presented are the range of the values attributed by different groups. ^cThe time refer to one single sample in one single run.

STATISTICAL ANALYSES

Statistical analyses were performed as described in the [Supplemental Methods](#).

Results

RATIONALE FOR THE SELECTION OF NCI-H441 AND NCI-H1563 LUNG CANCER CELL LINES FOR RING-TRIALS

For our testing platform for CTC-detection methods, we aimed to provide 2 lung cancer cell lines with strong differences in the expression of EpCAM, frequently used as cell surface antigen for label-dependent enrichment of CTCs (7, 17). In particular, we aimed to identify cell lines fulfilling 3 criteria: 1) All cell lines should express cytokeratin (CK), since this has become the standard marker for CTC identification by immunostaining; 2) Cell lines should have a differential expression of EpCAM to test marker-dependent and -independent platforms; 3) Cell line cells should be different in size to test size-dependent methods. Of the 21 NSCLC cell lines available among the CANCER-ID partners, we selected 9 for further analysis based on their EpCAM and CK RNA expression levels ([Supplemental Fig. 2](#)). As expected, EpCAM expression correlated positively with the expression of E-cadherin (CDH1) and other epithelial markers among the different NSCLC lines, but negatively with the mesenchymal markers vimentin (VIM) and N-cadherin (CDH2) ([Supplemental Fig. 2C](#)). Using flow cytometry, we quantified then the exact number of EpCAM (range: 4.3×10^3 — 1.1×10^6 antibodies bound per cell [ABC]) and CK (range: 1.6×10^4 — 1.1×10^5 ABC) epitopes per cell for each cancer cell line ([Supplemental Figs. 3 and 4](#)). Next, we determined the cell size, which did not vary substantially between the cancer cell lines (range: 14.7 - 18.2 μm) ([Supplemental Fig. 3](#)). Based on these results, we chose one EpCAM^{high} cell line (NCI-H411) and one EpCAM^{low} cell line (NCI-H1563) ([Fig. 1A–D](#)). Notably, each of the 2 cancer cell lines harbored a unique mutation pattern in KRAS, TP53, and EGFR genes ([Supplemental Fig. 2D](#)), and high intra-line genomic similarity ([Fig. 1E](#)).

RECOVERY OF SPIKED CELLS USING DIFFERENT TECHNOLOGIES

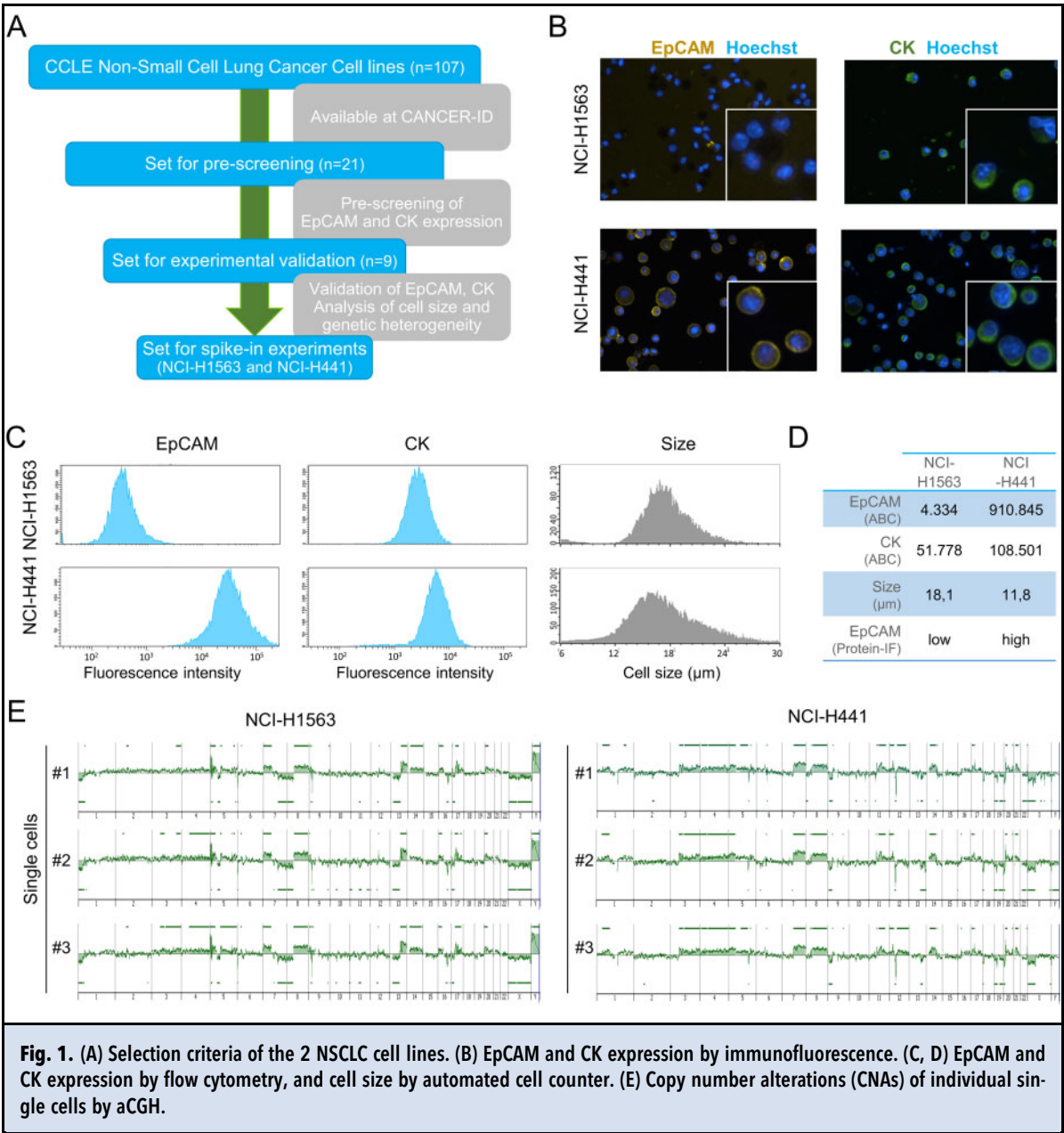
To test the 5 CTC-enrichment methods, a total of 98 samples were prepared at the central laboratory (IBBL, Luxembourg) and shipped to 9 participating sites in 6 countries (Germany, France, Belgium, Netherlands, Switzerland, Italy) according to the recommendations of the manufacturers of the preservative tubes ([Fig. 2A and B](#)). Siemens and VyCAP platforms were available at 4 participating sites, while Parsortix, CellSearch, and Rarecyte were tested in 3 sites ([Table 2](#)). The number of

cells spiked per sample ranged from 51 to 99 (mean: 77.5; median: 78) and it did not differ significantly between the samples to be analyzed with the different technologies. The mean viability over all the spike-in experiments for NCI-H441 was 95.1% (range: 91.8%—98.4%) and for NCI-H1563 was 96.6% (range: 93.0%—98.1%), and no significant variation in cellular size was observed during the experimental period.

In the present work, a majority of samples arrived at the participating sites on the next working day (within 24 h after samples preparation). The exceptions were 2 of the 27 shipments where there was a 1 day delay in delivery; as this was still within the recommended time limits of the tube manufacturers, samples were further processed. For 2 other samples, blood aggregates were visible upon arrival. These samples were sent to the same participating site during a period with atmospheric temperatures above 30 °C, the maximum recommended for correct stabilization in CellSave tubes, a factor that might have contributed to the poor condition of the samples. These were not further processed and were replaced by new samples sent in a new batch. Samples were processed at the analytical sites within 36 h after sample preparation. Spiked cells could be identified in 94 out of the remaining 96 samples processed ([Fig. 3A, Table 2](#)). The exceptions were 2 samples processed with the VyCAP Microsieves: one without stained cells and one with an abnormally high number of cells on the filter and nonspecific staining of CD45 on CK^{pos} cells. In some Siemens and VyCAP filters, the phenotypical evaluation of enriched cells, important for identification of intact cells, was compromised. This was likely due to the irregular surface of the filters (in the case of Siemens unit) and to the cellular distortions caused by the pressure necessary to make cells pass through the pores of the filters (in the case of both units). Standard automatic scanning of the irregular surface of the Siemens filters was not possible and was limited to one laboratory that was able to customize the scanning software for this application ([Supplemental Table 1](#), participating site #5). In addition, automatic scanning of Parsortix[®] was not practicable due to the large area and the depth of chamber in which cells are captured.

As expected, the EpCAM^{low} NCI-H1563 cells could not be detected by CellSearch[®] and were therefore excluded from the ring experiment testing this system ([Fig. 3B and C](#)). Collectively for NCI-H441 cells, recoveries with the Parsortix[®] (mean: 71%), CellSearch (mean: 75%), and RareCyte (mean: 68%) systems were significantly higher than with the Siemens (mean: 54%) and the VyCAP (mean: 49%) systems ($P < 0.05$ by Mann-Whitney U test).

For NCI-H1563 cells, recoveries with Parsortix[®] (mean: 67%) and RareCyte (mean: 76%) were

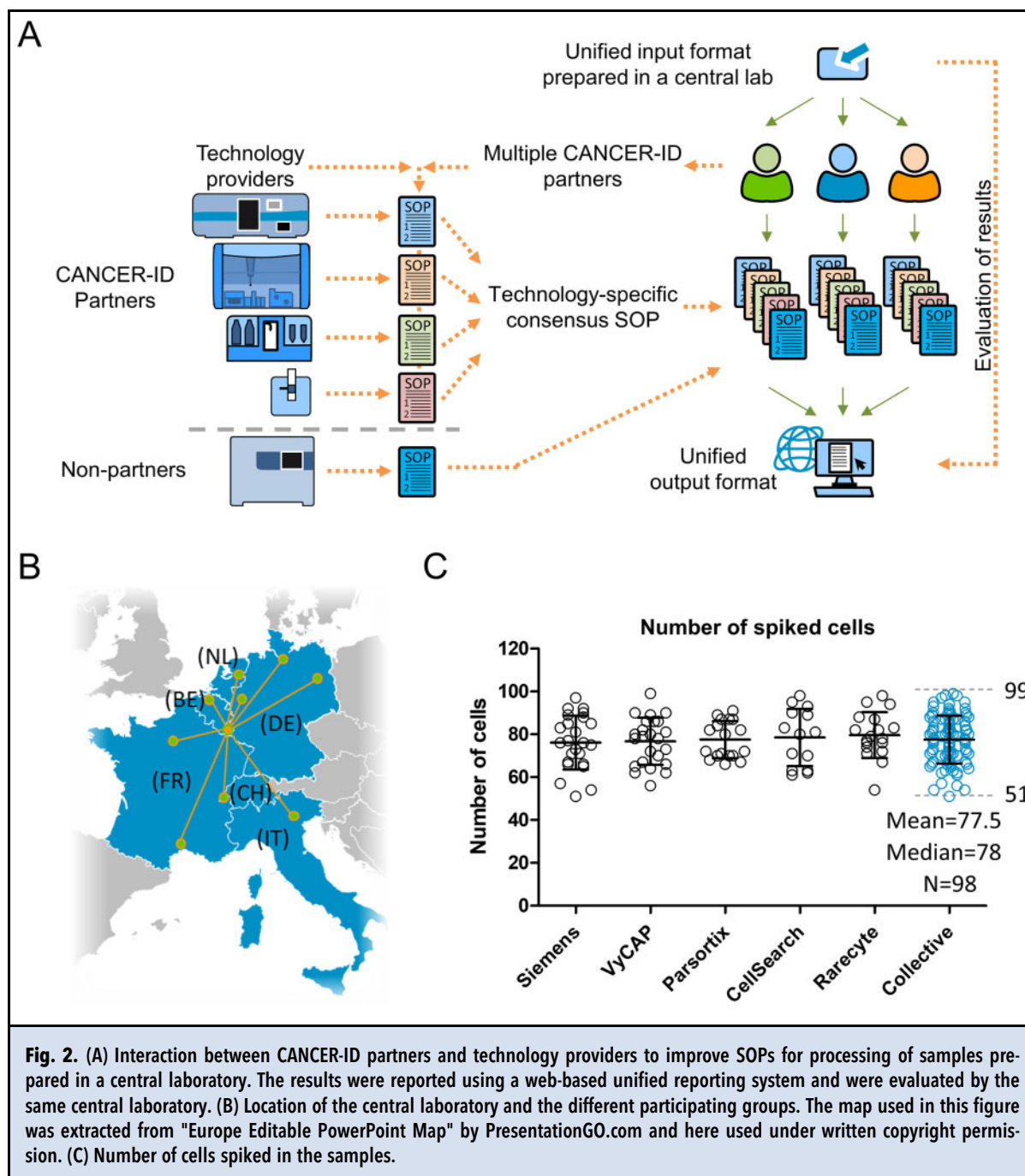


significantly higher than those with the VyCAP Microsieves (mean: 32%) ($P < 0.01$ by Mann-Whitney U test). Recovery with RareCyte was also significantly higher than that with Siemens (mean: 56%). We could not observe any statistically significant difference in the recovery of NCI-H441 and NCI-H1653 cells in the size-based technologies as expected due to the reduced differences in the cellular size between both lines. The smallest variance (measured as the standard deviation of all CTC enumerations done with a specific technology)

was obtained for the Siemens filtration unit followed by the CellSearch[®] system (Fig. 3D).

Discussion

In this multi-center study we established a platform enabling technical benchmarking of methods for CTC enrichment/isolation/detection. This platform was created within the frame of the European Innovative Medicines Initiative (IMI) consortium CANCER-ID (15) in which



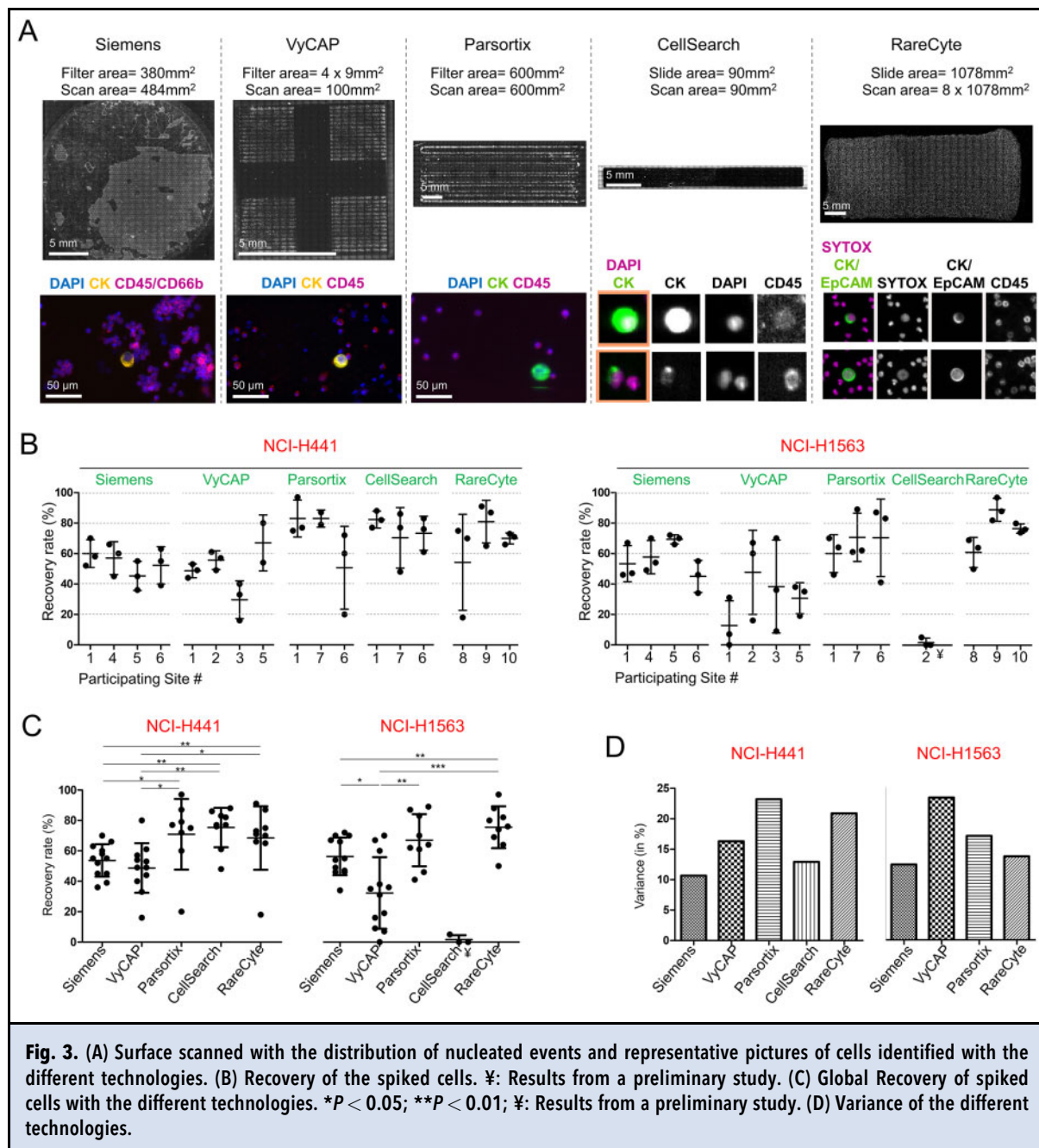
scientists from academic, clinical, and industrial sites in Europe and in the USA have joined forces to evaluate innovative technologies in the field of liquid biopsy. Currently, there is an increasing number of technologies available for CTC detection and their performance and reproducibility across multiple and real-life laboratories sites are very difficult to infer as all the data available is dispersed and quite difficult to

compare. Facing this, this CANCER-ID platform was created to generate comparative data with multiple technologies and to be used as a tool for technology developers to assess the technical performance characteristics of their technologies and standard operating procedures (SOPs) in multiple academic sites using standardized samples. From the numerous CTC detection technologies commercially available, we

Table 2. Recoveries obtained in each individual experiment and number of spiked cells/mL of PB.																						
Platform	Cell line	Round	Participating site																			
			#1		#2		#3		#4		#5		#6		#7		#8		#9		#9	
			(DE)		(NL)		(IT)		(DE)		(FR)		(DE)		(FR)		(CH)		(BE)		(BE)	
			R	S	R	S	R	S	R	S	R	S	R	S	R	S	R	S	R	S	R	S
Siemens	H441	#1	70	9.2					60	9.4	36	10.0	63	7.9								
		#2	52	7.3					66	10.8	55	8.4	55	9.8								
		#3	58	9.0					45	8.1	45	7.4	39	10.2								
	H1563	#1	67	8.3					70	9.9	66	10.2	55	7.3								
		#2	46	8.4					54	7.2	70	8.6	34	9.4								
		#3	47	5.7					49	7.9	72	6.0	46	6.3								
VyCAP	H441	#1	53	7.8	49	8.6	16	6.2			80	8.0										
		#2	44	9.0	61	5.6	40	7.0			(F1)	8.6										
		#3	49	8.2	57	9.9	33	8.0			54	8.9										
	H1563	#1	7	9.0	16	6.2	9	7.8			35	6.5										
		#2	31	8.6	67	7.2	36	7.3			19	7.9										
		#3	0	6.6	60	8.1	70	6.7			38	6.4										
Parsortix	H441	#1	75	10.1									20	8.9	(F2)	9.7						
		#2	77	7.8									60	7.6	87	7.4						
		#3	97	7.3									72	9.1	79	8.0						
	H1563	#1	70	7.9									87	9.3	89	9.7						
		#2	64	7.8									61	7.8	41	8.0						
		#3	46	9.7									83	9.9	62	9.1						
Cell Search*	H441	#1	(F3)	7.0									61	6.3	77	9.3						
			88	6.2																		
		#2	(F4)	9.5									76	8.3	48	8.9						
		77	6.1																			
	#3	82	8.1									83	9.8	86	9.0							
		H1563	#1			5 [‡]	8.0															
	#2			0 [‡]	6.3																	
	#3			0 [‡]	7.1																	
RareCyte*	H441	#1															75	9.1	65	8.4	73	9.1
		#2															18	6.0	91	8.8	66	7.4
		#3															70	8.4	87	10.9	71	10.6
	H1563	#1															64	8.6	82	9.8	74	9.2
		#2															50	8.2	97	8.7	76	7.9
		#3															69	10.4	88	8.0	80	9.7
R: Recoveries expressed as the percentage of spiked cells that could be identified after enrichment according to the respective SOP; S: the number of spiked cells/mL of blood; F1: sample with abnormal high number of cells on the filter and nonspecific staining of CD45 on CK ^{pos} cells; F2: Control plate positive but no labeling in the cassette. F3 and F4: samples showed macroscopic aggregates detected upon arrival and were repeated; [‡] : Results from a preliminary study performed at one single site. These results were not considered for further statistical analyses. *For CellSearch and RareCyte, the recovery was normalized to the volume of blood used on the assay (see Supplemental Methods).																						

selected methods from companies that were members of CANCER-ID or that approached us directly for testing their own technology.

This CANCER-ID proficiency testing platform organized ring trials to benchmark enrichment and detection of NSCLC cells spiked in healthy donor blood



samples. It was designed to assess the between-laboratory reproducibility of the methods (rather their repeatability). With the 1-week interval between sample shipments, the values reported for each site represent the intermediate precision, and combining the intermediate precision results from all participating laboratories per platform, we determine the reproducibility (i.e., the precision between measurements obtained at different laboratories).

As preanalytical variables can account for more than 50% of the errors in general clinical laboratory testing (18), in these ring trials measures were taken to limit/eliminate the confounding impact that preanalytical variables could have on the results. To limit variability in cancer cell line culture conditions, blood sample draw, cell spiking, and sample transport, all samples were prepared in one same reference laboratory and shipped to different participating sites under similar

transport conditions. To increase accuracy for cell-spiking, we chose direct enumeration over an uncontrolled dilution approach. However, irrespective the spiking-strategy, it is impossible to verify the exact cancer cell number in the blood sample, which may inevitably contribute to preanalytical variation. To mitigate any biological/biochemical effects by mixing allogeneous cells and to guarantee optimal sample stabilization, cancer cell lines and blood samples were stabilized separately before spiking using the blood collection tubes indicated by the respective SOPs. Furthermore, in order to obtain uniform analytical conditions across the participating sites, staff received on-site training from the technology providers and could sufficiently test the feasibility of the SOPs.

For these experiments we have used 2 lung cancer cell lines with distinct phenotypic and molecular characteristics: NCI-H441 (EpCAM^{high}, CK^{pos}, KRAS^{mut}, TP53^{mut}, and EGFR^{mut}) and NCI-H1563 (EpCAM^{low}, CK^{pos}, KRAS^{wt}, TP53^{wt}, and EGFR^{wt}). As part of standard procedure, cells were confirmed to be mycoplasma-free just before the first shipment, and cell viability and size were controlled prior every shipment. Although these 2 cancer cell lines may not represent the whole tumor cell diversity observed in lung cancer patients, their different EpCAM expression levels constitute an opportunity to challenge the known fundamental principles of the chosen technologies. This is best reflected in the results obtained with the CellSearch[®] system that could enrich EpCAM^{high} NCI-H441 cells but strikingly failed to enrich EpCAM^{low} NCI-H1563 cells, consistent with the dependency of this method on EpCAM expression previously demonstrated in various other cellular models and tumor entities (19–22). Among the panel of cell lines tested, we could not find a model with a cellular size small enough to challenge the limits of size-based technologies (Parsortix[®], VyCAP, and Siemens) with pore/gap sizes between 5 and 8 µm. As the cutoff of these technologies is clearly below the cell size of the 2 cell lines, the recovery for these 2 cell lines did not differ significantly in any of the platforms performing size-based enrichment. Additional smaller NSCLC cellular models could eventually help to validate the cutoffs of the technologies but these were not available.

The mean recovery rates for all tested systems ranged between 49% and 75% for NCI-H411 and 32% and 76% for NCI-H1563, respectively. Because of its inability to enrich EpCAM negative cells, CellSearch[®] was excluded from the ring trial involving (EpCAM-negative) NCI-H1563 cells. CellSearch[®], Parsortix[®], and RareCyte all allowed higher recoveries, however, the 2 last systems displayed also the highest variance between measurements with NCI-H441 cells while enumeration with the CellSearch[®] and the Siemens filtration unit were the most reproducible

(Fig. 3D). Of note, in CellSearch[®] and Siemens, enrichment and staining procedures are performed in a single streamlined automated protocol. Furthermore, the CellSearch[®] system includes a dedicated detection unit. Differences in the light source, optical filters, and detection cameras, might account for the larger assay variances observed in some of the other technologies, despite the fact that the different participating groups have used microscope systems globally suitable to identify the fluorescent dyes used (Supplemental Table 1). In general, these results suggest the advantages of automated protocols and dedicated instrumentation covering the complete analytical workflow to increase technical reproducibility, a key aspect for introduction of a new technology in the clinics. Processing laboratories interested in applying any CTC enrichment/isolation technologies without dedicated detection system that were tested here (i.e., Parsortix[®], Siemens, and VyCAP) need extra efforts to verify the procedure on their in-house detection equipment, and eventually additional investment to adapt the enrichment/isolation procedure and/or the detection equipment.

For the laboratory routine, the practicability of sample management and the throughput of the assay are paramount. In this context, the BCT with fixation solution recommended for each assay is an important issue for flexible sample shipment and efficient sample processing. Although BCT fixatives increase sample stability, it should be noted that they compromise downstream gene expression analyses in CTCs (23). The storage times of the BCTs varied between 3 (AccuCyte[®]) and 5 days (TransFix), which needs to be taken into consideration before routine use. Another important issue regarding laboratory practicability is the possibility to pause a workflow at a stable point. The majority of the workflows tested require all steps to be performed consecutively, including the microscope-based detection to avoid fading of the fluorescent dyes. An exception is RareCyte that allows long-term storage of processed samples at -20 °C (up to 1 year) prior to immunostaining, which can increase the flexibility for study design or sample management. The indicated maximum throughput of the assays (Table 1) was irrelevant for the proficiency testing but needs to be taken into consideration for clinical studies in real-life laboratories.

One other foreseeable important issue for implementation of any of these assays in the clinics is proper documentation of the results. In this aspect, the CellSearch[®] and RareCyte systems are clearly ahead of all the other tested technologies by performing automatic microscopic scanning of the entire fraction of enriched cells and making possible subsequent software-assisted identification of CTCs by different users. In contrast, the uneven surface of the Whatmann filters used in the Siemens unit and the lack of dedicated

detection systems able to deal with the specificities of the filters, forced the groups to perform a manual scanning which limits the documentation of the findings and their later verification.

Choosing the best method for CTC enrichment can be challenging and in this field, there is a lack of standardization and data from inter-laboratory testing raising questions on the technical reproducibility of the methods. Furthermore, comparison of results from different studies is hampered owing to different preanalytic conditions, protocols, cellular models, and patient samples, which also raises questions on the reproducibility of the results. The platform and the multi-national ring-trials established by CANCER-ID aimed to tackle some of these problems by using centrally prepared samples, consensus SOPs, and a unified reporting system. This ring-testing platform for CTCs does not intend to replace the efforts required from technology providers to prove the technical capabilities of their technologies, but rather to provide accountable information on assay reproducibility. Nevertheless, it can be adapted to test other relevant parameters of their technologies (e.g., intra-lab repeatability and linearity of recovery). Subsequently, it will be of utmost importance to clinically validate the technologies (if not done yet) in the context of clinical trials, which was beyond the scope of our project. This platform is not restricted to CANCER-ID partner companies as documented by the participation of RareCyte. In fact, this structure is meant to be useful to the broad community of technology providers who can thus compare the performance of their technologies in different real-life laboratories, as well as to the analytical sites for external quality assurance purposes. Furthermore, we believe that this proficiency testing program could help to define minimal requirements for performance qualification prior to clinical validation of technologies. For all these reasons, the program will remain in operation beyond the funding period of CANCER-ID. These activities will be sustained by the establishment of the European Liquid Biopsy Society (ELBS) (24) which comprises a large network of almost 100 institutions from academia and industry.

Supplemental Material

[Supplemental material](#) is available at *Clinical Chemistry* online.

Nonstandard Abbreviations CTCs, circulating tumor cells; EpCAM, epithelial cell adhesion molecule; EMT, epithelial-to-

mesenchymal transition; FDA, U.S. Food and Drug Administration; SMEs, small- and medium-sized enterprises; IMI, innovative medicines initiative; SOPs, standard operating procedures; NSCLC, non-small cell lung cancer; ATCC, American type culture collection; CK, cytokeratin; PE, phycoerythrin; WGA, whole genome amplification; CNA, copy number alterations; BCT, blood collection tube; BSA, bovine serum albumin; PBS, phosphate-buffered saline; IBBL, Integrated BioBank of Luxembourg; ABC, antibodies bound per cell.

Author Contributions: All authors confirmed they have contributed to the intellectual content of this paper and have met the following 4 requirements: (a) significant contributions to the conception and design, acquisition of data, or analysis and interpretation of data; (b) drafting or revising the article for intellectual content; (c) final approval of the published article; and (d) agreement to be accountable for all aspects of the article thus ensuring that questions related to the accuracy or integrity of any part of the article are appropriately investigated and resolved.

R.P.L. Neves, statistical analysis; W. Ammerlaan, provision of study material or patients; E. Rossi, provision of study material or patients; F. Betsou, provision of study material or patients; F. Farace, administrative support; T. Schlange, administrative support; R. Zamarchi, statistical analysis; K. Pantel, financial support, administrative support; N.H. Stoecklein, financial support, administrative support.

Authors' Disclosures or Potential Conflicts of Interest: Upon manuscript submission, all authors completed the author disclosure form. Disclosures and/or potential conflicts of interest:

Employment or Leadership: M.V. Luetke-Eversloh, Bayer AG; T. Schlange, Bayer AG; S. Bender, Bayer AG.

Consultant or Advisory Role: K. Pantel, Menarini/Silicon Biosystems.

Stock Ownership: T. Schlange, Bayer AG; L.W.M.M. Terstappen, VyCAP.

Honoraria: None declared.

Research Funding: The authors participate in the Innovative Medicines Initiative consortium CANCER-ID. CANCER-ID is supported by the Innovative Medicines Initiative (IMI) Joint Undertaking under grant agreement No115749, resources of which are composed of financial contributions from the European Union's Seventh Framework Program (FP7/2007–2013) and EFPIA companies' in-kind contributions. The European Union's Horizon 2020 research and innovation program under the Marie Skłodowska-Curie grant agreement No765492 (H. Wikman, K. Pantel).

Expert Testimony: R.P.L. Neves, Thermo Fisher Scientific, Terumo BCT.

Patents: L.W.M.M. Terstappen, patents related to the CellSearch and VyCAP platform.

Other Remuneration: R.P.L. Neves, Menarini Silicon Biosystems, Thermo Fisher Scientific, Terumo BCT; N.H. Stoecklein, Menarini Silicon Biosystems.

Role of Sponsor: The funding organizations played no role in the design of study, choice of enrolled patients, review and interpretation of data, preparation of manuscript, or final approval of manuscript.

Acknowledgments: The consortium thanks all blood donors, and Olga Kofanova and Kate Sokolowska (IBBL), Oliver Mauermann (UKE), Arjan Tibbe and Joska Broekmaat (VyCAP), Michael O'Brien and Lara Stevanato (ANGLE), Karen Marfurt, Michael Puglia and Guido Hennig (Siemens), Nicolò Manaresi and Tim Pitfield (Menarini Silicon Biosystems), and Tad George and Michael Rooney (Rarecyte) for their support.

References

1. Lianidou E, Pantel K. Liquid biopsies. *Genes Chromosomes Cancer* 2019;58:219-32.
2. Alix-Panabieres C, Pantel K. Clinical applications of circulating tumor cells and circulating tumor DNA as liquid biopsy. *Cancer Discov* 2016;6: 479-91.
3. Blackhall F, Frese KK, Simpson K, Kilgour E, Brady G, Dive C. Will liquid biopsies improve outcomes for patients with small-cell lung cancer? *Lancet Oncol* 2018; 19:e470-e81.
4. Pawlikowska P, Faugeroux V, Oulhen M, Aberlenc A, Tayoun T, Pailler E, Farace F. Circulating tumor cells (CTCs) for the noninvasive monitoring and personalization of non-small cell lung cancer (NSCLC) therapies. *J Thorac Dis* 2019;11:S45-S56.
5. Stoecklein NH, Fischer JC, Niederacher D, Terstappen LW. Challenges for CTC-based liquid biopsies: Low CTC frequency and diagnostic leukapheresis as a potential solution. *Expert Rev Mol Diagn* 2016;16:147-64.
6. Krebs MG, Metcalf RL, Carter L, Brady G, Blackhall FH, Dive C. Molecular analysis of circulating tumour cells: biology and biomarkers. *Nat Rev Clin Oncol* 2014;11: 129-44.
7. Pantel K, Alix PC. Liquid biopsy and minimal residual disease - latest advances and implications for cure. *Nat Rev Clin Oncol* 2019;16:409-24.
8. Keller L, Werner S, Pantel K. Biology and clinical relevance of EpCAM. *Cell Stress* 2019;3:165-80.
9. Harouaka RA, Nisic M, Zheng SY. Circulating tumor cell enrichment based on physical properties. *J Lab Autom* 2013;18:455-68.
10. Swennenhuis JF, van Dalum G, Zeune LL, Terstappen LW. Improving the cell search(r) system. *Expert Rev Mol Diagn* 2016;16:1291-305.
11. Allard WJ, Terstappen LW. CCR 20th anniversary commentary: paving the way for circulating tumor cells. *Clin Cancer Res* 2015;21:2883-5.
12. Riethdorf S, O'Flaherty L, Hille C, Pantel K. Clinical applications of the cell search platform in cancer patients. *Adv Drug Deliv Rev* 2018;125:102-21.
13. Lindsay CR, Blackhall FH, Carmel A, Fernandez-Gutierrez F, Gazzaniga P, Groen HJM, et al. EPAC-lung: Pooled analysis of circulating tumour cells in advanced non-small cell lung cancer. *Eur J Cancer* 2019;117:60-8.
14. Market research future. Circulating tumor cell market overview. <https://www.marketresearchfuture.com/reports/circulating-tumor-cell-market-1362> (Accessed November 2020).
15. CANCER-ID. Cancer treatment and monitoring through identification of circulating tumor cells and tumor related nucleic acids in blood. www.cancer-id.eu (Accessed November 2020).
16. IBBL Biospecimen proficiency testing programme. <http://biospecimenpt.ibbl.lu/> (Accessed November 2020).
17. Keller L, Pantel K. Unravelling tumour heterogeneity by single-cell profiling of circulating tumour cells. *Nat Rev Cancer* 2019;19:553-67.
18. Green SF. The cost of poor blood specimen quality and errors in preanalytical processes. *Clin Biochem* 2013;46: 1175-9.
19. Rao CG, Chianese D, Doyle GV, Miller MC, Russell T, Sanders RA, Jr., Terstappen LW. Expression of epithelial cell adhesion molecule in carcinoma cells present in blood and primary and metastatic tumors. *Int J Oncol* 2005;27:49-57.
20. de Wit S, Manicone M, Rossi E, Lampignano R, Yang L, Zill B, et al. EpCAM(high) and EpCAM(low) circulating tumor cells in metastatic prostate and breast cancer patients. *Oncotarget* 2018;9:35705-16.
21. Lindgren G, Wennerberg J, Ekblad L. Cell line dependent expression of EpCAM influences the detection of circulating tumor cells with Cellsearch. *Laryngoscope Investig Otolaryngol* 2017;2:194-8.
22. de Wit S, van Dalum G, Lenferink AT, Tibbe AG, Hiltermann TJ, Groen HJ, et al. The detection of EpCAM(+) and EpCAM(-) circulating tumor cells. *Sci Rep* 2015;5:12270.
23. Luk AWS, Ma Y, Ding PN, Young FP, Chua W, Balakrishnar B, et al. CTC-mRNA (AR-V7) analysis from blood samples-impact of blood collection tube and storage time. *Int J Mol Sci* 2017;18:
24. Elbs - European Liquid Biopsy Society. www.elbs.eu (Accessed November 2020).



Characterization of circulating breast cancer cells with tumorigenic and metastatic capacity

Claudia Koch^{1,†}, Andra Kuske^{1,†}, Simon A Joosse¹ , Gökhan Yigit², George Sflomos³ , Sonja Thaler⁴, Daniel J Smit⁵ , Stefan Werner¹, Kerstin Borgmann⁶, Sebastian Gärtner¹, Parinaz Mossahebi Mohammadi¹, Laura Battista³, Laure Cayrefourcq^{7,8}, Janine Altmüller⁹, Gabriela Salinas-Riester¹⁰, Kaamini Raithatha¹⁰, Arne Zibat², Yvonne Goy⁶, Leonie Ott¹, Kai Bartkowiak¹, Tuan Zea Tan¹¹ , Qing Zhou¹² , Michael R Speicher¹² , Volkmar Müller¹³, Tobias M Gorges¹, Manfred Jücker⁵, Jean-Paul Thiery¹⁴ , Cathrin Brisken^{3,15,‡}, Sabine Riethdorf^{1,‡} , Catherine Alix-Panabieres^{7,8,‡} & Klaus Pantel^{1,*}

Abstract

Functional studies giving insight into the biology of circulating tumor cells (CTCs) remain scarce due to the low frequency of CTCs and lack of appropriate models. Here, we describe the characterization of a novel CTC-derived breast cancer cell line, designated CTC-ITB-01, established from a patient with metastatic estrogen receptor-positive (ER⁺) breast cancer, resistant to endocrine therapy. CTC-ITB-01 remained ER⁺ in culture, and copy number alteration (CNA) profiling showed high concordance between CTC-ITB-01 and CTCs originally present in the patient with cancer at the time point of blood draw. RNA-sequencing data indicate that CTC-ITB-01 has a predominantly epithelial expression signature. Primary tumor and metastasis formation in an intraductal PDX mouse model mirrored the clinical progression of ER⁺ breast cancer. Downstream ER signaling was constitutively active in CTC-ITB-01 independent of ligand availability, and the CDK4/6 inhibitor Palbociclib strongly inhibited CTC-ITB-01 growth. Thus, we established a functional model that opens a new avenue to study CTC biology.

Keywords breast cancer; circulating tumor cells; functional studies; liquid biopsy; metastasis

Subject Categories Cancer; Stem Cells & Regenerative Medicine

DOI 10.15252/emmm.201911908 | Received 16 December 2019 | Revised 15 June 2020 | Accepted 17 June 2020 | Published online 15 July 2020

EMBO Mol Med (2020) 12: e11908

Introduction

Detection and characterization of circulating tumor cells (CTCs) have prognostic value in various tumor entities as demonstrated by several large clinical studies, e.g., for patients with breast and prostate cancer (Bidard *et al*, 2014; Goldkorn *et al*, 2014; Scher *et al*, 2015; Alix-Panabieres & Pantel, 2016). Moreover, these cells have the potential to be exploited as monitoring markers and might function as a blood-based biopsy guiding personalized treatment decisions (Keller & Pantel, 2019; Pantel & Alix-Panabieres, 2019). The perspective to accompany or even replace invasive tumor tissue biopsies in order to gain important diagnostically and therapeutically relevant information makes CTCs an essential contribution to

1 Department of Tumor Biology, Center of Experimental Medicine, University Medical Center Hamburg-Eppendorf, Hamburg, Germany

2 Institute of Human Genetics, University Medical Center Göttingen, Göttingen, Germany

3 ISREC – Swiss Institute for Experimental Cancer Research, School of Life Sciences, Ecole Polytechnique Fédérale de Lausanne (EPFL), Lausanne, Switzerland

4 European Centre for Angioscience (ECAS), Medical Faculty Mannheim, University of Heidelberg, Mannheim, Germany

5 Institute of Biochemistry and Signal Transduction, University Medical Center Hamburg-Eppendorf, Hamburg, Germany

6 Radiobiology & Experimental Radiooncology, University Medical Center Hamburg-Eppendorf, Hamburg, Germany

7 Laboratory of Rare Human Circulating Cells (LCCRH), University Medical Centre, Montpellier, France

8 Montpellier University, Montpellier, France

9 Cologne Center for Genomics, University of Cologne, Cologne, Germany

10 NGS Integrative Genomics Core Unit, Institute of Human Genetics, University Medical Center Göttingen, Göttingen, Germany

11 Cancer Science Institute of Singapore, National University of Singapore, Singapore City, Singapore

12 Institute of Human Genetics, Diagnostic and Research Center for Molecular BioMedicine, Medical University of Graz, Graz, Austria

13 Department of Gynecology, University Medical Center Hamburg-Eppendorf, Hamburg, Germany

14 INSERM Unit 1186, Comprehensive Cancer Center, Institut Gustave Roussy, Villejuif, France

15 Breast Cancer Now Research Centre, Institute of Cancer Research, London, UK

*Corresponding author. Tel: +49 40 741053503; Fax: 49 40 7410-55379; E-mail: pantel@uke.de

†These authors contributed equally to this work as first authors

‡These authors contributed equally to this work as senior authors

non-invasive “real-time liquid biopsies” (Pantel & Alix-Panabieres, 2010; Bardelli & Pantel, 2017).

In spite of an enormous progress in the development of approaches for the detection and molecular characterization of CTCs up to the single cell level (Joosse *et al*, 2012; Alix-Panabieres & Pantel, 2014a,b; Pantel & Alix-Panabieres, 2019), information on the functional properties of CTCs is still limited due to the very low concentrations of these cells in the peripheral blood of patients with cancer (Alix-Panabieres & Pantel, 2014a).

Not all CTCs possess the potential to extravasate at distant sites and grow out to form a novel metastatic lesion (Wicha & Hayes, 2011). A plethora of different factors play into the survival of these CTCs in the blood stream and their capacity to extravasate and metastasize (Strilic & Offermanns, 2017; Giuliano *et al*, 2018), including the hemodynamic forces within the circulation (Follain *et al*, 2018) and genomic make-up of the tumor cells (Joosse & Pantel, 2016; Gkoutela *et al*, 2019). Experimental models indicate that only few tumor cells are viable, survive shear forces within the blood flow, evade the immune system as well as systemic therapies, reach distant organs, and eventually have the potential to form an overt metastasis (Chambers *et al*, 2002, Y. Kang & Pantel, 2013). Adaptation to a new microenvironment and proliferation of a single tumor cell or a CTC cluster in a distant site requires highly specialized traits, most of which are largely unknown. In order to understand these underlying mechanisms of the metastatic cascade, functional characterization of viable CTCs capable of forming distant metastasis is required.

A prerequisite for these analyses were therefore the recent advances in the ability to culture CTCs *in vitro* (Zhang *et al*, 2013; Yu *et al*, 2014; Cayrefourcq *et al*, 2015) or expand the CTC pool *in vivo* using xenografts (Baccelli *et al*, 2013; Hodgkinson *et al*, 2014; Carter *et al*, 2017). However, to our knowledge, none of these studies compared the characteristics of the original CTCs captured from the patients with cancer directly to the CTC line. Besides unraveling the biology of CTCs in patients with cancer, these studies allow testing of the unknown activity of cancer drugs against CTCs. In this context, the low number of estrogen receptor-positive (ER⁺) breast cancer cell lines presently available is disturbing, since 70–80% of patients with breast cancer harbor ER⁺ tumors and ER is the primary target of endocrine therapies in breast cancer (Pan *et al*, 2017).

Here, we report the establishment and in-depth characterization of an ER⁺ breast CTC line with unique properties. Comparison of CTCs *in situ* before cell culture with the CTC line indicates that it

mirrors the situation in ER⁺ breast cancer patients and therefore provides novel insights into the biology and drug response of patient-derived CTCs in the most common breast cancer subtype.

Results

Patient characteristics

The patient with MBC the CTC-ITB-01 cell line derived from presented with a bilateral mammary carcinoma, lymph node (LN) metastases, and bone metastases (BM) at age 75, 2 years prior to blood collection for CTC analysis and begin of cultivation (Fig 1A). Histopathological analysis of biopsies performed for both breast tumors revealed a well-differentiated (G1) invasive lobular carcinoma (ILC) of the left breast and a well-differentiated (G1) invasive ductal carcinoma (IDC) of the right breast (Table EV1). E-cadherin re-staining of the tissue biopsies from both tumors revealed that the tumor described as lobular showed a sub-fraction of E-cadherin⁺ (Fig EV1A) besides E-cadherin[−] tumor cells (Fig EV1B). This could point toward a ducto-lobular histopathology. Both the primary right ductal tumor (Fig EV1C) and the vaginal metastasis (Fig EV1D) contained strongly E-cadherin⁺ tumor cells.

Both primary tumors were classified as estrogen receptor-positive (ER⁺ in ≥ 80% of nuclei), progesterone receptor positive (PR⁺ in ≥ 80% of nuclei), ERBB2 negative (ERBB2[−]), and presented with a low Ki67⁺ cell fraction of 5%. At time of blood collection, additional metastases in the spleen, liver, and vagina had been diagnosed. An overview of the disease progression and treatment scheme of this patient can be found in Fig 1A and in Appendix Supplementary Methods.

Establishment of a CTC-derived breast cancer cell line

The peripheral blood sample of this patient with metastatic breast cancer (MBC) was screened for CTCs using the CellSearch[®] System, resulting in a tumor cell count of 1,547 CTCs per ml of blood (total of 7.5 ml). In parallel, blood of the same patient was processed for cell culture. This led to the establishment of a permanent cancer cell line, designated CTC-ITB-01. The original CTCs at blood draw were comprised of single cells of various shapes and diameters (Fig 1B, e.g., panels 1–3), as well as approximately 700 small cell clusters of CTCs (Fig 1B, panels 5–6). CTCs showed negative or very weak (Fig 1B, panels 4 and 8) immunostaining for ERBB2. CTC-ITB-01

Figure 1. CTC cell line establishment from peripheral blood of an mBCa patient.

- A Scheme of the breast cancer patient's clinical status and therapies. Course of disease progression (blue) and treatment scheme (green) of the patient giving rise to CTC-ITB-01 are indicated. Timeline of progression and treatment indicated in years and months (mo). Drugs were administered at standard dosage according to indicated pattern. The red star represents the time point of blood sample collection. More detailed information is available the in Appendix Supplementary Methods.
- B Representative pictures of different CTCs from the initial CellSearch[®] analysis of the metastatic breast cancer patient who gave rise to the breast CTC line. The detected tumor cells display clear keratin and DAPI staining. CD45 negativity as well as lack of, or very weak (4, 8), ERBB2 expression. Cells of small (about 5 μm in diameter, 1, 2) and large size (larger than 10 μm in diameter, 3) were detected. While some CTCs displayed dot-like perinuclear keratin signals (1, 2), the majority showed diffuse keratin staining. Additionally, CTC clusters of more than 4 cells were present (5, 6). Some CTCs showed multiple/lobed nuclei (7, 8).
- C Bright field images of CTC-ITB-01 cells growing adherently.
- D Bright field images of CTC-ITB-01 cells growing non-adherently (relation between adherent and non-adherent cells: 80/20%).

Data information: White scale bars represent 10 μm. Black scale bars represent 40 μm.
Source data are available online for this figure.

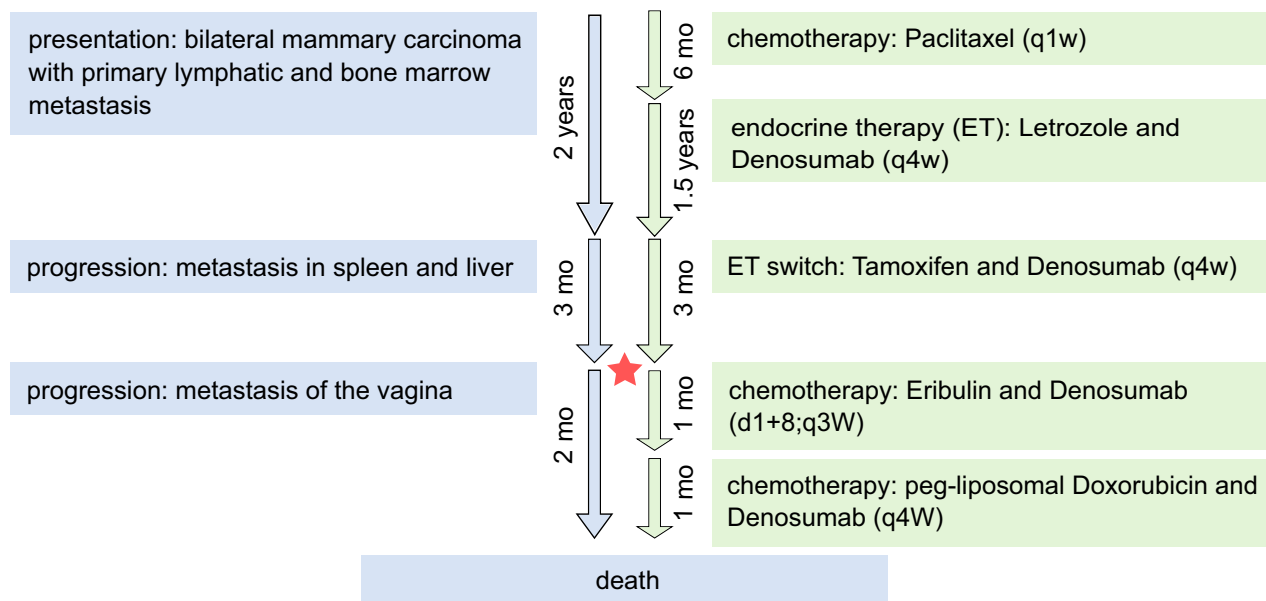
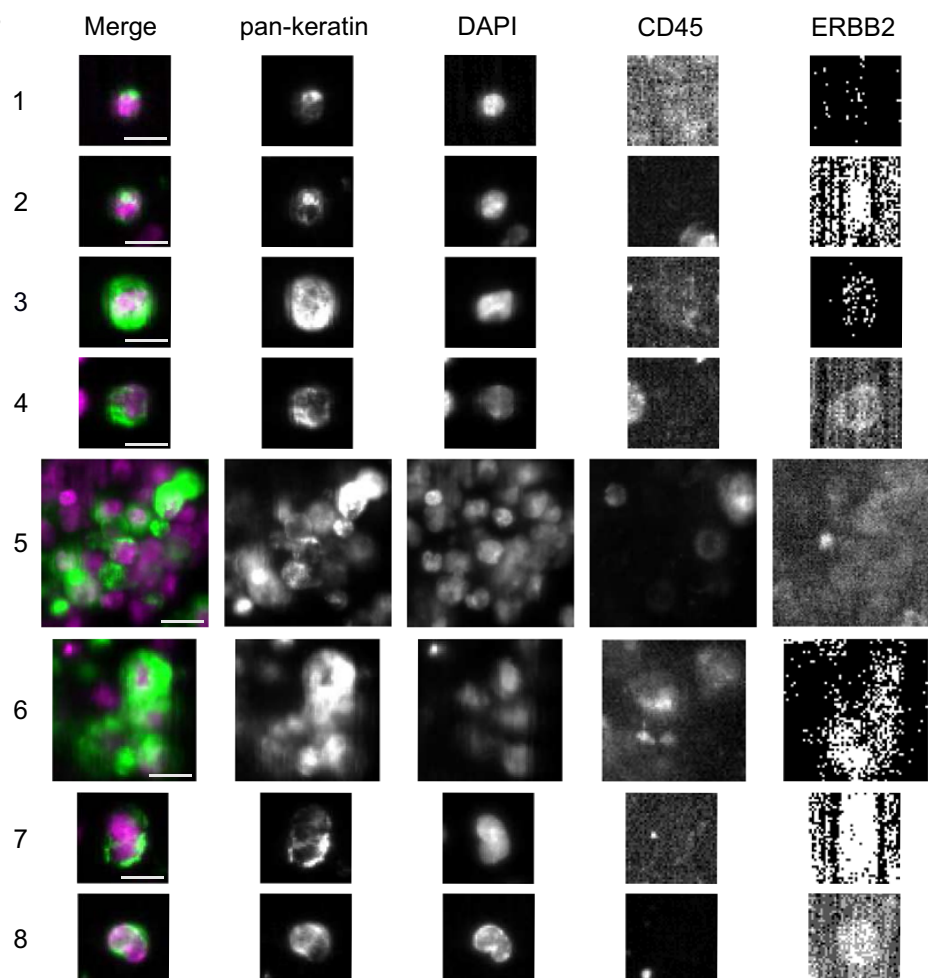
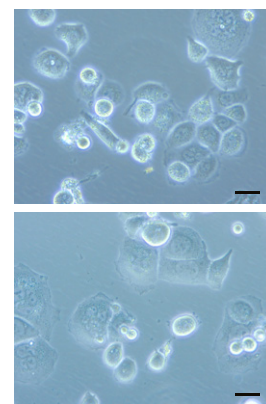
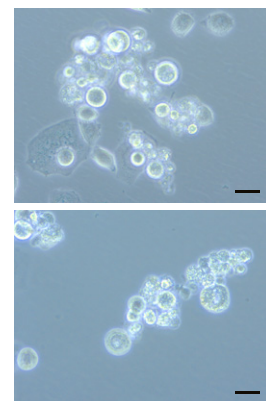
A**B****C****D**

Figure 1.

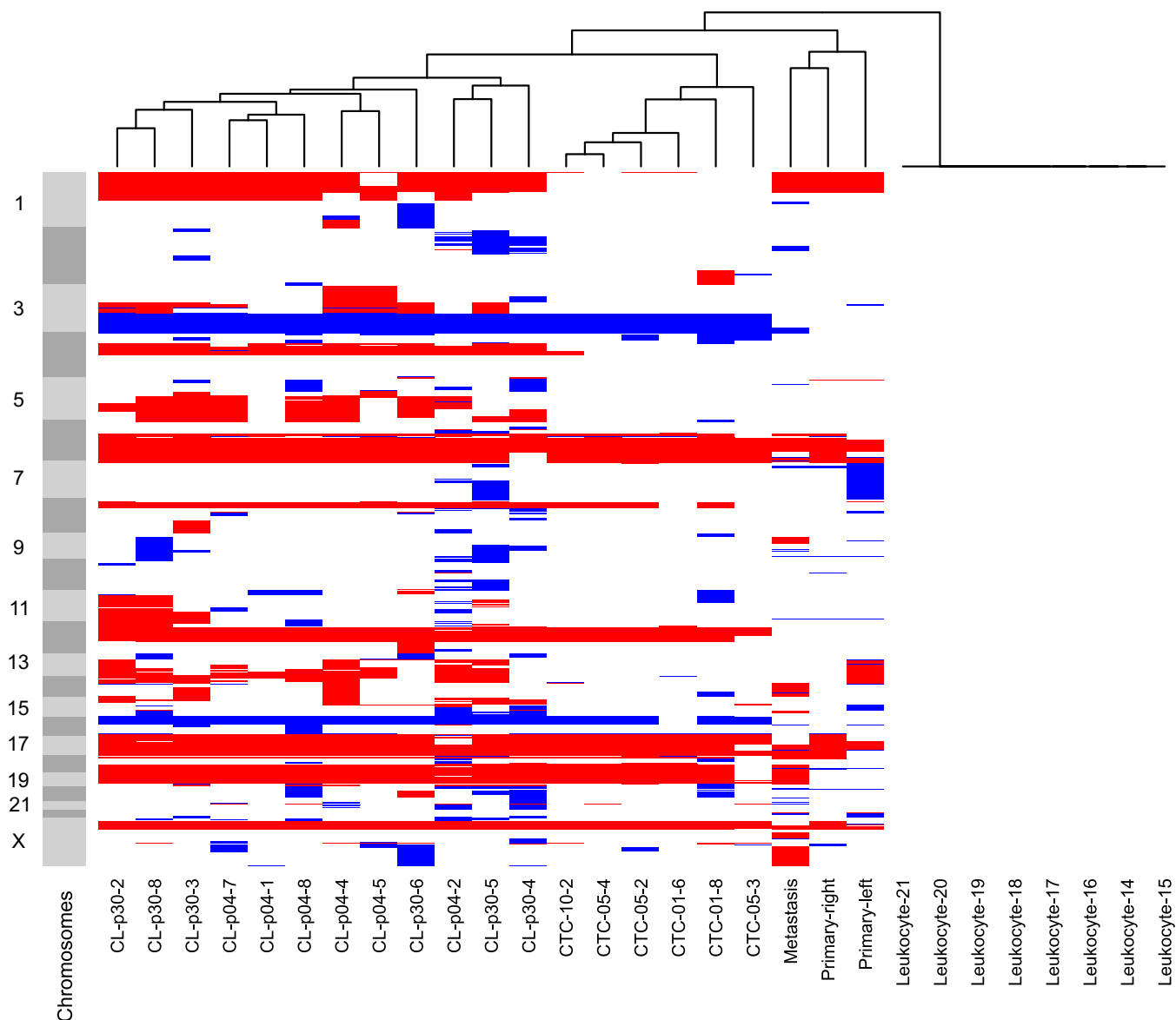


Figure 2. Hierarchical clustering analysis of CTC-ITB-01.

Unsupervised hierarchical clustering (Ward linkage with Euclidean distance) of CNA profiles generated from patient primary tumors, the vaginal metastasis, isolated single and pooled CTCs from the primary blood collection and CTC-ITB-01 (early and later passage) and leukocytes. “CL” represents the cell line, followed by the passage analyzed (p04/p30). “CTC” marks circulating tumor cells isolated from the initial blood draw, followed by 01/05/10 indicating single (01) or pooled cells (5 or 10, respectively). Light and dark gray bars to the left signify chromosomes, starting from the top with chromosome 1. Red color represents chromosome loss, blue represents gain. All copy number aberrations were calculated using the patient’s own germline DNA extracted from leukocytes as reference to eliminate copy number variations (CNVs).

has now been successfully cultured for more than 4 years and cells grow in a mixed epithelial–mesenchymal morphology (Fig 1C) as well as in adherent (Fig 1C) and non-adherent fractions (Fig 1D).

Genomic characteristics of CTC-ITB-01 cells

Remarkably, a considerable number of the CTC cell line cells carried multiple and lobed nuclei, probably due to abnormal cytokinesis (Fig EV2A). Those cells were also detectable in the original Cell-Search analysis (Fig 1B, panels 7–8), indicating that this is not an artificial effect originating in cell culture. Giant cancer cells carrying multiple nuclei have recently been associated with metastasis and

disease relapse (Mirzayans *et al*, 2018). Karyotyping of the cell line showed a broad range of chromosomes per cell (32–110), resulting in a mean of 70.7 ($s = 17.66$) chromosomes (Fig EV2B and C).

Whole-genome next-generation sequencing of single cells of the CTC-ITB-01 line revealed a wide spectrum of copy number alterations (CNA) including loss of large areas of chromosome 16q (Fig 2), typical for ER⁺ breast cancers (Horlings *et al*, 2010). Hierarchical clustering analysis showed that the primary CTCs within the patient’s blood and the resulting CTC-ITB-01 line cluster separately to the original primary tumors (left and right breast) and the vaginal metastasis, indicating tumor evolution during the course of the disease (Fig 2).

Overall, the highest concordance in CNA profiles was detected between the arbitrarily collected sample of original CTCs analyzed and the CTC-ITB-01 line (Fig 2), providing strong evidence that the CTC line derived from a subpopulation of CTCs in circulation at time point of blood draw. We furthermore directly compared the CNA profiles of CTC-ITB-01 cells to those of the primary CTCs present in the patient's blood (Fig 3A). Common aberrations include gain of chromosomes 3q and 15q as well as loss of chromosomes 6q, 12p, 16q, 17p, 18, and 22q (Fig 3A). Additionally, CTC-ITB-01 remains stable in its CNA profile during culture, shown by direct comparison of an early (04) with a late passage (30) of the line (Fig 3B). The fact that early and late passages of the line cluster together (Fig 2) represents another strong indicator of the CTC line's stability. Loss of chromosome 1p represents the largest significant difference measured between the early and late passages (Fig 3B).

Whole exome sequencing (WES) of CTC-ITB-01 cells, the two primary tumors, and the distant vaginal metastasis was performed and data were analyzed for mutations in common cancer-related genes (Table 1). We detected a one base pair deletion in *MAP3K1* (c.2782delT; p.S928Lfs*9) leading to an amino acid frameshift, thereby causing protein truncation and loss-of-function of the protein (Pham et al, 2013; Avivar-Valderas et al, 2018) in all four samples. Further, the two primary tumors, the vaginal metastasis and the CTC cell line also shared a mutation in the gene region encoding the kinase domain of the PIK3CA protein (c.3140A>G; p.H1047R, Table 1), a somatic hot spot mutation site in lobular and ductal breast cancer that has been associated with increased enzymatic activity of PIK3CA (Kang et al, 2005; Stemke-Hale et al, 2008). Besides shared variations with the primary tumors, CTC-ITB-01 and the vaginal metastasis exhibited an additional, less frequent *PIK3CA* mutation (c.1252G>A; p.E418K, Table 1), located in the region encoding the C2 calcium/lipid-binding domain (Saal et al, 2005; Stemke-Hale et al, 2008). Moreover, we identified a genomic aberration of the *NF1* gene that was shared between the CTC-ITB-01 cell line, the lobular tumor and the vaginal metastasis, but also "private" *CDH1* (c.2466delC; p.T823Qfs*23) and *TP53* (c.1024C>T; p.R342*) gene mutations in the vaginal metastasis not observed in the primary tumors or the CTC line (Table 1).

We furthermore checked for genes typically associated with hereditary breast cancer predisposition (e.g., *BRCA1/2*, *TP53*, *PTEN*, *STK11* or *CHEK2*), but found no mutations in the primary tumors. Also, no mutations were detected for other described breast cancer-associated genes (e.g., *RAD51*, *RAD50*, *p27*, *ESR1/2*, *ERBB2*, *ERBB3*, *AKT1*, *CCDN1*, *FGFR1*, *MYC*, and *RB1*) in any of the tissues or the CTC cell line.

Another specific variation of CTC-ITB-01 is a homozygous, mutation in the *TP53* tumor suppressor gene (c.853G>A; p.E285K)

(Table 1). The *TP53* gene sequence is commonly altered in breast cancer (Bertheau et al, 2013; Dumay et al, 2013), and this point mutation represents an established pathogenic variant (Fig EV3A–C) (Xu et al, 1997; Oh et al, 2000). Additionally, immunostaining of the p53 protein showed a strong accumulation of this tumor suppressor in the nucleus of CTC-ITB-01 cells (Fig EV3D).

Furthermore, the CTC-ITB-01 line carries a "private" variant in the *CDH1* gene (c.1204G>A; p.D402N, Table EV2) that differs from the *CDH1* mutation of the lobular primary tumor (c.1792C>T; p.R598*, Table 1). While the p.R598* mutation that has been previously detected in ER⁺ BCa tissue (Ma et al, 2017) represents a nonsense substitution leading to loss-of-function of the CDH1 protein, the *CDH1* mutation of the CTC cell line is a relatively uncharacterized missense mutation in E-cadherin's extracellular domain 3 (EC3) which is necessary for homophilic adhesion (Shiraishi et al, 2005). Apart from *CDH1*, we also checked for variations in other genes distinguishing the different histopathological subtypes of the two primary tumors (i.e., ILC and IDC), such as *GATA3*, *FOXA1*, and *TBX3*; however, no additional mutations of these genes were detected in the CTC line. Further analysis of WES data revealed additional variants in common cancer-related genes involved in DNA replication and DNA damage (e.g., *ATM*, *CDKN1A*), cell polarization (*SCRIB*), proliferation (*RNASEL*), VEGF expression (*MAP3K1*, *MAP3K6*), and in genes encoding growth factors (*FGF2*) (Table EV2). These variants were predicted to impair protein function by different *in silico* prediction tools; however, experimental data on the functional relevance of these variants are still inconsistent.

Finally, the CTC-ITB-01 line displayed a high degree of loss of heterozygosity (LOH) as assessed by runs of homozygosity (ROH) within the exome. In comparison with the primary tumors which showed homozygosity within < 90 Mb of the genome, 601 Mbs of homozygous sequences were detected for the breast CTC line, potentially indicating heterozygous mutations that became homozygous and contributed to tumor evolution. The 15 largest regions of LOH found solely in CTC-ITB-01 are listed in Table EV3 and are also discernible in Fig 2.

Expression signature of CTC-ITB-01 cells

CTC-ITB-01 cells were first characterized for ER and ERBB2 protein expression (receptors relevant to the major breast cancer subtypes) by Western blot (Fig 4A). ER expression in CTC-ITB-01 cells was strong, albeit less pronounced than in MCF-7 cells, the standard model for ER⁺ breast cancer cells (Fig 4A). ER positivity was confirmed via immunocytochemistry (Fig 4B). Consistent with the lack of *ERBB2* amplification (Appendix Fig S1A), *ERBB2* expression was

Figure 3. CNA profile analysis of CTC-ITB-01.

Direct comparisons of CNA profiles. Percentages of gene copy number gains and losses across the chromosomes for different sample types. Copy number gains are displayed in green, losses in red.

- A CNAs generated from CTCs from the primary blood collection (upper panel) and CTC-ITB-01, indicated as "CL" (medium panel). Significant distinctions between both samples were calculated using Fisher's exact test (Joosse et al, 2018) and are indicated in lowest panel (blue). Increased blue color intensity represents lower *P*-value and therefore higher statistical significance.
- B CNA comparison between early (p04) and late (p30) CTC-ITB-01 passages (upper and medium panel). Significant distinctions between both samples were calculated using Fisher's exact test (Joosse et al, 2018) and are indicated in lowest panel (in blue). Increased blue color intensity represents lower *P*-value and therefore higher statistical significance.

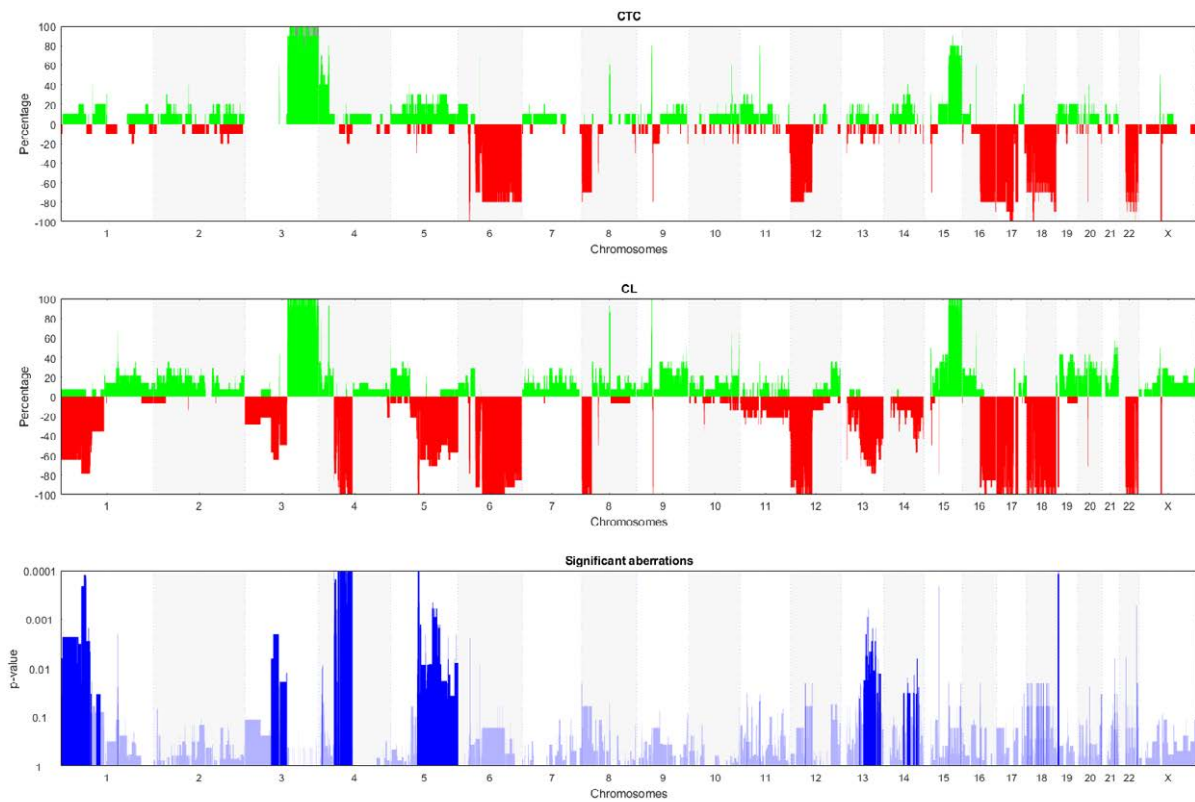
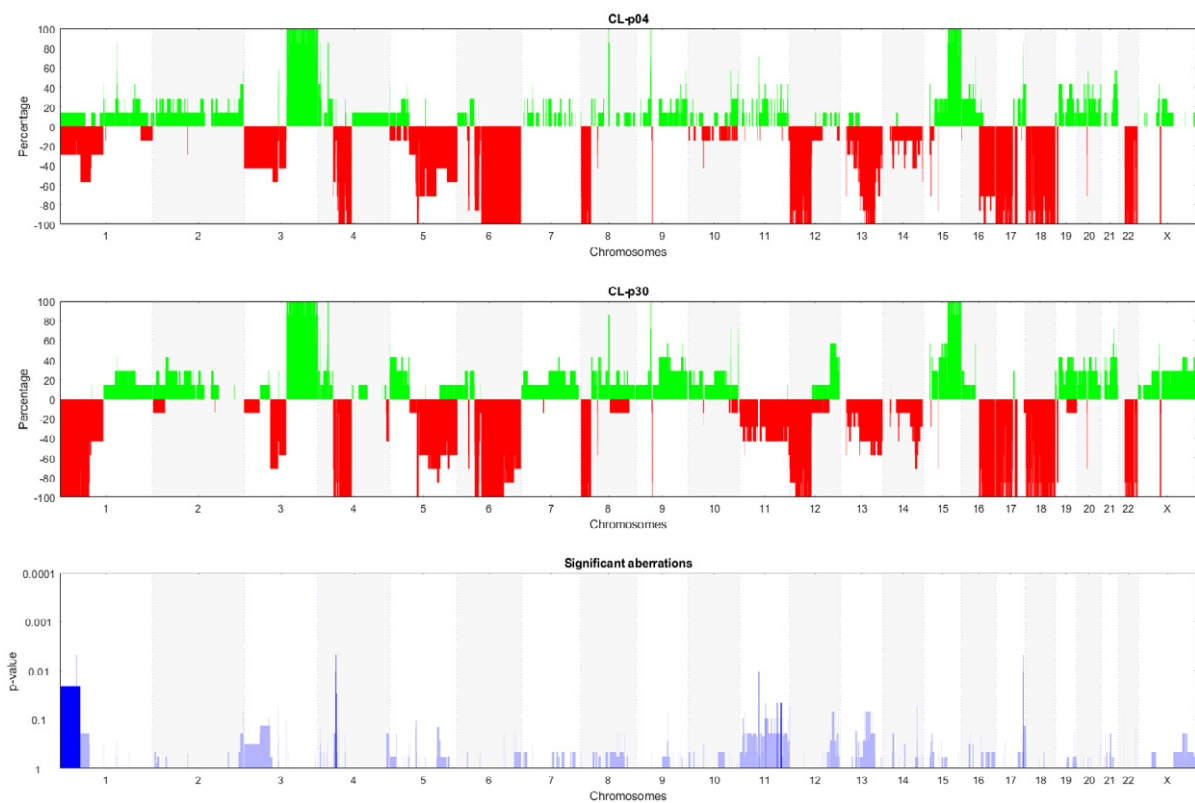
A**B**

Figure 3.

Table 1. Functionally relevant mutations in CTC-ITB-01, vaginal metastasis, and primary tumors identified by whole-exome sequencing.

Gene name	CTC-ITB-01	Vaginal metastasis	Left primary tumor	Right primary tumor
CDH1	–	–	c.1792C>T; p.R598* (13%)	–
	–	c.2466delC; p.T823Qfs*23 (37%)	–	–
MAP3K1	c.2782delT; p.S928Lfs*9 (41%)	c.2782delT; p.S928Lfs*9 (15%)	c.2782delT; p.S928Lfs*9 (22%)	c.2782delT; p.S928Lfs*9 (16%)
MAP3K6	c.2837C>T; p.P946L (30%)	c.2837C>T; p.P946L (40%)	c.2837C>T; p.P946L (30%)	c.2837C>T; p.P946L (45%)
NF1	c.4528_4529insG; p.L1510Rfs*20 (90%)	c.4528_4529insG; p.L1510Rfs*20 (37%)	c.4528_4529insG; p.L1510Rfs*20 (4%)	–
PIK3CA	c.1252G>A; p.E418K (26%)	c.1252G>A; p.E418K (33%)	–	–
	c.3140A>G; p.H1047R (74%)	c.3140A>G; p.H1047R (40%)	c.3140A>G; p.H1047R (21%)	c.3140A>G; p.H1047R (23%)
TP53	c.853G>A; p.E285K (92%)	–	–	–
	–	c.1024C>T; p.R342*(39%)	–	–

All four samples were analyzed for rare (MAF, minor allele frequency, <1%), functionally relevant variants with an allele frequency of 10% of reads and higher in at least one of the samples. 219 cancer-associated genes curated from the COSMIC, HGMD, and OMIM databases were analyzed, and 9 pathogenic mutations in 6 genes were identified. Gene symbols were used as approved by the HGNC, and location of variants on cDNA and protein (one letter code) level, and allele frequency is shown. del, deletion; ins, insertion; *, stop codon; fs, frameshift.

weak in CTC-ITB-01 cells (Fig 4A, Appendix Fig S1B). This phenotype mirrors the ER positivity and ERBB2 negativity of both primary tumors (Table EV1). We furthermore used RNA sequencing to perform expression-based subtyping of the CTC cell line using the PAM50 and scmod2 classifiers (Wirapati *et al*, 2008; Parker *et al*, 2009). Pooled cell line cells, as well as the adherent and non-adherent cell fraction, were classified as the breast cancer luminal B subtype (Fig 4C and D).

CTC-ITB-01 cells showed reduced expression of epithelial intermediate filaments K8 and K18 as compared to MCF-7 (Fig 4A), while the mesenchymal markers N-cadherin and vimentin were not expressed (Fig 4A). We further investigated the expression of breast cancer stemness markers. Aldehyde dehydrogenase activity (termed ALDH⁺) and CD44⁺/CD24[–] mark two largely non-overlapping populations of cancer stem cells, which have epithelial-like and mesenchymal-like phenotypes, respectively (Liu *et al*, 2014). CTC-ITB-01 cells were CD44[–]/CD24⁺ (Fig 4A) and a large proportion (77.92%) were ALDH⁺ as revealed by flow cytometric analysis (Fig 4E) and confirmed by ICC (Fig EV4).

The capacity of CTC-ITB-01 cells to secrete specific proteins of interest was assessed via functional fluoro-EPISPOT assays.

Besides keratin 19, recently described as CTC marker for breast cancer and other epithelial malignancies (Alix-Panabieres & Pantel, 2014a), viable CTC-ITB-01 cells actively secreted vascular endothelial growth factor (VEGF) known to induce tumor angiogenesis in patients with cancer (Saharinen *et al*, 2011) (Appendix Fig S2). While this secretion is comparable to that of the colon cancer CTC cell line CTC-MCC-41, CTC-ITB-01 does not secrete OPG (osteoprotegerin), EGFR (epidermal growth factor receptor) or FGF2 (fibroblast growth factor-2) characteristic for CTC-MCC-41 (Appendix Fig S2) (Cayrefourcq *et al*, 2015).

To find out whether stem cell pathways might be involved in the stem cell-like behavior of CTC-ITB-01, we tested a selection of index proteins by Western blot analysis. Interestingly, the expression level of NUMB indicative of activation of the NUMB pathway was strikingly increased compared with MCF-7, while NOTCH1 and NOTCH3 as components of the NOTCH pathway are rather weaker expressed in CTC-ITB-01 than in MCF-7. The levels of Cleaved NOTCH-1 expressed in CTC-ITB-01 and MCF-7 were similar (Fig EV5). Our results imply a participation of these pathways in the regulation of stem cell features in the CTC-ITB-01 cell line (Bocci *et al*, 2017; Saha *et al*, 2017).

Figure 4. CTC-ITB-01 phenotype in culture.

- Western blot analysis of selected protein markers, including ER α , EGFR, ERBB2, EpCAM, K18, K19, K8, E-cadherin, N-cadherin, vimentin, CD44, CD24, SNAIL, SLUG, TWIST1, and α -tubulin (as a loading control) ($n = 3$ replicates). CTC-ITB-01 was compared to more mesenchymal ER[–] Hs578t and epithelial ER⁺ MCF-7 breast cancer cell lines.
- ICC staining of CTC-ITB-01 for pan-keratin (orange), ER (green), and DAPI (blue). The scale bar corresponds to 20 μ m. Two representative panels are shown for CTC-ITB-01 (1) and (2). MCF-7 cells are depicted as reference cell line.
- PAM50 classifier results showing probabilities of pooled CTC-ITB-01 cells matching specific molecular breast cancer subtypes. Starting from lowest probability, CTC-ITB-01 was classified as 1.02% ($s = 2.5\%$) normal-like, 3.11% ($s = 6.6\%$) Basal-like, 13.11% ($s = 9.3\%$) ERBB2-positive, 16.77% ($s = 23.7\%$) luminal A, and 65.22% ($s = 16.6\%$) luminal B breast cancer subtype. Data were generated from $n = 3$ replicates.
- PAM50 classifier results showing probabilities of the non-adherent and adherent CTC-ITB-01 fractions matching molecular subtypes. Selected bars are not visible due to extremely low probability (close to zero). Both fractions show greatest alignment with a luminal B subtype. Starting from lowest probability, the adherent fraction of CTC-ITB-01 was classified as 0% ($\pm 0\%$) normal-like, 6.22% ($\pm 9.0\%$) Basal-like, 17.85% ($\pm 8.6\%$) ERBB2-positive, 0% ($s = 0\%$) luminal A, and 75.92% ($s = 0.7\%$) luminal B breast cancer subtype. The suspension cell fraction of CTC-ITB-01 was classified as 2.04% ($s = 3.5\%$) normal-like, 0% ($s = 0\%$) Basal-like, 17.32% ($s = 9.7\%$) ERBB2-positive, 33.5% ($s = 23.8\%$) luminal A, and 68.67% ($s = 18.6\%$) luminal B breast cancer subtype, respectively. Data were generated from $n = 3$ replicates.
- ALDH activity measurement on viable cells via flow cytometry using the ALDEFLUOR[™] assay. CTC-ITB-01 is compared to A549 as recommended control cell line. An internal (DEAB) control is also depicted. 77.92% of the gated CTC-ITB-01 population are ALDH⁺.

Source data are available online for this figure.

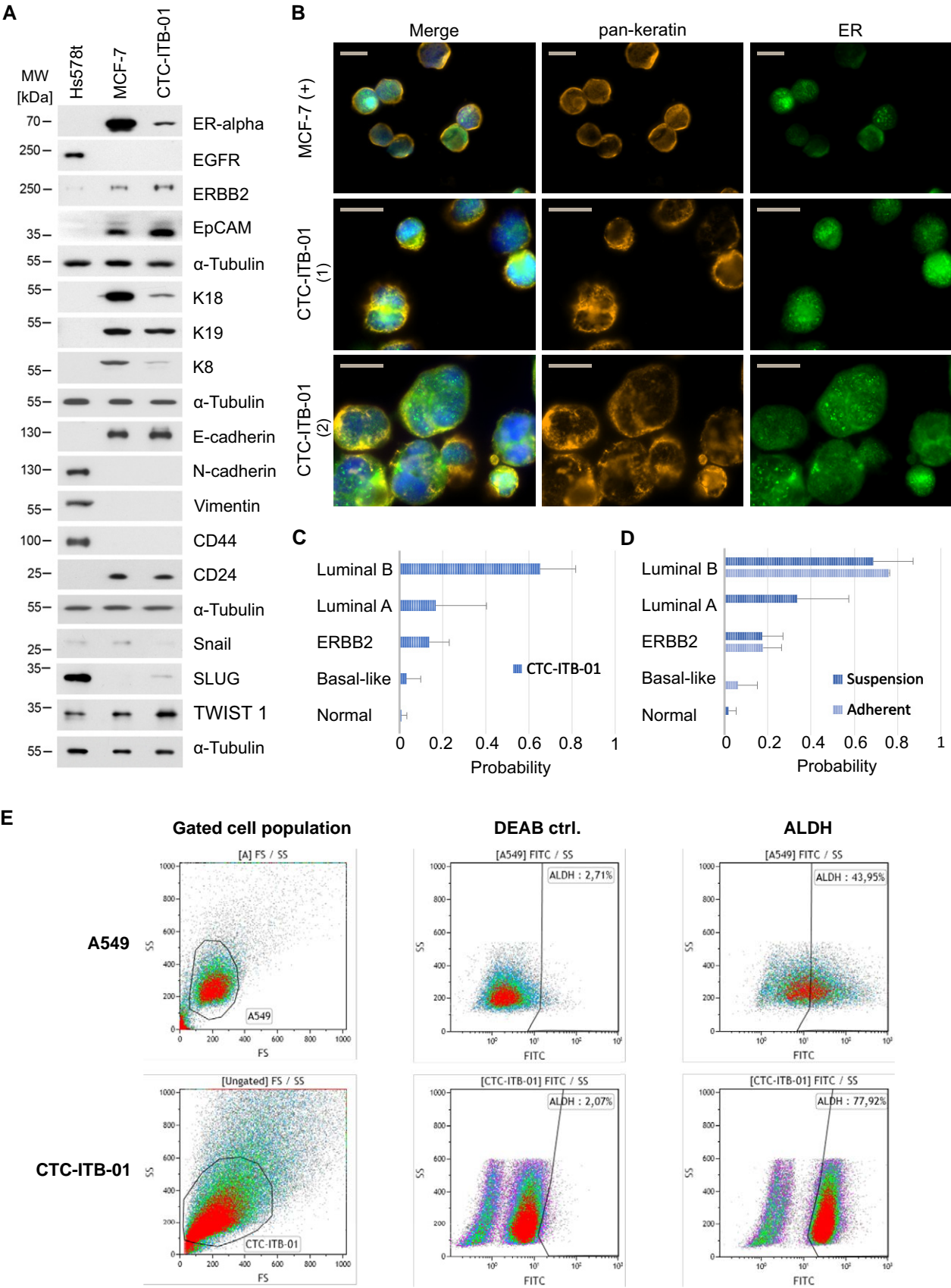


Figure 4.

Epithelial–mesenchymal plasticity of CTC-ITB-01 cells

In the initial blood sample of the patient with breast cancer, the high number of more than 1000 CTCs per ml of blood was detected with

the FDA-cleared CellSearch® system. CellSearch® uses magnetic particles coupled to antibodies against EpCAM to enrich fixed CTCs and subsequently identifies single CTCs by immunostaining of epithelial keratins. Thus, we conclude that this patient harbored

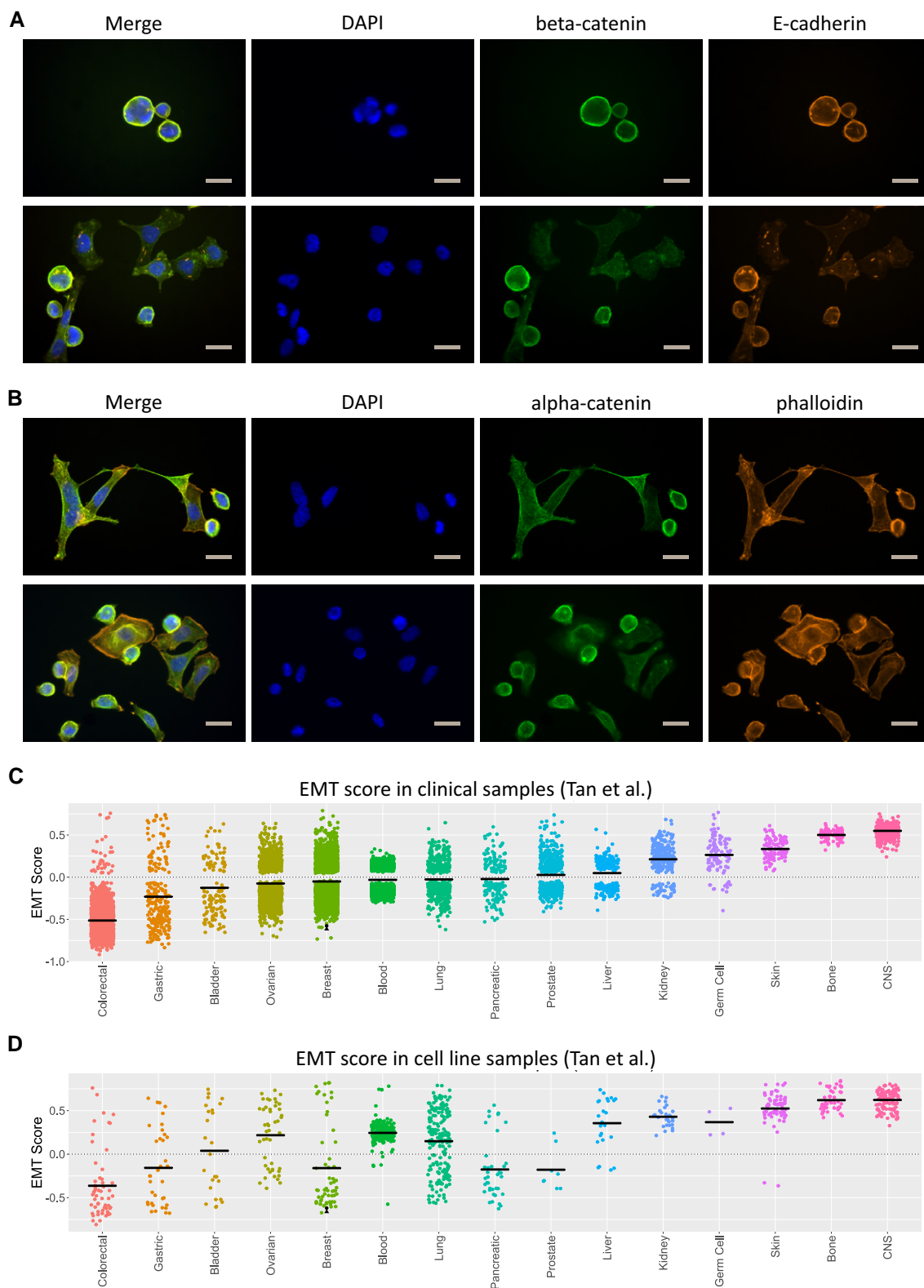


Figure 5.

Figure 5. Epithelial adhesion and EMT analysis of CTC-ITB-01.

- A ICC staining of CTC-ITB-01 for β -catenin (green), E-cadherin (orange), and DAPI (blue). The scale bar corresponds to 20 μ m. Two representative panels are shown for CTC-ITB-01.
- B ICC staining of CTC-ITB-01 for α -catenin (green), visualization of actin filaments by phalloidin (orange), and nuclei by DAPI (blue). The scale bar corresponds to 20 μ m. Two representative panels are shown for CTC-ITB-01.
- C Generic EMT score of the adherent and non-adherently growing CTC-ITB-01 fractions in relation to tumor samples from different cancer entities. Scaling ranges from 1 (completely mesenchymal) to -1 (entirely epithelial). The adherent fraction is shown with a black dot, the non-adherent fraction with a black triangle, and the mean score per cancer entity by a black line.
- D Generic EMT score of the adherent and non-adherently growing CTC-ITB-01 fractions in relation to established cancer cell lines. Scaling ranges from 1 (completely mesenchymal) to -1 (entirely epithelial). The adherent fraction is shown with a black dot, the non-adherent fraction with a black triangle, and the mean score per cancer entity by a black line.

Source data are available online for this figure.

many CTCs with an epithelial phenotype. However, we could not exclude that mesenchymal CTC phenotypes lacking EpCAM or keratin expression were also present in the blood of this patient but remained undetected by CellSearch[®], as shown in previous CTC studies (de Wit *et al*, 2018; Keller *et al*, 2019). To avoid selection bias for a particular phenotype of CTCs (Alix-Panabieres & Pantel, 2014a), we therefore took another blood sample from the same patient and cultured CTCs that were enriched by depletion of leukocytes using the Rosette Sep technology allowing an enrichment independent from the CTC phenotype. Thus, CTCs with epithelial and mesenchymal attributes had the same chance to be enriched and grown in culture.

This might explain why the morphology of the CTC-ITB-01 cell line is heterogeneous and not typical for an epithelial-like breast cancer cell line such as MCF-7. CTC-ITB-01 cells grow in parallel as adherent and non-adherent cell fractions (Fig 1C and D) and in varying cell sizes (Appendix Fig S3). The non-adherent cells grow out from the adherent cells into the medium resembling a string of pearls. Cultivating of either fraction separately results in adherently growing cells and subsequently similarly gives rise to the development of cells in suspension, indicating a high plasticity of CTC-ITB-01 cells (Pei *et al*, 2019).

The epithelial–mesenchymal morphology is characterized by a mixed population of epithelial cells in close cell–cell contact together with elongated, spindle-like cells growing disconnectedly (Fig 5A and B).

The expression of epithelial cell adhesion proteins detected via immunocytochemistry in adherently growing CTC-ITB-01 cells mirrors this phenotypic heterogeneity. While a subpopulation of these cells displays strong membranous E-cadherin staining with beta-catenin co-localization (Fig 5A), others show a more diffuse and weak expression of these proteins. Alpha-catenin displays

similarly diverse expression patterns (Fig 5B). Interestingly, E-cadherin appears to aggregate in small filaments, visible in all cells (Fig 5A).

To provide evidence for EMT features of our cell line, we analyzed the expression of the EMT transcription factors TWIST, SLUG, and SNAIL by Western blot analysis. Compared to MCF-7, increased levels of TWIST and SLUG were observed, while SNAIL was rather weaker expressed in CTC-ITB-01 (Fig 4A), providing further evidence that CTC-ITB-01 cells exhibit some signs of EMT.

To gain deeper insights into the EMT status of both cellular fractions, CTC-ITB-01 cells were assessed by analyzing RNA-sequencing data (from biological triplicates) using an EMT-scoring algorithm (Tan *et al*, 2014). This classifier compares data gained from hundreds of cancer cell line and tumor samples to allocate a score between -1 (completely epithelial) and +1 (completely mesenchymal) on the EMT spectrum. Both the adherent ($\bar{x} = -0.619$, $s = 0.002$) and non-adherent ($\bar{x} = -0.661$, $s = 0.011$) CTC fractions were clearly designated epithelial (Fig 5C and D). Compared with clinical breast cancer tumor tissue samples (Fig 5C) as well as other cancer cell lines (Fig 5D), CTC-ITB-01 appears to fall on the more epithelial end of the EMT spectrum, well below the established median value in both cases.

Xenograft formation and metastasis in immunocompromised mice

To assess tumorigenic as well as metastatic potential of the CTC-ITB-01 line, a GFP-luciferase transduced cell population was directly injected into the mouse milk duct system of four 10-week-old immunodeficient NOD scid gamma (NSG) females. This has proven to be an efficient model for ER⁺ cancer cell lines, allowing outgrowth under physiological systemic estrogen and low SLUG

Figure 6. Xenograft of CTC-ITB-01 in immunodeficient mice confirms tumorigenic and metastatic potential.

- A *In vivo* bioluminescence imaging of CTC-ITB-01 in four NSG mice. Blue indicates low radiance, red indicates high radiance.
- B Logarithmic plotting of *in vivo* radiance increase over time. Curves represent means \pm SEM of measurements performed on multiple glands ($n = 8$).
- C H&E staining of xenografted mouse mammary glands show formation of primary tumors.
- D Stereoscope image of a mammary gland of immunodeficient NSG mouse. Fluorescently tagged CTC-ITB-01 cells in green.
- E IHC staining for ER, confirms retained *in vivo* ER positivity of formed tumors. Representative images of ER staining in higher (left panel) and lower (right panel) magnification of 2 different areas of a xenografted mammary gland.
- F Representative *ex vivo* luminescence images of indicated organs from engrafted mice. Organs include brain (1), lung (2), liver (3), and bones (4).
- G Scatter plot showing *ex vivo* radiance intensity of metastatic organs in three different mice (M1, M2, M3), indicating highest intensity in liver and bone. Data represent means \pm SD of measurements performed on metastatic organs derived from three different mice.

Source data are available online for this figure.

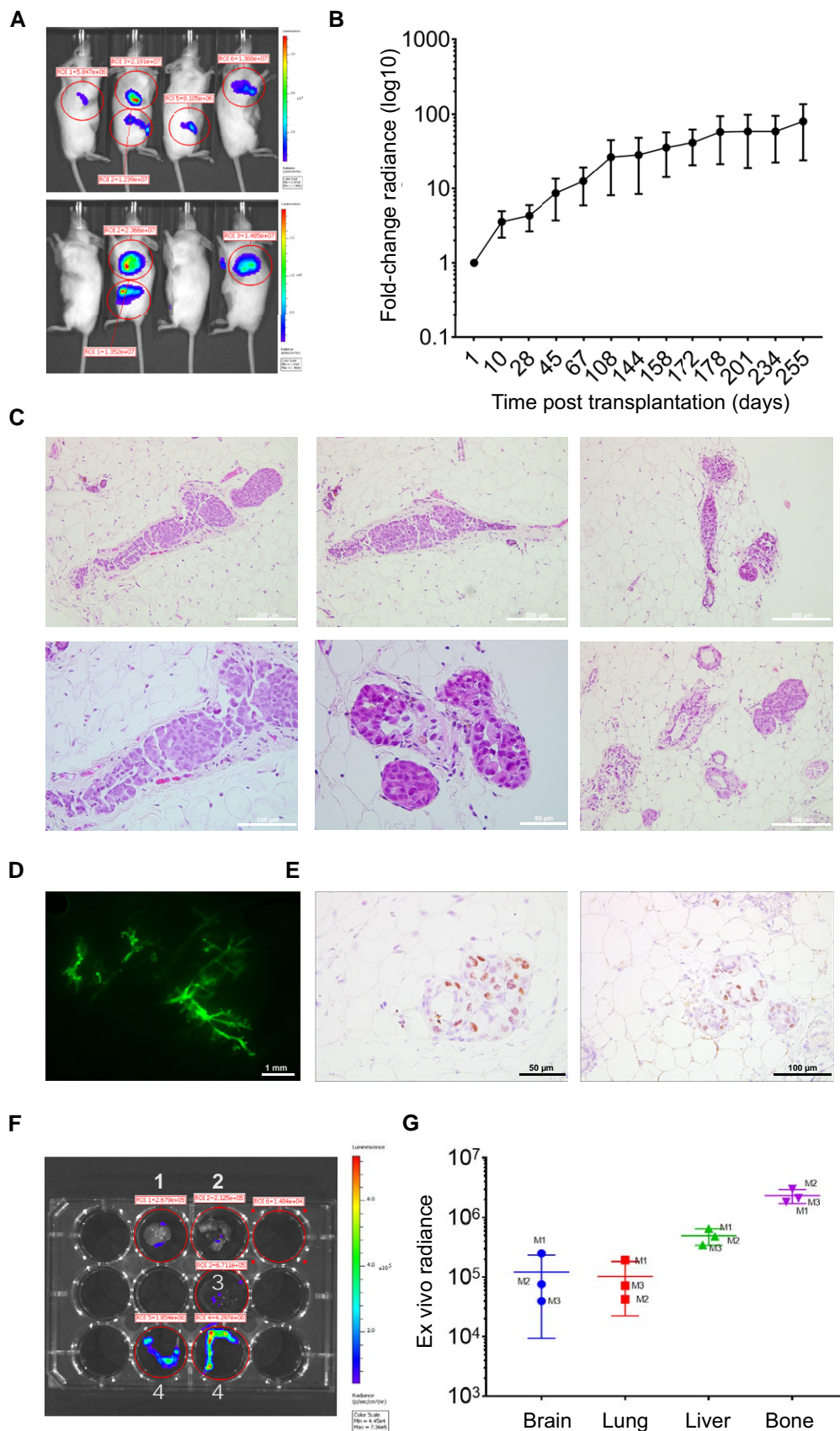


Figure 6.

levels (Sflomos *et al*, 2016; Ozdemir *et al*, 2018). Mice were monitored by *in vivo* bioluminescence imaging to assess the formation and proliferation of primary tumors and spontaneous metastases in clinical relevant tissues.

Primary tumor formation was seen in all mice bearing intraductally injected glands (Fig 6A). Tumor burden increased steadily over time until sacrificing after 8.5 months, assessed by the fold change radiance in bioluminescence imaging *in vivo* (Fig 6B). H&E sections of the mouse milk duct tissue (Fig 6C) confirmed the tumorigenic potential of CTC-ITB-01 in NSG mice. Fig 6D shows a stereoscope image of intraductal fluorescently tagged CTC-ITB-01 cells. Immunohistochemical staining for ER furthermore revealed that the ER⁺ status of the cell line was maintained on the CTC-derived xenografts (CDX), confirming that histopathologic features are preserved (Fig 6E). Upon sacrificing, three out of four mice displayed micrometastases in the brain, lung, bone, and liver (Fig 6F and G). The fourth mouse had to be sacrificed early due to health reasons unrelated to tumor growth. The overall highest *ex vivo* radiance was detected within the bone metastasis of the mice, mirroring the predominant metastatic site of ER⁺ breast cancer patients (Fig 6G). Interestingly, both bone and liver represented metastatic sites in the patient who harbored the CTCs that gave rise to CTC-ITB-01 and displayed high *ex vivo* bioluminescence in the MIND mouse model.

Conclusively, CTC-ITB-01 cells have tumorigenic potential in NSG mice upon intraductal injection and metastasize to clinically relevant organs such as bone, liver, brain, and lung.

Estrogen sensitivity and relevance of the ER-alpha for growth of CTC-ITB-01

CTC-ITB-01 cells were isolated after the patient progressed under two different endocrine therapy regimens based on the aromatase inhibitor letrozole and later tamoxifen (Fig 1A). Therefore, CTC-ITB-01 cells were tested for their ability to respond to 17- β -estradiol (E2). To rule out unspecific effects of estrogens and other substances which could cause activation of ER-alpha within the culture medium, the experiment was carried out using phenol red-free RPMI substituted with charcoal-stripped FBS. When cultured

under estrogen-free conditions or in the presence of E2 concentrations $\leq 10^{-11}$, CTC-ITB-01 cells showed slower outgrowth than when cultured in the presence of higher E2 concentrations (Fig 7A right panel). This indicates that the ER-alpha within CTC-ITB-01 cells is still functional and high estrogen concentrations cause accelerated cell growth. No differences in the morphology of CTC-ITB-01 cultured in the absence or in the presence of different E2 concentrations were observed (Fig 7A left panel). The fact that CTC-ITB-01 cells still grow and show no significant morphological changes under estrogen-free conditions point to these cells being able to tolerate estrogen deprivation and therefore endocrine regimens.

To investigate the potential relevance of the ER-alpha for outgrowth of CTC-ITB-01, stable knockdowns of ER-alpha with two different shRNAs were performed. Knockdown of ER-alpha with both shRNAs showed strong reduction of colonies in comparison with non-targeted shRNAs in colony-forming assays (Fig 7B left upper and lower panel). Efficiency of ER-alpha knockdowns were evidenced by Western blotting (Fig 7B right panel). This demonstrates that the ER-alpha is relevant for growth of CTC-ITB-01 under the given culture conditions. To investigate potential differences in the functionality of ER-alpha between CTC-ITB-01 and MCF-7 cells, both cell lines were cultured under identical conditions within estrogen-free, charcoal-stripped, phenol red-free medium. Both cell lines were cultured under E2-free conditions or incubated in the presence of E2 as indicated. After 24 h cells were harvested and differences in expression levels of certain ER-alpha target genes were tested by Western blotting. MCF-7 cells express ER-alpha target genes only in the presence of E2, whereas CTC-ITB-01 cells continue to express these genes in the absence of E2 (Fig 7C). This data suggests that ER-alpha within CTC-ITB-01 cells is active even in the absence of E2, which might explain why CTC-ITB-01 can tolerate low E2 levels. Interestingly, while MCF-7 expresses PR-A (progesterone receptor α) and B (progesterone receptor β) in an E2-dependent manner, CTC-ITB-01 cells display low amounts of PR-A but not B. However, both cell lines show reduced levels of ER-alpha in the presence of E2 indicating that both cell lines have functional mechanisms that regulate ER-alpha expression under the influence of estrogen (Martin *et al*, 1993).

Figure 7. Estrogen and Palbociclib sensitivity of CTC-ITB-01.

- A Equal numbers of CTC-ITB-01 cells were seeded on 6-well culture plates and grown in the presence or absence of different 17- β -estradiol concentrations as indicated. After 10 days, cells were fixed and stained with Coomassie blue staining (right panel). Macroscopic photographs are shown of the fixed cell colonies from cells grown in the absence or presence of the indicated E2 concentrations (right panel). Scale bar 200 μ m.
- B Stable knockdown of ER-alpha within CTC-ITB-01 cells was performed by using lentiviral transfer of non-targeted (scramble) or two different targeted shRNAs against ER-alpha. CTC-ITB-01 cells were seeded on 6-well plates. After 10 days, cells were fixed and stained (left upper panel). Macroscopic photos are shown of the fixed cells (left lower panel), scale bar 200 μ m. Western blots of lysates from knockdown of ER-alpha expression in CTC-ITB-01 cells transduced with the same amounts of lentiviral vectors were probed with the indicated antibodies. The extracts were obtained 72 h after lentiviral transduction (right panel). Where indicated, Western blots were visualized at long exposure (l.e.) and/or short exposure (s.e.).
- C CTC-ITB-01 and MCF-7 cells were grown under the same culture conditions in the presence or absence of E2 as indicated. 24 h after E2 deprivation or E2-treatment cells were harvested. Western blots of the protein lysates were probed with antibodies targeting ER-alpha, FOXM1, Bcl-2, PR-A, PR-B and ID1, actin was used as loading control, visualized at long exposure (l.e.) and/or short exposure (s.e.).
- D, E (D) Growth curves of CTC-ITB-01 and (E) MCF-7 cells under varying concentrations of Palbociclib treatment were measured using an IncuCyte Zoom live cell imaging system. The mean values from three technical triplicates (one experiment) with standard deviation are shown.
- F, G (F) Influence of Palbociclib on CTC-ITB-01 growth after 300 h and (G) MCF-7 after 80 h. Data were chosen from one representative time point during the exponential growth phase. Statistical significance was analyzed with a one-way ANOVA with Dunnett's multiple comparisons test and compared to the vehicle substance dimethyl sulfoxide (DMSO). The mean values from technical triplicates (one experiment) with standard deviation are shown.
- H, I (H) Effect of Palbociclib on the growth of CTC-ITB-01 cells and (I) MCF-7 cells. Concentrations were transformed to common logarithm. Three-parameter non-linear logistic regression was used to determine the IC₅₀. The mean values from three technical triplicates (one experiment) with standard deviation are shown. Error bars for standard deviation smaller than the symbols are not displayed.

Source data are available online for this figure.

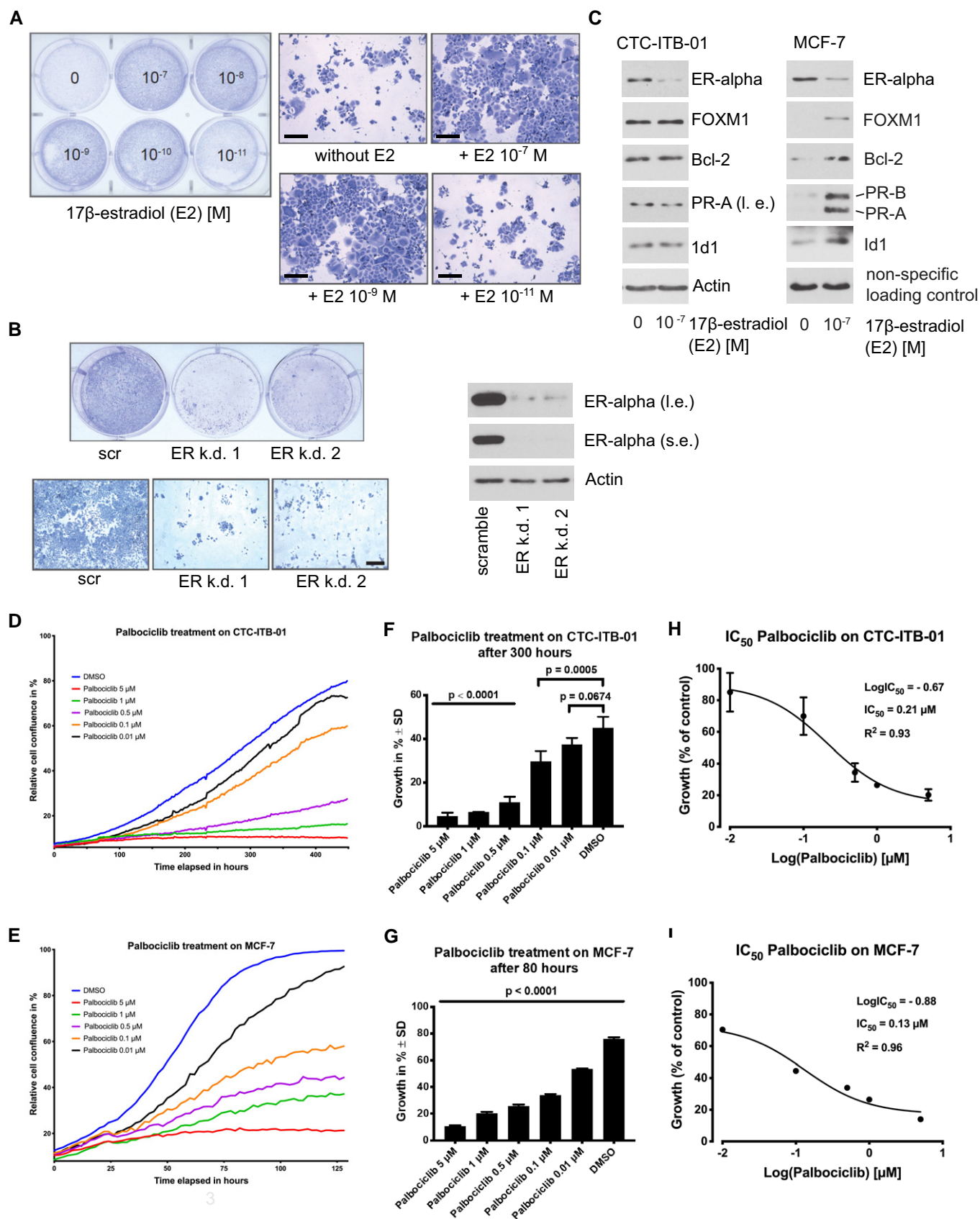


Figure 7.

Response of CTC-ITB-01 to cyclin-dependent kinase (CDK) 4/6 inhibitors

While the patient with breast cancer giving rise to CTC-ITB-01 progressed on endocrine and later chemotherapy, the added benefit of novel cyclin-dependent kinase (CDK) 4/6 inhibitors has only recently been described for ER⁺ breast cancer patients (Finn *et al*, 2015, 2016). At the time point when the patient had been treated, CDK inhibitors were not available for standard of care therapy in patients with breast cancer in Germany. To test the potential sensitivity of CTC-ITB-01 toward CDK4/6-inhibitors, CTC-ITB-01 and MCF-7 cells were treated with different concentrations of Palbociclib (Fig 7D and E). Cell growth is significantly reduced in CTC-ITB-01 already at a dose of 0.1 μ M of this CDK4/6 inhibitor ($P < 0.001$) in relation to the DMSO control (Fig 7F). Compared to the MCF-7 cell line, CTC-ITB-01 shows similar sensitivity toward Palbociclib at lower inhibitor doses (e.g., 0.1 μ M Palbociclib) and slightly increased sensitivity at higher doses of 0.5–5 μ M (Fig 7F and G). The IC₅₀ values were 0.21 μ M for CTC-ITB-01 (Fig 7H) and 0.13 μ M for MCF-7 (Fig 7I), respectively, indicating that the patient might have benefited from treatment with CDK4/6 inhibitors.

Discussion

The functional properties of CTCs are still largely unknown due to the rarity of functional models such as cell lines derived from CTCs that mirror the *in situ* CTCs in patients with cancer. A frequent argument raised against the use of cell lines is that tumor cells may change their original characteristics rapidly in cell culture. Here we provide, for the first time, a direct genomic comparison of the original CTCs isolated from a patient with breast cancer to the cell line established from these CTCs. Our results demonstrate that our ER⁺ breast CTC line resembles largely the CNA patterns of *in situ* CTCs, suggesting that the cell line has not undergone substantial genomic changes during the culturing period (passage 4 and passage 30) and might represent a good model for studying CTC biology.

The high number of CTCs isolated was certainly one precondition for the establishment of our CTC line. However, high CTC numbers on its own are no guarantee to obtain a permanent cell line (Tayoun *et al*, 2019; Faugeroux *et al*, 2020). Thus, we assume that the cells of our cell line have also the right biological properties of the most “aggressive” subset of CTCs. Future studies comparing CTC lines with CTCs that will stop proliferating after short term culture might help to define the molecular make up required for permanent survival and growth of CTCs.

CTC-ITB-01 cells showed a luminal B breast cancer subtype (ER⁺, ERBB2⁻); in particular the stable ER expression is remarkable in view of the paucity of ER⁺ breast cancer cell lines. Thus, our CTC cell line provides a novel model to study ER⁺ breast cancer CTCs. Moreover, for the first time, genomic aberrations of a breast cancer CTC-derived cell line were compared between the initially isolated CTCs, primary tumors and a distant metastasis.

The half-life of CTCs in the circulation is very short (few hours) (Meng *et al*, 2004) and the blood sample in our study was obtained years after primary tumor diagnosis in a highly metastatic setting. Thus, the CTC line is most likely derived from CTCs released from one or multiple metastatic sites (bone, lymph node, liver, vagina, or

spleen) of our patient. While CTC-ITB-01 cells showed a *CDH1* variant [c.1204G>A; p.D402N] in combination with loss of 16q (Ciriello *et al*, 2015), this variant differs from mutations of the left, primarily lobular tumor and the distant metastasis. Additionally, CTC-ITB-01 retains strong *CDH1* expression, arguing against a lobular origin. However, *CDH1* molecules expressed by the CTC-ITB-01 cell line are potentially adhesion-deficient (mutation in EC3), which might be the cause for the observation that subcellular distribution is disturbed. Furthermore, the CTC-ITB-01 cell line shares a mutation in the *NF1* gene, which belongs to the 9 frequently mutated driver genes in hormone receptor-positive breast cancer (Bertucci *et al*, 2019), with the primary lobular tumor and the vaginal metastasis. Besides shared variations with the primary tumors, CTC-ITB-01 and the vaginal metastasis exhibited an additional, less frequent *PIK3CA* mutation (c.1252G>A; p.E418K, Table 1), located in the region encoding the C2 calcium/lipid-binding domain (Saal *et al*, 2005; Stemke-Hale *et al*, 2008). Taken together, we can speculate that the vaginal metastasis might have contributed to the pool of CTCs but it appears not be the exclusive source.

In addition, CTC-ITB-01 cells have accumulated large genomic areas showing increased LOH as compared to the primary tumors, including large parts of chromosome 17p (13.905–18.391.123) harboring the *TP53* gene locus. In combination with the *TP53* mutation of CTC-ITB-01, this provides hints for a role of TP53 in dissemination and survival of CTCs in the bloodstream.

The in-depth characterization of CTC-ITB-01 cells on RNA and protein levels demonstrated a predominantly epithelial phenotype; additionally, CTC-ITB-01 cells showed phenotypic and functional *in vitro* and *in vivo* characteristics of cancer stem cells. EMT is assumed to play a crucial role in migration of tumor cells (Alix-Panabieres *et al*, 2017) and has been implicated in cancer progression, metastasis (Chaffer *et al*, 2016) and resistance to chemotherapy (Nieto *et al*, 2016). It has furthermore been established that CTCs display plasticity on the EMT spectrum (Armstrong *et al*, 2011; Nieto *et al*, 2016; Alix-Panabieres *et al*, 2017), shifting between epithelial and mesenchymal states depending on therapy and stages of disease progression (Yu *et al*, 2013). However, EMT enables invasiveness while simultaneously reducing the self-renewal capacity of tumor cells, thus reducing their potential to outgrow at distant sites (Celia-Terrassa *et al*, 2012). Interestingly, CTC-ITB-01 and the *in situ* CTCs of our index patient expressed epithelium-specific proteins such as EpCAM and keratins. EMT-scoring, using an established algorithm further revealed that CTC-ITB-01 resides on the epithelial end of the EMT spectrum.

Interestingly, CTC-ITB-01 cells showed an interchangeable adherent and non-adherent cell population similar to the behavior described for cancer stem cells (Cariati *et al*, 2008). This growth pattern was consistent with the observed dysregulated subcellular distribution of cell adhesion proteins such as E-cadherin, alpha-, and beta-catenin, with a significant expression of some transcription factors (TWIST1, SLUG) known to be involved in EMT regulation as well as with activation of the NUMB pathway. Nevertheless, RNA sequencing of both adherent and non-adherent cell layer of CTC-ITB-01 showed predominantly an epithelial signature, which is consistent with a recent report (Ebright *et al*, 2020), indicating that proliferating CTCs with an epithelial signature were the most aggressive subset associated with an unfavorable clinical outcome in breast cancer.

There have been multiple studies linking EMT and stemness in CTCs, revealing that both cellular programs are closely intertwined (Raimondi *et al*, 2011; Papadaki *et al*, 2014). Originally a CD44⁺/CD24⁻ phenotype was associated with breast cancer stemness (Al-Hajj *et al*, 2003). While the CTC-ITB-01 cell line was CD44⁻/CD24⁺, it showed a high expression of ALDH1, a more recent breast cancer stemness marker (Ginestier *et al*, 2007; Charafe-Jauffret *et al*, 2010). It has been reported that CD44⁻/CD24⁺ and ALDH1⁺ tumor cells represent two distinct tumor cell populations not only localized in different regions of the primary tumor tissue but also expressing distinct EMT and MET gene profiles (Liu *et al*, 2014; Colacino *et al*, 2018). Furthermore, ALDH1-expressing stem cells have been described as epithelial and proliferative in contrast to the more mesenchymal and quiescent CD44⁺/CD24⁻ stem cells (Ginestier *et al*, 2007; Liu *et al*, 2014; Colacino *et al*, 2018), which is consistent with the CD44⁻/CD24⁺/ALDH1⁺ epithelial phenotype of CTC-ITB-01 cells that were capable of *ex vivo* growth. Although CTC-ITB-01 shows some signs of cancer stem cells, more detailed future investigations are required to further determine whether our CTC line fulfills all criteria of cancer stem cells.

Apart from intrinsic attributes of CTCs, the interaction with the surrounding microenvironment is crucial for successful extravasation and colonization of distant organs. The cancer secretome can therefore function as an indicator of how the CTCs attempt to manipulate the host tissue. Here, we analyzed selected secreted proteins, known to be involved in different aspects of tumor development, progression and metastasis via the EPISPOT assay (Ramirez *et al*, 2014; Cayrefourcq *et al*, 2015). Apart from K19, CTC-ITB-01 secreted VEGF, a known angiogenic inducer as well as promoter of cancer stem cell self-renewal (Beck *et al*, 2011; Saharinen *et al*, 2011; Zhao *et al*, 2015; Liu *et al*, 2017).

The tumorigenic nature of CTC-ITB-01 was further demonstrated in CDX models. Growing ER⁺ cell lines as xenografts *in vivo* has not been successful without addition of exogenous 17 β -estradiol in the past (Guiu *et al*, 2014; Sikora *et al*, 2014). This hormonal treatment, however, has detrimental effects on the health of the mice and induces estrogen levels equivalent to premenopausal conditions. It therefore does not adequately mirror disease development in the patient as most women develop ER⁺ breast cancer in a postmenopausal setting. PDX are similarly difficult to establish displaying an engraftment rate of around 2.5% in immune-compromised mice (Cottu *et al*, 2012). This has contributed to underrepresentation of ER⁺ tumors in mouse models due to a favoring of more aggressive histological subtypes (ERBB2⁺ and triple-negative). Sflosmos *et al* recently developed an elegant *in vivo* model circumventing many of these issues and allowing outgrowth of ER⁺ cell lines under physiological hormone levels, thus increasing the engraftment rate to 30–100% (Sflosmos *et al*, 2016). Using this model, we confirmed the tumorigenic capacity of CTC-ITB-01 in immunodeficient NSG mice. Apart from primary tumor formation in the mouse milk ducts of all four animals, three out of four mice displayed metastasis in organs equal to those of the patient with breast cancer, thus mirroring disease development in the patient with cancer. Additionally, all xenografts preserved the histopathological features (ER⁺) of their clinical counterpart.

As the CTC line was derived from a patient progressing first on hormone therapy and subsequently on chemotherapy, it could provide a valuable model to study resistance to therapy. While the

ER remains partly functional and relevant for CTC-ITB-01 growth, downstream signaling appears to be constitutively active independent of ligand availability. This might provide a survival benefit for CTC-ITB-01 under extremely low ligand levels achieved by endocrine therapy, which might explain why the patient progressed under endocrine therapy. While ESR1 mutations represent a common mechanism of acquired resistance to endocrine therapy (Jeselsohn *et al*, 2015), we did not detect these mutations in CTC-ITB-01, suggesting a different mechanism of resistance in our index patient. Interestingly, treatment with the CDK4/6 inhibitor Palbociclib showed a concentration-dependent inhibition of CTC-ITB-01 growth, suggesting that the patient may have benefitted from this new line of therapy recently approved for ER⁺ patients (Turner *et al*, 2015; Finn *et al*, 2016). However, our *in vitro* data should be further tested by *in vivo* xenotransplantation models.

In conclusion, we characterize a unique CTC-derived ER⁺ breast cancer cell line that shares important features of *in situ* CTCs. This CTC line therefore represents a promising new tool for functional studies on CTC biology and response to novel drugs envisaged for ER⁺ breast cancer.

Materials and Methods

Blood collection and processing

Informed consent was obtained from all subjects, and the experiments conformed to the principles set out in the WMA Declaration of Helsinki and the Department of Health and Human Services Belmont Report as well as to the guidelines for experimentation with humans by the Chambers of Physicians of the State of Hamburg ("Hamburger Ärztekammer"). For this study, the blood of 50 patients with metastatic breast cancer was collected and processed. Samples were drawn into standard 7.5 ml ethylenediaminetetraacetic acid (EDTA) vacutainers or a CellSave[®] (Menarini Silicon Biosystems) preservation tube, respectively. The patients therefore provided a matched sample of blood in an EDTA (for *in vivo* culture) and CellSave[®] tube (CTC enumeration) for further analysis. The blood sample collected into the CellSave[®] preservation tube was processed with the CellSearch[®] system (Riethdorf *et al*, 2007). All analyses were performed by experienced scientists. CTCs were defined as keratin-positive, CD45-negative cells with a nuclear DAPI staining.

Isolation and cultivation of CTC-ITB-01

CTCs were enriched from 7.5 ml of EDTA blood by Rosette Sep[™] (StemCell Technologies) according to the manufacturer's instructions but using 20 μ l of Rosette Sep[™] solution per ml of blood instead of 50 μ l/ml. The cell pellet gained from Rosette Sep[™] enrichment was resuspended in 3 ml of RPMI *complete* medium. RPMI *complete* comprises RPMI 1640 (Gibco), 10% Fetal Calf Serum (FCS) (Gibco), 1% penicillin-streptomycin mix (Gibco), 1% L-glutamine (Gibco), 1% Insulin-Transferrin-Selenium-A Supplement (100X) liquid (Life Technologies), 10 ng/ml FGF2 (Miltenyi), 50 ng/ml EGF (Miltenyi), 0.1 μ g/ml hydrocortisone (Sigma-Aldrich), and 0.2 μ g/ml cholera Toxin (Sigma-Aldrich). Additional information is provided in Appendix Supplementary Methods. The cell solution

was distributed into a 96-well plate and cultured in standard cell culture conditions (37°C, 5% CO₂). After 14 days of cell culture, medium was changed. At 90% confluence, outgrowing cells were transferred to a 12-well cell culture dish and expanded.

Standard cell culture

MCF-7 (ATCC[®] HTB-22), Hs578T (ATCC[®] HTB-126), SKBR3 (ATCC[®] HTB-30), MDA-MB-468 (ATCC[®] HTB-132), MDA-MB-231 (ATCC[®] HTB-26), NBTII (bladder tumor), and 11B (laryngeal squamous cell carcinoma) cell lines were maintained in DMEM (Dulbecco's Modified Eagle's medium, Gibco) with 10% of FCS and 1% penicillin/streptomycin. A549 cells were cultured in DMEM supplemented with 10 mM of HEPES, 10% of FBS, and 1% penicillin/streptomycin. CTC-MCC-41 cell line was sustained in micrometastatic medium (RPMI1640, Growth factors: EGF and FGF-2, Insulin-Transferrin-Selenium supplement, L-Glutamine).

Karyotyping

For metaphase spreads, cells were treated with colcemid (0.02 µg/ml) overnight, incubated with 0.0075 M KCl, fixed with methanol/acetic acid (3:1), dropped onto wet slides, stained with 5% giemsa, and mounted with entellan before imaging with the Axioplan 2 microscope (Zeiss). 25 metaphases per experiment were counted.

DNA isolation from cell culture and FFPE tissue

Genomic DNA (gDNA) was isolated from cell culture using the *Nucleospin[®] Tissue Kit* (Macherey & Nagel) according to the manufacturer's instructions. gDNA from FFPE material was isolated with the *innuPREP DNA Micro Kit* (Analytik Jena) according to the manufacturer's instructions. To increase gDNA yield, the lysis step was extended overnight. DNA was stored at −20°C until further use.

Next-generation sequencing and CNA profiling

Single or pools of cells were picked via micromanipulation using a fluorescence microscope and underwent whole genome amplification using the PicoPLEX DNA-seq kit followed by library preparation according to manufacturer's instructions (Takara Bio). Sequencing was performed using an Illumina NextSeq 550. Copy number aberrations of all CTCs were analyzed against 8 single leukocytes from the same patient (control cells) according to a previous publication (Heitzer et al, 2013).

Whole-exome sequencing and WES data analysis

Exonic and adjacent intronic sequences were enriched from genomic DNA of the primary tumor, the vaginal metastasis and the CTC line using the Agilent SureSelect Human All Exon V6 enrichment kit and were run on an Illumina HiSeq4000 sequencer by the Cologne Center for Genomics (CCG). Data analysis and filtering of mapped target sequences were performed with the "Varbank" exome and genome analysis pipeline v.2.1 (CCG) and data were filtered for high-quality (coverage of more than 6 reads, a minimum quality score of 10) variants. WES data were analyzed for variants in 219 (Appendix Table S1) of the frequently mutated genes based on the

COSMIC, HGMD and OMIM databases (Tate et al, 2019) and genes involved in hereditary cancer predispositions syndromes. We filtered for variants with an allele frequency ≥ 10% in at least one of the four samples, a minor allele frequency (MAF) < 1% in the gnomAD database (Karczewski et al, 2020), and a predicted mutational effect on the encoded protein. Silent mutations and intronic variants were included as long as a functional effect on splicing was predicted.

Immunocytochemical staining

For ICC on cytopins and chamber slides, the following primary antibodies were applied: pan-keratin (Alexa488 or Alexa555 conjugated clone: AE1/AE3; eBioscience, 1:300), CD45 (Alexa647 conjugated, clone: Hi-30; BioLegend, 1:200), ER (clone SP1; Sigma-Aldrich, 1:100), ERBB2 (clone 29D8; Cell Signaling, 1:100), ALDH1 (clone 44; BD Pharmingen, 1:100), p53 (clone DO-1, Merck Millipore, 1:100) E-cadherin (Alexa555 conjugated, clone 36, BD Pharmingen, 1:200), α-catenin (clone D9R5E; Cell Signaling, 1:200), and β-catenin (clone D10A8; Cell Signaling, 1:100).

CTC-ITB-01 cells as well as appropriate tumor cell line controls were spun down on glass slides (190 × g for 5 min). Having dried overnight, cells were fixed with 4% PFA (Sigma-Aldrich), permeabilized using 0.1% Triton (Sigma-Aldrich), and blocked with 10% AB-serum (Bio-Rad).

For chamber slide ICC staining, 30,000 CTC-ITB-01 cells were seeded into 2-well chamber slides (Nunc Lab-Tek Chamber Slide System, 2-well Permanox slide, Thermo Fisher Scientific) and incubated under standard culture conditions for 48 h. Subsequently, medium was discarded and cells were washed with 1× PBS (Gibco) three times prior to being fixed with 2% PFA (Sigma-Aldrich) for 10 min. Washing was repeated prior to permeabilization with 0.1% Triton X-100 (Sigma-Aldrich). Following another washing with 1× PBS, slides were blocked for 20 min using 10% AB-serum (Bio-Rad). Primary antibodies were incubated for 60 min.

Secondary antibodies for ICC on cytopins and chamber slides were applied for 60 min. Species-specific secondary antibodies consisted of rabbit-anti-mouse-A546 (polyclonal, Thermo Fisher Scientific), rabbit-anti-mouse-A488 (polyclonal, Thermo Fisher Scientific), and mouse-anti-rabbit-A488 (polyclonal, Thermo Fisher Scientific).

For multiple immunofluorescence stainings, either different fluorescently conjugated antibodies were used as cocktail or subsequently to the sequential application of an unconjugated primary antibody and a fluorescently labeled secondary antibody, additional primary antibodies directly conjugated with fluorochromes were added.

After a final washing step with 1× PBS, cytopins and chamber slides were covered in Prolong Gold Antifade Mountant (Thermo Fisher Scientific) and cover-slipped for analysis. For visualization of actin filaments, phalloidin (Alexa555 conjugated, Life Technologies, 1:100) was used. DAPI was used to counterstain nuclei. Immunofluorescence was evaluated with the fluorescence microscope (Axioplan 2, Zeiss).

Chromogenic immunocytochemical analysis was performed using the DAKO REAL[™] EnVision Detection System Peroxidase/DAB+ Rabbit/Mouse kit (DakoCytomation). Cytopins were fixed with 2% PFA (Sigma-Aldrich) and permeabilized with 1% Triton for 10 min each. Following H₂O₂ blocking, cells were incubated with the P53 antibody diluted in 10% AB-serum (Bio-Rad) for 45 min prior to incubation with the peroxidase-labeled EnVision[™]

polymer coupled with goat anti-rabbit/mouse immunoglobulins (DakoCytomation) for 15 min at room temperature. Subsequently, cells were treated with DAB (3, 3'-diaminobenzidine) in substrate buffer containing hydrogen peroxide reagent for 10 min and coverslipped using Eukitt mounting medium (Sigma-Aldrich). Immunostaining was evaluated using the microscope Axioplan 2 (Zeiss).

Immunohistochemical assays

Patient as well as mouse-derived tumor tissues were formalin-fixed and paraffin-embedded (FFPE) for immunohistochemical analysis (IHC). Paraffin-embedded tissue specimens were taken from tissues acquired for routine diagnostic purposes at the Department of Pathology, University Medical Center Hamburg-Eppendorf. Immunohistochemical analysis was performed using the DAKO REAL™ Detection System Peroxidase/DAB+ Rabbit/Mouse kit (DakoCytomation). In brief, after pressure cooker pre-treatment of deparaffinized sections in citrate buffer (Bio-Genex Laboratories) for 5 min at 120°C and incubation with TBST (20 mM Tris, 150 mM NaCl, 0.1% Tween-20) for 5 min, the primary antibody (Mouse anti-E-cadherin, clone 36, BD Biosciences, final concentration: 1.25 µg/ml) was applied overnight at 4°C. Subsequent application of the biotinylated secondary antibodies for 10 min and endogenous peroxidase blocking solution for 5 min were followed by incubation with streptavidin peroxidase for 10 min. For visualization of E-cadherin-specific immunostaining, DAB diluted in substrate buffer containing hydrogen peroxide was utilized as chromogen. Counterstaining of nuclei was performed with Mayer's hemalum solution (Merck).

For mouse experiments, engrafted glands were dissected, fixed for 4 h in 4% paraformaldehyde, and paraffin-embedded. Four micrometer sections were cut, mounted onto 76 × 26 mm microscope slides (Rogo-Sampaic), and stained with hematoxylin–eosin (H&E). IHC was performed using estrogen receptor (cat#790-4324, clone SP1) by the Ventana-automated staining device (Ventana Medical Systems Inc, Roche AG).

Western blot analysis

Cells were harvested and homogenized by ultrasonic treatment. Protein concentration was measured using the Pierce BCA Protein Assay Kit (Pierce). All samples were generated in biological triplicates. For Western blot analysis, 20 µg of total protein per sample (EpCAM: 40 µg of total protein per sample) was applied. The primary antibodies were utilized according to the instruction manual of the supplier using appropriate dilutions (Table EV4). The appropriate secondary antibodies conjugated with horseradish peroxidase (DakoCytomation) according to the species of the primary antibody were used at dilutions from 1:500 to 1:10,000 depending on the signal intensity. Protein bands were visualized using SignalFire™ Plus ECL reagent (Cell Signaling Technology) and X-ray films (CEA) according to the instruction manual. More detailed information is given in Appendix Supplementary Methods.

Erbb2 fish

ERBB2 gene copy numbers of CTC-ITB-01 line cells were determined by fluorescence *in situ* hybridization using the *ERBB2/Cen17*

Zytovision probes (Zytomed) as described previously (Riethdorf et al, 2010). Briefly, after denaturation at 80°C for 2 min, dehydration in a series of ascending ethanol, and air-drying, cells were digested with a pepsin solution at 37°C for 7 min in a humidity chamber. Subsequently to renewed dehydration and air-drying, hybridization with the probe previously denatured for 7 min at 75°C was carried out at 37°C for 16 h. After different washing steps, dehydration, and air-drying, nuclei were stained with DAPI.

ALDH activity measurement

Aldehyde dehydrogenase (ALDH) activity was measured using the ALDEFLUOR™ kit (StemCell™ Technologies) following the instruction of StemCell™ Technologies. Briefly, 5 µl of ALDEFLUOR™ Reagent was added to the cell suspension and half of the cell mixture was immediately transferred into another tube with ALDEFLUOR™ DEAB Reagent (an inhibitor of ALDH activity) to serve as internal negative control. ALDH activity was analyzed in comparison with the internal negative control for each cell line. As recommended by the manufacturer, the A549 cell line was used as positive control.

EPISPOT assay

The fluoro-EPISPOT assay is able to detect low concentrations of secreted/released/shed proteins from viable cells at the single cell level (Alix-Panabieres et al, 2009). Cells are cultured for a short time (48 h) on a membrane coated with antibodies against K19, VEGF, OPG, EGFR, or FGF2 aimed to capture the secreted/released/shed proteins. In the next step, a second either directly fluorescently conjugated antibody or biotin-labeled antibodies detecting the captured proteins are applied. Biotin-labeled antibodies are then detected by streptavidin conjugated to Alexa 555 (Invitrogen). For detailed information about the antibodies used, see Appendix Supplementary Methods. Single fluorescent immunospots were evaluated under an ELISPOT reader (C.T.L ImmunoSpot).

Assessment of cell size

For immunofluorescence staining, cells were seeded on culture slides. Cells were fixed, permeabilized, and blocked overnight. Cytoskeleton was detected using anti-pan-keratin eFluor 570 clone AE1/AE3 (eBioscience, 1:80) and counterstained with DAPI. Fluorescence images were captured using a Zeiss Axioplan 2 epifluorescence microscope equipped with a charge-coupled device camera and AxioVision software. Cell size was measured using ImageJ.

RNA Sequencing and bioinformatics analysis

RNA sequencing was performed at the NGS Integrative Genomics Core Unit (NIG), University Medical Center, Goettingen, in biological triplicates for all CTC samples. RNA was extracted using the NucleoSpin RNA Plus kit (Macherey Nagel). Following RNA extraction, quality and integrity of RNA were assessed with the Fragment Analyzer from Advanced Analytical by using the standard sensitivity RNA Analysis Kit (DNF-471). All samples selected for sequencing exhibited an RNA integrity number over 8 and RNA-seq libraries were generated using an mRNA-Seq protocol from Illumina, the

TruSeq stranded mRNA prep Kit (Cat. No. RS-122-2101), and quantified using the QuantiFluor™dsDNA System from Promega. The size of final cDNA libraries was determined and exhibited an average size of 300 bp. Libraries were pooled and sequenced on a HiSeq 4000 (Illumina) generating 50 bp single-end reads (30–40 Mio reads/sample).

Sequencing images obtained after sequencing in the form of .bcl files are demultiplexed and converted to fastq files using Illumina software bcl2fastq v2.17.1.14. Quality check of resulting sequence reads is performed using FastQC version 0.11.5. Generated raw reads are aligned to the reference Human genome version hg38 sourced from ENSEMBL database using aligner STAR version 2.5. BAM files generated from alignment step are used to perform read counting using software featureCounts from subread package version 1.5.0. Counts generated are used to perform the differential gene expression analysis in R environment version 3.4.3 loading R/Bioconductor package DESeq2 version 1.14.1. Candidate genes generated were filtered to a minimum log2fold change of 1 and a FDR-corrected *P*-value of 0.05. Heatmap/s depicting top 50 candidate genes are generated using R/Bioconductor package pheatmap version 1.0.8.

Mouse model

CTC-ITB-01 cells were fluorescently tagged with a luciferase gene (GFP-*fluc2*) using lentiviral technology. Efficiency of the lentiviral transduction lay at around 30–40%. A single-cell suspension of 300,000 cells was injected into the milk duct of NSG mice (*N* = 4). Mice were kept for 8.5 months prior to sacrificing. The tumor growth was monitored in real time at multiple time points following transplantation by Xenogen IVIS bioluminescence imaging system 200 (Caliper Life Sciences) in accordance with the manufacturer's recommendations and protocols 12–15 min after intraperitoneal administration of 150 mg/kg luciferin (cat# L-8220, Biosynth AG). Images were analyzed with Living Image software (Caliper Life Sciences, Inc.). For metastasis *ex vivo* detection, mice were injected with luciferin 10 min prior to sacrifice and resected organs were imaged immediately.

Colony-forming assay

For colony-forming assays, cells were seeded at the same density per well of 6-well cell culture plates. Cells were fixed with 70% ethanol and stained with Coomassie blue staining solution.

Viral transduction

The packaging cell line HEK293T was used for generation of lentiviruses (shRNA: NM_000125 TRCN0000003298 pLKO.1 CMV-tGFP, NM_000125 TRCN0000003300 pLKO.1 CMV-tGFP, Non-target pLKO.1 CMV-tGFP) following standard calcium phosphate protocol. Transduction efficiency was monitored by flow cytometric detection of EGFP and efficiency of knockdown was tested by Western blotting.

In vitro drug testing of Palbociclib

CTC-ITB-01 or MCF-7 cells were seeded in a density of 2×10^3 cells per well in technical triplicates into a flat bottom 96-well plate and

The paper explained

Problem

Metastases developing upon dissemination of tumor cells from the primary tumor, access to the blood circulation and outgrowth at distant organs are the most frequent causes of breast cancer-related death. The vast majority of breast cancer cases is driven by hormone receptors enabling endocrine treatment as promising therapeutic strategy. However, tumor cells can develop resistance to this therapy, which constitutes a significant clinical problem, especially in the metastatic stage of the disease. Analyzing circulating tumor cells (CTCs) might be helpful to identify new therapeutic targets, but functional studies giving insight into the biology of CTCs are limited due to their low frequency and the lack of appropriate models.

Results

This study describes the establishment and characterization of a novel CTC-derived estrogen receptor (ER)-positive breast cancer cell line from a patient with metastatic ER-positive breast cancer, designated CTC-ITB-01. Downstream ER signaling is constitutively active in CTC-ITB-01 independent of ligand availability. This ER-positive cell line is resistant to endocrine therapy; however, the CDK4/6 inhibitor Palbociclib strongly inhibits CTC-ITB-01 growth. Genomic analyses revealed high concordance between CTC-ITB-01 and CTCs originally present in the patient with cancer at the time point of blood draw. Primary tumor and metastasis formation in an intraductal PDX mouse model reflected the clinical progression of ER-positive breast cancer.

Impact

Our work established and characterized a novel CTC cell line that mirrored *in situ* CTCs. This cell line allows first in-depth insights into the functional properties of CTCs in the most common ER⁺ breast cancer subtype and enables further experimental steps to uncover resistance mechanisms and to identify new therapeutic targets.

placed in the incubator at 37°C with 5% CO₂ overnight to adhere. The next day, Palbociclib (PD-0332991, Cayman Chemical), dissolved in DMSO, was serially diluted to the desired concentration in standard cell culture medium and added to the cells. Afterward, the plate was immediately transferred into the IncuCyte Zoom live cell imaging system (Essen Bioscience) and relative cell confluence was measured every 2 h. The processing definition and confluence mask of the IncuCyte system were created using the provided IncuCyte Zoom 2016B software (Essen Bioscience). Accuracy of fit of the confluence mask was verified on representative images at different states of growth during the experiment.

Statistical testing was performed with Prism 7.0a (GraphPad Software Inc.) using a one-way ANOVA followed by Dunnett's multiple comparisons test. A *P* < 0.05 was considered as statistically significant. IC₅₀ calculation was also achieved with Prism 7.0a using the implemented non-linear three-parameter logistic curve regression. Concentrations were transformed to common logarithm.

Data availability

NGS data are deposited at the European Nucleotide Archive with the following accession number: PRJEB37968 (<http://www.ebi.ac.uk/ena/browser/view/PRJEB37968>).

Expanded View for this article is available online.

Acknowledgements

The authors acknowledge Malgorzata Stoupiec, Cornelia Coith, Antje Andreas, and Olivier Mauermann from UKE Hamburg, and Alexandra Soler from CHU Montpellier for technical assistance. For preparation of the graphical synopsis, the figures were designed with the assistance of and modification to the images provided by the Servier Medical Art database <http://smart.servier.com/>. Further information pertaining to the license and disclaimer notices can be found here: <https://creativecommons.org/licenses/by/3.0/>. Klaus Pantel and Catherine Alix-Panabieres received funding from the European IMI research project CANCER-ID (115749-CANCER-ID). Klaus Pantel and Sabine Riethdorf received funding from the Deutsche Krebshilfe (Nr. 70112504). Klaus Pantel has received research funding from the Deutsche Forschungsgemeinschaft (DFG) SPP2084 μ Bone and ERC Advanced Investigator Grant INJURMET (Nr. 834974). Cathrin Briskén received a grant from the Swiss Cancer Ligue KFS-3701-08-2015, Sonja Thaler obtained funding from the Deutsche Forschungsgemeinschaft (DFG grant TH 1523/3-1 to S Thaler) and George Sflomos was supported by the Biltema and ISREC Foundation.

Author contributions

Conception and design: KP. Development and methodology: CK; AK; SR; KP. Acquisition of data: CK; AK; SAJ; SG; GY; GS; ST; DS; SG; PMM; LB; LC; JA; GS-R; KR; AZ; YG; KBa; LO; QZ; SR; SW. Analysis and interpretation of data: CK; AK; SAJ; GY; VM; GS; ST; DJS; KBa; LC; KBo; YG; TZT; MRS; LB; TMG; MJ; JPT; CB; SR; SW; CAP; KP. Administrative, technical, or material support: CK; SAJ; AK; MRS; VM; TMG; MJ; J-PT; CB; CA-P; KP. Study supervision: KP; SR; CK; AK; TMG. Writing, review, and/or revision of the manuscript: All authors. Final approval: All authors.

Conflict of interest

KP and CAP have ongoing patent applications related to CTCs. KP has received honoraria from Agena, Novartis, Roche, and Sanofi and research funding from European Federation of Pharmaceutical Industries and Associations (EFPIA) partners (Angle, Menarini and Servier) of the CANCER-ID program of the European Union–EFPIA Innovative Medicines Initiative. CAP has received honoraria from Janssen and grant support from Menarini. The remaining authors declare no conflict of interest.

References

- Al-Hajj M, Wicha MS, Benito-Hernandez A, Morrison SJ, Clarke MF (2003) Prospective identification of tumorigenic breast cancer cells. *Proc Natl Acad Sci USA* 100: 3983–3988
- Alix-Panabieres C, Vendrell JP, Slijper M, Pelle O, Barbotte E, Mercier G, Jacot W, Fabbro M, Pantel K (2009) Full-length cytokeratin-19 is released by human tumor cells: a potential role in metastatic progression of breast cancer. *Breast Cancer Res* 11: R39
- Alix-Panabieres C, Pantel K (2014a) Challenges in circulating tumour cell research. *Nat Rev Cancer* 14: 623–631
- Alix-Panabieres C, Pantel K (2014b) Technologies for detection of circulating tumor cells: facts and vision. *Lab Chip* 14: 57–62
- Alix-Panabieres C, Pantel K (2016) Clinical applications of circulating tumor cells and circulating tumor DNA as liquid biopsy. *Cancer Discov* 6: 479–491
- Alix-Panabieres C, Mader S, Pantel K (2017) Epithelial-mesenchymal plasticity in circulating tumor cells. *J Mol Med* 95: 133–142
- Armstrong AJ, Marengo MS, Oltean S, Kemeny G, Bitting RL, Turnbull JD, Herold CL, Marcom PK, George DJ, Garcia-Blanco MA (2011) Circulating tumor cells from patients with advanced prostate and breast cancer display both epithelial and mesenchymal markers. *Mol Cancer Res* 9: 997–1007
- Avivar-Valderas A, McEwen R, Taheri-Ghahfarokhi A, Carnevalli LS, Hardaker EL, Maresca M, Hudson K, Harrington EA, Cruzalegui F (2018) Functional significance of co-occurring mutations in PIK3CA and MAP3K1 in breast cancer. *Oncotarget* 9: 21444–21458
- Baccelli I, Schneeweiss A, Riethdorf S, Stenzinger A, Schillert A, Vogel V, Klein C, Saini M, Bauerle T, Wallwiener M et al (2013) Identification of a population of blood circulating tumor cells from breast cancer patients that initiates metastasis in a xenograft assay. *Nat Biotechnol* 31: 539–544
- Bardelli A, Pantel K (2017) Liquid biopsies, what we do not know (yet). *Cancer Cell* 31: 172–179
- Beck B, Driessens G, Goossens S, Youssef KK, Kuchnio A, Caauwe A, Sotiropoulou PA, Loges S, Lapouge G, Candi A et al (2011) A vascular niche and a VEGF-Nrp1 loop regulate the initiation and stemness of skin tumours. *Nature* 478: 399–403
- Bertheau P, Lehmann-Che J, Varna M, Dumay A, Poirot B, Porcher R, Turpin E, Plassa LF, de Roquancourt A, Boursstyn E et al (2013) p53 in breast cancer subtypes and new insights into response to chemotherapy. *Breast* 22 (Suppl 2): S27–S29
- Bertucci F, Ng CKY, Patsouris A, Droin N, Piscuoglio S, Carbuccioni N, Soria JC, Dien AT, Adnani Y, Kamal M et al (2019) Genomic characterization of metastatic breast cancers. *Nature* 569: 560–564
- Bidard FC, Peeters DJ, Fehm T, Nole F, Gisbert-Criado R, Mavroudis D, Grisanti S, Generali D, Garcia-Saenz JA, Stebbing J et al (2014) Clinical validity of circulating tumour cells in patients with metastatic breast cancer: a pooled analysis of individual patient data. *Lancet Oncol* 15: 406–414
- Bocci F, Jolly MK, Tripathi SC, Aguilar M, Hanash SM, Levine H, Onuchic JN (2017) Numb prevents a complete epithelial-mesenchymal transition by modulating Notch signalling. *J R Soc Interface* 14: 20170512
- Cariati M, Naderi A, Brown JP, Smalley MJ, Pinder SE, Caldas C, Purushotham AD (2008) Alpha-6 integrin is necessary for the tumorigenicity of a stem cell-like subpopulation within the MCF7 breast cancer cell line. *Int J Cancer* 122: 298–304
- Carter L, Rothwell DG, Mesquita B, Smowton C, Leong HS, Fernandez-Gutierrez F, Li Y, Burt DJ, Antonello J, Morrow CJ et al (2017) Molecular analysis of circulating tumor cells identifies distinct copy-number profiles in patients with chemosensitive and chemorefractory small-cell lung cancer. *Nat Med* 23: 114–119
- Cayrefourcq L, Mazard T, Joosse S, Solassol J, Ramos J, Assenat E, Schumacher U, Costes V, Maudelonde T, Pantel K et al (2015) Establishment and characterization of a cell line from human circulating colon cancer cells. *Cancer Res* 75: 892–901
- Celia-Terrassa T, Meca-Cortes O, Mateo F, Martinez de Paz A, Rubio N, Arnal-Estape A, Ell BJ, Bermudo R, Diaz A, Guerra-Rebollo M et al (2012) Epithelial-mesenchymal transition can suppress major attributes of human epithelial tumor-initiating cells. *J Clin Invest* 122: 1849–1868
- Chaffer CL, San Juan BP, Lim E, Weinberg RA (2016) EMT, cell plasticity and metastasis. *Cancer Metastasis Rev* 35: 645–654
- Chambers AF, Groom AC, MacDonald IC (2002) Dissemination and growth of cancer cells in metastatic sites. *Nat Rev Cancer* 2: 563–572
- Charafe-Jauffret E, Ginestier C, Iovino F, Tarpin C, Diebel M, Esterni B, Houvenaeghel G, Extra JM, Bertucci F, Jacquemier J et al (2010) Aldehyde dehydrogenase 1-positive cancer stem cells mediate metastasis and poor clinical outcome in inflammatory breast cancer. *Clin Cancer Res* 16: 45–55

- Ciriello G, Gatza ML, Beck AH, Wilkerson MD, Rhee SK, Pastore A, Zhang H, McLellan M, Yau C, Kandoth C *et al* (2015) Comprehensive molecular portraits of invasive lobular breast cancer. *Cell* 163: 506–519
- Colacino JA, Azizi E, Brooks MD, Harouaka R, Fouladdel S, McDermott SP, Lee M, Hill D, Madden J, Boerner J *et al* (2018) Heterogeneity of human breast stem and progenitor cells as revealed by transcriptional profiling. *Stem Cell Rep* 10: 1596–1609
- Cottu P, Marangoni E, Assayag F, de Cremoux P, Vincent-Salomon A, Guyader C, de Plater L, Elbaz C, Karboul N, Fontaine JJ *et al* (2012) Modeling of response to endocrine therapy in a panel of human luminal breast cancer xenografts. *Breast Cancer Res Treat* 133: 595–606
- Dumay A, Feugeas JP, Wittmer E, Lehmann-Che J, Bertheau P, Espie M, Plassa LF, Cottu P, Marty M, Andre F *et al* (2013) Distinct tumor protein p53 mutants in breast cancer subgroups. *Int J Cancer* 132: 1227–1231
- Ebright RY, Lee S, Wittner BS, Niederhoffer KL, Nicholson BT, Bardia A, Truesdell S, Wiley DF, Wesley B, Li S *et al* (2020) Deregulation of ribosomal protein expression and translation promotes breast cancer metastasis. *Science* 367: 1468–1473
- Faugeroux V, Pailler E, Oulhen M, Deas O, Brulle-Soumare L, Hervieu C, Marty V, Alexandrova K, Andree KC, Stoecklein NH *et al* (2020) Genetic characterization of a unique neuroendocrine transdifferentiation prostate circulating tumor cell-derived eXplant model. *Nat Commun* 11: 1884
- Finn RS, Crown JP, Lang I, Boer K, Bondarenko IM, Kulyk SO, Ettl J, Patel R, Pinter T, Schmidt M, *et al* (2015) The cyclin-dependent kinase 4/6 inhibitor palbociclib in combination with letrozole versus letrozole alone as first-line treatment of oestrogen receptor-positive, HER2-negative, advanced breast cancer (PALOMA-1/TRIO-18): a randomised phase 2 study. *Lancet Oncol* 16: 25–35
- Finn RS, Martin M, Rugo HS, Jones S, Im SA, Gelmon K, Harbeck N, Lipatov ON, Walshe JM, Moulder S *et al* (2016) Palbociclib and letrozole in advanced breast cancer. *N Engl J Med* 375: 1925–1936
- Follain G, Osmani N, Azevedo AS, Allio G, Mercier L, Karreman MA, Solecki G, Garcia Leon MJ, Lefebvre O, Fekonja N *et al* (2018) Hemodynamic forces tune the arrest, adhesion, and extravasation of circulating tumor cells. *Dev Cell* 45: 33–52 e12
- Ginestier C, Hur MH, Charafe-Jauffret E, Monville F, Dutcher J, Brown M, Jacquemier J, Viens P, Kleer CG, Liu S *et al* (2007) ALDH1 is a marker of normal and malignant human mammary stem cells and a predictor of poor clinical outcome. *Cell Stem Cell* 1: 555–567
- Giuliano M, Shaikh A, Lo HC, Arpino G, De Placido S, Zhang XH, Cristofanilli M, Schiff R, Trivedi MV (2018) Perspective on circulating tumor cell clusters: why it takes a village to metastasize. *Cancer Res* 78: 845–852
- Gkoutela S, Castro-Giner F, Szczerba BM, Vetter M, Landin J, Scherrer R, Krol I, Scheidmann MC, Beisel C, Stirnimann CU *et al* (2019) Circulating tumor cell clustering shapes DNA methylation to enable metastasis seeding. *Cell* 176: 98–112 e114
- Goldkorn A, Ely B, Quinn DI, Tangen CM, Fink LM, Xu T, Twardowski P, Van Veldhuizen PJ, Agarwal N, Carducci MA *et al* (2014) Circulating tumor cell counts are prognostic of overall survival in SWOG S0421: a phase III trial of docetaxel with or without atrasentan for metastatic castration-resistant prostate cancer. *J Clin Oncol* 32: 1136–1142
- Guiu S, Wolfer A, Jacot W, Fumoleau P, Romieu G, Bonnetain F, Fiche M (2014) Invasive lobular breast cancer and its variants: how special are they for systemic therapy decisions? *Crit Rev Oncol Hematol* 92: 235–257
- Heitzer E, Ulz P, Belic J, Gutschl S, Quehenberger F, Fischereder K, Benezeder T, Auer M, Pischler C, Mannweiler S *et al* (2013) Tumor-associated copy number changes in the circulation of patients with prostate cancer identified through whole-genome sequencing. *Genome Med* 5: 30
- Hodgkinson CL, Morrow CJ, Li Y, Metcalf RL, Rothwell DG, Trapani F, Polanski R, Burt DJ, Simpson KL, Morris K *et al* (2014) Tumorigenicity and genetic profiling of circulating tumor cells in small-cell lung cancer. *Nat Med* 20: 897–903
- Horlings HM, Lai C, Nuyten DS, Halfwerk H, Kristel P, van Beers E, Joosse SA, Klijn C, Nederlof PM, Reinders MJ *et al* (2010) Integration of DNA copy number alterations and prognostic gene expression signatures in breast cancer patients. *Clin Cancer Res* 16: 651–663
- Jeselson R, Buchwalter G, De Angelis C, Brown M, Schiff R (2015) ESR1 mutations—a mechanism for acquired endocrine resistance in breast cancer. *Nat Rev Clin Oncol* 12: 573–583
- Joosse SA, Hannemann J, Spotter J, Bauche A, Andreas A, Muller V, Pantel K (2012) Changes in keratin expression during metastatic progression of breast cancer: impact on the detection of circulating tumor cells. *Clin Cancer Res* 18: 993–1003
- Joosse SA, Pantel K (2016) Genetic traits for hematogeneous tumor cell dissemination in cancer patients. *Cancer Metastasis Rev* 35: 41–48
- Joosse SA, Souche FR, Babayan A, Gasch C, Kerkhoven RM, Ramos J, Fabre JM, Riethdorf S, Konig A, Wikman H *et al* (2018) Chromosomal aberrations associated with sequential steps of the metastatic cascade in colorectal cancer patients. *Clin Chem* 64: 1505–1512
- Kang S, Bader AG, Vogt PK (2005) Phosphatidylinositol 3-kinase mutations identified in human cancer are oncogenic. *Proc Natl Acad Sci USA* 102: 802–807
- Kang Y, Pantel K (2013) Tumor cell dissemination: emerging biological insights from animal models and cancer patients. *Cancer Cell* 23: 573–581
- Karczewski KJ, Francioli LC, Tiao G, Cummings BB, Alföldi J, Wang Q, Collins RL, Laricchia KM, Ganna A, Birnbaum DP *et al* (2020) The mutational constraint spectrum quantified from variation in 141,456 humans. *Nature* 581: 434–443
- Keller L, Pantel K (2019) Unravelling tumour heterogeneity by single-cell profiling of circulating tumour cells. *Nat Rev Cancer* 19: 553–567
- Keller L, Werner S, Pantel K (2019) Biology and clinical relevance of EpCAM. *Cell Stress* 3: 165–180
- Liu SL, Cong Y, Wang D, Sun Y, Deng L, Liu YJ, Martin-Trevino R, Shang L, McDermott SP, Landis MD *et al* (2014) Breast cancer stem cells transition between epithelial and mesenchymal states reflective of their normal counterparts. *Stem Cell Reports* 2: 78–91
- Liu K, Hao M, Ouyang Y, Zheng J, Chen D (2017) CD133(+) cancer stem cells promoted by VEGF accelerate the recurrence of hepatocellular carcinoma. *Sci Rep* 7: 41499
- Ma CX, Gao F, Luo J, Northfelt DW, Goetz M, Forero A, Hoog J, Naughton M, Ademuyiwa F, Suresh R *et al* (2017) NeoPalAna: neoadjuvant palbociclib, a cyclin-dependent kinase 4/6 inhibitor, and anastrozole for clinical stage 2 or 3 estrogen receptor-positive breast cancer. *Clin Cancer Res* 23: 4055–4065
- Martin MB, Saceda M, Lindsey RK (1993) Regulation of estrogen receptor expression in breast cancer. *Adv Exp Med Biol* 330: 143–153
- Meng S, Tripathy D, Frenkel EP, Shete S, Naftalis EZ, Huth JF, Beitsch PD, Leitch M, Hoover S, Euhus D *et al* (2004) Circulating tumor cells in patients with breast cancer dormancy. *Clin Cancer Res* 10: 8152–8162
- Mirzayans R, Andrais B, Murray D (2018) Roles of polyploid/multinucleated giant cancer cells in metastasis and disease relapse following anticancer treatment. *Cancers* 10: 118
- Nieto MA, Huang RY, Jackson RA, Thiery JP (2016) EMT: 2016. *Cell* 166: 21–45

- Oh SJ, Jung JY, Shim SS, Im MY, Kim HD, Chung SY, Yoon JH (2000) Identification of p53 gene mutations in breast cancers and their effects on transcriptional activation function. *Mol Cells* 10: 275–280
- Ozdemir BC, Sflomos G, Brisken C (2018) The challenges of modeling hormone receptor-positive breast cancer in mice. *Endocr Relat Cancer* 25: R319–R330
- Pan H, Gray R, Braybrooke J, Davies C, Taylor C, McGale P, Peto R, Pritchard KI, Bergh J, Dowsett M et al (2017) 20-year risks of breast-cancer recurrence after stopping endocrine therapy at 5 years. *N Engl J Med* 377: 1836–1846
- Pantel K, Alix-Panabieres C (2010) Circulating tumour cells in cancer patients: challenges and perspectives. *Trends Mol Med* 16: 398–406
- Pantel K, Alix-Panabieres C (2019) Liquid biopsy and minimal residual disease - latest advances and implications for cure. *Nat Rev Clin Oncol* 16: 409–424
- Papadaki MA, Kallergi G, Zafeiriou Z, Manouras L, Theodoropoulos PA, Mavroudis D, Georgoulis V, Agelaki S (2014) Co-expression of putative stemness and epithelial-to-mesenchymal transition markers on single circulating tumour cells from patients with early and metastatic breast cancer. *BMC Cancer* 14: 651
- Parker JS, Mullins M, Cheang MC, Leung S, Voduc D, Vickery T, Davies S, Fauron C, He X, Hu Z et al (2009) Supervised risk predictor of breast cancer based on intrinsic subtypes. *J Clin Oncol* 27: 1160–1167
- Pei D, Shu X, Gassama-Diagne A, Thiery JP (2019) Mesenchymal-epithelial transition in development and reprogramming. *Nat Cell Biol* 21: 44–53
- Pham TT, Angus SP, Johnson GL (2013) MAP3K1: genomic alterations in cancer and function in promoting cell survival or apoptosis. *Genes Cancer* 4: 419–426
- Raimondi C, Gradilone A, Naso G, Vincenzi B, Petracca A, Nicolazzo C, Palazzo A, Saltarelli R, Spremberg F, Cortesi E et al (2011) Epithelial-mesenchymal transition and stemness features in circulating tumor cells from breast cancer patients. *Breast Cancer Res Treat* 130: 449–455
- Ramirez JM, Fehm T, Orsini M, Cayrefourcq L, Maudelonde T, Pantel K, Alix-Panabieres C (2014) Prognostic relevance of viable circulating tumor cells detected by EPISPOT in metastatic breast cancer patients. *Clin Chem* 60: 214–221
- Riethdorf S, Fritsche H, Muller V, Rau T, Schindlbeck C, Rack B, Janni W, Coith C, Beck K, Janicke F et al (2007) Detection of circulating tumor cells in peripheral blood of patients with metastatic breast cancer: a validation study of the cell search system. *Clin Cancer Res* 13: 920–928
- Riethdorf S, Muller V, Zhang L, Rau T, Loibl S, Komor M, Roller M, Huober J, Fehm T, Schrader I et al (2010) Detection and HER2 expression of circulating tumor cells: prospective monitoring in breast cancer patients treated in the neoadjuvant GeparQuattro trial. *Clin Cancer Res* 16: 2634–2645
- Saal LH, Holm K, Maurer M, Memeo L, Su T, Wang XM, Yu JS, Malmstrom PO, Mansukhani M, Enoksson J et al (2005) PIK3CA mutations correlate with hormone receptors, node metastasis, and ERBB2, and are mutually exclusive with PTEN loss in human breast carcinoma. *Can Res* 65: 2554–2559
- Saha SK, Choi HY, Kim BW, Dayem AA, Yang GM, Kim KS, Yin YF, Cho SG (2017) KRT19 directly interacts with beta-catenin/RAC1 complex to regulate NUMB-dependent NOTCH signaling pathway and breast cancer properties. *Oncogene* 36: 332–349
- Saharinen P, Eklund L, Pulkki K, Bono P, Alitalo K (2011) VEGF and angiopoietin signaling in tumor angiogenesis and metastasis. *Trends Mol Med* 17: 347–362
- Scher HI, Heller G, Molina A, Attard G, Danila DC, Jia X, Peng W, Sandhu SK, Olmos D, Riisnaes R et al (2015) Circulating tumor cell biomarker panel as an individual-level surrogate for survival in metastatic castration-resistant prostate cancer. *J Clin Oncol* 33: 1348–1355
- Sflomos G, Dormoy V, Metsalu T, Jeitziner R, Battista L, Scabia V, Raffoul W, Delaloye JF, Treboux A, Fiche M et al (2016) A Preclinical model for ERalpha-positive breast cancer points to the epithelial microenvironment as determinant of luminal phenotype and hormone response. *Cancer Cell* 29: 407–422
- Shiraishi K, Tsuzaka K, Yoshimoto K, Kumazawa C, Nozaki K, Abe T, Tsubota K, Takeuchi T (2005) Critical role of the fifth domain of E-cadherin for heterophilic adhesion with alpha E beta 7, but not for homophilic adhesion. *J Immunol* 175: 1014–1021
- Sikora MJ, Cooper KL, Bahreini A, Luthra S, Wang G, Chandran UR, Davidson NE, Dabbs DJ, Welm AL, Oesterreich S (2014) Invasive lobular carcinoma cell lines are characterized by unique estrogen-mediated gene expression patterns and altered tamoxifen response. *Cancer Res* 74: 1463–1474
- Stemke-Hale K, Gonzalez-Angulo AM, Lluch A, Neve RM, Kuo WL, Davies M, Carey M, Hu Z, Guan Y, Sahin A et al (2008) Integrative genomic and proteomic analysis of PIK3CA, PTEN, and AKT mutations in breast cancer. *Can Res* 68: 6084–6091
- Strlic B, Offermanns S (2017) Intravascular survival and extravasation of tumor cells. *Cancer Cell* 32: 282–293
- Tan TZ, Miow QH, Miki Y, Noda T, Mori S, Huang RY, Thiery JP (2014) Epithelial-mesenchymal transition spectrum quantification and its efficacy in deciphering survival and drug responses of cancer patients. *EMBO Mol Med* 6: 1279–1293
- Tate JG, Bamford S, Jubb HC, Sondka Z, Beare DM, Bindal N, Boutselakis H, Cole CG, Creatore C, Dawson E et al (2019) COSMIC: the catalogue of somatic mutations in cancer. *Nucleic Acids Res* 47: D941–D947
- Tayoun T, Faugeroux V, Oulhen M, Aberlenc A, Pawlikowska P, Farace F (2019) CTC-derived models: a window into the seeding capacity of circulating tumor cells (CTCs). *Cells* 8: 1145
- Turner NC, Ro J, Andre F, Loi S, Verma S, Iwata H, Harbeck N, Loibl S, Huang Bartlett C, Zhang K et al (2015) Palbociclib in hormone-receptor-positive advanced breast cancer. *N Engl J Med* 373: 209–219
- Wicha MS, Hayes DF (2011) Circulating tumor cells: not all detected cells are bad and not all bad cells are detected. *J Clin Oncol* 29: 1508–1511
- Wirapati P, Sotiriou C, Kunkel S, Farmer P, Pradervand S, Haibe-Kains B, Desmedt C, Ignatiadis M, Sengstag T, Schutz F et al (2008) Meta-analysis of gene expression profiles in breast cancer: toward a unified understanding of breast cancer subtyping and prognosis signatures. *Breast Cancer Res* 10: R65
- de Wit S, Manicone M, Rossi E, Lampignano R, Yang L, Zill B, Rengel-Puertas A, Ouhlen M, Crespo M, Berghuis AMS et al (2018) EpCAM(high) and EpCAM(low) circulating tumor cells in metastatic prostate and breast cancer patients. *Oncotarget* 9: 35705–35716
- Xu X, Stower MJ, Reid IN, Garner RC, Burns PA (1997) A hot spot for p53 mutation in transitional cell carcinoma of the bladder: clues to the etiology of bladder cancer. *Cancer Epidemiol Biomarkers Prev* 6: 611–616
- Yu M, Bardia A, Wittner BS, Stott SL, Smas ME, Ting DT, Isakoff SJ, Ciciliano JC, Wells MN, Shah AM et al (2013) Circulating breast tumor cells exhibit dynamic changes in epithelial and mesenchymal composition. *Science* 339: 580–584
- Yu M, Bardia A, Aceto N, Bersani F, Madden MW, Donaldson MC, Desai R, Zhu H, Comaills V, Zheng Z et al (2014) Cancer therapy. *Ex vivo* culture of

circulating breast tumor cells for individualized testing of drug susceptibility. *Science* 345: 216–220

Zhang L, Ridgway LD, Wetzel MD, Ngo J, Yin W, Kumar D, Goodman JC, Groves MD, Marchetti D (2013) The identification and characterization of breast cancer CTCs competent for brain metastasis. *Sci Transl Med* 5: 180ra148

Zhao D, Pan C, Sun J, Gilbert C, Drews-Elger K, Azzam DJ, Picon-Ruiz M, Kim M, Ullmer W, El-Ashry D et al (2015) VEGF drives cancer-initiating stem

cells through VEGFR-2/Stat3 signaling to upregulate Myc and Sox2. *Oncogene* 34: 3107–3119



License: This is an open access article under the terms of the Creative Commons Attribution 4.0 License, which permits use, distribution and reproduction in any medium, provided the original work is properly cited.

In Situ Detection and Quantification of AR-V7, AR-FL, PSA, and *KRAS* Point Mutations in Circulating Tumor Cells

Amin El-Heliebi,^{1*†} Claudia Hille,^{2†} Navya Laxman,^{3†} Jessica Svedlund,^{3†} Christoph Haudum,^{1,4} Erkan Ercan,¹ Thomas Kroneis,¹ Shukun Chen,¹ Maria Smolle,⁴ Christopher Rossmann,⁵ Tomasz Krzywkowski,³ Annika Ahlford,^{3,6} Evangelia Darai,³ Gunhild von Amsberg,⁷ Winfried Alsdorf,⁷ Frank König,⁸ Matthias Löhr,⁹ Inge de Kruijff,¹⁰ Sabine Riethdorf,² Tobias M. Gorges,² Klaus Pantel,² Thomas Bauernhofer,^{4,5} Mats Nilsson,³ and Peter Sedlmayr¹

BACKGROUND: Liquid biopsies can be used in castration-resistant prostate cancer (CRPC) to detect androgen receptor splice variant 7 (AR-V7), a splicing product of the androgen receptor. Patients with AR-V7-positive circulating tumor cells (CTCs) have greater benefit of taxane chemotherapy compared with novel hormonal therapies, indicating a treatment-selection biomarker. Likewise, in those with pancreatic cancer (PaCa), *KRAS* mutations act as prognostic biomarkers. Thus, there is an urgent need for technology investigating the expression and mutation status of CTCs. Here, we report an approach that adds AR-V7 or *KRAS* status to CTC enumeration, compatible with multiple CTC-isolation platforms.

METHODS: We studied 3 independent CTC-isolation devices (CellCollector, Parsortix, CellSearch) for the evaluation of AR-V7 or *KRAS* status of CTCs with in situ padlock probe technology. Padlock probes allow highly specific detection and visualization of transcripts on a cellular level. We applied padlock probes for detecting AR-V7, androgen receptor full length (AR-FL), and prostate-specific antigen (PSA) in CRPC and *KRAS* wild-type (wt) and mutant (mut) transcripts in PaCa in CTCs from 46 patients.

RESULTS: In situ analysis showed that 71% (22 of 31) of CRPC patients had detectable AR-V7 expression ranging from low to high expression [1–76 rolling circle products (RCPs)/CTC]. In PaCa patients, 40% (6 of 15) had *KRAS* mut expressing CTCs with 1 to 8 RCPs/CTC. In

situ padlock probe analysis revealed CTCs with no detectable cytokeratin expression but positivity for AR-V7 or *KRAS* mut transcripts.

CONCLUSIONS: Padlock probe technology enables quantification of AR-V7, AR-FL, PSA, and *KRAS* mut/wt transcripts in CTCs. The technology is easily applicable in routine laboratories and compatible with multiple CTC-isolation devices.

© 2017 American Association for Clinical Chemistry

Liquid biopsies gained enormous momentum in recent years. Minimally invasive blood tests that detect circulating tumor cells (CTCs)¹¹ and cell-free circulating tumor DNA are highly beneficial compared with invasive tissue biopsies (1), but they face challenges in their usability to guide treatment selection. Although several techniques have been developed to allow characterization of CTCs and circulating tumor DNA (2–6), they have not been put into widespread clinical use. Recently, however, promising studies have been published, investigating the role of androgen receptor splice variant 7 (AR-V7) in prostate cancer (7, 8). The authors showed that patients with AR-V7-positive CTCs had greater benefit of taxane-based therapy compared with enzalutamide or abiraterone therapy (8–10). This indicates that the assessment of CTC-based AR-V7 status may serve as a treatment-selection biomarker in metastatic castration-resistant prostate cancer (CRPC) patients. However,

¹ Institute of Cell Biology, Histology and Embryology, Medical University Graz, Austria; ² Department of Tumor Biology, University Medical Center Hamburg-Eppendorf, Hamburg, Germany; ³ Science for Life Laboratory, Department of Biophysics and Biochemistry, Stockholm University, Solna, Sweden; ⁴ Center for Biomarker Research in Medicine (CBmed); Graz, Austria; ⁵ Division of Oncology, Department of Internal Medicine, Medical University of Graz, Austria; ⁶ Devyser AB, Stockholm, Sweden; ⁷ Department of Hematology and Oncology, University Medical Center Hamburg-Eppendorf, Hamburg, Germany; ⁸ ATURO, Urology Practice, Berlin, Germany; ⁹ Center for Digestive Diseases, Karolinska University Hospital and Division of Surgery, CLINTEC, Karolinska Institutet, Stockholm, Sweden; ¹⁰ Erasmus MC Cancer Institute, Department of Medical Oncology and Cancer Genomics Netherlands, Rotterdam, the Netherlands.

* Address correspondence to this author at: Institute of Cell Biology, Histology, and Embryology, Medical University Graz, Neue Stiftingtalstraße 6/II, 8010 Graz, Austria. Fax +43-316-385-79612; e-mail amin.elheliebi@medunigraz.at.

† A. El-Heliebi, C. Hille, N. Laxman, and J. Svedlund contributed equally to this work. Received September 1, 2017; accepted December 11, 2017.

Previously published online at DOI: 10.1373/clinchem.2017.281295

© 2017 American Association for Clinical Chemistry

¹¹ Nonstandard abbreviations: CTC, circulating tumor cell; AR-V7, androgen receptor splice variant 7; CRPC, castration-resistant prostate cancer; PaCa, pancreatic cancer; mut, mutant; wt, wild type; AR-FL, androgen receptor full length; PSA, prostate-specific antigen; RCP, rolling circle products; NHT, novel hormonal therapy.

published assays require sophisticated technologies for CTC isolation, which are available only at specialized centers (8), or are based on pooled (CTC) lysates that do not yield any quantitative information on the number of CTCs in circulation or the fraction of cells expressing clinically relevant AR-V7 transcripts (7, 10).

In parallel to splice variants, determining *KRAS*¹² point mutations in CTCs from pancreatic cancer (PaCa) patients could be used to improve diagnostics and stratification. Mutational activation of *KRAS* occurs in approximately 95% of pancreatic ductal adenocarcinoma cases (11) and is associated with worse prognosis (12), making it a potential biomarker. PaCa has a high mortality rate because of late diagnosis, often at advanced stages with metastatic disease (13, 14). Owing to the difficult access of the primary tumor with its high desmoplastic reaction in its microenvironment and false-negative biopsy results, CTC characterization could represent an important additional tool in diagnosis and treatment monitoring as a tumor-specific marker, as well as a prognostic marker suitable for stratification of these patients.

Thus, there is an urgent need for reliable and easily accessible technologies to investigate CTCs and their expression profile or mutational status. Here, we aimed at developing (a) an assay that adds clinically relevant molecular information of CTCs such as AR-V7 or *KRAS* status and (b) is compatible with multiple CTC isolation platforms. Our assay is based on padlock probe technology (15). Padlock probes consist of oligonucleotides that specifically bind to their target sequence (e.g., AR-V7, *KRAS*) and form a DNA circle that is amplified by rolling circle amplification (16). These amplified products are subsequently targeted by fluorescent probes, resulting in bright quantifiable signals. Padlock probes are highly specific, allowing differentiation between sequences differing in only a single base [e.g., splice variants or mutant (mut) vs wild type (wt)] (15). Here, we report an mRNA-based in situ padlock probe approach that allows visualization and quantification of prostate-specific transcripts (AR-V7), androgen receptor full length (AR-FL), prostate-specific antigen (PSA), and *KRAS* point mutations directly within single CTCs. Enrichment of CTCs was performed with the EpCAM-dependent in vivo CellCollector device, the CellSearch system, and the EpCAM-independent microfluidic Parsortix device.

Materials and Methods

CELL LINES

The following prostate cancer cell lines were used: VCaP (kindly provided by Martina Auer, Medical University

Graz, Austria), LNCaP (kindly provided by Martine Mazel, Montpellier, France), PC-3, and 22RV1 (ATCC). The CAPAN-1 and BxPC-3 [European Collection of Authenticated Cell Cultures (UK)] cell lines were used for PaCa experiments. Cells were cultured in cell culture flasks as recommended by the distributor. Cell lines received from other laboratories (VCaP and LNCaP) were verified by short tandem repeat analysis using the PowerPlex 16 System Kit (Promega) and were tested free of *Mycoplasma* (Bioutil).

SEEDING OF CELL LINES

Cultured cells were seeded on slides as previously described (17). Seeding of cells onto CellCollectors (Gilupi) is described in the Materials and Methods section of the Data Supplement that accompanies the online version of this article at <http://www.clinchem.org/content/vol64/issue3>.

SPIKING OF CELL LINES INTO HEALTHY DONOR BLOOD

For spiking experiments, cell line cells were counted in a Neubauer chamber and spiked into blood. If defined cell counts were needed, cells were spread to a petri dish filled with medium, manually counted, picked under a light microscope, and spiked into blood.

PATIENT SAMPLES AND ETHICS

The study enrolled patients from 4 centers. Patients with histologically confirmed CRPC were enrolled at the Division of Clinical Oncology, Medical University Graz (Austria), University Medical Center Hamburg-Eppendorf (Germany), and the Erasmus MC Cancer Institute (the Netherlands). Histologically confirmed PaCa patients were treated at Karolinska Institutet Hospital (Sweden). Patient characteristics are summarized in Tables 1 and 2 of the online Data Supplement. Healthy donor and patient blood samples were obtained in accordance with the World Medical Association Declaration of Helsinki, and all patients gave written informed consent. Each center received approval of the study from their ethical committees (Medical University Graz EK28–177-ex-15/16; Karolinska Institutet Hospital Dnr2013/1783–31/3; University Medical Center Hamburg PV3779; Erasmus MC MEC-2016–464). For samples from the Erasmus MC Cancer Institute, written informed consent was obtained for only the blood samples and their analysis and explicitly excluded any detailed clinical data.

IN VIVO CTC ISOLATION: CELLCOLLECTOR

CellCollectors were applied in 13 patients with CRPC and in 15 patients with PaCa as previously described (18). In short, an intravenous catheter (20 gauge, BD Venflon) was placed into the patients' cubital vein, and the CellCollector was carefully inserted until the wire was extended 2 cm into the vein. After 30 min, the Cell-

¹² Human Genes: *KRAS*, *KRAS* proto-oncogene, GTPase; *ACTB*, actin beta.

Collector was removed, washed 3 times in 1×PBS, fixed in 100% acetone for 10 min, air-dried for 5 min, and stored at −20 °C until further usage.

CTC ISOLATION: PARSORTIX

Thirty-eight blood samples were drawn from 17 CRPC patients into standard 7.5-mL EDTA vacutainers or CellSave[®] (Menarini-Silicon Biosystems) preservation tubes. Each patient, therefore, provided a matched sample of EDTA and CellSave blood for further analysis. Two patients donated an additional set of blood samples on a second visit. CTCs were enriched from EDTA blood using the size-dependent, label-free Parsortix system (ANGLE plc) as described previously (19, 20). A separation pressure of 99 mbar was chosen to process the blood samples. After cell harvest into a cytospin funnel on a glass slide, samples were spun down (190g, 5 min) via cytocentrifuge, dried overnight at room temperature, and stored at −80 °C. More detailed information on the general separation mechanism of the Parsortix is found in the Materials and Methods section of the online Data Supplement.

CTC ANALYSIS USING THE CELLSEARCH SYSTEM

The patient cohort of the University Medical Center Hamburg-Eppendorf (Germany) was analyzed with Parsortix and CellSearch in parallel. Patient blood samples were collected into CellSave preservation tubes and processed with the CellSearch system using the CellSearch[®] CXC Kit (21). This specific kit uses anti-CK-fluorescein, diaminopyrolylindole 4,6-diamino, 2-pyrolylindole, and anti-CD45-APC to identify CTCs and leukocytes. All analyses were performed by trained CellSearch analysts using the CellTracks Analyzer II. The AR-FL status was assessed in the fourth fluorescence channel of the CellSearch with a phycoerythrin-labeled Celltracks anti-androgen receptor antibody (Janssen Diagnostics). To test whether CellSearch-processed samples can be analyzed by in situ analysis, 1 patient sample from the Erasmus MC Cancer Institute was processed with the CellSearch system and forwarded for in situ analysis. The blood was collected in an EDTA tube and processed within 24 h on the CellSearch system. After enrichment of the CTCs with the CellSearch CTC Profile Kit (Menarini Silicon Biosystems), the enriched cell fraction was cytocentrifuged on slides (first, 300g, 4 min; after removal of the remaining fluid, 1000g, 1 min) using 4-mL CytoSystem funnels (Hettich Laboratory technology) supported by a magnetic device. The sample was then dried and fixed with 3.7% formaldehyde (Sigma) for 15 min. After fixation, the slides were dried again and run through an ethanol series. Afterward, slides were stored at −20 °C before being forwarded for in situ analysis.

IN SITU REACTIONS

Oligonucleotides for prostate cancer were designed according to published guidelines by Weibrecht et al. using CLC Main Workbench software (CLC Bio Workbench version 7.6, Qiagen) (17). Sequences with the GenBank accession number NM_000044.3 (AR-FL), FJ235916.1 (AR-V7), and NM_001030047 (PSA) were retrieved from the National Center for Biotechnology Information. For AR-FL and PSA, single padlock probes were used. As expression levels of AR-V7 are generally low (1.2 and 0.4 copies/cell in VCaP and LNCaP, respectively) (22), we amplified the signals by an array of AR-V7 padlocks. Details for the padlock probes can be found in the Materials and Methods section of the online Data Supplement. Oligonucleotides for PaCa were designed as previously described for *KRAS* codon 12 (23). A mixture of padlock probes targeting the housekeeping gene *ACTB*, *KRAS* codon 12 wt, and mut G12S, G12R, G12C, G12D, G12V, and G12A were combined with immunofluorescence staining of cytokeratin and CD45.

For cytokeratin immunostaining, we combined antibodies directed against a broad panel of cytokeratins, namely, the C-11 (Exbio), AE1/AE3 (Thermo Fisher Scientific), and DC-10 (Exbio) antibodies, which detect multiple keratins. The C-11 clone reacts with cytokeratins 4, 5, 6, 8, 10, 13, and 18; the AE1/AE3 clone recognizes cytokeratins 1, 2, 3, 4, 5, 6, 7, 8, 10, 14, 15, 16, and 19; and the DC-10 clone reacts with cytokeratin 18. A detailed protocol for immunostaining can be found in the Materials and Methods section of the online Data Supplement. All oligonucleotides are summarized in Table 3 of the online Data Supplement.

In situ reactions were performed as described previously (24) with slight modifications, including the doubling of all enzyme concentrations for in situ reactions of patient material, as blood cells show an inhibitory effect on PCR reactions (25). The in situ reactions for the CellCollectors were performed in glass pipettes as described in the Materials and Methods section of the online Data Supplement.

For imaging of a CellCollector, the wire was placed and fixed onto a metal frame object slide with an imaging window (Carl Zeiss) using tape or fixed onto a wire holder (Gilupi). Then, wires were scanned across the whole length of the functional part. To image the whole surface of the CellCollector, it was rotated in 90° angles until fully processed. To verify rolling circle products (RCPs) to be specific, each signal was checked in all other fluorescent channels. Signals present in all channels were considered unspecific (17) (see Fig. 1 in the online Data Supplement).

Quantification of RCPs was performed with CellProfiler software (version 2.1.1) (26). We modified the previously published quantification pipeline (27). A detailed description can be found in the Materials and Methods section of the online Data Supplement.

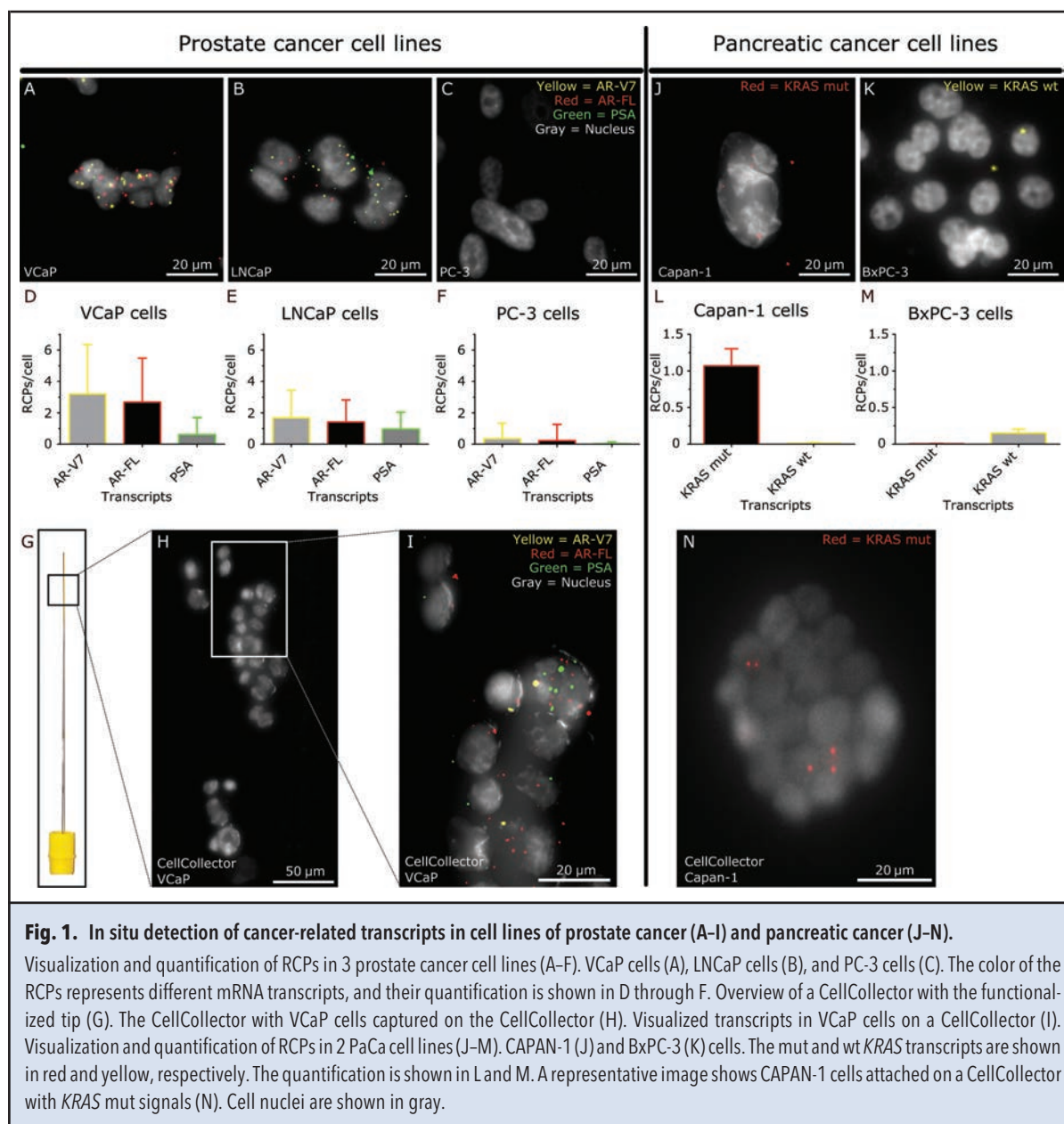


Fig. 1. In situ detection of cancer-related transcripts in cell lines of prostate cancer (A-I) and pancreatic cancer (J-N). Visualization and quantification of RCPs in 3 prostate cancer cell lines (A-F). VCaP cells (A), LNCaP cells (B), and PC-3 cells (C). The color of the RCPs represents different mRNA transcripts, and their quantification is shown in D through F. Overview of a CellCollector with the functionalized tip (G). The CellCollector with VCaP cells captured on the CellCollector (H). Visualized transcripts in VCaP cells on a CellCollector (I). Visualization and quantification of RCPs in 2 PaCa cell lines (J-M). CAPAN-1 (J) and BxPC-3 (K) cells. The mut and wt *KRAS* transcripts are shown in red and yellow, respectively. The quantification is shown in L and M. A representative image shows CAPAN-1 cells attached on a CellCollector with *KRAS* mut signals (N). Cell nuclei are shown in gray.

Results

AR-V7, AR-FL, AND PSA CAN BE VISUALIZED AND QUANTIFIED IN PROSTATE CANCER CELL LINES

Three prostate cancer cell lines were selected for validation of specificity and sensitivity of padlock probes. AR-V7, AR-FL, and PSA were detected in the “positive” cell lines VCaP and LNCaP and were not expressed in the “negative” PC-3 cell line cells (Fig. 1). The terms positive and negative refer to previously published data as detectable and not detectable mRNA, respectively (22). For VCaP cells, the average numbers of RCPs/

cell for AR-V7, AR-FL, and PSA were 3.2 (range, 0–20), 2.7 (range, 0–19), and 0.6 (range, 0–7), respectively. The corresponding numbers of RCPs for the LNCaP cells were 1.7 RCPs/cell (range, 0–17) for AR-V7, 1.4 (range, 0–6) for AR-FL, and 1.0 (range, 0–7) for PSA. PC-3 cells yielded an average RCP/cell of 0.3 (range, 0–9) for AR-V7 and 0.2 (range, 0–11) for AR-FL, but negligible expression of PSA with 0.0 (range, 0–2) RCPs/cell. In total, 252 VCaP, 108 LNCaP, and 186 PC-3 cells were evaluated and RCPs quantified by CellProfiler software. The in situ results reflect previously published data (22). VCaP cells

seeded onto the CellCollector showed results comparable with cells on a slide (Fig. 1).

IN SITU AR-V7 DETECTION CAN BE COMBINED WITH IMMUNOSTAINING FOR PANCK AND CD45 OF PARSORTIX-PROCESSED PROSTATE CANCER CELL LINE CELLS

To evaluate whether our novel approach can also be applied to samples obtained from other CTC isolation platforms, spiked prostate cancer cell line cells were enriched from whole blood by the EpCAM-independent Parsortix system (20). 22VRv1 and PC-3 cells were chosen for these experiments, having high and low AR-V7 expression, respectively. After enrichment, cells were processed via in situ padlock probe technology and immunofluorescent staining of panCK and CD45. This combination of mRNA and protein analysis allows for effective discrimination between CTCs and background blood cells (see Fig. 2 in the online Data Supplement). Accordingly, both cell lines showed expression of panCK and no expression for CD45. 22VRv1 cells also exhibited clear AR-V7 signals, whereas PC-3 cells were AR-V7-negative. Based on these data, we concluded in situ padlock probes can be successfully combined with immunostaining after enrichment with the Parsortix system.

KRAS WT AND MUT TRANSCRIPTS CAN BE VISUALIZED AND QUANTIFIED IN PACA CELL LINES

To validate specificity and sensitivity of padlock probes and antibodies, experiments were performed using the 2 pancreatic cell lines CAPAN-1 [EpCAM(+), panCK(+), CD45(-), and *KRAS* G12V homozygous mutation] and BxPC3 (*KRAS* wt) (28, 29). As expected, CAPAN-1 displayed homozygous expression of *KRAS* mut (1.1 RCP/cell), as well as positive protein staining for panCK and negative staining for CD45. BxPC3 cells expressed *KRAS* wt (0.2 RCP/cell) and had a low false-positive rate for the mutation (0.004 RCP/cell) (Fig. 1).

AR-V7, AR-FL, AND PSA CAN BE DETECTED IN CTC ISOLATED BY CELLCOLLECTOR

We assessed the CTC status of 13 patients with CRPC by applying in situ padlock probe technology on cells attached to the CellCollector. Multiplex in situ analysis for expression of AR-V7, AR-FL, and PSA was directly performed on CTCs attached to the surface of the CellCollector. An overview of the results is provided in Table 4 of the online Data Supplement. In all, 62% (8 of 13) of the patients were CTC-positive (range, 1–15 CTCs/patient). In situ analysis revealed that 54% (7 of 13) of patients had CTCs with AR-V7 mRNA expression (range, 1–10 RCPs/CTC) (Fig. 2). AR-FL-positive CTCs were detectable in 39% (5 of 13) of patients (expression range, 1–9 RCPs/CTC), and PSA-positive CTCs were found in 23% (3 of 13) of patients (expression

range, 1–2 RCPs/cell) (Fig. 2). Representative CTCs on the CellCollector are shown in Fig. 2.

DIFFERENT SUBTYPES OF CTC CAN BE IDENTIFIED BY IN SITU AR-V7 DETECTION AND PANCK IMMUNOSTAINING OF CTC ISOLATED BY PARSORTIX

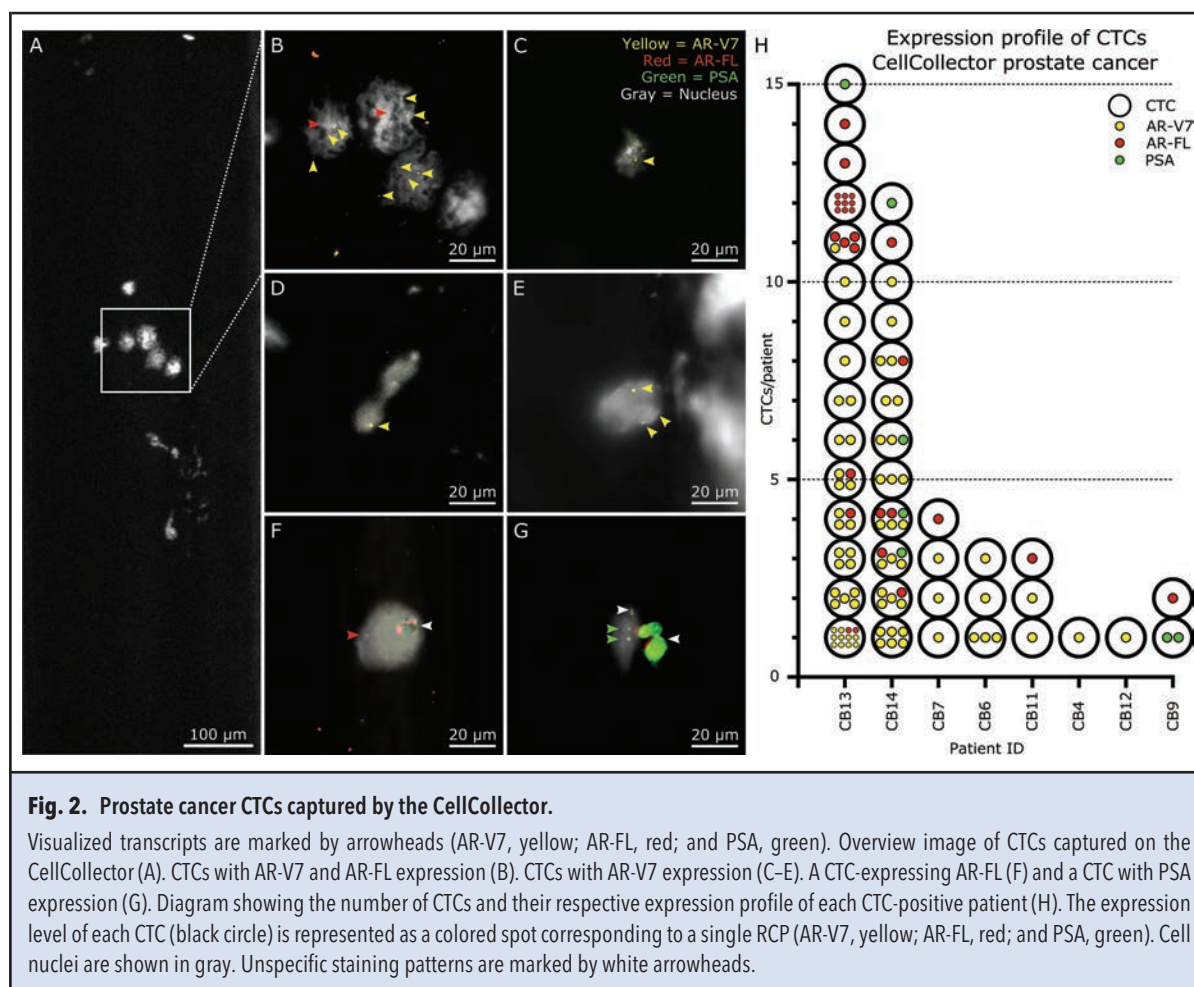
We evaluated the CTC status of 17 patients (19 samples) with CRPC using the Parsortix system to isolate CTCs. CTCs were evaluated by applying in situ padlock probe technology for AR-V7 in combination with panCK and CD45 immunostaining. In all, 89% of the samples (17 of 19) were positive for CTCs (range, 1–158 CTCs/7.5 mL of blood). In situ analysis revealed that 79% of samples (15 of 19) also contained CTCs with AR-V7 mRNA expression (range, 1–30 RCPs/CTC) (Fig. 3). We observed 3 types of CTCs by combining in situ AR-V7 detection with panCK immunostaining: (a) panCK(+)/AR-V7(-), (b) panCK(-)/AR-V7(+), and (c) panCK(+)/AR-V7(+). An overview of the distribution of the different CTC subtypes is shown in Fig. 3. Images of representative CTCs are shown in Fig. 4. In all, 84% of the samples (16 of 19) were positive for panCK(+)/AR-V7(-) CTCs, 68% of samples (13 of 19) were positive for panCK(+)/AR-V7(+) CTCs, and 32% of samples (6 of 19) were positive for panCK(-)/AR-V7(+) CTCs. In rare cases, single cells were detected showing staining for both, panCK and CD45, similar to the results of others (30). These cells were not counted as CTCs. An overview of the results is provided in Table 4 of the online Data Supplement.

AR-V7 CAN BE DETECTED IN CTC ISOLATED BY CELLSEARCH

One CRPC sample was processed with the CellSearch System and analyzed by in situ padlock probe technology for AR-V7 expression. In total, 557 AR-V7(+) CTCs/7.5 mL of blood were detected, with AR-V7 expression ranging from 1 to 76 RCPs/CTC (mean, 10 RCPs/CTC) (Fig. 5).

KRAS WT AND MUT TRANSCRIPTS CAN BE DETECTED IN CTC ISOLATED BY CELLCOLLECTOR

The CTC status of 15 patients with PaCa was characterized by in situ padlock probe technology combined with immunostaining for CK18/panCK and CD45, directly on patient cells attached to the CellCollector. Representative CTCs on the CellCollector are shown in Fig. 6. In all, 47% of the patients (7 of 15) were CTC-positive (range, 1–3 CTCs/patient). The expression of *KRAS* and panCK/CK18 showed intrapatient and interpatient heterogeneity (Fig. 6). The *KRAS* mut expression ranged from 1 to 8 RCPs/CTC, and *KRAS* wt ranged from 1 to 2 RCPs/CTC. The overall rate of *KRAS* mutated CTCs was 75% (9 of 12). In all, 50% (6 of 12) of CTCs detected were also positive for cytokeratin protein, demonstrating that in situ padlock probes can be successfully



combined with immunostaining using the CellCollector. CD45 immunostaining showed only weak staining of mononuclear cells attached to the wire with stronger staining of a certain lymphocyte subpopulation. The *KRAS* mutation status of the corresponding primary tumor DNA in 5 of the CTC-positive patients was further tested with a diagnostic PCR analysis. A similar mutation pattern could be observed (see Fig. 3 of the online Data Supplement). An overview of the results is provided in Table 5 of the online Data Supplement.

CHARACTERISTICS OF THE PATIENT COHORTS

As this study aimed to develop a CTC-based assay (e.g., AR-V7 detection), patients with advanced disease were enrolled to obtain a high number of CTCs. Basic clinical data were obtained from the patients with additional follow-up data from a subset of patients. A detailed overview of both patient cohorts for each individual patient can be found in Tables 1 and 6 of the online Data Supplement. An overview of PSA response is shown in a waterfall plot (see Fig. 4 of the online Data Supplement).

Discussion

We evaluated the feasibility and utility of in situ padlock probe technology for the analysis of clinically relevant splice variants and point mutations in CTCs isolated by 3 independent enrichment technologies. Our data show that CTCs from prostate cancer patients can be analyzed for AR-V7, AR-FL, and PSA expression and that CTCs from PaCa patients can be analyzed for *KRAS* point mutations. We further demonstrate the feasibility of combining immunostaining (panCK and CD45) with in situ padlock probe technology. Our approach allows for quantification of CTC and simultaneous interrogation of clinically relevant markers.

Our padlock approach for AR-V7 mRNA detection shows robust signals in isolated CTCs. A strength of the method is the possibility to easily quantify expression levels by simply counting the fluorescent signals. Another advantage is the option to investigate nucleic acids without lysis of CTCs and, therefore, allowing the quantification of CTCs, which serves as a prognostic marker. In

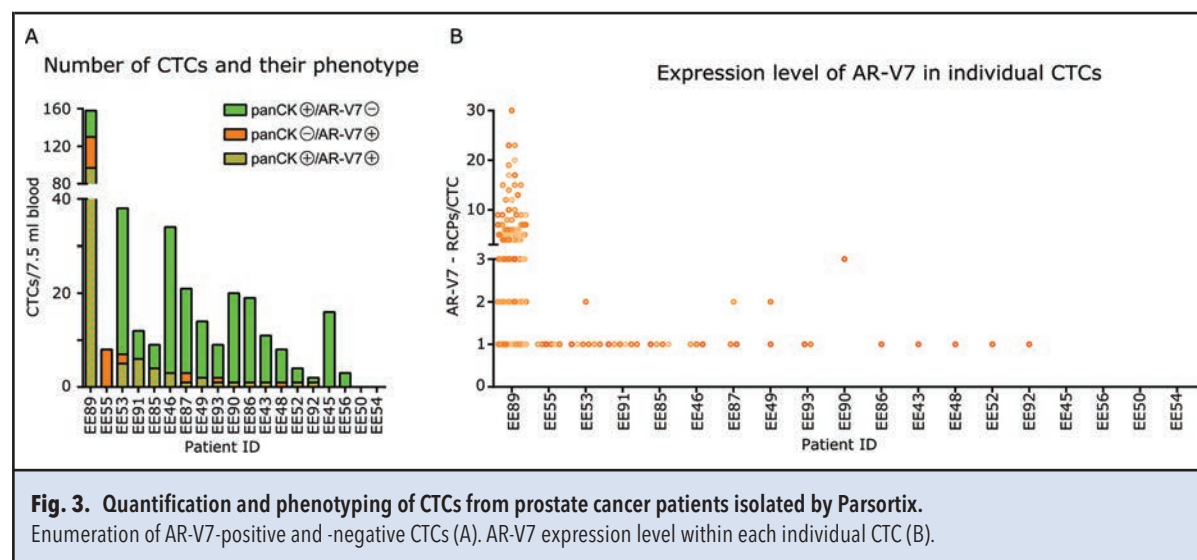


Fig. 3. Quantification and phenotyping of CTCs from prostate cancer patients isolated by Parsortix. Enumeration of AR-V7-positive and -negative CTCs (A). AR-V7 expression level within each individual CTC (B).

addition, heterogeneity among CTCs can be easily visualized. Although the AR-V7 mRNA expression is shown to correlate with worse clinical outcomes in recent literature, we cannot simply conclude that every mRNA transcript will be translated to protein (31). Indeed, Scher et al. showed that resistance toward novel hormonal therapy (NHT) depends on the nuclear-specific location of AR-V7 protein rather than on cytoplasmic localization (32). To investigate the location of AR- protein in CTCs, we analyzed a subset of CellSearch-processed samples. The CellSearch samples were immunostained for AR in addition to panCK and CD45 (see Table 4 in the online Data Supplement) as recently published (33). The used AR- antibody targets the N-terminal part of the protein, thereby also detecting AR-V7 but without the possibility to discriminate between the full length and splice variant. Interestingly, the patient with one of the highest AR-V7(+) CTC counts showed localization of AR protein in the nucleus of CTCs analyzed by CellSearch (see Table 4 in the online Data Supplement). This indicates that high expression of AR-V7 may correlate with active AR-V7 protein in the nucleus. A recent publication showed that another splice variant may also play an important role in the NHT resistance mechanism. Kohli et al. stated that initial annotation of the splice variant AR-V9 needs to be reevaluated, as they revealed by short- and long-read sequencing that the sequences of the 3'-UTR of AR-V7 and AR-V9 overlap (34). This implies that our AR-V7 assay may partially also detect AR-V9. Nevertheless, the authors also found that AR-V9-expressing cells had similar therapeutic resistance toward the NHT drug enzalutamide as the AR-V7-expressing cells (34). The patients we enrolled in our study were selected for establishing the in situ assay, rather than an evaluation of patient outcome. To do so,

our patients were selected for advanced stage, rather than a clearly defined timepoint or treatment regimen. For example, most of the recruited CRPC patients already acquired resistance toward enzalutamide and abiraterone. Our rationale was to increase the probability of AR-V7 detection among the patients, as AR-V7 positivity increases in later lines of therapy to approximately 20% of CRPC patients (8). Our assay for the quantification of AR-V7 expression may become an important tool to stratify patients into AR-V7 "high" or "low" expressers or to supply a cutoff value for potential resistance to NHT. However, our assay needs validation in a prospective clinical study.

Moreover, we successfully characterized the mutation status of *KRAS* in CTCs of PaCa patients. The number of CTCs detected ranged from 1 to 3 CTCs per patient. In this study, all pancreatic tumors were surgically resectable with relatively little tumor burden, so the number of CTCs was expected to be low. For those with advanced disease, for whom we would expect a higher frequency of CTCs, a low CTC count might not be sufficient for monitoring progression; however, it could still be useful for diagnostics.

In our hands, the CellCollector has proven to be a usable in vivo CTC enrichment device. The application into a cubital vein for 30 min is somewhat more laborious than simple blood drawing, but the wire can be easily processed and stored for at least 1 month at -20°C without any noticeable degradation of in situ signals. Furthermore, for performing in situ reactions and follow-up screening of the CellCollector, only a routine molecular biology lab, equipped with a fluorescent microscope, is needed. Processing and screening time of the CellCollector is short and generates results within 48 h. Recent data show that the CellCollector can detect

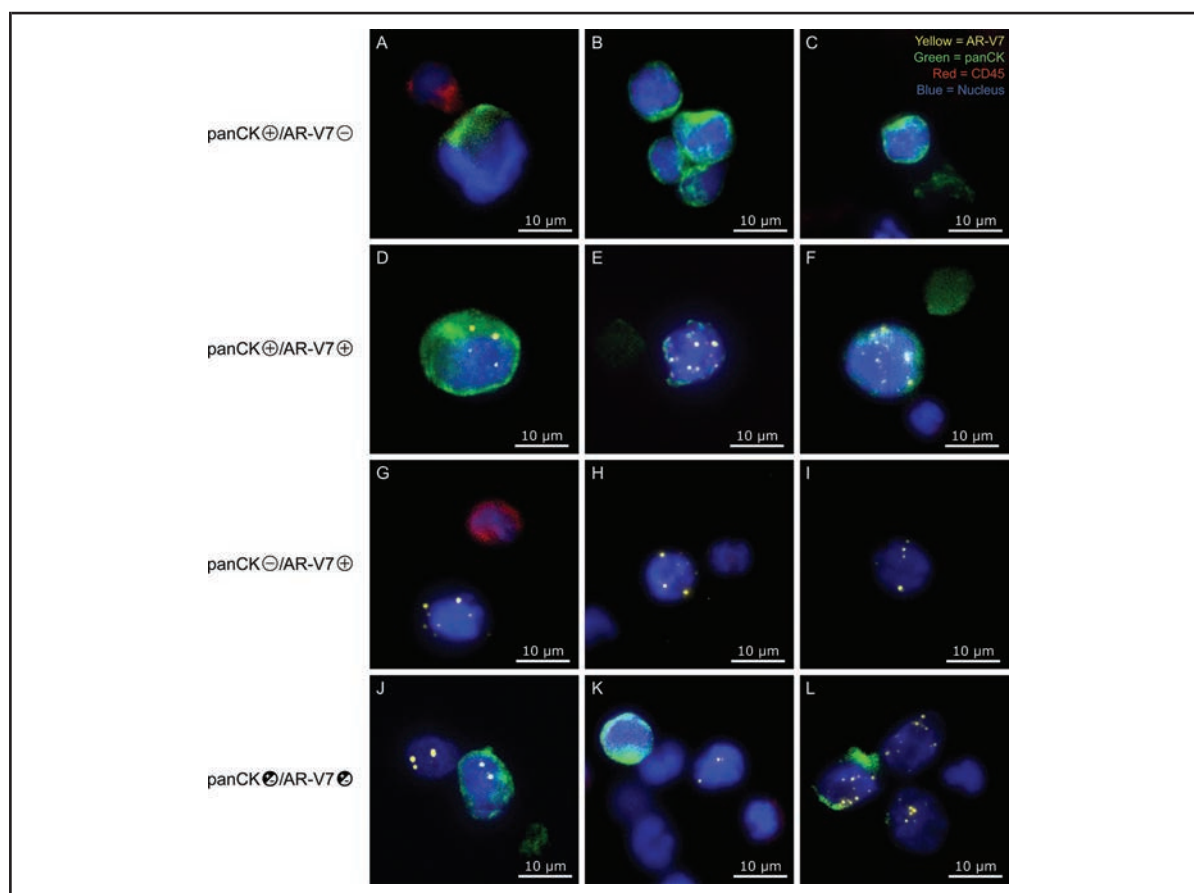
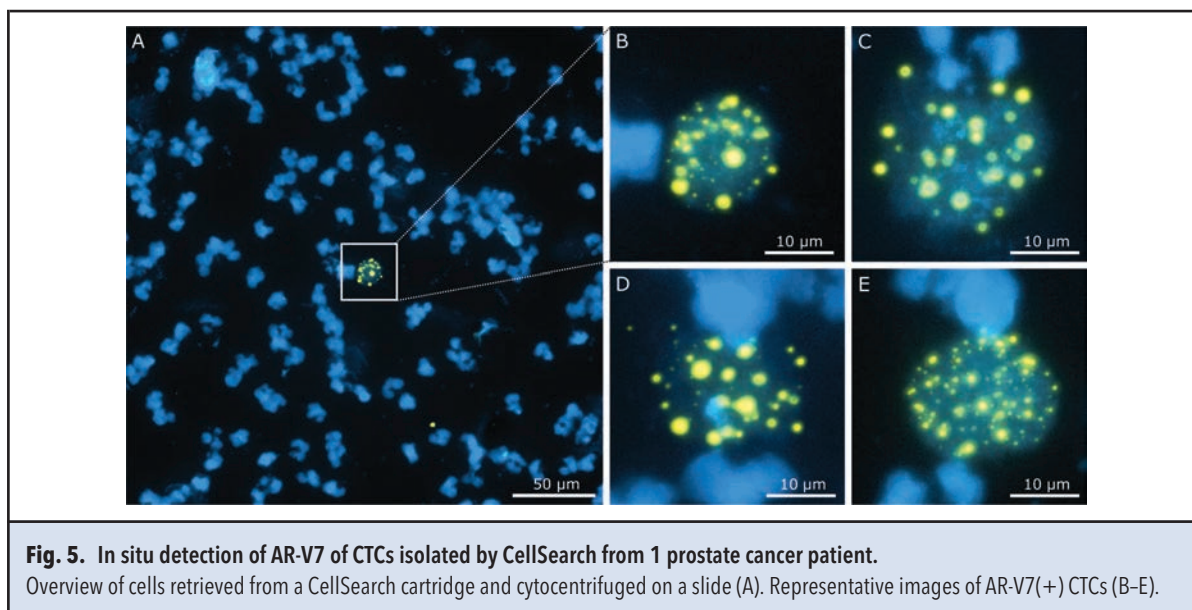


Fig. 4. In situ detection of AR-V7 in CTCs from prostate cancer patients isolated by Parsortix.

CTCs and a CTC cluster with positive immunostaining for panCK but lack of AR-V7 expression (A–C). panCK(+) and AR-V7(+) CTCs with varying degree of AR-V7 expression (4–20 AR-V7 RCP signals) (D–F). panCK(–) and AR-V7(+) CTCs (G–I). Mixed populations of CTCs and clusters, with and without panCK and AR-V7 expression (J–L). AR-V7 (yellow), panCK (green), leukocyte common antigen (CD45, red), and nucleus (blue).

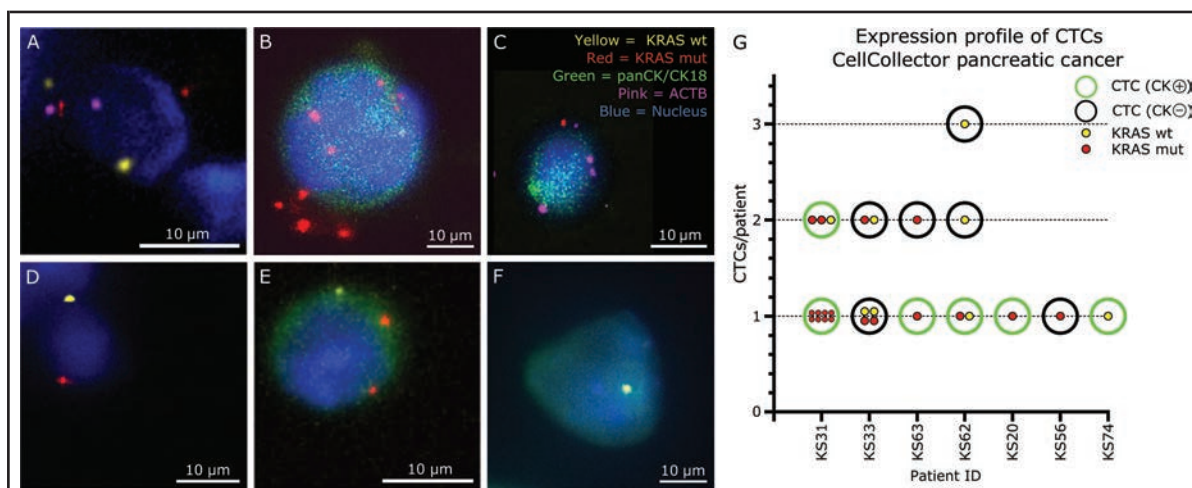
higher rates of patients positive for CTCs as compared with other technologies (18). The CTCs are firmly attached to the CellCollector and will not be lost during the in situ process. Indeed, the cells cannot be released from the wire without their lysis. For more elaborate single-cell molecular characterization (e.g., next-generation sequencing), a novel CellCollector was developed, namely, the Catch & Release CellCollector (Gilupi). The Catch & Release CellCollector allows EpCAM-based capturing of cells and their release by a releasing buffer for subsequent single-cell analysis, but it is not yet cleared for use in patients (35). As the CellCollector is based on anti-EpCAM antibodies for CTC isolation, it may miss several other CTC subpopulations with downregulated epithelial markers (36). To evade limitation by EpCAM, we combined the in situ padlock approach with the EpCAM-independent Parsortix platform (20), demonstrating that the in situ padlock approach is generally applicable to different isolation platforms. By combining

the in situ AR-V7 detection with the Parsortix system, we observed heterogeneous cytokeratin expression of CTCs. Heterogeneity among CTCs is well described, including a wide range of differentiation states from epithelial to mesenchymal types (37). With this approach, in situ padlock probes allowed the detection of several CTCs that had no sign of cytokeratin expression, suggesting cells in an active state of epithelial to mesenchymal transition. These CTCs actively expressed AR-V7 or *KRAS* transcripts and would have been “missed” by EPCAM-dependent assays. It might be hypothesized that these CTCs are of high clinical relevance. We observed 6 CRPC patients with panCK(–)/AR-V7(+) CTCs. Five of these 6 patients also showed panCK(+)/AR-V7(+) CTCs (see Table 4 in the online Data Supplement), making it difficult to distinguish which of the AR-V7-positive populations is “most relevant” for clinical resistance toward enzalutamide and abiraterone. Nevertheless, this reflects the selection of resistant clones toward enzalut-



amide and abiraterone treatment (38). In situ padlock probes can thereby add an extra layer of information to CTCs, including diagnostic data and proof of CTC origin. Indeed, the traditional definition of CTCs (positive for EpCAM/panCK and negative for CD45) becomes extended by molecular characterization. As we have shown with our combined in situ AR-V7 and panCK/CD45 immunostaining approach, CTCs can be clearly

identified and grouped into different subtypes. The sole immunostaining profile is insufficient to stratify CTCs into different subtypes. Moreover, recent studies identified cells in circulation with common epithelial/CTC-like features and balanced copy number profiles (39). Others have shown that CK+/CD45− cells can be found in healthy volunteer samples. The clinical relevance of these cells is currently unknown (40). This un-



derlines the importance of molecular characterization in liquid biopsies beyond the traditional EpCAM/panCK immunostaining. Deeper molecular insight into different CTC populations may lead to a better understanding of how metastatic disease and therapy resistance form and which cells contribute to their formation.

As a proof of principle, we also applied our in situ AR-V7 approach to CellSearch-enriched CTCs from 1 patient. Although just a single case, we clearly identified CTCs with high AR-V7 expression, suggesting that the in situ padlock probe approach is applicable to multiple independent CTC enrichment technologies.

In conclusion, we have shown detection and quantification of clinically relevant molecular markers in single CTCs using our in situ approach. We thereby could add additional information beyond simple CTC enumeration, which likely will improve the predictive and prognostic value of CTC analysis in the clinic.

Author Contributions: All authors confirmed they have contributed to the intellectual content of this paper and have met the following 3 requirements: (a) significant contributions to the conception and design, acquisition of data, or analysis and interpretation of data; (b) drafting or revising the article for intellectual content; and (c) final approval of the published article.

Authors' Disclosures or Potential Conflicts of Interest: Upon manuscript submission, all authors completed the author disclosure form. Disclosures and/or potential conflicts of interest:

Employment or Leadership: P. Sedlmayr, Medical University of Graz. **Consultant or Advisory Role:** None declared.

Stock Ownership: None declared.

Honoraria: G. von Amsberg, Roche, Astellas, Sanofi, MSD, BMS, AstraZeneca.

Research Funding: A. El-Heliebi, Start Funding of the Medical University Graz, Austria; Franz Lanyar Foundation of the Medical University Graz, Austria; N. Laxman, European Commission CanDo project (FP7-610472) to institution; J. Svedlund, European Commission CanDo project (FP7-610472) to institution; T. Krzykowski, European Commission CanDo project (FP7-610472) to institution; A. Ahlford, European Commission CanDo project (FP7-610472) to institution; E. Darai, European Commission CanDo project (FP7-610472) to institution; I. de Kruijff, Pieter de Mulder award from the Dutch Society for Medical Oncology (NVMO) sponsored by Pfizer Oncology; T. Bauernhofer, Center for Biomarker Research in Medicine (CBmed, Graz, Austria), FFG Comet K1 to institution; M. Nilsson, European Commission CanDo project (FP7-610472) to institution; P. Sedlmayr, Austrian Science Fund project I 1220-B19.

Expert Testimony: None declared.

Patents: A. El-Heliebi, WO2017081049 A1; A. Ahlford, PCT/EP2016/077068; M. Nilsson, PCT/EP2016/077068.

Role of Sponsor: The funding organizations played no role in the design of study, choice of enrolled patients, review and interpretation of data, or final approval of manuscript.

Acknowledgments: The authors thank Lisa Jaritz, Sylvia Tripolt, Karin Groller, Eva Maria Wascher, and Carina Kreuter for their support in patient recruitment. They also thank Birgitta Holmgren for supporting wire collection from patients at the Huddinge Hospital and Merlin Verena Luetke-Eversloh for providing antibodies. The authors thank Devyser AB for the diagnostic PCR-based analysis of *KRAS* mutations. Icons were made by Freepik from www.flaticon.com.

References

- Perakis S, Speicher MR. Emerging concepts in liquid biopsies. *BMC Med* 2017;15:75.
- El-Heliebi A, Kroneis T, Zohrer E, Haybaeck J, Fischeder K, Kampel-Kettner K, et al. Are morphological criteria sufficient for the identification of circulating tumor cells in renal cancer? *J Transl Med* 2013;11:214.
- Kroneis T, Geigl JB, El-Heliebi A, Auer M, Ulz P, Schwarzbraun T, et al. Combined molecular genetic and cytogenetic analysis from single cells after isothermal whole-genome amplification. *Clin Chem* 2011;57:1032–41.
- Ulz P, Belic J, Graf R, Auer M, Laferl, Fischeder K, et al. Whole-genome plasma sequencing reveals focal amplifications as a driving force in metastatic prostate cancer. *Nat Commun* 2016;7:12008.
- Ulz P, Thallinger GG, Auer M, Graf R, Kashofer K, Jahn SW, et al. Inferring expressed genes by whole-genome sequencing of plasma DNA. *Nat Genet* 2016;48:1273–8.
- Gorges TM, Kuske A, Röck K, Mauermann O, Müller V, Peine S, et al. Accession of tumor heterogeneity by multiplex transcriptome profiling of single circulating tumor cells. *Clin Chem* 2016;62:1504–15.
- Antonarakis ES, Lu C, Wang H, Lubber B, Nakazawa M, Roeser JC, et al. AR-V7 and resistance to enzalutamide and abiraterone in prostate cancer. *N Engl J Med* 2014;371:1028–38.
- Scher HI, Lu D, Schreiber NA, Louw J, Graf RP, Vargas HA, et al. Association of AR-V7 on circulating tumor cells as a treatment-specific biomarker with outcomes and survival in castration-resistant prostate cancer. *JAMA Oncol* 2016;2:1441.
- Antonarakis ES, Lu C, Lubber B, Wang H, Chen Y, Nakazawa M, et al. Androgen receptor splice variant 7 and efficacy of taxane chemotherapy in patients with metastatic castration-resistant prostate cancer. *JAMA Oncol* 2015;1:582–91.
- Onstenk W, Sieuwerts AM, Kraan J, Van M, Nieuweboer AJM, Mathijssen RHJ, et al. Efficacy of cabazitaxel in castration-resistant prostate cancer is independent of the presence of AR-V7 in circulating tumor cells. *Eur Urol* 2015;68:939–45.
- Bryant KL, Mancias JD, Kimmelman AC, Der CJ. KRAS: feeding pancreatic cancer proliferation. *Trends Biochem Sci* 2014;39:91–100.
- Tao L, Zhang L, Xiu D, Yuan C, Ma Z, Jiang B. Prognostic significance of K-ras mutations in pancreatic cancer: a meta-analysis. *World J Surg Oncol* 2016;14:146.
- Siegel RL, Miller KD, Jemal A. Cancer statistics, 2017. *CA Cancer J Clin* 2017;67:7–30.
- Stathis A, Moore MJ. Advanced pancreatic carcinoma: current treatment and future challenges. *Nat Rev Clin Oncol* 2010;7:163–72.
- Larsson C, Grundberg I, Söderberg O, Nilsson M. In situ detection and genotyping of individual mRNA molecules. *Nat Methods* 2010;7:395–7.
- Ke R, Mignardi M, Pacureanu A, Svedlund J, Botling J, Wahlby C, et al. In situ sequencing for RNA analysis in preserved tissue and cells. *Nat Methods* 2013;10:857–60.
- Weibrecht I, Lundin E, Kiflemariam S, Mignardi M, Grundberg I, Larsson C, et al. In situ detection of individual mRNA molecules and protein complexes or post-translational modifications using padlock probes combined with the in situ proximity ligation assay. *Nat Protoc* 2013;8:355–72.
- Gorges TM, Penkalla N, Schalk T, Joosse SA, Riethdorf S, Tucholski J, et al. Enumeration and molecular characterization of tumor cells in lung cancer patients using a novel in vivo device for capturing circulating tumor cells. *Clin Cancer Res* 2016;22:2197–206.
- Chudziak J, Burt DJ, Mohan S, Rothwell DG, Mesquita B, Antonello J, et al. Clinical evaluation of a novel microfluidic device for epitope-independent enrichment of circulating tumour cells in patients with small cell lung cancer. *Analyst* 2016;141:669–78.
- Hvichia GE, Parveen Z, Wagner C, Janning M, Quidde J, Stein A, et al. A novel microfluidic platform for size and deformability based separation and the subsequent molecular characterization of viable circulating tumor cells. *Int J Cancer* 2016;138:2894–904.
- Alix-Panabières C, Vendrell J-P, Pellé O, Rebillard X, Riethdorf S, Müller V, et al. Detection and characterization of putative metastatic precursor cells in cancer patients. *Clin Chem* 2007;53:537–9.
- Ma Y, Luk A, Young F, Lynch D, Chua W, Balakrishnar B, et al. Droplet digital PCR based androgen receptor variant 7 (AR-V7) detection from prostate cancer patient blood biopsies. *Int J Mol Sci* 2016;17:1264.
- Grundberg I, Kiflemariam S, Mignardi M, Imgenberg-

- Kreuz J, Edlund K, Micke P, et al. In situ mutation detection and visualization of intratumor heterogeneity for cancer research and diagnostics. *Oncotarget* 2013; 4:2407–18.
24. Siwetz M, Blaschitz A, El-Heliebi A, Hiden U, Desoye G, Huppertz B, et al. TNF- α alters the inflammatory secretion profile of human first trimester placenta. *Lab Invest* 2016;96:428–38.
25. Al-Soud WA, Rådström P. Purification and characterization of PCR-inhibitory components in blood cells. *J Clin Microbiol* 2001;39:485–93.
26. Carpenter AE, Jones TR, Lamprecht MR, Clarke C, Kang IH, Friman O, et al. CellProfiler: image analysis software for identifying and quantifying cell phenotypes. *Genome Biol* 2006;7:R100.
27. Kühnemund M, Wei Q, Darai E, Wang Y, Hernández-Neuta I, Yang Z, et al. Targeted DNA sequencing and in situ mutation analysis using mobile phone microscopy. *Nat Commun* 2017;8:13913.
28. Brummelkamp TR, Bernards R, Agami R. Stable suppression of tumorigenicity by virus-mediated RNA interference. *Cancer Cell* 2002;2:243–7.
29. Deer EL, Gonzalez-Hernandez J, Coursen JD, Shea JE, Ngatia J, Scaife CL, et al. Phenotype and genotype of pancreatic cancer cell lines. *Pancreas* 2010; 39:425–35.
30. Lustberg MB, Balasubramanian P, Miller B, Garcia-Villa A, Deighan C, Wu Y, et al. Heterogeneous atypical cell populations are present in blood of metastatic breast cancer patients. *Breast Cancer Res* 2014;16:R23.
31. Antonarakis ES, Lu C, Luber B, Wang H, Chen Y, Zhu Y, et al. Clinical significance of androgen receptor splice variant-7 mRNA detection in circulating tumor cells of men with metastatic castration-resistant prostate cancer treated with first- and second-line abiraterone and enzalutamide. *J Clin Oncol* 2017;35:2149–56.
32. Scher HI, Graf RP, Schreiber NA, McLaughlin B, Lu D, Louw J, et al. Nuclear-specific AR-V7 protein localization is necessary to guide treatment selection in metastatic castration-resistant prostate cancer. *Eur Urol* 2017;71: 874–82.
33. Crespo M, van Dalum G, Ferraldeschi R, Zafeiriou Z, Sideris S, Lorente D, et al. Androgen receptor expression in circulating tumour cells from castration-resistant prostate cancer patients treated with novel endocrine agents. *Br J Cancer* 2015;112:1166–74.
34. Kohli M, Ho Y, Hillman DW, Van Etten JL, Henzler C, Yang R, et al. Androgen receptor variant AR-V9 is coexpressed with AR-V7 in prostate cancer metastases and predicts abiraterone resistance. *Clin Cancer Res* 2017;23:4704–15.
35. Chen S, El-Heliebi A, Tauber G, Langsenlehner T, Pötscher M, Kashofer K, et al. Catch and Release: rare cell analysis from a functionalised medical wire. *Sci Rep* 2017;7:43424.
36. Lamouille S, Xu J, Derynck R. Molecular mechanisms of epithelial-mesenchymal transition. *Nat Rev Mol Cell Biol* 2014;15:178–96.
37. Yu M, Bardia A, Wittner BS, Stott SL, Smas ME, Ting DT, et al. Circulating breast tumor cells exhibit dynamic changes in epithelial and mesenchymal composition. *Science* 2013;339:580–4.
38. Misale S, Yaeger R, Hobor S, Scala E, Janakiraman M, Liska D, et al. Emergence of KRAS mutations and acquired resistance to anti-EGFR therapy in colorectal cancer. *Nature* 2012;486:532–6.
39. Dago AE, Stepansky A, Carlsson A, Luttgen M, Kendall J, Baslan T, et al. Rapid phenotypic and genomic change in response to therapeutic pressure in prostate cancer inferred by high content analysis of single circulating tumor cells. *PLoS One* 2014;9:e101777.
40. McDaniel AS, Ferraldeschi R, Krupa R, Landers M, Graf R, Louw J, et al. Phenotypic diversity of circulating tumour cells in patients with metastatic castration-resistant prostate cancer. *BJU Int* 2017;120:E30–44.

Article

Detection of Androgen Receptor Variant 7 (ARV7) mRNA Levels in EpCAM-Enriched CTC Fractions for Monitoring Response to Androgen Targeting Therapies in Prostate Cancer

Claudia Hille ¹, Tobias M. Gorges ¹, Sabine Riethdorf ¹, Martine Mazel ² , Thomas Steuber ³, Gunhild Von Amsberg ⁴, Frank König ⁵, Sven Peine ⁶, Catherine Alix-Panabieres ^{2,†}  and Klaus Pantel ^{1,*,†} 

¹ Department of Tumor Biology, University Medical Center Hamburg-Eppendorf, 20246 Hamburg, Germany; c.hille@uke.de (C.H.); t.gorges@uke.de (T.M.G.); s.riethdorf@uke.de (S.R.)

² Laboratory of Rare Human Circulating Cells (LCCRH), University Medical Centre of Montpellier–UM EA2415, 34295 Montpellier, France; martine-mazel@chu-montpellier.fr (M.M.); c-panabieres@chu-montpellier.fr (C.A.-P.)

³ Martini Clinic, University Medical Center Hamburg-Eppendorf, 20246 Hamburg, Germany; steuber@uke.de

⁴ Department of Hematology and Oncology, University Medical Center Hamburg-Eppendorf, 20246 Hamburg, Germany; g.von-amsberg@uke.de

⁵ ATURO, Urology Practice, 14197 Berlin, Germany; frank.koenig@aturo.berlin

⁶ Department of Transfusion Medicine, University Medical Center Hamburg-Eppendorf, 20246 Hamburg, Germany; s.peine@uke.de

* Correspondence: pantel@uke.de; Tel.: 49-40-741053503; Fax: 49-40-7410-55379

† There authors contributed equally to this work.

Received: 15 August 2019; Accepted: 10 September 2019; Published: 11 September 2019



Abstract: Expression of the androgen receptor splice variant 7 (ARV7) in circulating tumor cells (CTCs) has been associated with resistance towards novel androgen receptor (AR)-targeting therapies. While a multitude of ARV7 detection approaches have been developed, the simultaneous enumeration of CTCs and assessment of ARV7 status and the integration of validated technologies for CTC enrichment/detection into their workflow render interpretation of the results more difficult and/or require shipment to centralized labs. Here, we describe the establishment and technical validation of a novel ARV7 detection method integrating the CellSearch[®] technology, the only FDA-cleared CTC-enrichment method for metastatic prostate cancer available so far. A highly sensitive and specific qPCR-based assay was developed, allowing detection of ARV7 and *keratin 19* transcripts from as low as a single ARV7⁺/K19⁺ cell, even after 24 h of sample storage. Clinical feasibility was demonstrated on blood samples from 26 prostate cancer patients and assay sensitivity and specificity was corroborated. Our novel approach can now be included into prospective clinical trials aimed to assess the predictive values of CTC/ARV7 measurements in prostate cancer.

Keywords: prostate cancer; biomarkers; circulating tumor cells; androgen receptor; ARV7; abiraterone; enzalutamide

1. Introduction

Prostate cancer (PCa) remains the second most commonly diagnosed cancer among men worldwide with an estimated 1.3 million new cases each year [1]. In contrast to other cancer types such as pancreatic cancer, routine preventive medical screens for PCa are accessible to a broad spectrum of the public and have been widely accepted, leading to a drastic increase of newly diagnosed PCa cases. Tissue

biopsies are invasive and can be associated with adverse effects for the patient [2]. Furthermore, routine tissue biopsy is challenging in metastatic PCa (mPCa). In recent years, minimally invasive liquid biopsies, focusing on the identification of circulating tumor cells (CTCs) and circulating nucleic acids (ctDNA, miRNA) from whole blood samples, have gained tremendous attention [3–7]. While the prognostic relevance of CTCs in PCa, especially in the metastatic setting, has been thoroughly shown in large clinical trials [8–11], predictive value of CTC analysis and their clinical utility are still being debated [12–17]. While a multitude of therapeutic approaches exist, aimed at treating PCa in various disease stages, a subset of patients develop aggressive PCa subtypes that defy current therapeutic options. Therefore, simple detection of PCa is not sufficient and robust biomarkers are urgently needed to discern aggressive subtypes from clinically well treatable cancers, preferably without exposing patients to unnecessary tissue biopsies.

With the advent of novel hormone therapies such as enzalutamide and abiraterone and the emergence of innate and acquired resistance towards these therapies, the androgen receptor splice variant 7 (ARV7) has become a leading target of CTC research in PCa [17–19]. Multiple studies indicate that ARV7 mRNA and ARV7 protein expression in CTCs is associated with resistance towards novel hormone therapies [20–25] and that ARV7 expressing patients benefit more from taxane-based therapy [25–27]. This implicates ARV7 as a possible treatment selection biomarker for PCa patients prior to receiving novel hormone therapy (e.g., enzalutamide, abiraterone). Additionally, the ARV7 status is subject to change during therapy regimens [25,28,29], underlining the benefit of sequential sampling which becomes possible through liquid biopsy. ARV7 could therefore also represent a biomarker to monitor treatment response and predict upcoming therapy resistance.

While many approaches have been developed to assess ARV7 either on protein or mRNA level [20,24,30], only very few of these approaches allow for parallel CTC enumeration and morphological characterization while giving information on ARV7 status for individual CTCs [24,31], a limitation recently highlighted [32]. Additionally, even fewer were designed to use the only FDA-cleared CTC enrichment and detection technology shown to have clinical prognostic relevance in prostate cancer, the CellSearch® system [33]. Here, we aimed to develop a protocol for ARV7 detection using the CellSearch® technology. With our novel workflow we were able to detect ARV7 mRNA in as low as one CTC in 7.5 mL of whole blood.

2. Materials and Methods

2.1. Cancer Cell Lines

The human prostate cancer cell lines 22Rv1 (ATCC® CRL-2505), VCaP (ATCC® CRL-2876), LNCaP (ATCC® CRL-1740) and PC3 (ATCC® CRL-1345) were obtained from the American Type Culture Collection (ATCC, Manassas, VA, USA) and cultured according to ATCC recommendations.

LNCaP and 22Rv1 cells were cultured in RPMI 1640 medium, while the VCaP and PC3 cells were maintained in Dulbecco's Modified Eagle Medium (DMEM). Media were additionally fortified with 10% fetal calf serum (FCS) (Gibco—Life Technologies, Darmstadt, Germany), 1% L-glutamine (Gibco—Life Technologies, Darmstadt, Germany) and 1% penicillin/streptomycin (Gibco—Life Technologies, Darmstadt, Germany), as recommended by ATCC. Cells were cultured in 25 cm² flasks at 37 °C in a humidified atmosphere containing 5% CO₂.

2.2. Blood Collection and Processing

Male healthy donor (HD) and patient blood samples were acquired in accordance to the World Medical Association Declaration of Helsinki and the guidelines for experimentation with humans by the Chambers of Physicians of the State of Hamburg (“Hamburger Ärztekammer”). All patients gave informed, written consent prior to blood collection (Ethics Approval: PV3779). Samples were drawn from 26 metastatic prostate cancer (mPCa) patients into standard 7.5 mL ethylenediaminetetraacetic acid (EDTA) vacutainers or CellSave® (Menarini-Silicon Biosystems, Florence, Italy) preservation tubes respectively. Each patient therefore provided a matched sample of EDTA-KE (Sarstedt, Rheinbach, Germany) and CellSave® blood for further analysis. CTCs from EDTA blood samples were enriched via the CellSearch® Profile Kit (Menarini-Silicon Biosystems, Florence, Italy) and further analyzed for ARV7 expression as described below. Samples collected into CellSave® blood preservation tubes were processed via the CellSearch® CXC-Kit (FITC labelled pan-keratin) [34]. Phycoerythrin labelled androgen receptor CellTracks Anti-Androgen Receptor (Janssen Diagnostics) antibody (10 µg/mL) was used for full-length AR (AR-FL) detection in the fourth channel of the CellSearch® for 12/26 mPCa patients. All analyses were performed by trained CellSearch® analyst. CTCs were defined as keratin positive and CD45 negative cells with a nuclear DAPI staining.

2.3. Spiking of Healthy Donor Blood

For spiking experiments, cell line cells were washed once with 1 x PBS (Gibco-Life Technologies, Darmstadt, Germany) and treated with 0.25% trypsin-EDTA (Gibco-Life Technologies, Darmstadt, Germany) for 5 min at 37 °C prior to being resuspended in culture medium. The cell suspension was centrifuged at 190× g for 5 min after which the supernatant was discarded and the cells were again resuspended in fresh culture medium. The cells were spread to a petri dish filled with corresponding medium, manually counted and picked under a light microscope. Defined cell counts were added directly to healthy donor blood samples.

2.4. Immunocytochemical Stainings on Cell Culture Plates

Cells were seeded into 24-well plates at the rate of 50,000 cells/well, and maintained at 37 °C in a humidified atmosphere containing 5% CO₂ until reaching 80% confluence. Cells were then fixed and permeabilized using IntraPrep Permeabilization Reagent (A07803, Beckman Coulter, Brea, CA, USA), and blocked with 10% Goat serum for 1 h at room temperature. Cells were subsequently incubated with (i) primary antibodies Anti-AR (AR-V7 specific) antibody [EPR15656] (Abcam, Cambridge, United Kingdom) at a final concentration of 10 µg/mL, or (ii) Rabbit IgG, monoclonal [EPR25A]-Isotype Control (Abcam, Cambridge, United Kingdom) (our negative control) at a final concentration of 10 µg/mL. All wells were also incubated with the anti-PanCK^{PE} (Menarini-Silicon Biosystems, Florence, Italy). Following this first incubation, cells were washed with 1% goat serum in PBS, incubated with the FITC-conjugated secondary antibody (1:20 in PBS containing 10% Goat serum), and washed twice with 1% goat serum in PBS.

In parallel, the presence of the androgen receptor (AR) was tested using the anti-AR^{AF488} [D6F11] XP Rabbit antibody (0.5 µg/mL, Ozyme, Saint Cyr L'Ecole, France); in the control wells, the Rabbit [DA1E] IgG^{AF488} XP isotype (0.5 µg/mL, Ozyme, Saint Cyr L'Ecole, France) was used. Cell imaging was obtained under 20x magnification using a Fluorescent Axio Observer microscope (Carl Zeiss, Oberkochen, Germany).

2.5. Immunocytochemical Stainings on Cytospins

Cell suspensions of selected prostate cancer cell lines (22Rv1, LNCap, PC3) were spun down on glass slides (190× g, 5 min) and dried at room temperature (RT) over night. Cells were subsequently fixed and permeabilized using the respective CellSearch CXC Kit reagents (Menarini-Silicon Biosystems, Florence, Italy) and blocked with 10% AB-Serum (BioRad, Rüdigenheim, Germany). Primary antibodies targeting ARV7, 4 µg/mL of clone AG10008 (unlabeled, Precision, Columbia, Maryland, USA) and 6 µg/mL EPR15656 (unlabeled, Abcam, Cambridge, United Kingdom) were tested. Secondary antibodies were applied and contained a DAPI nuclear counterstain. Secondary rabbit-anti mouse (Alexa 546, polyclonal, Thermo Fisher Scientific, Dreieich, Germany) and mouse-anti-rabbit (Alexa 546, polyclonal, Thermo Fisher Scientific, Dreieich, Germany) antibodies were used. Cytospins were covered in Prolong Gold Antifade Reagent (Thermo Fisher Scientific, Dreieich, Germany) and cover slipped for analysis. Slides were manually assessed using a fluorescence microscope (Axioplan 2, Carl Zeiss, Oberkochen, Germany).

2.6. Western Blots

Cell lines (22Rv1, VCaP, LNCaP, and PC3) were cultured to 70% confluency, harvested in urea lysis buffer (9.8 M Urea, 15 mM EDTA, 30 mM Tris) and homogenized by ultrasonic treatment. Protein concentration was measured with the Pierce BCA Protein Assay Kit (Pierce, Rockford, Illinois, USA). 40 µg of total protein was applied for Western Blot analysis for each respective cell line alongside pre-stained pEqGold protein marker-V (VWR, Erlangen, Germany). Proteins were separated according to size using a Laemmli buffer system and 8% polyacrylamide separation gel. Two ARV7 antibodies, mouse-AG10008 (Precision, Columbia, MD, USA; 2 µg/mL) and rabbit-EPR15656 (Abcam, Cambridge, United Kingdom; 1.5 µg/mL) were applied in dilutions according to the supplier's instruction manual in 5% milk powder. Alpha-tubulin was used as a loading control (Cell Signaling Technology, Danvers, MA, USA). Species specific secondary antibodies (horseradish peroxidase conjugated, DAKO, Glostrup, Germany) were applied at 1:10.000 dilution in 5% milk powder. Protein bands were visualized using SignalFire™ Plus ECL reagent (Cell Signaling Technology, Danvers, MA, USA) and X-ray films (CEA, Hamburg, Germany) according to the instruction manual.

2.7. RNA Extraction and cDNA Synthesis

For cell line characterization and PCR establishment RNA was isolated from prostate cancer cell lines grown in a T25 culture flask at 70% confluency using the NucleoSpin® RNA isolation kit (Macherey-Nagel, Düren, Germany) according to manufacturer's instructions. RNA concentration and purity were controlled via NanoDrop 1000 spectrophotometer (Thermo Fisher Scientific, Dreieich, Germany) following isolation. 0.5 µg of RNA per cell line were used for DNA synthesis with the First Strand cDNA Synthesis Kit (Thermo Fisher Scientific, Dreieich, Germany) according to manufacturer's instructions. cDNA Synthesis was carried out in a PqSTAR 96 Universal Gradient thermocycler (VWR International, Darmstadt, Germany).

Following CTC enrichment via the CellSearch® Profile Kit (Menarini-Silicon Biosystems, Florence, Italy) samples were transferred to a fresh 1.5 mL tube (Sarstedt, Rheinbach, Germany). To do so, a 1000 µL pipette tip was first coated with a solution of 0.1 mg/mL of BSA/PBS to circumvent binding and sticking of CTCs to the pipette surface. All RNA work was performed using sterile, DNA/RNA-free, filtered Biosphere® plus pipette tips (Sarstedt, Rheinbach, Germany). The Profile® sample tube was washed with 500 µL of 1x DPBS (cell culture use) (Thermo Fisher Scientific, Dreieich, Germany), which was also added to the sample. Subsequently the sample was placed in a magnetic rack (Magnetoclect; R&D systems, Minneapolis, MN, USA) for 10 min. The supernatant was discarded, and the sample was washed with 1000 µL of 1x DPBS, followed by another 10 min attached to the magnetic rack. This step was repeated with 500 µL of 1x DPBS prior to resuspension of the Profile® beads in 150 µL of lysis buffer (Dynabeads mRNA DIRECT Kit; Thermo Fisher Scientific, Dreieich, Germany). Samples were

immediately frozen at -80°C . Sample lysates were stored for a maximum of 14 days prior to RNA isolation and cDNA synthesis.

For RNA extraction, the Dynabeads mRNA DIRECT Kit (Thermo Fisher Scientific, Dreieich, Germany) was applied according to manufacturer's instructions. Following the last wash step with Wash buffer B, supernatant was removed, and beads were resuspended in $14.75\ \mu\text{L}$ of Nuclease-free H_2O (Qiagen, Hilden, Germany) and placed in a PCR cycler at 75°C for 5 min to ensure elution of mRNA from the beads. Subsequently cDNA was synthesized using the Sensiscript Reverse Transcription Kit (Qiagen, Hilden, Germany) with Recombinant Rnasin[®] (Promega, Mannheim, Germany) as an added RNase inhibitor. Primer addition was not necessary as the contained dynabeads function as oligo-dT primers. RNase inhibitor was limited to $0.25\ \mu\text{L}$, leading to a total mastermix of $5.25\ \mu\text{L}$ added to each RNA sample (total reaction volume of $20\ \mu\text{L}$). Following cDNA synthesis, beads were removed via magnet and supernatant was transferred to a fresh PCR tube for subsequent qPCR analysis.

2.8. Polymerase-Chain Reaction (PCR) Analysis

For *AR-FL* and *ARV7* primer evaluation, 10 ng of cDNA of each prostate cancer cell line was applied per PCR. The PCR reaction conditions for initial primer testing were adapted from the original Antonarakis et al. publication by the Johns Hopkins Group [20]. Reactions were run in a PeqSTAR 96 Universal Gradient thermocycler (VWR International, Darmstadt, Germany).

PCR primer pairs (Sigma Aldrich, Steinheim, Germany) chosen for PCR targeted *AR-FL* (fw-CAGCCTATTGCGAGAGAGCTG, rev-GAAAGGATCTTGGGCACTTGC, fragment size of 125 bp) [20] and *ARV7* (Antonarakis et al. [20]: fw-CCATCTTGTCGTCTTCGGAAATGTGA, rev-TTTGAATGAGGCAAGTCAGCCTTTCT, fragment size of 125 bp; Guo et al. [35]: fw-CTACTCCGGACCTTACGGGGACATGCG, rev-TGCCAACCCGGAATTTTCTCCC, fragment size of 314 bp; Liu et al. [36]: fw- CAGGGATGACTCTGGGAGAA, rev- GCCCTCTAGAGCCCTCATTT, fragment size of 112 bp; UKE: fw-AGAAAGGCTGACTTGCCTCA, rev- CGCCAGGTTTCTCCAGACTA, fragment size of 73 bp) gene sequences. Novel UKE primers were designed using the Primer 3 software [37]. Primers were aliquoted at stock concentrations of $100\ \mu\text{M}$ with Nuclease-free H_2O (Qiagen, Hilden, Germany) and frozen at -20°C . Final concentrations of $10\ \mu\text{M}$ were applied to PCRs.

To visualize PCR products, they were mixed with DNA Gel loading dye (6x) (Thermo Fisher Scientific, Dreieich, Germany) and applied to 2% agarose gels containing GelRed[®] Nucleic Acid Gel Stain (Biotum, Fremont, CA, USA) at $1/\mu\text{L}$ per ml of agarose gel. The Quick-Load[®] 100 bp DNA Ladder (New England Biolabs, Frankfurt am Main, Germany) was used as a size standard. PCR fragments were visualized using the Gene Genius bioimaging system (Syngene, Bangalore, India).

2.9. Quantitative Polymerase-Chain Reaction (qPCR) Analysis

qPCRs were pipetted under a separate flow hood with sterile, DNA/RNA-free, filtered Biosphere[®] plus pipette tips (Sarstedt, Rheinbach, Germany) and performed in a CFX96 Touch[™] Real Time PCR Detection System (BioRad, Rüdigenheim, Germany). Maxima SYBR-Green fluorescent dye (Thermo Fisher Scientific, Dreieich, Germany) was used for product detection. Amplification was performed under the following conditions: after an initial denaturation step (10 min at 95°C), 40 amplification cycles were carried out, consisting of denaturation at 95°C for 30 seconds, annealing at 60°C for 30 s, and elongation for 30 s at 72°C . A final elongation step at 72°C (10 min) was followed by a melting curve analysis and storage of the samples at 4°C . Data was summarized and converted into Excel files using the CFX Manager Software (BioRad, Rüdigenheim, Germany). For qPCR analysis, two additional primer sets targeting *K19* (fw-CGAACCAAGTTTGAGACGGA; rev-GATCTGCATCTCCAGGTCGG; fragment size of 117 bp) and *Actin* (x) gene sequences were applied. Samples were applied in triplicates and average Cq values as well as standard deviations were calculated. Primers were aliquoted at stock concentrations of $100\ \mu\text{M}$ with Nuclease-free H_2O (Qiagen, Hilden, Germany) and frozen at -20°C . Final concentrations of $10\ \mu\text{M}$ were applied to qPCRs.

Relative gene expression of *AR-FL* and *ARV7* in initial primer testing and cell line characterization was normalized from data sets by the comparative Cq method [38]. Briefly, the first amplification cycle showing significant increase of fluorescence signal over background level was defined as the cycle of quantification (Cq). Cq data of *AR-FL* and *ARV7* was normalized by subtracting the Cq value of *Actin* from the respective target gene for each cell line tested, generating a ΔCq value. Subsequently, the $\Delta\Delta Cq$ values were calculated by subtracting the ΔCq of each specific gene calculated for the different cell lines (22Rv1, VCap, and LNCaP) from the ΔCq values calculated for gene expression in PC3 cells. Finally, $\Delta\Delta Cq$ values were converted to log2 fold changes by applying $2^{-\Delta\Delta Cq}$. Ten nanograms of cDNA were applied per triplicate well.

Following RNA isolation and cDNA transcription from CellSearch® Profile Kit (Menarini-Silicon Biosystems, Florence, Italy) enriched samples, the 20 μ L of cDNA mix was applied in triplicates for each gene (2 μ L/well). No absolute quantification or normalization of genes was performed as levels of *Actin* gene expression is variable depending on background leucocyte cDNA co-amplified following CTC enrichment. Gene expression was confirmed when at least 2/3 triplicates showed detectable transcript levels under a Cq threshold of 35. Quality of the results was furthermore corroborated by melting curve analysis and subsequent visualization of amplified products on 2% agarose gels (see above).

3. Results

3.1. Test of Commercially Available ARV7 Antibodies for Fourth CellSearch® Channel

To allow assessment of ARV7 protein levels in parallel to CTC enumeration on a cell-specific level, we initially tested available ARV7 antibodies with the aim of adding them to the fourth channel of the CellSearch® system. Currently only few commercial antibodies are available, aimed at detecting ARV7 protein either via immunohistochemistry (IHC), immunocytochemistry (ICC) and/or western blot.

Three established prostate cancer cell lines were chosen for method establishment, each cell line representing a specific status of AR-full length (AR-FL) and ARV7 protein expression: 22Rv1 (AR-FL⁺/AR-V7⁺), LNCaP (AR-FL⁺/AR-V7^{+/-}), and PC3 (AR-FL⁻/AR-V7⁻). First, the cell lines were characterized for AR-FL (Figure 1a), resulting in cell line specific nuclear ICC staining (22Rv1 and LNCaP) or absence of staining (PC3) for the full-length protein, seen in green. Next, we tested the anti-ARV7 antibody [EPR15656] described in literature to specifically stain nuclear ARV7 [25]. This antibody did not result in cell line specific staining results, as all three tested cell lines including the ARV7⁻ PC3 cells showed green nuclear ARV7 staining (Figure 1b). Similar results were obtained using the antibody [EPR15656] as well as an additional commercially available ARV7 antibody on cell line cytopins (Figure S1). In western blot analysis the anti-ARV7 antibody [AG10008] by Precision showed cell line specific results, correctly detecting 22Rv1 and VCap lysate as ARV7⁺, LNCaP protein levels as below detection limit and identifying PC3 cells as ARV7⁻ (Figure S1a). In contrast, the anti-ARV7 antibody [EPR15656], showed an unspecific western blot signal for PC3 cells (Figure S1a). In ICC both antibodies failed to correctly characterize the chosen prostate cancer cell lines, giving unspecific staining results (Figure S1b,c).

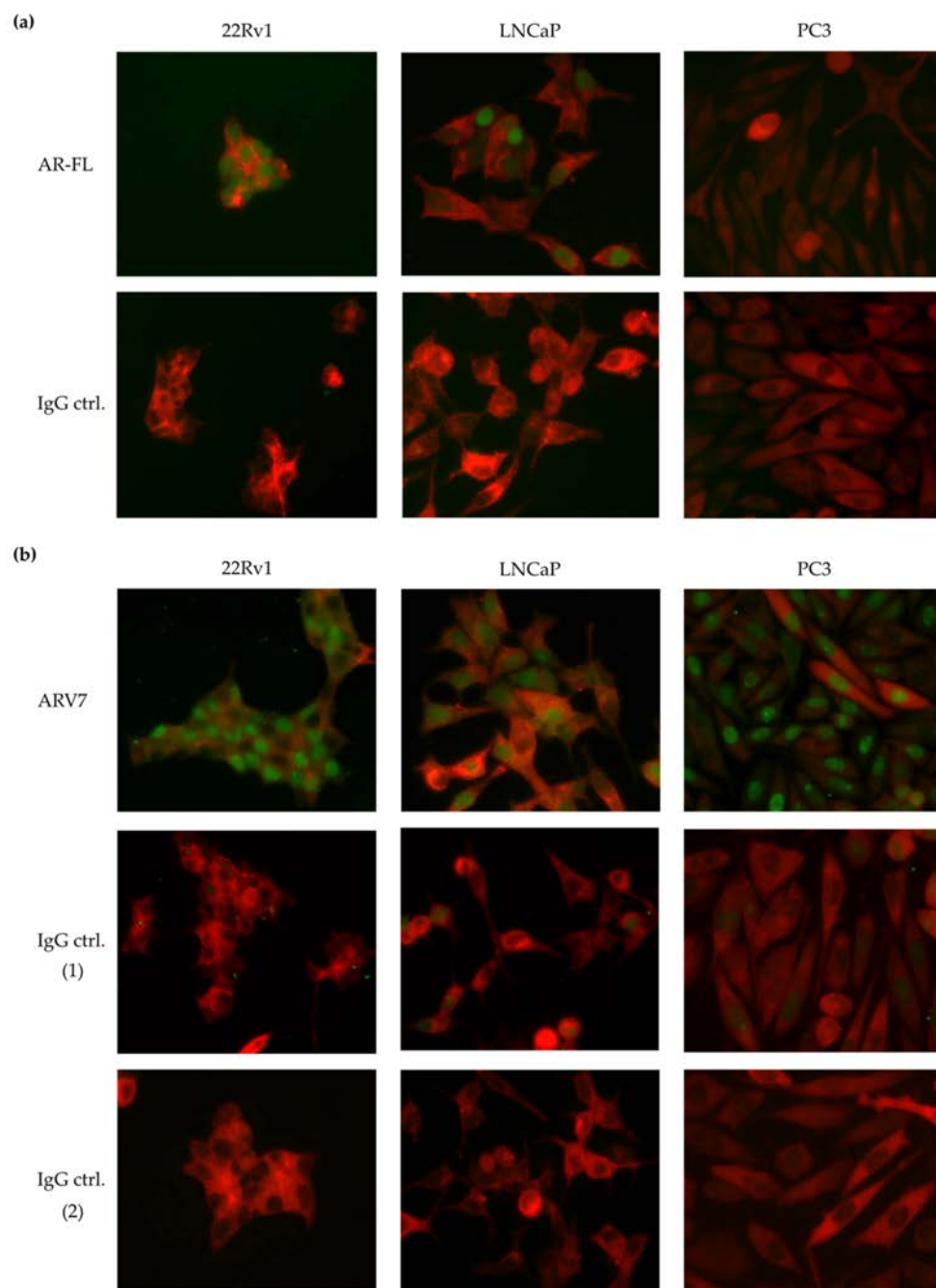


Figure 1. Immunocytochemical (ICC) staining of full-length androgen receptor (AR-FL) and ARV7 on three selected prostate cancer cell lines. Cells are stained for pan-keratin in red (anti-PanCK, CellSearch[®], Menarini) in all images. **(a)** Upper panel: ICC staining performed using the anti-AR-FL antibody (7395S Ozyme) in green. AR-FL positive cells lines 22Rv1 and LNCaP show positive nuclear AR-FL staining, while PC3 cells remain unstained. Lower panel: ICC control staining using Rabbit [DA1E] IgG XP isotype (2975S Ozyme) in green showing the absence of unspecific staining on 22Rv1, LNCaP and PC3 cells. **(b)** Upper panel: ICC staining performed using the anti-ARV7 antibody [EPR15656] (209491 Abcam) detected by a FITC-conjugated secondary antibody. A positive nuclear staining is observable on all three cell lines (in green), indicating unspecific signal of the antibody in PC3. Medium panel: ICC staining performed with the Rabbit IgG, monoclonal [EPR25A]-Isotype Control (172730 Abcam) detected with FITC-conjugated secondary antibody (97050, Abcam) showing negativity on 22Rv1, LNCaP, and PC3 cells. Lower panel: ICC staining performed with FITC-conjugated secondary antibody (97050, Abcam) showing negativity on 22Rv1, LNCaP, and PC3 cells.

In conclusion, none of the tested antibodies were deemed suitable for characterization of ARV7 protein on CTCs via the CellSearch® system. Additionally, the most intensively tested anti-ARV7 antibody [EPR15656] [25], described to give a specific nuclear and unspecific cytoplasmic staining did not show reliable results in our hands (Figure 1b), giving unspecific nuclear staining signals in ARV7[−] PC3 cells, even when neglecting the cytoplasmic staining and considering the described, relevant nuclear staining.

3.2. Development of a qPCR Based Assay to Detect ARV7 mRNA

As an alternative to protein-based detection we subsequently aimed at establishing a qPCR-based approach to detect ARV7 on an mRNA level. We added an additional prostate cancer cell line to the analysis, to further confirm the robustness of our method. VCaP cells show similar AR-FL and ARV7 expression profiles as 22RV1 cells (AR-FL⁺/AR-V7⁺) and were used as a second ARV7⁺ cell line during method establishment. An overview of the AR-FL and ARV7 status for all four cell lines is listed in Figure 2a. Initially, we planned on using the AR-FL and ARV7 primer sets already published [20] for our qPCR-based detection and then modifying the CTC pre-enrichment steps. However, when testing the primers using PCR according to the published protocol, it became clear that while the AR-FL primers showed specific bands at the correct expected size of 125 bp (Figure 2b), an additional, undescribed PCR fragment of around 250 bp was detected using the ARV7 primers in 22Rv1 but not in LNCaP cells (Figure 2b). To ensure optimal primer quality for ARV7 detection, additional ARV7 primer sets described in literature [35,36] as well as an own design (UKE), were employed. To exclude that the unspecific PCR fragments detected were generated due to incorrect annealing temperature or incorrect cDNA synthesis, we tested all four primer sets in a gradient PCR on freshly generated 22Rv1 and LNCaP cDNA (Figure 2c). Again, an additional PCR product was detected for the Antonarakis [20] and Guo [35] primer sets across all annealing temperatures in 22Rv1 cells but not LNCaP cells (Figure 2c, lines 1,2). This could represent an additional AR splice variant, similar to ARV7 [30]. Using the original protocol of 40 amplification cycles [20,23] this additional transcript could come up in clinical samples, especially those with high CTC counts, and result in an unaccounted bias. In contrast, the Liu [36] and UKE primer sets, resulted in specific PCR fragments at 112 bp and 73 bp, respectively (Figure 2c, lines 3,4). The fragment signal intensity appeared slightly higher for the UKE primers (Figure 2c, line 4) in comparison to the Liu primers [36] (Figure 2c, line 3), which could indicate a higher amount of generated PCR product. However, this cannot be conclusively deduced from qualitative PCR. Decreasing the PCR cycles from 39 to 30 (Figure 2d), reduced the unspecific PCR signals down to hardly visible levels for the Antonarakis [20] and Guo [35] primer sets (Figure 2d). However, as quantitative PCR represents a much more sensitive method than qualitative PCR, both primer sets were discarded for further experiments. Both the Liu [36] and UKE primer sets displayed cell line specific PCR results and PCR fragments at correct sizes, resulting in further evaluation of these two primer sets via qPCR.

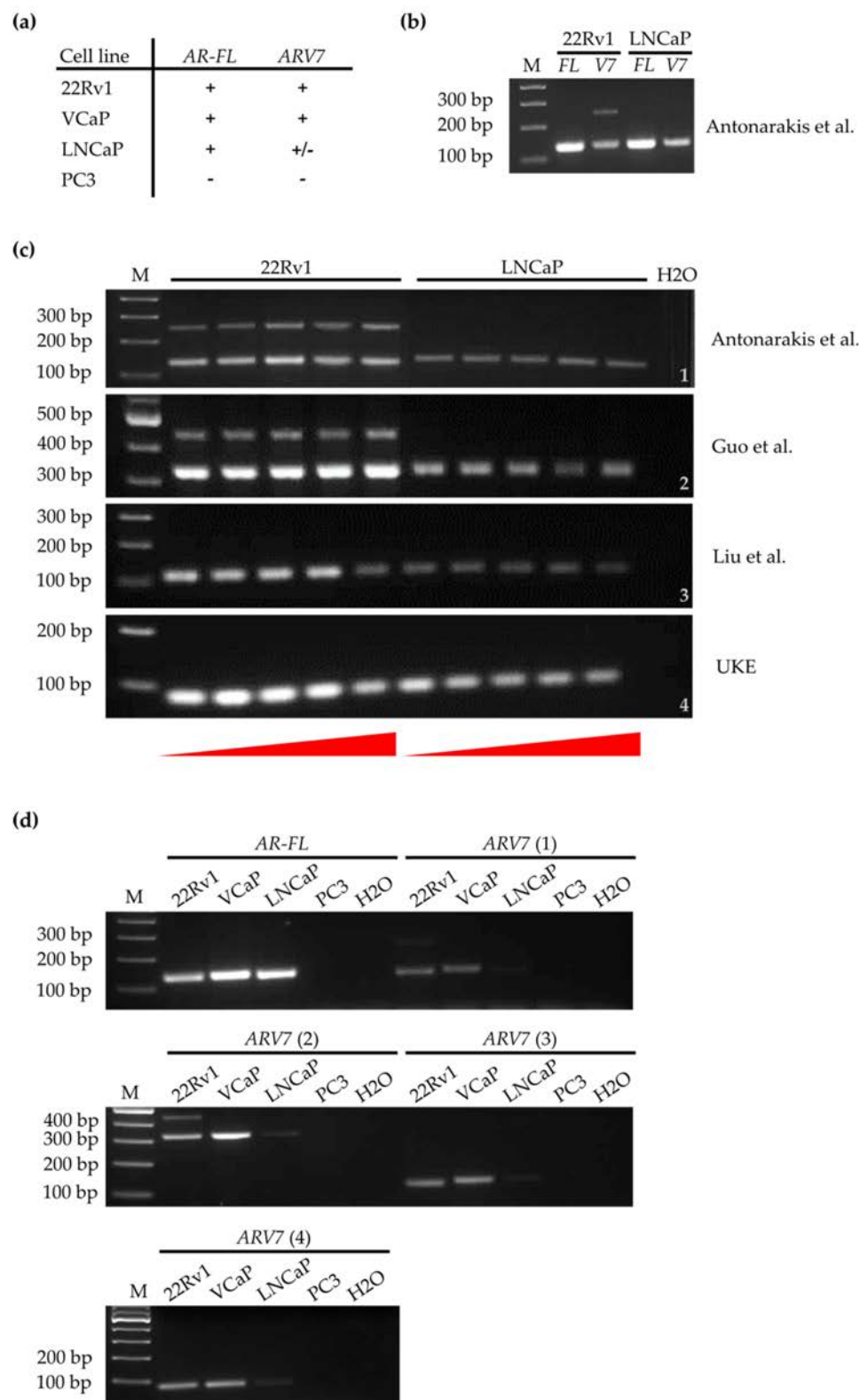


Figure 2. PCR-based detection of AR-FL and androgen receptor splice variant 7 (ARV7) in selected prostate cancer cell lines. Letter M indicating DNA ladder (marker) lanes. Ten nanograms of cDNA were analyzed for each PCR sample. (a) Schematic overview of AR-FL and ARV7 positivity (+) and negativity (−) for established prostate cancer cell lines, as described in literature. (b) Agarose gels of a PCR detecting AR-FL and ARV7 in cDNA isolated from 22RV1 and LNCaP cells. ARV7 cDNA was detected using the primers described by Antonarakis et al. [20]. PCRs were performed for 39 cycles.

125 bp PCR products are expected for both *AR-FL* and *ARV7*. The *ARV7* PCR shows an additional, uncharacterized band at between 250–300 bp for 22RV1 cells, but not for LNCaP cells. (c) Agarose gel of a gradient PCR for *ARV7* on 22RV1 and LNCaP cDNA using different primer pairs. PCRs were performed for 39 cycles. Temperatures increasing from 58.5 °C to 65.5 °C, indicated by red triangles below gel images. Antonarakis (1) and Guo (2) primers both show secondary PCR bands on 22RV1 cDNA (between 200–300bp and between 400–500 bp, respectively). Liu (3) and UKE (4) primers both give expected PCR bands for *ARV7* at 112 bp and 73 bp. Signal intensity appears higher, possibly indicating more generated PCR product, for UKE primers. (d) Agarose gels of PCRs detecting *AR-FL* and *ARV7* in cDNA of 22RV1, VCaP, LNCaP, and PC3 prostate cancer cell line cells. PCRs were performed for 30 cycles. *AR-FL* primer set, results in specific PCR signals in *AR*⁺ and *AR*[−] cell lines. *ARV7* (1) corresponds to Antonarakis et al., *ARV7* (2) corresponds to Guo et al., *ARV7* (3) corresponds to Liu et al., and *ARV7* (4) corresponds to our newly developed UKE primer sets.

Gene expression levels of *AR-FL* and *ARV7* (using the Liu and UKE primers) were assessed for 22RV1, LNCaP, and VCaP cells in relation to their respective expression in PC3 cells (Figure 3a). As expected, both *AR-FL* and *ARV7* gene expression were dramatically increased in all three cell lines compared to PC3 cells. Additionally, the UKE primers showed most effective detection of *ARV7* (Figure 3a). All further experiments were therefore carried out using the newly designed UKE primers.

Apart from *AR-FL* and *ARV7*, *K19*, and *Actin* gene expression were also measured via qPCR. *Actin* functioning as a gene for normalization and a confirmation of successful cDNA synthesis, and *K19* as an established marker for CTC detection in blood [39,40] thus allowing confirmation of the presence of CTCs in future clinical samples. Figure 3b shows representative qPCR curves for all four cell lines (in different colors) for each gene. Due to the high sensitivity of qPCR analysis, *ARV7* expression can be detected at around 36 cycles for cDNA inputs generated from high PC3 cell counts (Figure 3b). This is an enormous difference to the approximately 22 cycles necessary for detection of *ARV7*⁺ cell lines (Figure 3b). Despite the fact that such high CTC cell counts are extremely rarely to be expected in clinical samples, a cut-off of ≤35 cycles was established for gene expression to be counted as positive for the analyzed genes in all further analysis.

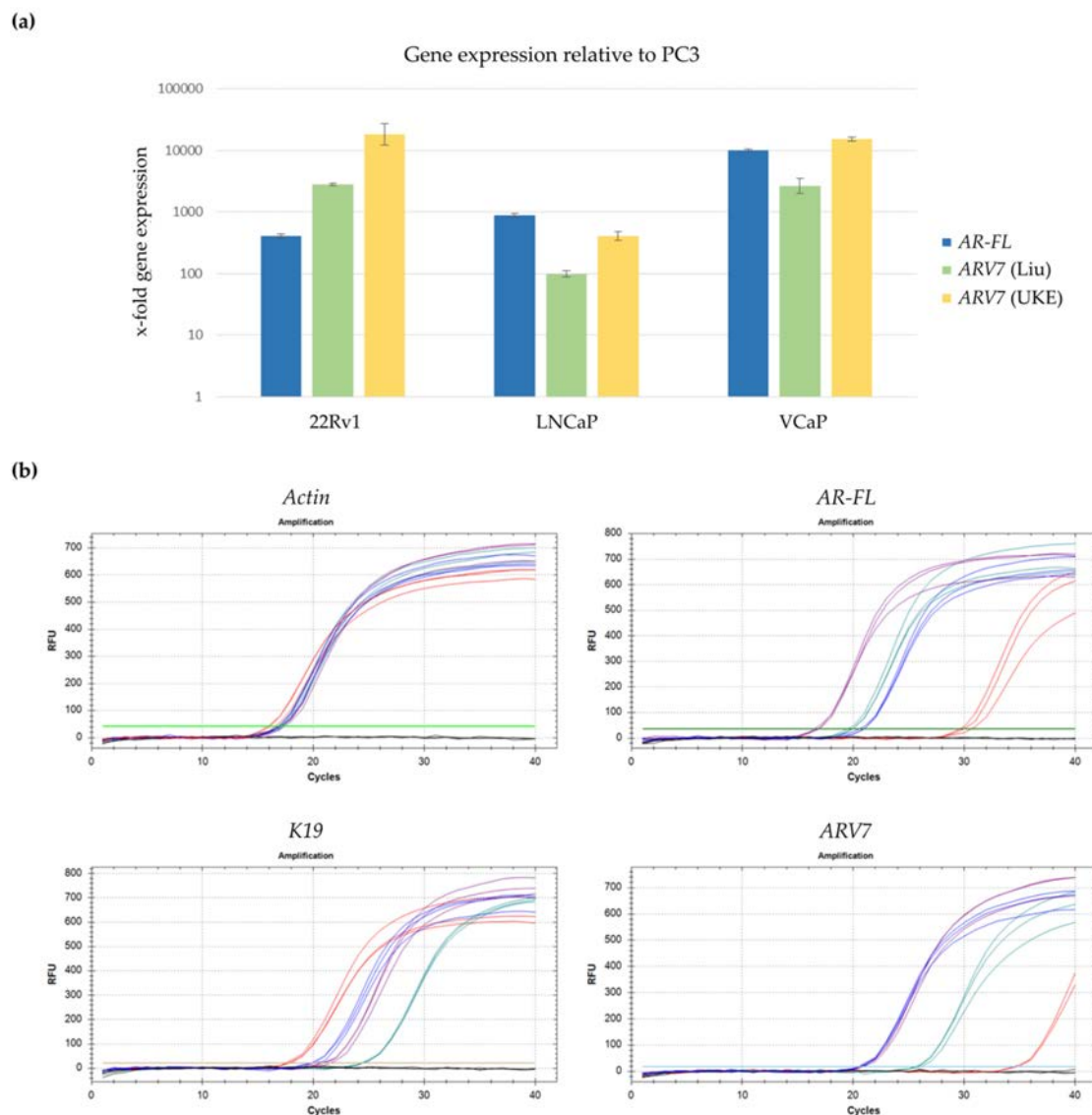


Figure 3. qPCR-based characterization of selected prostate cancer cell line cDNA. cDNA was generated from RNA isolated from 22RV1, VCaP, LNCaP, and PC3 cells and analyzed via qPCR. (a) Relative gene expression of AR-FL and ARV7 using primers by Liu et al. and our newly developed primers (UKE). Gene expression was first normalized to actin and subsequently displayed relative to PC3 gene expression. Standard deviation is indicated as brackets. (b) Representative qPCR expression profiles for different target genes (*Actin*, *AR-FL*, *K19* and *ARV7*) across all four chosen cell lines: 22RV1 (blue), VCaP (purple), LNCaP (green), and PC3 (red). All samples were applied in triplicates.

3.3. Combining Profile-Kit-Based CTC Enrichment with ARV7 mRNA Detection

To allow for use of the CellSearch[®] system to isolate prostate cancer CTCs for ARV7 detection on the one hand and enable parallel CTC quantification on the other, a two-armed approach was designed (Figure 4). 7.5 mL of whole blood was taken in parallel into standard EDTA tubes for RNA isolation and CellSave[®] blood preservation tubes for CTC enumeration, respectively. From EDTA blood, CTCs were enriched via the CellSearch[®] Profile Kit for subsequent RNA analysis. RNA was isolated and cDNA synthesized prior to analysis of *ARV7*, *K19*, and *Actin* via qPCR. In parallel CellSave[®] preserved blood was processed using the CellSearch[®] CXC Kit thus allowing for parallel AR-FL protein characterization in the fourth fluorescent channel of the device (Figure 4).

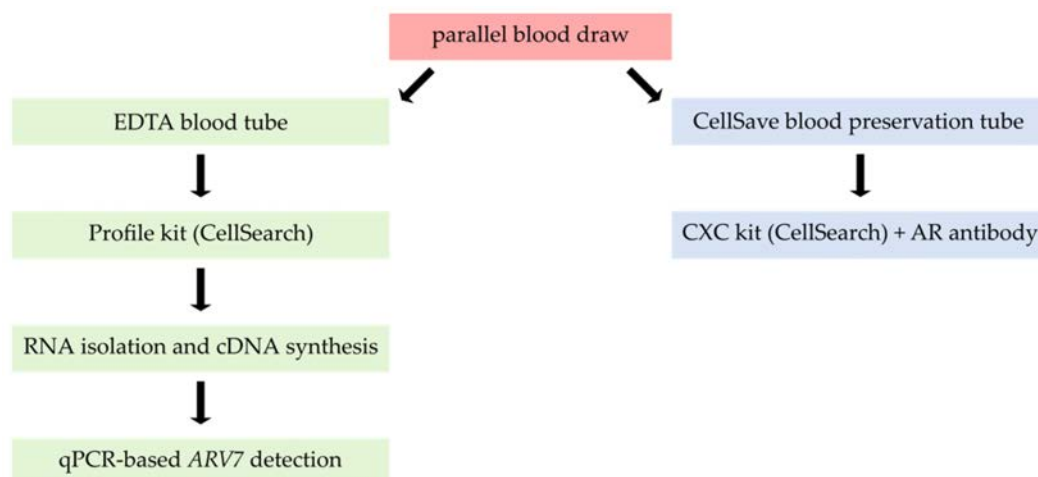


Figure 4. Schematic workflow of ARV7 detection combined with parallel circulating tumor cell (CTC) enumeration.

“Mock” samples were generated to mimic clinical sample handling. Differing amounts of ARV7[−] and ARV7⁺ cell line cells were manually spiked into healthy donor (HD) blood and directly processed by our workflow (Table 1). Following the qPCR run, generated products were applied to a gel electrophoresis allowing final confirmation of gene expression status (data not shown).

Table 1. Validation of protocol specificity and sensitivity. Titration experiments of spiked cell lines in blood from healthy donor (HD) samples. Indicated cell counts of ARV7⁺ (22Rv1) and ARV7[−] (PC3) cells were manually spiked into HD blood and processed by our protocol. ARV7 status is highlighted as “+” for positive and “−” for negative samples. Detection of gene expression was confirmed when at least 2/3 triplicates were positive in qPCR analysis. Unamplified qPCR samples are marked as N/D (not detected). HD samples were processed in parallel as a negative control for ARV7 and *K19*. The bar (−) in the respective table column of detection indicates no further experiments were conducted.

Cell Line	ARV7 Status	Cell Amount	Target	Detection	Detection (n = 2)	Detection (n = 3)
HD	−	0	ARV7	N/D	N/D	N/D
			<i>K19</i>	N/D	N/D	N/D
			<i>Actin</i>	yes	yes	yes
PC3	−	50	ARV7	N/D	−	−
			<i>K19</i>	yes	−	−
			<i>Actin</i>	yes	−	−
		100	ARV7	N/D	−	−
			<i>K19</i>	yes	−	−
			<i>Actin</i>	yes	−	−
22RV1	+	50	ARV7	yes	−	−
			<i>K19</i>	yes	−	−
			<i>Actin</i>	yes	−	−
		20	ARV7	yes	−	−
			<i>K19</i>	yes	−	−
			<i>Actin</i>	yes	−	−
		10	ARV7	yes	yes	yes
			<i>K19</i>	yes	yes	yes
			<i>Actin</i>	yes	yes	yes
		5	ARV7	yes	yes	yes
			<i>K19</i>	yes	yes	yes
			<i>Actin</i>	yes	yes	yes

All HD samples measured ($n = 3$) were ARV7 and K19 negative (Table 1). PC3 samples were negative for ARV7 and positive for K19, confirming the specificity of the established assay. ARV7 and keratin 19 were still detectable down to 5 ARV7⁺ 22RV1 cells using our protocol ($n = 3$), demonstrating high sensitivity (Table 1).

3.4. Assessment of Sample Storage Parameters

mRNA instability represents a common issue for RNA analysis. Sample processing time frames and optimal blood collection tubes therefore need to be carefully assessed to allow for reliable mRNA detection. As cells are not fixed in EDTA blood tubes, which is essential for subsequent RNA isolation, potential CTCs could deteriorate over time. This is especially crucial when calculating time frames for shipment of clinical samples. EDTA blood spiked with cell lines was left at room temperature (RT) for 24 h (Table 2) and 48 h (Table 3), respectively, to test processing windows. Following the qPCR run, generated products were applied to a gel electrophoresis allowing final confirmation of gene expression status (data not shown).

Table 2. Validation of protocol specificity and sensitivity after 24 h. Influence of sample storage on ARV7 detection limits and assay robustness. ARV7 status is highlighted as “+” for positive and “−” for negative samples. Detection of gene expression was confirmed when at least 2/3 triplicates were positive in qPCR analysis. N represents the number of repetitions performed per experimental setting. The ratio is defined as the frequency at which any specific gene was detected out of the N repetitions. N/D signifies no gene expression or gene expression above the set threshold of 35 cycles.

Cell Line	ARV7 Status	Cell Amount	Target	Detection	N	Ratio [detection/N]
HD	−	0	ARV7	N/D	3	3/3
			K19	N/D		
			Actin	yes		
22RV1	+	10	ARV7	yes	1	1/1
			K19	yes		
			Actin	yes		
		5	ARV7	yes	2	2/2
			K19	yes		
			Actin	yes		
		3	ARV7	yes	4	1/4
			K19	yes		3/4
			Actin	yes		4/4
		1	ARV7	yes	3	1/3
			K19	yes		2/3
			Actin	yes		3/3
VCaP	+	10	ARV7	yes	2	2/2
			K19	yes		
			Actin	yes		
		5	ARV7	yes	1	1/1
			K19	N/D		
			Actin	yes		

After 24 h of sample storage at RT, 5 ARV7⁺ cells were still reliably detected using the assay (Table 2). This was confirmed on two ARV7⁺ cell lines (22Rv1 and VCaP). Additionally, as low as 3 and down to 1 ARV7⁺ cells were detectable (Table 2). With these low cell counts, detection frequency is more variable as cell enrichment from whole blood and extremely careful sample handling play crucial roles. Still, correct detection down to a single ARV7⁺ cell is possible. After 48 h, detection of ARV7 and K19 transcripts is subject to even higher fluctuation and increased cell counts would be needed to robustly detect transcripts of interest from these samples (Table 3). The specificity of our assay was

demonstrated as no signals for *ARV7* or *K19* were seen in blood samples from healthy individuals in EDTA blood tested for 24h (3/3) as well as 48 h (3/3) of sample storage (Tables 2 and 3).

Blood tube types vary and some may be more suitable for our assay than others. Therefore, we additionally tested the performance of AdnaCollect blood collection tubes (Qiagen, Hilden, Germany), designed for mRNA characterization by the AdnaTest Prostate Cancer (Qiagen, Hilden, Germany) with our assay. This tube has been used for PCR-based detection of RNA transcripts from whole blood and could therefore provide an alternative to EDTA, potentially prolonging the sample processing window. Again, different cell counts were spiked into HD blood, this time in AdnaCollect blood collection tubes, and processed after 48 h of storage with our protocol. In our hands, these tubes were able to detect *ARV7* in spiked samples, down to 5 *ARV7*⁺ cells (Table 3). However, as *ARV7* and *K19* signals were seen in all three tested HD samples (Table 3) indicating low specificity, the use of this blood tube type was not further continued.

Table 3. Influence of sample tubes and sample storage times on *ARV7* detection limits and assay specificity. *ARV7* status is highlighted as “+” for positive and “−” for negative samples. Detection of gene expression was confirmed when at least 2/3 triplicates were positive in qPCR analysis. N represents the number of repetitions performed per experimental setting. The ratio is defined as the frequency at which any specific gene was detected out of the N repetitions. N/D signifies no gene expression or gene expression above the set threshold of 35 cycles.

Tube	Cell Line	ARV7 Status	Cell Amount	Target	Detection	N	Ratio [detection/N]
EDTA	HD	−	0	<i>ARV7</i>	N/D	3	3/3
				<i>K19</i>	N/D		
				<i>Actin</i>	yes		
	22RV1	+	10	<i>ARV7</i>	N/D	1	1/1
				<i>K19</i>	yes		
				<i>Actin</i>	yes		
Adnagen	HD	−	0	<i>ARV7</i>	yes	3	1/3
				<i>K19</i>	yes		2/3
				<i>Actin</i>	yes		3/3
	22RV1	+	10	<i>ARV7</i>	N/D	1	1/1
				<i>K19</i>	N/D		
				<i>Actin</i>	yes		
	22RV1	+	5	<i>ARV7</i>	yes	3	3/3
				<i>K19</i>	yes		1/3
				<i>Actin</i>	yes		3/3

Our protocol ensures specific detection of tumor cell transcripts in 7.5 mL of blood down to a single cell level even after 24 h of sample storage (Table 2). Conclusively, a sample preparation window of 24 h was determined for the evaluation of clinical samples taken into EDTA blood to allow for sample shipment while ensuring robust detection of *ARV7* from CTCs.

3.5. Clinical Feasibility of the Complete *ARV7* Detection Workflow

The clinical feasibility of our assay was demonstrated by analyzing blood samples of 26 metastatic prostate cancer (mPCa) patients. Detailed clinical patient data is listed in Table S1. qPCR based *ARV7* analysis was performed within 24 h of sample collection from 7.5 ml of EDTA blood for all 26 patients. Parallel blood draws to assess CTC counts via CellSearch[®] were collected and processed for 23/26 patients. AR-FL staining in the fourth fluorescent channel was available for 12/23 patient samples processed via CellSearch[®] (Table 4).

Table 4. Correlation of qPCR results, AR-FL detection and CTC enumeration via CellSearch for 26 mPCa patients analyzed. Detection of a gene was confirmed when at least 2/3 triplicates were positive in qPCR analysis. N/D signifies no gene expression or gene expression above the set threshold of 35 cycles. CTC enumeration via CellSearch® was not conducted for the first three patient samples, indicated by a bar in the respective table column (-). This also applies to 14 samples collected regarding AR occurrence. The number of CTCs with detectable AR-FL expression is indicated in brackets.

Sample	CellSearch			qPCR		
	CTC Count	AR (nucl.)	AR (cytopl.)	ARV7	K19	Actin
UKE-1	-	-	-	yes	yes	yes
UKE-2	-	-	-	N/D	N/D	yes
UKE-3	-	-	-	N/D	N/D	yes
UKE-4	0	-	-	N/D	N/D	yes
UKE-5	0	-	-	N/D	N/D	yes
UKE-6	0	-	-	N/D	N/D	yes
UKE-7	0	0	0	N/D	N/D	yes
UKE-8	1	0	yes (1)	N/D	N/D	yes
UKE-9	1	yes (1)	0	N/D	N/D	yes
UKE-10	1	0	0	N/D	yes	yes
UKE-11	1	0	yes (1)	N/D	yes	yes
UKE-12	1	-	-	yes	yes	yes
UKE-13	1	0	0	yes	yes	yes
UKE-14	2	yes (1)	yes (1)	N/D	yes	yes
UKE-15	6	0	0	N/D	N/D	yes
UKE-16	6	-	-	N/D	N/D	yes
UKE-17	8	yes (3)	yes (4)	yes	yes	yes
UKE-18	9	0	yes (9)	yes	yes	yes
UKE-19	11	0	yes (11)	yes	yes	yes
UKE-20	11	0	yes (11)	yes	yes	yes
UKE-21	14	-	-	N/D	yes	yes
UKE-22	16	-	-	yes	yes	yes
UKE-23	22	-	-	yes	N/D	yes
UKE-24	80	-	-	yes	yes	yes
UKE-25	156	-	-	yes	yes	yes
UKE-26	398	-	-	yes	yes	yes

Of the patient samples analyzed via CellSearch® 86.2% (19/23) were found to have ≥ 1 CTC in 7.5 mL of blood. In 52.2% (12/23) of patients ≥ 5 CTCs were detected in 7.5 ml of whole blood, reaching the clinically prognostic cut-off value for worse overall survival for metastatic mPCa patients [8]. The median of detected CTCs for our cohort is 6 (range: 0–398 CTCs) and the average is 32 CTCs/7.5 mL of blood. ARV7 mRNA was detected in 46.2% (12/26) of mPCa patients, K19 was detected in 57.7% (15/26) of samples and Actin was detected in all samples (26/26), indicating effective cDNA transcription. Four measured patients were negative for the androgen receptor splice variant and positive for K19 (e.g., samples UKE-10 and UKE-11). Additionally, one patient was positive for ARV7 expression and negative for K19 (UKE-23). No ARV7 or K19 gene expression was found in samples classified as CTC negative by the CellSearch® system. Evaluation of the first 26 clinical samples resulted in 42.3% of ARV7⁺/K19⁺ of all cases (11/26) and 52.6% of ARV7⁺/K19⁺ cases (10/19) with ≥ 1 detectable CTC. Representative CellSearch® images of AR-FL staining are shown in Figure 5.

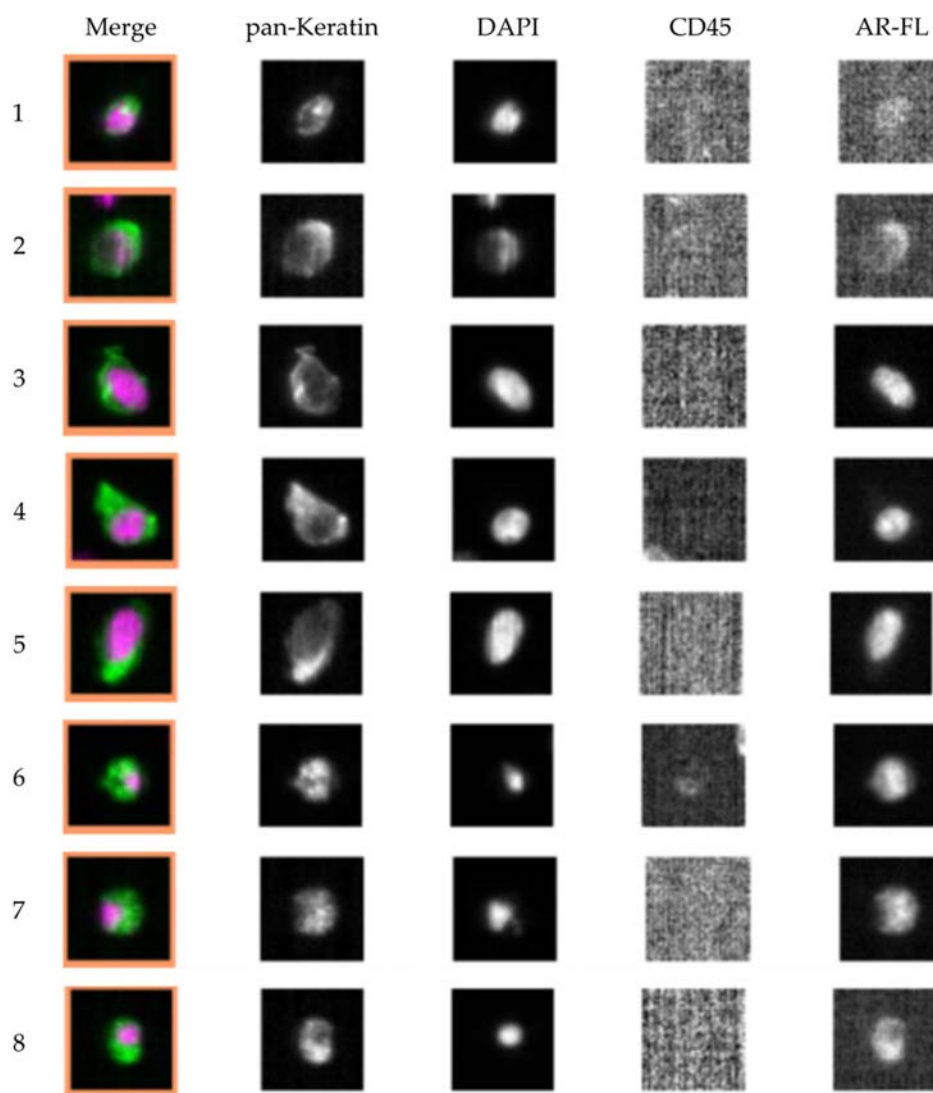


Figure 5. Representative CellSearch® images of CTCs and AR-FL staining from a single prostate cancer patient case. This patient had detectable AR-FL negative (1), weakly positive (2), nuclear AR-FL positive (3–5) and cytoplasmatically AR-FL positive (6–8) CTCs.

Only three of the 12 cases in which AR-FL protein staining was assessed in the CellSearch® (UKE-9, UKE-14, UKE-17) had detectable nuclear AR-FL protein levels (Table 4). Two of these three patients (UKE-14, UKE-17) had a mixed CTC population of nuclear and cytoplasmic AR-FL⁺ CTCs. Of these three patients, two were ARV7 negative with our assay (UKE-9, UKE-14). Additional five patients showed cytoplasmic AR-FL protein expression, more than half of these patients were ARV7 positive (3/5).

For the majority of patient samples tested (88.4% or 23/26), the CTC count as measured by the CellSearch® system was in accordance to *K19* detection in parallel samples (Table 4). Detection of ARV7 was possible in 2/6 patients with only a single CTC detected in the patient's blood (UKE-12, UKE-13) confirming the assays sensitivity (Table 4). *K19* was detected in 4/6 patients with only a single CTC indicating careful and effective sample handling (Table 4).

4. Discussion

The CellSearch[®] Profile technology allows a reliable, standardized, and automated enrichment of EpCAM-positive cancer cells. ARV7 expression in CTCs of prostate cancer patients has been linked to resistance toward AR-targeted therapy, in particular enzalutamide and abiraterone [20,25]. Our novel approach ensures specific detection of ARV7 transcripts in CTCs isolated by the CellSearch[®] system down to the single cell level. The specificity of our assay was indicated as no signals for ARV7 or K19 were seen in 9 blood samples from healthy, male individuals (Tables 1–3). Our protocol ensures specific detection of tumor cell transcripts in 7.5 mL of blood even after 24 h of sample storage (Table 2). Robust ARV7 and K19 detection is feasible in as low as 5 ARV7⁺/K19⁺ cells (Table 2). Transcript expression below 5 cells, even down to 1 ARV7⁺/K19⁺ cell, was possible (Table 2). The clinical feasibility of our assay and its high sensitivity (down to a single CTC) was demonstrated in a cohort of 26 mPca patients (Table 4).

Antonarakis et al. linked ARV7 mRNA expression on CTCs of mCRPC patients receiving enzalutamide and/or abiraterone therapy to lower PSA response rates, as well as shorter progression free and overall survival [20]. Following this initial study, conducted with a combination of bead-based CTC enrichment and subsequent qPCR multiplexing, the group confirmed their finding in a larger cohort of 202 CRPC patients [23]. In their study, CTC[−] patients were found to have the best outcome (judged by best PSA-response, PSA progression-free survival, progression-free survival, and overall survival), followed by CTC⁺/ARV7[−] and finally CTC⁺/ARV7⁺ patients [23]. Additionally, it was demonstrated that ARV7 status can change in the course of hormone therapy [25,28,29] and that within one patient ARV7 status on CTCs can be heterogeneous [41].

The CellSearch[®] system enables validated and automated enrichment of EpCAM-positive cancer cells [8,42–45]. Ideally, adding a specific and sensitive anti-ARV7 antibody to the fourth fluorescent channel of the CellSearch[®] device would therefore represent a valuable alternative to allow parallel CTC enumeration and the assessment of ARV7 status for each respective CTC. Unfortunately, detection of ARV7 protein using the CellSearch[®] technology was dramatically hampered by lacking specificity of most existing ARV7 antibodies (Figure 1, Figure S1). Recently, a novel commercially available antibody has been tested and validated for immunohistochemistry on primary tumor tissue, showing specific ARV7 staining results [32]. Whether this antibody might represent a promising novel candidate for immunocytochemical analysis and combination with CellSearch[®] needs to be investigated in future studies. However, so far most sources of CTC-related ARV7 information stems from RNA measurements.

The meaningful clinical impact of ARV7 expression of CTCs [20,46] has led to the development of a multitude of different assays targeting ARV7 protein [25] or ARV7 transcripts [30,31,47,48]. Primarily the developed methods are based on the analysis of pooled lysate of an enriched CTC fraction [26,30,48], only few perform whole blood gene expression analysis [47]. CTC are enriched by bead-based approaches [20,48], or the CellSearch[®] Profile kit and analyzed by subsequent qPCR or RNA-seq [26,30]. While these approaches effectively assess ARV7 status, they give no additional information on the abundance of CTCs in a patient at the time point of blood draw. This could, however, prove to be valuable information allowing more precise interpretation of the qualitative ARV7⁺ or ARV7[−] status of a patient. Without CTC count, an ARV7[−] status may refer to no available CTCs within the blood draw or to high amounts of ARV7[−] CTCs, respectively. The clinical information to be gained from both results is, however, very different, as no CTCs indicate good and ≥5 CTCs indicate poor outcome for the patient [8]. Multiplexing of additional genes such as prostate specific antigen (PSA) or prostate specific membrane antigen (PSMA), as well as epithelial genes is commonly used as a means of circumventing this issue and attempting to detect ARV7[−] CTCs [20,26,49]. While this is a feasible approach, it is limited by heterogeneous expression of these markers [31,41,49–51] and the required pre-amplification step can introduce bias.

Using our novel approach (Figure 4) information on both CTC count, AR-FL and ARV7 status is collected. One could argue that the amount of CTCs present in the blood tube destined for ARV7 assessment is also not directly assessed by our assay. However, studies have shown that CTC counts determined with the CellSearch® technology do not significantly fluctuate depending on circadian rhythm or serial blood draws [52,53], thereby indicating that stochastically, similar to equal CTC amounts would be expected in two sequential blood draws from the same patient at the same time (as is necessitated by our protocol). The importance of integrated CTC enumeration becomes apparent when looking at clinical cases such as UKE-23 (Table 4). While this patient had clearly detectable ARV7 transcripts, he did not show K19 positivity in our assay. Without the additional information of 22 CTCs being detected via CellSearch® analysis, interpretation of the qPCR results would have been impaired. This case also highlights the inert limitation of qPCR multiplexing, which lies in the before mentioned heterogeneity of gene and protein expression in CTCs [41,50,51]. In addition, CTC detection via the CellSearch® allows for morphological assessment of the CTCs in circulation and in our case, parallel characterization of AR-FL protein as well as its cellular location. Both represent important factors in resistance to androgen deprivation therapy [54]. The localization of the full length AR within the cell has been shown to be associated with disease progression on novel hormone therapies (e.g., enzalutamide and abiraterone) [55]. Therefore, it was critical for our assay to be able to distinguish both cytoplasmic and nuclear fractions of AR to support differentiation between “AR-on” and “AR-off” patients [54]. Apart from the AR-FL targeting antibody (by Janssen Diagnostics) used in this study, other well-established alternative antibodies have been published for AR-FL detection in the fourth channel of the CellSearch® [55].

To our knowledge, only two assays have been developed allowing parallel CTC enumeration and ARV7 protein [24,25] or transcript detection [31] on the same cell so far. El-Heliebi et al. isolated CTCs via the CellSearch® Profile kit or the size-dependent Parsortix™ platform (ANGLE plc, Guildford, UK) [56] and subsequently characterized them for ARV7, AR-FL, and PSA expression via in situ padlock probe technology [31]. This approach allows for absolute transcript quantification while keeping cell morphology intact and thereby enabling tumor cell enumeration [31]. In regards to CellSearch® Profile kit pre-enrichment, a single patient with high CTC load was included in this study to demonstrate general feasibility of the approach [31]. Additional technical validation will therefore be required to ensure sufficient sensitivity and specificity of this method for future clinical application.

The ARV7 assay most advanced in regards to clinical validation is the EPICs approach [24,25]. Here, the nuclear cell fraction is placed on slides, stained via ICC and automatically screened and evaluated. The assay focusses on nuclear ARV7 protein expression using the same antibody clone EPR15656 (Abcam) that we tested in our present study. While the EPICS approach allows for parallel CTC enumeration and ARV7 protein assessment, it requires sample shipment to a centralized lab in the US, a costs intensive approach when conducting larger clinical studies or when shipping patient samples for routine testing. A nuclear ARV7 staining has been postulated to be relevant to predict therapy outcome of AR-targeted therapies as well as taxanes in a cohort of 161 mCRPC patients, leading to a favorable coverage recommendation and certification of the approach in the state of California (USA) [57,58]. However, in our hands, the EPR15656 antibody did not result in specific nuclear staining signals for tested cancer cell line cells on chamber slides or cytopins (Figure 1, Figure S1).

While the ARV7 detection assay established in this study is highly specific and sensitive, some limitations require mentioning. The main limitation is the fact that our assay does not allow for simultaneous morphological and molecular ARV7 characterization of each single CTC. However, this is somewhat compensated by the use of a clinically validated CTC enrichment method, adding weight to the clinical relevance of the CTCs analyzed. Additionally, ARV7 and K19 transcript detection cannot be guaranteed down to a single CTC level in all patient samples. Nevertheless, we can secure determination of ARV7 status from ≥ 5 CTCs which is the prognostic cut-off value for patients with metastatic prostate cancer. Due to the high sensitivity and specificity of our ARV7 detection assay and the parallel nature of the CellSearch® CTC-enumeration, K19 detection is not a mandatory prerequisite

for robust ARV7 assessment and result interpretation. However, we believe K19 adds further valuable information in positive cases and represents an additional confirmation of successful CTC analysis.

Taken together, the use of a FDA-cleared enrichment technology, high assay sensitivity and specificity, a shipment window of 24 h and comparably low necessity of elaborate additional laboratory equipment (standard qPCR cycler) corroborate the value of our established method. Inclusion into prospective clinical trials will be now necessary to demonstrate clinical validity and utility. Furthermore, additional age-matched healthy donors and other control cohorts (e.g., prostatitis patients) should be included into future studies to further corroborate assay specificity. Head-to-head comparison with other ARV7/CTC technologies is desirable to assess to which extent different assays are redundant or complementary.

5. Conclusions

The novel workflow developed in this study allows for a semi-automated enrichment of CTCs followed by a qPCR assay measuring the ARV7 status of CTCs. This approach can now be integrated into future clinical trials assessing treatment responses to antiandrogen therapies in prostate cancer patients.

Supplementary Materials: The following are available online at <http://www.mdpi.com/2073-4409/8/9/1067/s1>. Figure S1: Assessment of ARV7 antibody performance on selected prostate cancer cell lines via Western Blot and immunocytochemical (ICC) staining; Table S1: Clinical data of 26 mPCa patients.

Author Contributions: C.H. collected and primarily analyzed data, developed the methodology, visualized the results and wrote the manuscript draft. T.M.G. conceptualized and supervised the project and contributed to the method establishment. S.R. and M.M. collected and analyzed data. M.M. additionally participated in writing of the manuscript. T.S., G.v.A., F.K. and S.P. contributed clinical as well as healthy donor samples and clinical data. They furthermore aided in the clinical interpretation of the results. C.A.-P. and K.P. participated in writing of the manuscript and supported data analysis. K.P. furthermore supervised and conceptualized the project and acquired funding. All authors contributed to the editing and writing of the manuscript. Conceptualization, T.M.G., C.A.-P., and K.P.; Funding acquisition, K.P.; Investigation, C.H., S.R., M.M., T.S., G.v.A., F.K. and S.P.; Methodology, C.H. and T.M.G.; Supervision, T.M.G.; Visualization, C.H.; Writing—original draft, C.H. and K.P.; Writing—review and editing, C.H., T.M.G., S.R., M.M., T.S., G.v.A., F.K., S.P., C.A.-P., and K.P.

Funding: Klaus Pantel and Catherine Alix-Panabières received funding from the European TRANSCAN PROLIPSY grant (Nr. 01KT1810).

Acknowledgments: The authors acknowledge Cornelia Coith, Antje Andreas and Oliver Mauermann from UKE Hamburg for technical support.

Conflicts of Interest: Klaus Pantel has ongoing patent applications related to circulating tumour cells. Klaus Pantel has received honoraria from Agena, Novartis, Roche, and Sanofi and research funding from European Federation of Pharmaceutical Industries and Associations (EFPIA) partners (Angle, Menarini and Servier) of the CANCER-ID programm (www.cancer-id.eu) of the European Union–EFPIA Innovative Medicines Initiative. CAP has received honoraria from Janssen and grant support from Menarini. The remaining authors declare no conflict of interest.

References

1. World Cancer Research Fund International, American Institute for Cancer Research. Prostate Cancer. 2018. Available online: <https://www.wcrf.org/dietandcancer/prostate-cancer> (accessed on 30 July 2019).
2. Ladjevardi, S.; Auer, G.; Castro, J.; Ericsson, C.; Zetterberg, A.; Häggman, M.; Wiksell, H.; Jorulf, H. Prostate Biopsy Sampling Causes Hematogenous Dissemination of Epithelial Cellular Material. *Dis. Markers* **2014**, *2014*, 1–6. [CrossRef] [PubMed]
3. Alix-Panabières, C.; Pantel, K. Clinical Applications of Circulating Tumor Cells and Circulating Tumor DNA as Liquid Biopsy. *Cancer Discov.* **2016**, *6*, 479–491. [CrossRef] [PubMed]
4. Pantel, K.; Speicher, M.R. The biology of circulating tumor cells. *Oncogene* **2016**, *35*, 1216–1224. [CrossRef] [PubMed]
5. Bardelli, A.; Pantel, K. Liquid Biopsies, What We Do Not Know (Yet). *Cancer Cell* **2017**, *31*, 172–179. [CrossRef] [PubMed]
6. Alix-Panabières, C.; Pantel, K. Circulating tumor cells: Liquid biopsy of cancer. *Clin. Chem.* **2013**, *59*, 110–118. [CrossRef] [PubMed]

7. Hille, C.; Pantel, K. Circulating tumour cells in prostate cancer. *Nat. Rev. Urol.* **2018**, *15*, 265–266. [[CrossRef](#)] [[PubMed](#)]
8. De Bono, J.S.; Scher, H.I.; Montgomery, R.B.; Parker, C.; Miller, M.C.; Tissing, H.; Doyle, G.V.; Terstappen, L.W.W.M.; Pienta, K.J.; Raghavan, D. Circulating tumor cells predict survival benefit from treatment in metastatic castration-resistant prostate cancer. *Clin. Cancer Res.* **2008**, *14*, 6302–6309. [[CrossRef](#)] [[PubMed](#)]
9. Scher, H.I.; Jia, X.Y.; de Bono, J.S.; Fleisher, M.; Pienta, K.J.; Raghavan, D.; Heller, G. Circulating tumour cells as prognostic markers in progressive, castration-resistant prostate cancer: A reanalysis of IMMC38 trial data. *Lancet. Oncol.* **2009**, *10*, 233–239. [[CrossRef](#)]
10. Scher, H.I.; Heller, G.; Molina, A.; Attard, G.; Danila, D.C.; Jia, X.; Peng, W.; Sandhu, S.K.; Olmos, D.; Riisnaes, R.; et al. Circulating Tumor Cell Biomarker Panel As an Individual-Level Surrogate for Survival in Metastatic Castration-Resistant Prostate Cancer. *J. Clin. Oncol.* **2015**, *33*, 1348–1355. [[CrossRef](#)]
11. Heller, G.; Fizazi, K.; McCormack, R.; Molina, A.; MacLean, D.; Webb, I.J.; Saad, F.; de Bono, J.S.; Scher, H.I. The Added Value of Circulating Tumor Cell Enumeration to Standard Markers in Assessing Prognosis in a Metastatic Castration-Resistant Prostate Cancer Population. *Clin. Cancer Res.* **2017**, *23*, 1967–1973. [[CrossRef](#)]
12. Miller, M.C.; Doyle, G.V.; Terstappen, L.W. Significance of Circulating Tumor Cells Detected by the CellSearch System in Patients with Metastatic Breast Colorectal and Prostate Cancer. *J. Oncol.* **2010**, *2010*, 617421. [[CrossRef](#)] [[PubMed](#)]
13. Goodman, O.B.; Symanowski, J.T.; Loudyi, A.; Fink, L.M.; Ward, D.C.; Vogelzang, N.J. Circulating Tumor Cells as a Predictive Biomarker in Patients With Hormone-sensitive Prostate Cancer. *Clin. Genitourin. Cancer* **2011**, *9*, 31–38. [[CrossRef](#)] [[PubMed](#)]
14. Danila, D.C.; Fleisher, M.; Scher, H.I. Circulating tumor cells as biomarkers in prostate cancer. *Clin. Cancer Res.* **2011**, *17*, 3903–3912. [[CrossRef](#)] [[PubMed](#)]
15. Gorges, T.M.; Pantel, K. Circulating tumor cells as therapy-related biomarkers in cancer patients. *Cancer Immunol. Immunother.* **2013**, *62*, 931–939. [[CrossRef](#)] [[PubMed](#)]
16. Singhal, U.; Wang, Y.; Henderson, J.; Niknafs, Y.S.; Qiao, Y.; Gursky, A.; Zaslavsky, A.; Chung, J.-S.; Smith, D.C.; Karnes, R.J.; et al. Multigene Profiling of CTCs in mCRPC Identifies a Clinically Relevant Prognostic Signature. *Mol. Cancer Res.* **2018**, *16*, 643–654. [[CrossRef](#)]
17. Pantel, K.; Hille, C.; Scher, H.I. Circulating Tumor Cells in Prostate Cancer: From Discovery to Clinical Utility. *Clin. Chem.* **2019**, *65*, 87–99. [[CrossRef](#)] [[PubMed](#)]
18. Luo, J.; Attard, G.; Balk, S.P.; Bevan, C.; Burnstein, K.; Cato, L.; Cherkasov, A.; De Bono, J.S.; Dong, Y.; Gao, A.C.; et al. Role of Androgen Receptor Variants in Prostate Cancer: Report from the 2017 Mission Androgen Receptor Variants Meeting. *Eur. Urol.* **2018**, *73*, 715–723. [[CrossRef](#)]
19. Antonarakis, E.S.; Armstrong, A.J.; Dehm, S.M.; Luo, J. Androgen receptor variant-driven prostate cancer: Clinical implications and therapeutic targeting. *Prostate Cancer Prostatic Dis.* **2016**, *19*, 231–241. [[CrossRef](#)]
20. Antonarakis, E.S.; Lu, C.; Wang, H.; Luber, B.; Nakazawa, M.; Roeser, J.C.; Chen, Y.; Mohammad, T.A.; Chen, Y.; Fedor, H.L.; et al. AR-V7 and Resistance to Enzalutamide and Abiraterone in Prostate Cancer. *New Engl. J. Med.* **2014**, *371*, 1028–1038. [[CrossRef](#)]
21. Antonarakis, E.S.; Luo, J. Blood Based Detection of Androgen Receptor Splice Variants in Patients with Advanced Prostate Cancer. *J. Urol.* **2016**, *196*, 1606–1607. [[CrossRef](#)]
22. Lokhandwala, P.M.; Riel, S.L.; Haley, L.; Lu, C.; Chen, Y.; Silberstein, J.; Zhu, Y.; Zheng, G.; Lin, M.-T.; Gocke, C.D.; et al. Analytical Validation of Androgen Receptor Splice Variant 7 Detection in a Clinical Laboratory Improvement Amendments (CLIA) Laboratory Setting. *J. Mol. Diagn.* **2017**, *19*, 115–125. [[CrossRef](#)] [[PubMed](#)]
23. Antonarakis, E.S.; Lu, C.; Luber, B.; Wang, H.; Chen, Y.; Zhu, Y.; Silberstein, J.L.; Taylor, M.N.; Maughan, B.L.; Denmeade, S.R.; et al. Clinical Significance of Androgen Receptor Splice Variant-7 mRNA Detection in Circulating Tumor Cells of Men With Metastatic Castration-Resistant Prostate Cancer Treated With First- and Second-Line Abiraterone and Enzalutamide. *J. Clin. Oncol.* **2017**, *35*, 2149–2156. [[CrossRef](#)]
24. Scher, H.I.; Graf, R.P.; Schreiber, N.A.; Jayaram, A.; Winkquist, E.; McLaughlin, B.; Lu, D.; Fleisher, M.; Orr, S.; Lowes, L.; et al. Assessment of the Validity of Nuclear-Localized Androgen Receptor Splice Variant 7 in Circulating Tumor Cells as a Predictive Biomarker for Castration-Resistant Prostate Cancer. *JAMA Oncol.* **2018**, *4*, 1179–1186. [[CrossRef](#)]

25. Scher, H.I.; Lu, D.; Schreiber, N.A.; Louw, J.; Graf, R.P.; Vargas, H.A.; Johnson, A.; Jendrisak, A.; Bambury, R.; Danila, D.; et al. Association of AR-V7 on Circulating Tumor Cells as a Treatment-Specific Biomarker With Outcomes and Survival in Castration-Resistant Prostate Cancer. *JAMA Oncol.* **2016**, *2*, 1441–1449. [[CrossRef](#)] [[PubMed](#)]
26. Onstenk, W.; Sieuwerts, A.M.; Kraan, J.; Van, M.; Nieuweboer, A.J.; Mathijssen, R.H.; Hamberg, P.; Meulenbeld, H.J.; De Laere, B.; Dirix, L.Y.; et al. Efficacy of Cabazitaxel in Castration-resistant Prostate Cancer Is Independent of the Presence of AR-V7 in Circulating Tumor Cells. *Eur. Urol.* **2015**, *68*, 939–945. [[CrossRef](#)] [[PubMed](#)]
27. Antonarakis, E.S.; Lu, C.; Luber, B.; Wang, H.; Chen, Y.; Nakazawa, M.; Nadal, R.; Paller, C.J.; Denmeade, S.R.; Carducci, M.A.; et al. Androgen Receptor Splice Variant 7 and Efficacy of Taxane Chemotherapy in Patients With Metastatic Castration-Resistant Prostate Cancer. *JAMA Oncol.* **2015**, *1*, 582–591. [[CrossRef](#)] [[PubMed](#)]
28. Bernemann, C.; Schnoeller, T.J.; Luedeke, M.; Steinestel, K.; Boegemann, M.; Schrader, A.J.; Steinestel, J. Expression of AR-V7 in Circulating Tumour Cells Does Not Preclude Response to Next Generation Androgen Deprivation Therapy in Patients with Castration Resistant Prostate Cancer. *Eur. Urol.* **2017**, *71*, 1–3. [[CrossRef](#)]
29. Nakazawa, M.; Lu, C.; Chen, Y.; Paller, C.J.; Carducci, M.A.; Eisenberger, M.A.; Luo, J.; Antonarakis, E.S. Serial blood-based analysis of AR-V7 in men with advanced prostate cancer. *Ann. Oncol.* **2015**, *26*, 1859–1865. [[CrossRef](#)]
30. De Laere, B.; Van Dam, P.-J.; Whittington, T.; Mayrhofer, M.; Diaz, E.H.; Eynden, G.V.D.; Vandebroek, J.; Del-Favero, J.; Van Laere, S.; Dirix, L.; et al. Comprehensive Profiling of the Androgen Receptor in Liquid Biopsies from Castration-resistant Prostate Cancer Reveals Novel Intra-AR Structural Variation and Splice Variant Expression Patterns. *Eur. Urol.* **2017**, *72*, 192–200. [[CrossRef](#)]
31. El-Heliebi, A.; Attard, G.; Balk, S.P.; Bevan, C.; Burnstein, K.; Cato, L.; Cherkasov, A.; De Bono, J.S.; Dong, Y.; Gao, A.C.; et al. In Situ Detection and Quantification of AR-V7, AR-FL, PSA, and KRAS Point Mutations in Circulating Tumor Cells. *Clin. Chem.* **2018**, *64*. [[CrossRef](#)]
32. Sharp, A.; Welti, J.C.; Lambros, M.B.; Dolling, D.; Rodrigues, D.N.; Pope, L.; Aversa, C.; Figueiredo, I.; Fraser, J.; Ahmad, Z.; et al. Clinical Utility of Circulating Tumour Cell Androgen Receptor Splice Variant-7 Status in Metastatic Castration-resistant Prostate Cancer. *Eur. Urol.* **2019**. [[CrossRef](#)]
33. Riethdorf, S.; O’Flaherty, L.; Hille, C.; Pantel, K. Clinical applications of the CellSearch platform in cancer patients. *Adv. Drug Deliv. Rev.* **2018**, *125*, 102–121. [[CrossRef](#)] [[PubMed](#)]
34. Riethdorf, S.; Fritsche, H.; Müller, V.; Rau, T.; Schindlbeck, C.; Rack, B.; Janni, W.; Coith, C.; Beck, K.; Jänicke, F.; et al. Detection of Circulating Tumor Cells in Peripheral Blood of Patients with Metastatic Breast Cancer: A Validation Study of the CellSearch System. *Clin. Cancer Res.* **2007**, *13*, 920–928. [[CrossRef](#)] [[PubMed](#)]
35. Guo, Z.; Yang, X.; Sun, F.; Jiang, R.; Linn, D.E.; Chen, H.; Chen, H.; Kong, X.; Melamed, J.; Tepper, C.G.; et al. A novel androgen receptor splice variant is up-regulated during prostate cancer progression and promotes androgen depletion-resistant growth. *Cancer Res.* **2009**, *69*, 2305–2313. [[CrossRef](#)] [[PubMed](#)]
36. Liu, L.L.; Xie, N.; Sun, S.; Plymate, S.; Mostaghel, E.; Dong, X. Mechanisms of the androgen receptor splicing in prostate cancer cells. *Oncogene* **2014**, *33*, 3140–3150. [[CrossRef](#)] [[PubMed](#)]
37. Untergasser, A.; Cutcutache, I.; Koressaar, T.; Ye, J.; Faircloth, B.C.; Remm, M.; Rozen, S.G. Primer3—New capabilities and interfaces. *Nucleic Acids Res.* **2012**, *40*, e115. [[CrossRef](#)]
38. Livak, K.J.; Schmittgen, T.D. Analysis of relative gene expression data using real-time quantitative PCR and the 2(-Delta Delta C(T)) Method. *Methods* **2001**, *25*, 402–408. [[CrossRef](#)]
39. Stathopoulou, A.; Angelopoulou, K.; Perraki, M.; Georgoulas, V.; Malamos, N.; Lianidou, E. Quantitative RT-PCR luminometric hybridization assay with an RNA internal standard for cytokeratin-19 mRNA in peripheral blood of patients with breast cancer. *Clin. Biochem.* **2001**, *34*, 651–659. [[CrossRef](#)]
40. Stathopoulou, A.; Gizi, A.; Perraki, M.; Apostolaki, S.; Malamos, N.; Mavroudis, D.; Georgoulas, V.; Lianidou, E.S. Real-time quantification of CK-19 mRNA-positive cells in peripheral blood of breast cancer patients using the lightcycler system. *Clin. Cancer Res.* **2003**, *9*, 5145–5151.
41. Gorges, T.M.; Kuske, A.; Röck, K.; Mauermann, O.; Müller, V.; Peine, S.; Verpoort, K.; Novosadova, V.; Kubista, M.; Riethdorf, S.; et al. Accession of Tumor Heterogeneity by Multiplex Transcriptome Profiling of Single Circulating Tumor Cells. *Clin. Chem.* **2016**, *62*, 1504–1515. [[CrossRef](#)]

42. Cristofanilli, M.; Budd, G.T.; Ellis, M.J.; Stopeck, A.; Matera, J.; Miller, M.C.; Reuben, J.M.; Doyle, G.V.; Allard, W.J.; Terstappen, L.W.; et al. Circulating Tumor Cells, Disease Progression, and Survival in Metastatic Breast Cancer. *New Engl. J. Med.* **2004**, *351*, 781–791. [[CrossRef](#)] [[PubMed](#)]
43. Cohen, S.J.; Punt, C.J.; Iannotti, N.; Saidman, B.H.; Sabbath, K.D.; Gabrail, N.Y.; Picus, J.; Morse, M.; Mitchell, E.; Miller, M.C.; et al. Relationship of Circulating Tumor Cells to Tumor Response, Progression-Free Survival, and Overall Survival in Patients With Metastatic Colorectal Cancer. *J. Clin. Oncol.* **2008**, *26*, 3213–3221. [[CrossRef](#)] [[PubMed](#)]
44. Ligthart, S.T.; Coumans, F.A.W.; Attard, G.; Cassidy, A.M.; De Bono, J.S.; Terstappen, L.W.M.M. Unbiased and Automated Identification of a Circulating Tumour Cell Definition That Associates with Overall Survival. *PLoS ONE* **2011**, *6*, e27419. [[CrossRef](#)] [[PubMed](#)]
45. Scholtens, T.M.; Schreuder, F.; Ligthart, S.T.; Swennenhuis, J.F.; Greve, J.; Terstappen, L.W. Automated identification of circulating tumor cells by image cytometry. *Cytometry A* **2012**, *81A*, 138–148. [[CrossRef](#)] [[PubMed](#)]
46. Markowski, M.C.; Silberstein, J.L.; Eshleman, J.R.; Eisenberger, M.A.; Luo, J.; Antonarakis, E.S. Clinical Utility of CLIA-Grade AR-V7 Testing in Patients With Metastatic Castration-Resistant Prostate Cancer. *JCO Precis. Oncol.* **2017**, 1–9.
47. Todenhöfer, T.; Azad, A.; Stewart, C.; Gao, J.; Eigl, B.J.; Gleave, M.E.; Joshua, A.M.; Black, P.C.; Chi, K.N. AR-V7 Transcripts in Whole Blood RNA of Patients with Metastatic Castration Resistant Prostate Cancer Correlate with Response to Abiraterone Acetate. *J. Urol.* **2017**, *197*, 135–142. [[CrossRef](#)] [[PubMed](#)]
48. Tommasi, S.; Pilato, B.; Carella, C.; Lasorella, A.; Danza, K.; Vallini, I.; De Summa, S.; Naglieri, E. Standardization of CTC AR-V7 PCR assay and evaluation of its role in castration resistant prostate cancer progression. *Prostate* **2018**, *79*, 54–61. [[CrossRef](#)] [[PubMed](#)]
49. Sieuwerts, A.M.; Mostert, B.; Van Der Vlugt-Daane, M.; Kraan, J.; Beaufort, C.M.; Van, M.; Prager, W.J.; De Laere, B.; Beije, N.; Hamberg, P.; et al. An In-Depth Evaluation of the Validity and Logistics Surrounding the Testing of AR-V7 mRNA Expression in Circulating Tumor Cells. *J. Mol. Diagn.* **2018**, *20*, 316–325. [[CrossRef](#)]
50. Gorges, T.M.; Riethdorf, S.; Von Ahsen, O.; Nastały, P.; Röck, K.; Boede, M.; Peine, S.; Kuske, A.; Schmid, E.; Kneip, C.; et al. Heterogeneous PSMA expression on circulating tumor cells—A potential basis for stratification and monitoring of PSMA-directed therapies in prostate cancer. *Oncotarget* **2016**, *7*, 34930–34941. [[CrossRef](#)] [[PubMed](#)]
51. Scher, H.I.; Graf, R.P.; Schreiber, N.A.; McLaughlin, B.; Jendrisak, A.; Wang, Y.; Lee, J.; Greene, S.; Krupa, R.; Lu, D.; et al. Phenotypic Heterogeneity of Circulating Tumor Cells Informs Clinical Decisions between AR Signaling Inhibitors and Taxanes in Metastatic Prostate Cancer. *Cancer Res.* **2017**, *77*, 5687–5698. [[CrossRef](#)]
52. Martín, M.; García-Sáenz, J.A.; Casas, M.L.M.D.L.; Vidaurreta, M.; Puente, J.; Veganzones, S.; Rodríguez-Lajusticia, L.; De La Orden, V.; Oliva, B.; De La Torre, J.-C.; et al. Circulating tumor cells in metastatic breast cancer: timing of blood extraction for analysis. *Anticancer. Res.* **2009**, *29*, 4185–4187. [[PubMed](#)]
53. Tibbe, A.G.J.; Miller, M.C.; Terstappen, L.W.M.M. Statistical considerations for enumeration of circulating tumor cells. *Cytom. Part. A* **2007**, *71*, 154–162. [[CrossRef](#)]
54. Miyamoto, D.T.; Lee, R.J.; Stott, S.L.; Ting, D.T.; Wittner, B.S.; Ulman, M.; Smas, M.E.; Lord, J.B.; Brannigan, B.W.; Trautwein, J.; et al. Androgen receptor signaling in circulating tumor cells as a marker of hormonally responsive prostate cancer. *Cancer Discov.* **2012**, *2*, 995–1003. [[CrossRef](#)] [[PubMed](#)]
55. Crespo, M.; Van Dalum, G.; Ferraldeschi, R.; Zafeiriou, Z.; Sideris, S.; Lorente, D.; Bianchini, D.; Rodrigues, D.N.; Riisnaes, R.; Miranda, S.; et al. Androgen receptor expression in circulating tumour cells from castration-resistant prostate cancer patients treated with novel endocrine agents. *Br. J. Cancer* **2015**, *112*, 1166–1174. [[CrossRef](#)] [[PubMed](#)]
56. Hvichia, G.; Parveen, Z.; Wagner, C.; Janning, M.; Quidde, J.; Stein, A.; Müller, V.; Loges, S.; Neves, R.; Stoecklein, N.; et al. A novel microfluidic platform for size and deformability based separation and the subsequent molecular characterization of viable circulating tumor cells. *Int. J. Cancer* **2016**, *138*, 2894–2904. [[CrossRef](#)]

57. Services, C.f.M.M. 2018. Available online: <https://med.noridianmedicare.com/documents/10546/6990981/MolDX+Circulating+Tumor+Cell+Marker+Assays+LCD/8eaf89f0-9970-455c-b048-ebaeaf42bd7d> (accessed on 30 July 2019).
58. Services C.f.M.M. 2018. Available online: <https://www.cms.gov/medicare-coverage-database/details/lcd-details.aspx?LCDId=37914&ver=2&Cntctr=All&UpdatePeriod=796&bc=AQAAEAAAAAAAAA&> (accessed on 30 July 2019).



© 2019 by the authors. Licensee MDPI, Basel, Switzerland. This article is an open access article distributed under the terms and conditions of the Creative Commons Attribution (CC BY) license (<http://creativecommons.org/licenses/by/4.0/>).

4. Discussion

Studying CTCs has provided a significant contribution to our understanding of various aspects of tumor biology. These include fundamental biological processes such as tumor invasion, metastasis tropism, and intra-tumor heterogeneity (1.2). CTCs have furthermore been applied as biomarkers for clinical patient management, providing information on patient prognosis, monitoring disease recurrence, and functioning as predictive markers (1.2.5). The results of this thesis have touched on multiple components of this broad potential in CTC research, beginning with the improvement of CTC enrichment, a crucial step in allowing for preferably un-biased and sound characterization of these extremely rare cells.

4.1. Improving the Enrichment of CTCs

The enrichment and detection of CTCs from the cellular background of a whole blood sample represents a crucial prerequisite for a more detailed subsequent biological characterization of these rare cells and requires highly sensitive and specific methods and work flows. The low concentration of CTCs in peripheral blood poses a challenge for any analytical system, thus rendering the identification and optimization of all additional factors potentially hindering ideal outcome extremely important. The success of this crucial initial step is highly dependent on technological factors including pre-analytical variables and the performance of the chosen enrichment technology. It is also determined by biological (e.g. specific marker expression) and clinical aspects (e.g. time point of blood draw in relation to administered therapy). Combined, these factors result in a mere 1-10 CTCs being identified on average in a 10 ml blood draw for most cancer patients [109]. Therefore to maximize the biological understanding to be gained from CTCs, it is paramount to increase the amount of tumor cells available for analysis as well as their morphological intactness, thus ensuring they become applicable to a broad spectrum of downstream assays. Within this thesis, significant steps have been taken in this direction [167-169].

4.1.1. Impact of Pre-Analytical and Analytical Variables on CTC Enumeration

The extent to which pre-analytical and analytical variables influence CTC enrichment is often overlooked. Pre-analytical procedures encompass all steps leading up to the initiation of CTC processing via a certain enrichment platform. They include the specimen collection by the physician, the choice of blood collection tubes, sample handling, and sample storage. These steps significantly impact whether the collection of blood samples of consistently high quality and thereby the analysis of unbiased analyte profiles (e.g. CTCs) is possible. Testing these pre-analytical parameters in combination with analytical variables for a specific enrichment assay is complex, requiring time as well as resources. It is therefore often bypassed or minimized during the development and initial use of novel enrichment technologies. The label-independent Parsortix® system has been in use for CTC capture in research labs for multiple years and has demonstrated significant capabilities across multiple tumor entities [170-173]. The size-based nature of this system potentially enables the enrichment of various CTC subpopulations, independent of specific marker expression, as well as viable CTCs and CTC clusters [139, 170]. Depending on the research question at hand, this can represent a distinct advantage to the “gold-standard” (EpCAM-based) CellSearch® system. The Parsortix® system also allows for certain user-defined flexibility in protocols and is therefore easily adaptable to the respective research question. However, despite its extensive use, information on how the interplay of pre-analytical and analytical variables influences CTC capture efficiency and CTC morphology for this device was lacking.

Initially, the efficiency of CTC capture was significantly increased by a reduction of the separation cassette gap from 10µm to 6.5µm. This was demonstrated not only in spiked whole blood samples but confirmed by a 4.7-fold increase in CTC count using the narrow cassette gap of 6.5µm compared to 10µm in actual breast cancer patient samples. This translated to 99 instead of 21 patient CTCs available for potential further analysis, a decisive gain of “starting material”. Already in these initial spike-in experiments, a substantial interplay between CTC capture efficiency and pre-analytical (blood sample processing) as well as analytical variables (separation pressure, cassette gap, processing time) was observed [167]. These experiments were subsequently further extended to include additional blood preservatives and separation pressures. Blood collection preservatives that allow for both morphological and molecular analysis of CTCs are rare. Through these extensive spike-in experiments using breast cancer cell line cells, two robust and optimized protocols suitable to answer distinct biological and clinical questions were developed [167]. The first protocol utilizes

un-fixed cells (EDTA blood sample), thus enabling transcriptional analysis and potentially CTC culture [125, 170]. A 99% viability rate of tumor cells passed through the Parsortix® system has already been demonstrated via transcriptional analysis and by use in mouse models in prior studies [139, 170, 174]. Furthermore, the established protocol was successfully applied to the analysis of single CTCs on a transcriptional level for *ARV7* expression via an *in situ* hybridization assay [171]. The second protocol was focused on cell preservation using a newly developed CE-certified fixative (TransFix®). Again, the results for both protocols were cross-checked and corroborated on actual clinical patient samples [167]. Furthermore, cells processed via these protocols were not only shown to be morphologically intact and thus well suited for immunocytochemical staining but also for amplification of single cell DNA of excellent quality via whole genome amplification (WGA), a key method facilitating subsequent molecular analysis of these cells [167]. In summary, these results speak for the successful enrichment of higher CTC counts as well as the combinability of the developed protocols with current downstream analytic options.

In a next step, Parsortix® based enrichment of CTCs, was paired with CTC capture and detection using a newly developed microfluidic chip [168]. Microfluidic systems have demonstrated comparable and at times even superior tumor cell capture rates to the CellSearch® system [175-178]. The CTC capture chip represents an innovative, novel tool to arrest and analyze CTCs. It's basic principle rests in the antibody based capture of tumor cells on streptavidin coated dots of a microfluidic chamber. In short, a cell suspension containing tumor cells and background leukocytes is inoculated with biotinylated antibodies targeting specific per-defined cell-surface antigens (e.g. EpCAM). These so called "sensitized" tumor cells subsequently pass through a microfluidic chamber in which chaotic flow leads to interaction with streptavidin coated dots that then immobilize the biotinylated cells of interest. Non-biotinylated cells freely pass through the device and are flushed out. The benefit of this approach lies in the high purity of the samples (below 500 remaining nucleated cell per 7.5 ml blood sample) and the co-localization of the tumor cells and streptavidin dots [168]. The latter reduces the necessity of elaborate subsequent identification procedures (e.g. immunocytochemistry), potentially damaging the captured cells and requiring additional time and resources. Skipping staining-based identification enables immediate single cell manipulation and molecular analysis of captured tumor cells. Selected analytical variables (e.g. temperature, cell concentration) of the microfluidic chip had already been assessed in a prior publication [111]. In this thesis, further modifications in the structure of the microfluidic chamber were implemented (e.g.

ceiling structure, streptavidin pattern) and tested for tumor cell recovery via spike-in experiments with breast cancer cell line cells [168].

In healthy blood samples manually spiked with defined tumor cell line counts, the newly developed herringbone structure ceiling (HC) combined with 50µm spaced streptavidin dots, significantly outperformed the other chip designs [168]. Factoring in the average of tumor cells lost during Parsortix® based pre-enrichment prior to chip processing, the CTC capture chip shows near full tumor cell recovery. Unfortunately, the CTC capture chip is not yet set up to directly process whole blood, a limitation that needs to be addressed in future experiments. However, the promising results of my thesis warrant further focus on the optimization of efficient sample pre-enrichment. Work in this direction is currently being continued. In addition to the demonstrated increase in CTC capture efficiency, the vast majority (around 90%) of the cell line cells processed by this workflow (Parsortix® pre-enrichment, microfluidic CTC capture) remained viable, indicating ideal conditions for subsequent cell culture [168]. Furthermore, feasibility of the workflow for downstream genomic analysis of single tumor cells was shown in form of successful whole genome amplification. In the future, experiments including actual cancer patient samples will be required to test this workflow in a clinical setting.

4.1.2. Influence of Cancer Entity and Clinical Setting on CTC Enrichment

The importance of head to head comparison between results generated by spike-in experiments and the processing of actual clinical samples from cancer patients was highlighted by this thesis [167]. The in-depth protocol comparison performed for the label-independent Parsortix® system revealed a significant discrepancy between results obtained for spike-in experiments and clinical samples. In the initial spike-in experiments using cancer cell line cells in healthy donor blood, both the EDTA and TransFix® protocols resulted in nearly equal CTC capture rates [167]. However, when applying these protocols to actual clinical samples, the cell preservative (TransFix®) clearly outperformed the unfixed EDTA blood samples in respect to the amount of CTCs captured (21 CTCs with TransFix® vs 7 CTCs with EDTA) and the overall positivity rate (46.2% with TransFix® vs 30,8% with EDTA), respectively. This data indicates that the efficiency of CTC enrichment is dependent on factors surpassing the sensitivity of the technology chosen. These additional factors include the short half-life of CTCs in blood. Physical and biological variables such as shear forces, anoikis, and attacks by the immune system influence tumor cell viability and perseverance (1.2.1.). Clinical factors, such

as the time point of sample collection in relation to therapy may also significantly affect the robustness of CTCs. The use of a cell preservative may therefore become highly beneficial when enriching more fragile or impacted CTCs. In this study, the protocols were furthermore tested on a broad spectrum of different tumor entities, thereby addressing another biological variable and increasing their applicability to various cancer types. It has become common knowledge that some tumor entities, such as breast and prostate cancer, lend themselves well to CTC analysis, displaying relatively high CTC counts especially in a metastatic setting [108]. Other entities, such as non-small cell lung cancer (NSCLC), are notoriously difficult to detect CTCs in, despite their high metastatic potential [108, 116]. The underlying cause of this discrepancy has not been uncovered to date. Hypotheses range from a reduction in CTC shed into the blood, to increased fragility of the tumor cells shed, or quicker extravasation. These tumor type specific biological factors might provide some explanation as to why the analysis of spike-in experiments and metastatic breast cancer patient samples at the onset of this study provided more closely aligned results [167].

Here, a set of more challenging entities were included into the analysis (e.g. NSCLC). Due to the label-independent nature of the chosen enrichment approach, it is to be assumed that CTCs stemming from most tumor types are captured using the Parsortix® system. The broad use of the device strengthens this assumption [170, 172, 173, 179]. Keeping in mind the challenging nature of some of the entities analyzed in this study, the resulting overall positivity rate (defined as ≥ 1 CTC) for both methods (46.2% with TransFix® vs 30.8% with EDTA) is comparable or even superior to most EpCAM dependent enrichment approaches [116]. These results might be further enhanced by the addition of more specific detection markers. Seeing as this represents a very small, mixed patient cohort, the results obtained here require cautious interpretation. Validation in larger clinical studies including higher patient numbers will be necessary to consolidate these initial indications. Overall, a combination of biological factors and the sensitivity/specificity of existing technologies and assays therefore appear to limit the robust and reproducible enrichment and identification of CTCs. CTC clusters have been associated with significantly increased metastatic capacity [138, 139, 180], as well as shorter progression free and overall survival in breast cancer patients [181, 182]. Interestingly, the enrichment of CTC clusters was on a comparable level for both the unfixed and fixed cell protocol, respectively [167]. This could hint at higher endurance of CTC clusters, potentially due to the reduced effect of shear forces and anoikis in these cellular aggregates. The latter hypothesis is supported by recent findings, indicating the overexpression of anti-apoptotic proteins, such as Bcl2,

and down-regulation of the whole apoptotic pathway in CTC clusters compared to single CTCs [139, 183].

4.1.3. Intra- and Inter-Laboratory Comparability of CTC Enumeration

While the optimization of performance is of great importance and represents an important prerequisite to ensure optimal CTC recovery, it is of equal importance to assess how well a technology performs under highly defined conditions compared to others. The multitude of label-dependent and label-independent enrichment technologies flooding the diagnostics market makes it highly difficult for researchers, and clinicians alike, to gauge which methods are robust and suitable for efficient CTC capture and detection. Most enrichment technologies have shown promising results in selected publications. However, due to the lack of available standardized and validated protocols, the use of different cellular models and pre-analytic conditions, results remain difficult to interpret and compare. The CANCER-ID consortium, funded by the European Innovative Medicines Initiative (IMI), attempted to tackle this issue in a collaborative effort to standardize protocols in the liquid biopsy realm and thus advance the analysis of blood based markers in research and in the clinical setting [184]. The consortium, which included PhD students such as myself, was active for 5 years (2015-2019) and encompassed 36 partners from academia and industry, dispersed over 13 countries. In this time, and also beyond expiration of the funding period, a multitude of scientific publications focusing on assay validation, standardization and comparison were published. The academic leads of this massive undertaking were Klaus Pantel (UKE, Hamburg; Scientific coordinator) and Leon Terstappen (University of Twente, Netherlands; Scientific Co-coordinator). One aspiration of the consortium was the establishment of a multinational platform to assess the technical validity of CTC enrichment systems. This platform was designed to directly compare selected, promising technologies across various sites (and users) and between one another. A successful demonstration of this platform was conducted via large multicenter ring-experiments [169]. Here, blood samples containing well defined NSCLC cell line cells of similar size range, showing ample Keratin expression (for use as detection criteria), and high as well as low EpCAM expressions were generated in an independent and central laboratory [169]. A total of 98 samples containing between 51 - 99 cells spiked per sample (mean: 77.5, median: 78) were subsequently shipped to 9 sites in 6 countries and processed in defined time frames [169]. Five different CTC enrichment methods were tested, including three size based filtration devices (Siemens, Parsortix®, VyCAP), one density based

approach (RareCyte®) and the immunomagnetic, label-dependent CellSearch® system. Semi-automated and integrated sample scanning was performed if available (CellSearch®, RareCyte®). For each method, detailed pre-analytical information (e.g. blood tube type and volume), and technical data were assessed (e.g. sample throughput, detection system, etc.). Also, user defined characteristics such as hands on time needed for sample processing were provided, thus, forming a detailed and educative picture of the respective assay for potential users [169]. Cell recoveries lay in a comparably high range for the CellSearch® (mean 75%), Parsortix® (mean 71%), and RareCyte® (mean 68%) systems when analyzing samples containing the EpCAM high NSCLC cell line cells [169]. For the EpCAM low NSCLC cell line, the Parsortix® (mean 67%) and RareCyte® (mean 78%) systems outperformed their competitors [167]. In line with expectations, the CellSearch® system did not detect the EpCAM low NSCLC cell line. In both experimental settings, the Siemens and VyCAP filtration units provided significantly lower recoveries [169]. While the Parsortix® and RareCyte® platforms demonstrate competitive results to the “gold-standard” CellSearch® system in terms of CTC recovery, the CellSearch® clearly displays the lowest variance between measurements [167]. This could originate from the fact that this system contains a dedicated detection unit and users are subjected to an in-depth training teaching them to adequately “call” CTCs using the device. Similar efforts will most likely need to be undertaken by the promising, novel label-independent enrichment approaches to increase their technical reproducibility.

In this thesis, an initial step has been taken in this direction by demonstrating compatibility of the Parsortix® technology with the XCyto® 10 Quantitative Cell Imager [167]. The capabilities of this semi-automated screening device were tested in direct comparison to traditional manual sample evaluation via fluorescence microscopy. To this end, a gating allowing the detection of pan-Keratin^{pos/neg} (Alexa Fluor 488) and CD45^{pos/neg} (APC) cells was developed on breast cancer cell line cells and subsequently applied to clinical samples [167]. The results from 27 blood samples stemming from 16mBC patient samples that had prior been manually evaluated for CTC positivity and count were juxtaposed. A significant portion of these samples (13/27) were negative for CTCs with both screening approaches. Similarly, a substantial portion (12/27) were found to be positive by both detection approaches. This resulted in a high, statistically validated, concordance between CTC-positive patients and total number of CTCs identified per sample between manual identification and semi-automated screening [167]. These promising results were complemented by the halving of hands-on time required for sample evaluation using the semi-automated XCyto® 10 (from 20min

to 10min). Also, the option of reapplying a standardized set of gating parameters to an entire study cohort would increase reproducibility, while reducing user bias from individual image analysis.

Overall, there is no one-fits-all approach to enrich and identify CTCs. Which technology or combination of assays are best suited heavily depends on the research question and the tumor entity at hand. Having said this, working with such rare events as CTCs, necessitates highly specific and sensitive technologies and protocols to maximize yield. In this thesis, the tumor cell yield of the technologies chosen was substantially increased [167, 168]. Furthermore, the understanding of the interplay between analytical variables was improved [167, 168]. Furthermore robust protocols were generated, ensuring the enrichment of intact CTCs that are combinable with various downstream analysis [167, 168]. This work thereby represents the crucial basis for successful further biological understanding of these cells. Validation studies such as the ones of this thesis were performed extensively during the development of the CellSearch® system and have contributed to its optimal function as well as its approval for clinical use in multiple cancer entities [146-148]. Apart from technological improvement, a complementary approach to overcoming the limitations posed by the rarity of CTCs is the drastic increase of sample volume by methods such as diagnostic leukapheresis (DLA). DLA represents a very promising tool, shown to significantly increase CTC yield [185, 186]. However, the DLA procedure is elaborate, time consuming, requires trained medical staff, and specialized appliances. It is therefore questionable whether cancer patients and clinicians would be willing to routinely undergo/initiate such a procedure or rather opt for the less invasive and time consuming standard blood draw. Also, most enrichment technologies currently available are unable to process the extremely cell-dense DLA samples, only enabling the analysis of a fraction of the cells obtained [185]. Further developments will therefore be needed to unlock the full potential of this approach.

Considering the plethora of technologies currently on the market, it is crucial to acquire credible and dependable data on the robustness and technical validity of an assay. In this regard, multinational ring studies, as conducted here, are of paramount importance [169]. More such efforts to benchmark technologies will be needed in the future to broaden the use of CTC analysis in research and in the clinical setting. Fortunately, the infrastructure set up via the CANCER-ID consortium, will be sustained within the newly founded European Liquid Biopsy Society (ELBS) consortium [187].

4.2. Development of a Model for Functional CTC Analysis

Despite the large number of CTCs shed into the bloodstream on a daily basis, only a fraction of these tumor cells are able to survive the harsh conditions of the bloodstream [98]. Even fewer CTCs possess the capacity to extravasate into the surrounding tissue at distant sites, survive within the novel microenvironment, and subsequently outgrow to form remote tissue metastases [100]. It has been postulated that only 0.01% of CTCs shed into the bloodstream are able to initiate metastatic outgrowth at distant sites [188]. This small, potent fraction of the CTC population, is therefore of paramount importance when trying to uncover the biological prerequisites and circumstances driving blood borne dissemination. The rarity of this CTC-subpopulation within the already scarce overall CTC pool in an average blood sample could provide a probable explanation as to why the generation of CTC-derived cell lines is so seldom successful. It furthermore illustrates why most existing CTC-derived cell lines (including the one described in this thesis) were obtained from patients with advanced disease stages that harbored unusually high CTC amounts [136, 143, 189, 190]. However, when successful the potential biological understanding to be gained by CTC-derived cell lines as functional models remains vast. Also, seeing as 90% of cancer related deaths are caused by the formation of distant metastasis, understanding and possibly preventing blood borne dissemination in a targeted manner would significantly increase survival odds for cancer patients.

4.2.1. Luminal CTC-Derived Cell Lines

The permanent breast cancer cell line, CTC-ITB-01, described in this thesis represents one of the few functional models in existence that are derived from estrogen receptor positive (ER⁺) breast cancer patient CTCs [133, 190]. In light of luminal (ER⁺ and/or PR⁺) breast cancers (BC) representing the predominant molecular BC subtype (65-80% of BC cases [20, 24]) they are underrepresented in functional BC models. This can partly be traced back to the fact that they tend to be less aggressive than other BC subtypes and therefore lend themselves less well to functional studies involving *in vitro* migration assays or *in vivo* mouse models [191, 192]. However, molecular BC subtypes show distinct differences in frequency, marker expression, prognosis, and response to treatment (Table 1), making working with appropriate *in vitro* and *in vivo* models corresponding to the molecular subtype of the BC studied a critical prerequisite. CTC-ITB-01 shows luminal protein expression patterns including epithelial keratins such as K18 and K19, hormone receptors ER α and progesterone

receptor (PR), while lacking ERBB2 amplification [190]. Molecular subtyping of RNA expression profiles using the PAM50 classifier resulted in CTC-ITB-01 matching the luminal subtype with a probability of 81.99% [190]. Most studies do not further stratify their cell lines into luminal A or B subtypes [193]. However, extensive molecular characterization studies capturing the heterogeneity of BC have demonstrated that intrinsic subtyping accurately reflects the vast majority of the biological diversity occurring in BC [194, 195]. Keeping in mind the reduced prognosis of the luminal B compared to the luminal A subtype (Table 1), this is a stratification that needs to be taken into account. As classified by the PAM50 gene signature, CTC-ITB-01 most closely aligns with the luminal B subtype, reaching a 65.22% probability. This finding is somewhat strengthened by the rapid clinical progression of the cancer patient giving rise to the CTC cell line, resulting in death two years after primary diagnosis. This potentially hints at a more invasive and aggressive disease, which has been described for luminal B compared to luminal A tumor subtypes [20, 24].

4.2.2. Metastatic Potential of CTC-ITB-01

Luminal breast cancer cell lines are often relatively well differentiated and show tight cell-cell junctions, rendering them less migratory and thus limiting their metastatic capability [192]. CTC-ITB-01 displays a more heterogeneous growth pattern, a mix of adherent and non-adherent cell fractions. While the chosen culture medium might support this type of growth, cultivating the cellular fractions separately (only adherent or only suspension) gives rise to the respective counterpart, hinting at a certain grade of cellular plasticity. Furthermore, the adherent cell fraction harbors heterogeneous cellular phenotypes including cells in close cell-cell contact as well as less cohesive spindle-like elongated cells that grow disconnectedly. The latter are typically more common for mesenchymal cell types. Research has hypothesized that in order to gain motility and detach from the interconnected tumor tissue, epithelial tumor cells undergo a process called epithelial to mesenchymal transition (EMT) [196]. In an effort to identify CTC subpopulations with the highest metastatic potential, EMT has been described to convey invasive properties to tumor cells otherwise unable to initiate outgrowth [73, 197]. Mesenchymal CTC populations have been described for multiple tumor types and have been associated with increased aggressiveness, higher metastatic potential, and disease progression [122, 144]. Originally it was assumed that EMT and its counterpart mesenchymal to epithelial transition (MET) propelled cells to two distinct cellular states, epithelial or mesenchymal. In recent years it has become clear, that tumor cells transition on an EMT spectrum

and that phenotypically partial-EMT subtypes exist [72, 73, 103]. While the distribution of specific adhesion proteins such as E-cadherin, α -catenin, and β -catenin was dysregulated for CTC-ITB-01 and selected EMT-associated transcription factors (SLUG, TWIST1) were increased in contrast to the MCF-7 cell line, CTC-ITB-01 was overall associated with an epithelial RNA and protein expression pattern. Both the adherent and the non-adherent tumor cell fraction were classified as epithelial when analyzing RNA-sequencing data via an EMT scoring algorithm. Despite its primarily epithelial phenotype, CTC-ITB-01 showed tumorigenic and metastatic capacity in immunodeficient NOD scid gamma (NSG) mice upon intermammary injection. These seemingly controversial findings are supported by more recent studies unlinking EMT and metastatic outgrowth [102, 198, 199]. Epithelial-type CTCs have recently been associated with higher metastasis initiating capacity than mesenchymal CTCs [199]. Also, EpCAM expressing CTC populations were found to significantly correlate with distant metastases and poor patient outcome in metastatic BC patients [199]. Data gained from primary tumors, and metastatic sites showing epithelial tumor cell phenotypes for both tissue types further corroborate the potential of epithelial tumor cells to foster metastatic growth [200-202]. EMT and the more mesenchymal cellular phenotype therefore appear to affect only a small percentage of tumor cells at very much defined time points. *In vivo* studies have furthermore indicated that while EMT is required for motility, it is not necessary for entering the circulation [102]. These observations hint at the possibility that EMT might play a subordinate role in metastasis of luminal BC and cells might disseminate via other pathways, such as cohesive migration [203]. The method chosen to isolate CTC-ITB-01 allowed for an EpCAM-independent CTC enrichment, giving both epithelial and mesenchymal CTC populations the chance to grow in culture. Therefore, it cannot be excluded that CTC-ITB-01 stems from more mesenchymal CTCs present in the circulation at time point of blood draw. However, the epithelial nature of the cell line in culture would hint at the transient nature of the parental CTCs mesenchymal status and the necessity of a more epithelial phenotype for outgrowth.

4.2.3. Cancer Stem Cell Pathways in CTC-ITB-01

As mentioned before, an infinitesimal fraction 0.01% of CTCs shed into the bloodstream are assumed to be able to initiate metastatic outgrowth at distant sites [188]. Similarly, only a fraction of the tumor cells present within the population of the bulk tumor mass isolated from BC patients have shown metastatic potential in mice [204]. These tumor cells are often referred to as cancer stem cells (CSC)

and have gained tremendous attention in recent years. Apart from driving metastatic spread, CSC are believed to be resistant to chemotherapy due to their efficient DNA repair, quiescence, decreased apoptosis and the expression of proteins mediating drug resistance [205]. CSC were traditionally characterized by a $CD44^+/CD24^{-/low}$ phenotype [143, 197]. Interestingly, apart from primary tumor tissue, $CD44^+/CD24^{-/low}$ cells have been identified among disseminated tumor cell (DTCs) populations in the bone marrow of early BC patients [206]. More recently, the expression of aldehyde dehydrogenase 1 (ALDH1) has been identified as an additional CSC marker in BC [207, 208]. ALDH1⁺ tumor cells have been shown to be more tumorigenic, proliferative, and epithelial than those expressing $CD44^+/CD24^{-/low}$ profiles [207, 209, 210]. This is concordant with the capability of the ALDH1⁺ and $CD44^+/CD24^+$ CTC-ITB-01 line to grow *ex vivo* and its tumorigenic capacity in an *in vivo* mouse model [190]. Injecting CTC-ITB-01 into the mouse milk duct of female immunodeficient NOD scid gamma (NSG) mice, resulted in primary tumor formation in four out of four mice [190, 191]. CTC-ITB-01 could therefore represent a suitable functional model to further study the role of ALDH1 in tumorigenesis and metastasis. Also, ALDH1 expression in primary tumors has been associated with clinicopathological factors associated with disease progression and poor prognosis, such as larger tumor size, higher clinical staging, and node metastasis [211, 212]. Furthermore, metastasis and recurrence rates were significantly increased in ALDH1⁺ compared to ALDH1⁻ breast tumors [213]. This is in line with additional studies identifying ALDH1 expression as an independent predictor of disease free survival (DFS), with ALDH1⁺ patients showing significantly reduced DFS and OS compared to their ALDH1⁻ counterparts [212]. While the ALDH1 status of our index patient's primary tumors and metastatic tissues are unknown, her rapid clinical progression somewhat mirrors these findings. Interestingly, ALDH1⁺ tumor cells are most commonly associated with more aggressive histological BC subtypes such as HER2⁺ or triple negative BC [212, 214]. In general, CSC are rarely described in ER+/PR+ tumors and their clinical significance is generally unknown. Therefore, while significant associations between ALDH1⁺ and poor prognosis have been explicitly described for luminal breast cancers [212], the identification of ALDH1⁺ tumor cells in ER+/PR+ tumors is rare [212, 214]. The large proportion of ALDH1⁺ cells within the CTC-ITB-01 cell line (77.9%) could result from selection-bias of these clones via the enrichment approach or the culture conditions chosen. Additional contributing factors such as potential survival advantages, as well as an increased proliferative capability could also be hypothesized and should be addressed in future experiments. Similarly, studies have demonstrated a significant increase in the ALDH1⁺ tumor cell population following disease recurrence, indicating a role of this cell population in metastatic

outgrowth [213]. As the CTC pool that gave rise to CTC-ITB-01 potentially stemmed from a host of different metastatic sites (bone, spleen, liver, vagina), this could provide further indication to the origin of the high level of ALDH1⁺ tumor cells in CTC-ITB-01.

Apart from CD44/CD24/ALDH1, additional index proteins involved in cellular stemness features were analyzed via Western blot for CTC-ITB-01. These include the NUMB and NOTCH1/3 proteins. In this analysis high NUMB expression was detected for CTC-ITB-01 compared to MCF-7 cell line cells, implying a role of this protein in the CTC cell lines stem cell features. Retained NUMB expression has been shown to positively correlate with an ER⁺/PR⁺ protein expression status, while negatively correlating with the CD44⁺/CD24^{-/low} phenotype for ER⁺ tumors [215]. The NUMB protein is involved in a multitude of cellular processes, the most established being its function as an inhibitor of the NOTCH receptor signaling pathway [216]. The high NUMB, combined with low NOTCH1 and NOTCH3, expression detected in the CTC cell line is in agreement with this role. However, NUMBs complex biological influence extends beyond NOTCH regulation towards cellular development, regulation of polarity and adhesion, as well as migration [216]. The NOTCH pathway is involved in cell differentiation, proliferation and survival [217]. ER⁻ breast cancer cells have been shown to become dependent on NOTCH-induced survivin expression for cell proliferation and apoptosis resistance [218]. No such effect was seen for ER⁺ breast cancer lines [218]. Furthermore, increased expression of NOTCH family proteins, such as NOTCH1 have been associated with poor prognosis in breast cancer [219]. NUMB, as a repressor of NOTCH activity is therefore handled as tumor suppressor. Interestingly, NUMB has also been associated with the regulation of p53, a key protein involved in cell cycle arrest and apoptosis in the face of DNA damage [220]. The *TP53* gene sequence is commonly mutated, and the p53 protein dysregulated, in many types of cancers [221]. The most common cancer associated *TP53* mutations are pathological missense mutations, as detected for the p53 DNA-binding domain in CTC-ITB-01 (c.853G>A; p.E285K) [221, 222]. Furthermore, loss of heterozygosity (LOH) within the *TP53* gene region, located on the 17q chromosome, often accompanies these missense mutations [222]. Such LOH was also seen for large parts of the 17q chromosome (13.905–18.391.123) of CTC-ITB-01. In addition to these genetic alterations, a strong accumulation of the p53 protein was detected in the nucleus of the CTC cell line via immunostaining, hinting at reduced degradation of the p53 protein. NUMB has been previously described to interact with p53 by preventing its ubiquitination and subsequent degradation [220, 223]. Together with a loss of feedback-loop by the inability of mutated p53 to

initiate the transcriptional activation of the ubiquitin ligase MDM2, high NUMB protein levels could further contribute to the stabilization of p53 protein detected in CTC-ITB-01 [223, 224].

While the cellular importance of wild-type p53 protein has been firmly established, an increasing body of evidence is pointing to mutant p53 gaining new functional activities surpassing the tumor-suppressor role of the wild type protein [225, 226]. Potential mutant p53 functions include increased survival, invasiveness, metastatic potential, and chemotherapy resistance [226]. These newly acquired cellular roles could result in distinct survival advantages thus driving tumor progression. The fact that the detected *TP53* gene mutation in CTC-ITB-01 was unique to the CTC cell line and not detectable in the primary tumor or the vaginal metastasis tissues, indicates a role of this *TP53* mutation in dissemination and survival. More detailed future experiments and analysis will need to be conducted to address the influence of *TP53* in CTC-ITB-01, as well as the cell lines stem cell capabilities to greater detail.

4.2.4. CTC-Derived Cell Lines as Surrogate Model for CTCs and Tumor Tissue

When working with cell lines as *in vitro* models of cancer, the question arises of how closely the established line mirrors the tumor cells of origin and how stable it remains in prolonged culture. There is mounting evidence that during the initial establishment of a novel cell line, dramatic genetic shifts can occur, indicating that the resulting cell line may have substantially evolved from the original source material [227]. Hierarchical clustering analysis of whole-genome next-generation sequencing data stemming from early (p04) and late (p30) passages of CTC-ITB-01, the primary tissue samples, and a collection CTCs collected in the initial blood draw, showed high concordance between both early and late CTC-ITB-01 passages and the original CTCs present at the time point of sample collection. Additionally, the direct comparison of copy number aberration (CNA) profiles between these early and late cell line passages and the original CTCs, provided further indication of the stability of CTC-ITB-01 in culture and its similarity to the original CTC population. This data strongly suggests that CTC-ITB-01 was derived from a subpopulation of the CTCs in circulation. Furthermore it indicates a high level of genomic stability of CTC-ITB-01 in culture. Similarly to genomic profiles, artificial culture environments may significantly modify RNA and subsequently protein expression. It is not to be expected that CTC-ITB-01 cells genetically or expression profile

wise exactly mirror the patients primary tumors, which were diagnosed and treated two years prior to blood collection and establishment of the CTC cell line. However, retaining consistent expression of key proteins describing the disease, such as the hormone receptors, renders broader transferability to the novel functional findings generated with CTC-ITB-01. While complete, comprehensive proteomic data of the primary tumor tissues, the metastatic sites, or the original CTCs was not available, selected relevant protein markers were compared to ensure congruence between the primary tumors, the vaginal metastasis, and the cell line. For CTC-ITB-01, protein expression profiles as assessed by immunocytochemical (ICC) staining and Western blot analysis, clearly indicated a strong retained ER positivity [190]. Furthermore, a lack of *ERBB2* amplification was demonstrated via *FISH* analysis and low *ERBB2* expression profiles. Similarly low *ERBB2* expression was also shared by the original CTCs in circulation. These expression profiles mirrored the classifications provided for the patient's primary tumors and the vaginal metastasis (ER⁺/PR⁺/ERBB2⁻).

Histopathologic features, such as ER positivity were also maintained by the CTC derived xenografts (CDX). In the chosen mouse model CTC-ITB-01 metastasize to clinically relevant organs of ER⁺ cancers including bone, liver, brain, and lung [228]. Two of these sites (bone and liver) constituted metastatic sites of the patient giving rise to the CTC cell line and were the most prominently affected organs *in vivo* as measured by *ex vivo* radiance signal of the isolated tissues. This finding indicates that the clinical progression of this patient could partially be mirrored by CTC-ITB-01 and the chosen mouse model. In combination, this data represents an important requirement to allow for the use of CTCs and in this case CTC derived cell lines as a form of surrogate for the analysis of solid tumor tissue, in particular for research on tumor specific or actionable mutations, tumor drivers, and as a model for drug testing. Initial steps in this direction have been taken by assessing CTC-ITB-01s susceptibility to cyclin-dependent kinase (CDK) 4/6 inhibitors (e.g. Palbociclib), a relatively novel therapeutic approach not available as standard care to the patient during her treatment [229-231]. While the patient had progressed on endocrine- and subsequently chemotherapy, CTC-ITB-01 showed sensitivity towards Palbociclib, indicating the patient may have profited from this line of therapy. These findings need to be expanded and corroborated in additional PDX mice models.

Functional CTC models have demonstrated their value in identifying CTC subpopulations with increased metastatic capability, their use for biomarker identification, the gain of fundamental

biological insight into the metastatic cascade and assessment of therapy response [133, 134, 232]. Despite the added difficulty in establishing these lines and the limitations they share with all cellular *in vitro* models, the vast potential insight CTC derived cell lines could provide in the realm of blood borne dissemination remains immense. CTC cell lines may thus supplement existing cancer models (e.g. cell lines and organoids) stemming from primary and metastatic tumor tissue [233]. The cell line generated in this thesis will substantially contribute to the understanding of pathways involved in blood borne dissemination and metastasis. It can furthermore be applied to the evaluation of drug candidates. In light of the paucity of tumorigenic ER⁺ BC cell lines, CTC-ITB-01 will represent a valuable model for future studies uncovering the functional properties of CTCs, and our report has been therefore highlighted with a photo of the cultured CTCs on the cover of the Journal EMBO Molecular Medicine.

4.3. Characterization of CTCs for Therapy Relevant Gene Expression

Similarly to breast cancer, prostate cancer (PC) is initially primarily hormone and hormone receptor driven. The androgen receptor (AR) and its ligands play a crucial role in PC progression and therefore represent the primary target for therapeutic approaches, such as androgen deprivation therapy (ADT) [234, 235]. Today, most patients receive local treatment upon early detection of their tumor(s) either in combination or without adjuvant ADT [30]. However, ADT in itself is not curative when used alone, meaning a proportion of PC patients, estimated at around 10-20%, progress to a castration-resistant stage of the disease (CRPC) within 5 years of follow up [236]. CRPC is declared as biochemical, radiological or clinical progression within a low androgen environment, yet, it is most commonly diagnosed by rising prostate-specific antigen (PSA) levels [237]. While the treatment landscape for these advanced patients was traditionally scarce, the advent of secondary hormone therapies has resulted in increased therapeutic options and survival benefits [30, 45-49]. Despite these advances, inert and acquired resistance to drugs targeting the androgen axis is prevalent and biomarkers allowing for early assessment of treatment response represent an urgent clinical need [238, 239]. Due to its AR-dependency, PSA does not qualify as a reliable biomarker for therapy response assessment with drugs that modulate the AR or AR ligand concentrations, such as secondary hormone therapy agents. CTCs on the other hand are AR independent and, when present, indicate active disease. They could therefore represent a suitable biomarker for tumor spread and disease burden. Prospective phase III studies conducted for mCPRC have shown that

CTC count combined with LDH activity satisfied all 4 Prentice criteria of surrogacy for overall survival (OS), thus indicating CTC enumeration could in fact serve as a surrogate marker for meaningful clinical endpoints [158, 240].

In addition to enumeration, further characterization of CTCs for therapy relevant gene expression could provide valuable supplementary information for clinicians concerning the selection of best suitable therapy. So far, the choice between secondary hormone therapy (e.g. enzalutamide and abiraterone) or taxanes is often empiric and not guided by predictive biomarkers. Mechanisms of resistance to androgen targeting therapies include mutations in the AR itself, AR gene amplification, androgen receptor bypass signaling, and the expression of androgen receptor splice variants, amongst others [42, 241-243]. Truncated AR splice variants can stimulate androgen-independent PC growth by dispensing with the need for ligand based activation and becoming constitutively active transcription factors [53, 244, 245]. The majority of patients express multiple splice variants, with ARV3 being the most prevalently expressed [246]. However, in the context of secondary hormone therapy resistance, the splice variant ARV7 has received most attention [54]. ARV7 protein status significantly increases from primary PC to CRPC [247]. While ARV7 is rarely expressed in primary PC tissue (<1%) it is commonly elevated after androgen deprivation therapy [247]. ARV7 mRNA and ARV7 protein expression detected in CTCs have been associated with resistance toward enzalutamide and abiraterone but not taxanes [50, 164, 165, 248-250]. The stratification of patients into CTC-/ARV7-, CTC+/ARV7- and CTC+/ARV7+ groups confirmed that CTC+/ARV7+ patients display inferior clinical outcomes (PSA response, progression-free and overall survival), compared to CTC+/ARV7- patients [163]. This effect was observed for first-line as well as second-line secondary hormone therapy treatment [163]. ARV7 detection could therefore represent the first CTC-based biomarker with predictive value for clinical decision making in the treatment choice between secondary hormone therapy and taxanes.

4.3.1. Label-Dependent and Label-Independent ARV7 Detection

Existing ARV7 mRNA and ARV7 protein detection approaches are primarily based on enrichment methods that have not comprehensively demonstrated their capacity to enrich clinically relevant CTC populations [50], or rely on centralized laboratories for sample analysis thus requiring extensive and costly sample shipment [51, 249]. Within this thesis two separate methods were developed allowing for detection of ARV7 mRNA in CTCs [171, 251]. Both workflows are compatible with [171],

or are explicitly designed to perform CTC enrichment via the FDA-approved CellSearch® system and can be conducted by laboratories on site [251]. They do not rely on elaborate equipment, or high-cost analysis (e.g. next-generation-sequencing), and allow for simple ARV7 read-out. The first approach is based on the detection of ARV7 mRNA transcripts via padlock-probe technology and subsequent microscopic evaluation, the second is a qPCR based assay performed on pooled CTC fractions. Both assays demonstrated a high level of sensitivity and specificity as well as clinical feasibility with PC patient samples [171, 251].

High CTC positivity rates of 86.2% (≥ 1 CTC; 52.2% ≥ 5 CTCs) and 64.7% (≥ 1 CTC), respectively, were detected using the CellSearch® system for the PC patient cohorts analyzed in this thesis [171, 251]. The high proportion of CTC positivity is reflective of the late disease stage of the patients enrolled in both studies and mirrors published data for metastatic prostate cancer patients [147]. Comparing technology performance across studies is error prone, however, the clinical similarity of both patient collectives allows for very tentative performative comparisons. Overall CTC positivity was comparable across enrichment methods of both studies at 86.2% (≥ 1 CTC) for the CellSearch® and 84.2% using the label-independent Parsortix® in combination with padlock-probe detection [171, 251]. However, direct comparison of both approaches revealed distinct variations in CTC counts detected for matched samples, alluding to the differences of label-dependent and label-independent CTC enrichment [171]. This discrepancy was also mirrored in an overall ARV7 positivity rate of 46.2% (CellSearch® and qPCR), versus 71% (Parsortix® and padlock-probe), respectively [171, 251]. While EpCAM dependent CTC enrichment, selects for primarily epithelial CTC phenotypes, label independent approaches possess the potential to enrich for more mesenchymal, keratin negative CTC subpopulations. Using the Parsortix® system for CTC enrichment and padlock-probe technology for detection, three different CTC populations were identified, panK+/ARV7-, panK+/ARV7+, and panK-/ARV7+ CTCs [171]. The last group of panK-/ARV7+ CTCs would most likely not have been detected using an EpCAM based enrichment approach such as the CellSearch® and could contribute to the discrepancy seen in overall ARV7 positivity. For breast cancer, studies indicate that EpCAM independent CTC isolation systems may underestimate the total number of tumor cells in circulation, but allow quantification of clinically relevant cells [199]. Similarly to other cancer entities, the biological functions and clinical relevance of mesenchymal, EpCAM-low or keratin-negative CTCs in prostate cancer is poorly understood and study results are conflicted [252-254]. However, research has linked mesenchymal CTC populations to increased rate of progression from hormone sensitive to castration resistant disease, indicating

that EpCAM negative CTC subpopulations potentially hold clinical relevance in PC [255]. The absence or downregulation of EpCAM is a strong indicator that the initially epithelial carcinoma cell has undergone epithelial to mesenchymal transition (EMT) [72]. As EMT is postulated to be required for cellular motility and has also been associated with resistance towards chemotherapy [102, 256], it could therefore be conceivable that panK-/ARV7+ CTC subpopulations represent one variable explaining why selected patients do not benefit from secondary hormone therapy even in absence of detectable panK+/ARV7+ CTCs [50, 163, 249].

4.3.2. Intensity and Localization of ARV7 Expression in Prostate Cancer Patient CTCs

Despite the fact that the link between ARV7 expression and resistance to secondary hormone therapy is now widely accepted, conflicting studies finding no such correlation, do exist [257]. Furthermore, even studies that demonstrate a correlation between ARV7 expression and therapeutic response have identified a small percentage (around 13%) of CTC+/ARV7+ patients that still respond to and benefit from secondary hormone therapy [163]. This raises questions as to how many ARV7-positive cells are necessary to confidently predict resistance and/or whether the level of ARV7 expression per cell plays into decreased treatment response. Especially in light of the advent of more and more sensitive ARV7 detection methods (e.g. down to a single ARV7+ CTC [251]), answering this question will become highly relevant. So far, only two ARV7 detection assays allow for the simultaneous quantification of CTCs and visualization of ARV7 positivity and intensity on a single cell level [51, 171]. The EPIC platform has been used to assess ARV7 protein expression and cellular localization and demonstrated its validity in clinical studies [51]. The detailed EPIC-based ARV7 detection parameters have already been published [258]. While the overall assay design is sound, some doubts have been cast as to the specificity of EPICs ARV7 detection due to reports by ourselves and others of unspecific ICC staining results by the utilized detection antibody [EPR15656] [247, 251]. Recently, a novel antibody clone, RM7, has been developed and tested, showing higher ARV7 specificity than [EPR15656] [247]. This clone could potentially be included into the fourth channel of the CellSearch® system in future studies, allowing for CTC enumeration by an FDA-approved technology for mPC in combination with ARV7 protein status determination. This represented our original assay approach but had to be discarded due to non-specific antibody signals, making qPCR based detection of ARV7 transcripts necessary [251]. In contrast, the padlock-

probe based assay published in this thesis represents an elegant approach to analyze nucleic acids without disrupting cellular integrity [171]. It uniquely allows for the assessment of *ARV7*, *AR-FL*, and *PSA* transcript levels combined with the immunocytochemical characterization of CTCs for pan-keratins and CD45.

Apart from shining light into *ARV7* heterogeneity in CTCs, the method enables the absolute quantification of *ARV7* transcript levels and their cellular localization thus facilitating comparability between samples [171]. A high range of *ARV7* expression [1-79 *ARV7* transcripts/CTC] was detected for the advanced patient cohort analyzed in this study [171]. Additionally, distinct CTC subpopulations were described for the majority of patient samples (panK+/ARV7-, panK+/ARV7+, and panK-/ARV7+ CTCs), indicating large intra-patient heterogeneity in *ARV7* expression and adding another layer of complexity to *ARV7* assessment [171]. These findings match the results of large genomic heterogeneity studies indicating that different tumor foci are genetically distinct within the same prostate cancer patients [259]. While the primary aim of this study was to demonstrate clinical feasibility for the developed method, it could in future contribute to the determination of an *ARV7* “threshold” on transcriptional or overall CTC-count level. This threshold could more accurately stratify patients into responders and non-responders towards secondary hormone therapies.

Similarly to other transcription factors cellular localization within the nucleus is a prerequisite for the *ARV7* to unfold its full effect. Scher et al. demonstrated that solely nuclear *ARV7* protein in CTCs is a relevant predictor for treatment selection [51]. In a study enrolling 193 mCRPC patients, those with nuclear *ARV7* protein had superior survival on taxanes while *ARV7*- patients showed better survival on hormone therapy [260]. Additionally, the use of *ARV7* status on CTCs was able to inform treatment choice and improve clinical outcome compared to decisions based solely on standard of care, thus demonstrating clinical utility [260]. In contrast, most established *ARV7* mRNA assays do not account for the splice variants localization within the cell [50, 246, 250, 251]. Furthermore it cannot be assumed that all detected *ARV7* mRNA transcripts will in fact be translated into protein [163]. Both of these aspects might further contribute to the observation that selected CTC+/ARV7+ patients still benefit from novel hormonal therapy (NHT) [163]. Despite these obvious drawbacks for mRNA-based *ARV7* detection assays, it has recently been demonstrated, that within the CRPC setting *ARV7* protein is predominantly nuclear (in 94% of cases), indicating that the fraction of *ARV7* mRNA that is translated to protein will most likely be active in the nucleus [247].

Additionally, an 82% agreement between protein and mRNA based ARV7 status assessment has been shown for CTCs [249]. Therefore, ARV7 mRNA detection remains clinically relevant.

CTC enumeration has extensively demonstrated its prognostic potential in metastatic prostate cancer [147]. Subsequent molecular characterization of CTCs for therapy relevant gene expression, such as for ARV7 in the context of secondary hormone therapy, has the potential to stratify patients towards best-suitable therapeutic options and facilitate the monitoring of treatment response, as well as the emergence of resistant clones. Conversions of ARV7 status under therapy have already been described hinting at the necessity of longitudinal monitoring of patients ARV7 status in the course of treatment [163]. Here, the analytical validation of two highly sensitive and specific methods for ARV7 mRNA detection have been described and their clinical feasibility has been demonstrated [171, 251]. These methods have the potential to answer urgent questions regarding the biological functions and clinical relevance of ARV7 in PC. The inclusion and comparison of both methods in clinical studies with large and more homogenous patient cohorts will be necessary to further corroborate assay specificity and determine to which extent both approaches are complementary or redundant.

5. Conclusion and Outlook

Research on CTCs has demonstrated vast potential to contribute to a plethora of different realms of tumor biology, the most prominent being blood borne dissemination. In this thesis, a multifaceted approach was adapted, reflecting the wealth of knowledge to be gained in this field. Improving CTC detection and making this rare and delicate biomarker available for un-biased molecular characterization represents a crucial prerequisite for all further CTC-based projects. Within this thesis, relevant improvements were initiated and successfully implemented in this respect [167-169]. Existing methods were analytically validated and additionally compared in large multi-center ring trials [167, 169]. Furthermore, an epithelial, ER⁺ breast cancer CTC-derived cell line model with tumorigenic and metastatic capability in mice was established [190]. This functional model represents a valuable tool for future in-depth studies addressing the biology of CTCs, their plasticity, and their role in dissemination and metastasis tropism [190]. Finally, the clinical relevance of CTC analysis was addressed by the characterization of the therapy relevant gene transcript, *ARV7*, in metastatic prostate cancer [171, 251]. The results of these studies have pointed to relevant questions of the field (e.g. the determination of *ARV7* thresholds) and illustrate a path to answer them [171, 251]. This ties in to the role of CTCs as biomarkers for clinical patient management and within the development of personalized therapy approaches. The results of this thesis have therefore contributed to CTC detection, the understanding of their biological role, and their translational value in clinical practice.

Despite the relevance of CTC enumeration in advanced cancer patients, reimbursement of CTC detection assays and the broad clinical use of CTC analysis as a biomarker has not been achieved as of today. This is mostly due to insufficient data demonstrating clinical utility of CTC analysis. Clinical utility, the ability of a diagnostic test to improve patient health outcomes by altering treatment, necessitated the integration of CTC analysis in interventional studies. Very recently, the results of the first successful interventional trial applying CTC count as a biomarker for clinical decision making has been published [261]. The STIC CTC trial (NCT01710605) assessed whether the first line treatment decision between endocrine therapy and chemotherapy for metastatic hormone receptor (HR)-positive BC patients could be based on CTC enumeration at baseline. To answer this question, a CTC-based arm (377 patients) was compared to a clinician-based arm (378 patients). In the CTC arm, patients received endocrine therapy at CTC values below <5 CTCs and received

chemotherapy at ≥ 5 CTCs per 7.5ml of blood. In the control arm, the choice of therapy was left to the investigator. The primary end-point of progression free survival (PFS) was reached (HR of 0.94). Median PFS was 13.9 months (95% CI; 12.2-16.3) in the control arm and 15.5 months (95% CI; 12.7-17.3) in the CTC arm, thus proving clinical utility of CTC enumeration for HR-positive BC patients in advance of first line therapy [261]. Additional trials aiming at demonstrating clinical utility are currently underway for breast cancer (e.g. DETECT III; NCT01619111), and prostate cancer (e.g. TACTIK study; NCT03101046). Their results will be necessary to further corroborate these findings and demonstrate clinical utility in other cancer entities and treatment settings to enable reimbursement and broad clinical use of CTC analysis as a biomarker. Initial promising results of the DETECT III trial were presented at the last San Antonio Breast Cancer Symposium and demonstrated that patients with metastatic breast cancer who initially presented with ER⁺/HER2⁻ tumors but showed HER2⁺ CTCs at the time of relapse had a prolonged overall survival if they received anti-HER2 therapy with Lapatinib in addition to standard therapy as compared to standard therapy alone. This demonstrates, for the first time, the clinical utility of CTC phenotyping. Insights provided by this thesis might further contribute to a better understanding of potential targets or pathways for novel therapeutic interventions specifically directed against CTCs.

6. Literature and References

1. Organization, W.H. *Cancer Fact Sheet*. 2018 [cited 2020 11.26.]; Available from: <https://www.who.int/news-room/fact-sheets/detail/cancer>.
2. Cancer, I.A.f.R.o. *Global Cancer Observatory, GLOBOCAN*. 2020 [cited 2021 13.01.]; Available from: <https://gco.iarc.fr/today/home>.
3. Stephens, F.O., Aigner, Karl Reinhard *Basics of Oncology*. 2016: p. 17-38.
4. La Thangue, N.B. and D.J. Kerr, *Predictive biomarkers: a paradigm shift towards personalized cancer medicine*. *Nat Rev Clin Oncol*, 2011. **8**(10): p. 587-96.
5. Hanahan, D. and R.A. Weinberg, *Hallmarks of cancer: the next generation*. *Cell*, 2011. **144**(5): p. 646-74.
6. Hawkes, N., *Cancer survival data emphasise importance of early diagnosis*. *BMJ*, 2019. **364**: p. l408.
7. Chaffer, C.L. and R.A. Weinberg, *A perspective on cancer cell metastasis*. *Science*, 2011. **331**(6024): p. 1559-64.
8. Richards, M.A., *The size of the prize for earlier diagnosis of cancer in England*. *Br J Cancer*, 2009. **101** Suppl 2: p. S125-9.
9. Bradley, C.J., C.W. Given, and C. Roberts, *Disparities in cancer diagnosis and survival*. *Cancer*, 2001. **91**(1): p. 178-88.
10. Hiom, S.C., *Diagnosing cancer earlier: reviewing the evidence for improving cancer survival*. *Br J Cancer*, 2015. **112** Suppl 1: p. S1-5.
11. Steeg, P.S., *Targeting metastasis*. *Nat Rev Cancer*, 2016. **16**(4): p. 201-18.
12. Botha, J.L., et al., *Breast cancer incidence and mortality trends in 16 European countries*. *Eur J Cancer*, 2003. **39**(12): p. 1718-29.
13. DeSantis, C.E., et al., *International Variation in Female Breast Cancer Incidence and Mortality Rates*. *Cancer Epidemiol Biomarkers Prev*, 2015. **24**(10): p. 1495-506.
14. Sant, M., et al., *Time trends of breast cancer survival in Europe in relation to incidence and mortality*. *Int J Cancer*, 2006. **119**(10): p. 2417-22.
15. Yang, X.R., et al., *Associations of breast cancer risk factors with tumor subtypes: a pooled analysis from the Breast Cancer Association Consortium studies*. *J Natl Cancer Inst*, 2011. **103**(3): p. 250-63.
16. Tabar, L., et al., *The incidence of fatal breast cancer measures the increased effectiveness of therapy in women participating in mammography screening*. *Cancer*, 2019. **125**(4): p. 515-523.
17. Shepardson, L.B. and L. Dean, *Current controversies in breast cancer screening*. *Semin Oncol*, 2020. **47**(4): p. 177-181.
18. Cardoso, F., et al., *Early breast cancer: ESMO Clinical Practice Guidelines for diagnosis, treatment and follow-up*. *Ann Oncol*, 2019. **30**(10): p. 1674.
19. Giuliano, A.E., et al., *Breast Cancer-Major changes in the American Joint Committee on Cancer eighth edition cancer staging manual*. *CA Cancer J Clin*, 2017. **67**(4): p. 290-303.
20. Makki, J., *Diversity of Breast Carcinoma: Histological Subtypes and Clinical Relevance*. *Clin Med Insights Pathol*, 2015. **8**: p. 23-31.
21. Prat, A., et al., *Clinical implications of the intrinsic molecular subtypes of breast cancer*. *Breast*, 2015. **24** Suppl 2: p. S26-35.
22. Holm, J., et al., *Assessment of Breast Cancer Risk Factors Reveals Subtype Heterogeneity*. *Cancer Res*, 2017. **77**(13): p. 3708-3717.

23. Hennigs, A., et al., *Prognosis of breast cancer molecular subtypes in routine clinical care: A large prospective cohort study*. BMC Cancer, 2016. **16**(1): p. 734.
24. van Maaren, M.C., et al., *Ten-year recurrence rates for breast cancer subtypes in the Netherlands: A large population-based study*. Int J Cancer, 2019. **144**(2): p. 263-272.
25. Cardoso, F., et al., *5th ESO-ESMO international consensus guidelines for advanced breast cancer (ABC 5)*. Ann Oncol, 2020. **31**(12): p. 1623-1649.
26. Culp, M.B., et al., *Recent Global Patterns in Prostate Cancer Incidence and Mortality Rates*. Eur Urol, 2020. **77**(1): p. 38-52.
27. Cuzick, J., et al., *Prevention and early detection of prostate cancer*. Lancet Oncol, 2014. **15**(11): p. e484-92.
28. Perez-Cornago, A., et al., *Prospective investigation of risk factors for prostate cancer in the UK Biobank cohort study*. Br J Cancer, 2017. **117**(10): p. 1562-1571.
29. Steele, C.B., et al., *Prostate cancer survival in the United States by race and stage (2001-2009): Findings from the CONCORD-2 study*. Cancer, 2017. **123** Suppl 24: p. 5160-5177.
30. Parker, C., et al., *Prostate cancer: ESMO Clinical Practice Guidelines for diagnosis, treatment and follow-up*. Ann Oncol, 2020. **31**(9): p. 1119-1134.
31. Kasivisvanathan, V., et al., *MRI-Targeted or Standard Biopsy for Prostate-Cancer Diagnosis*. N Engl J Med, 2018. **378**(19): p. 1767-1777.
32. Villers, A., et al., *Multiple cancers in the prostate. Morphologic features of clinically recognized versus incidental tumors*. Cancer, 1992. **70**(9): p. 2313-8.
33. Mellinger, G.T., *Prognosis of prostatic carcinoma*. Recent Results Cancer Res, 1977(60): p. 61-72.
34. Bailar, J.C., 3rd, G.T. Mellinger, and D.F. Gleason, *Survival rates of patients with prostatic cancer, tumor stage, and differentiation--preliminary report*. Cancer Chemother Rep, 1966. **50**(3): p. 129-36.
35. Schroder, F.H., et al., *Screening and prostate-cancer mortality in a randomized European study*. N Engl J Med, 2009. **360**(13): p. 1320-8.
36. Heinlein, C.A. and C. Chang, *Androgen receptor in prostate cancer*. Endocr Rev, 2004. **25**(2): p. 276-308.
37. Knudsen, K.E., K.C. Arden, and W.K. Cavenee, *Multiple G1 regulatory elements control the androgen-dependent proliferation of prostatic carcinoma cells*. J Biol Chem, 1998. **273**(32): p. 20213-22.
38. Wang, Q., et al., *Androgen receptor regulates a distinct transcription program in androgen-independent prostate cancer*. Cell, 2009. **138**(2): p. 245-56.
39. Xu, Y., et al., *Androgens induce prostate cancer cell proliferation through mammalian target of rapamycin activation and post-transcriptional increases in cyclin D proteins*. Cancer Res, 2006. **66**(15): p. 7783-92.
40. Shore, N.D., et al., *New considerations for ADT in advanced prostate cancer and the emerging role of GnRH antagonists*. Prostate Cancer Prostatic Dis, 2013. **16**(1): p. 7-15.
41. Mohler, M.L., et al., *Androgen receptor antagonists: a patent review (2008-2011)*. Expert Opin Ther Pat, 2012. **22**(5): p. 541-65.
42. Watson, P.A., V.K. Arora, and C.L. Sawyers, *Emerging mechanisms of resistance to androgen receptor inhibitors in prostate cancer*. Nat Rev Cancer, 2015. **15**(12): p. 701-11.
43. Merson, S., et al., *Focal amplification of the androgen receptor gene in hormone-naïve human prostate cancer*. Br J Cancer, 2014. **110**(6): p. 1655-62.
44. Robinson, D., et al., *Integrative Clinical Genomics of Advanced Prostate Cancer*. Cell, 2015. **161**(5): p. 1215-1228.

45. de Bono, J.S., et al., *Abiraterone and increased survival in metastatic prostate cancer*. N Engl J Med, 2011. **364**(21): p. 1995-2005.
46. Scher, H.I., et al., *Increased survival with enzalutamide in prostate cancer after chemotherapy*. N Engl J Med, 2012. **367**(13): p. 1187-97.
47. Ryan, C.J., et al., *Abiraterone acetate plus prednisone versus placebo plus prednisone in chemotherapy-naïve men with metastatic castration-resistant prostate cancer (COU-AA-302): final overall survival analysis of a randomised, double-blind, placebo-controlled phase 3 study*. Lancet Oncol, 2015. **16**(2): p. 152-60.
48. Beer, T.M. and B. Tombal, *Enzalutamide in metastatic prostate cancer before chemotherapy*. N Engl J Med, 2014. **371**(18): p. 1755-6.
49. Basch, E., et al., *Abiraterone acetate plus prednisone versus prednisone alone in chemotherapy-naïve men with metastatic castration-resistant prostate cancer: patient-reported outcome results of a randomised phase 3 trial*. Lancet Oncol, 2013. **14**(12): p. 1193-9.
50. Antonarakis, E.S., et al., *AR-V7 and resistance to enzalutamide and abiraterone in prostate cancer*. N Engl J Med, 2014. **371**(11): p. 1028-38.
51. Scher, H.I., et al., *Nuclear-specific AR-V7 Protein Localization is Necessary to Guide Treatment Selection in Metastatic Castration-resistant Prostate Cancer*. Eur Urol, 2017. **71**(6): p. 874-882.
52. Guo, Z., et al., *A novel androgen receptor splice variant is up-regulated during prostate cancer progression and promotes androgen depletion-resistant growth*. Cancer Res, 2009. **69**(6): p. 2305-13.
53. Hu, R., et al., *Ligand-independent androgen receptor variants derived from splicing of cryptic exons signify hormone-refractory prostate cancer*. Cancer Res, 2009. **69**(1): p. 16-22.
54. Cato, L., et al., *ARv7 Represses Tumor-Suppressor Genes in Castration-Resistant Prostate Cancer*. Cancer Cell, 2019. **35**(3): p. 401-413 e6.
55. Ladjevardi, S., et al., *Prostate biopsy sampling causes hematogenous dissemination of epithelial cellular material*. Dis Markers, 2014. **2014**: p. 707529.
56. Joosse, S.A., T.M. Gorges, and K. Pantel, *Biology, detection, and clinical implications of circulating tumor cells*. EMBO Mol Med, 2015. **7**(1): p. 1-11.
57. Liotta, L.A., J. Kleinerman, and G.M. Saidel, *Quantitative relationships of intravascular tumor cells, tumor vessels, and pulmonary metastases following tumor implantation*. Cancer Res, 1974. **34**(5): p. 997-1004.
58. Butler, T.P. and P.M. Gullino, *Quantitation of cell shedding into efferent blood of mammary adenocarcinoma*. Cancer Res, 1975. **35**(3): p. 512-6.
59. Martin, M., et al., *Circulating tumor cells in metastatic breast cancer: timing of blood extraction for analysis*. Anticancer Res, 2009. **29**(10): p. 4185-7.
60. Bardelli, A. and K. Pantel, *Liquid Biopsies, What We Do Not Know (Yet)*. Cancer Cell, 2017. **31**(2): p. 172-179.
61. Reimers, N. and K. Pantel, *Liquid biopsy: novel technologies and clinical applications*. Clin Chem Lab Med, 2019. **57**(3): p. 312-316.
62. Alix-Panabieres, C. and K. Pantel, *Clinical Applications of Circulating Tumor Cells and Circulating Tumor DNA as Liquid Biopsy*. Cancer Discovery, 2016. **6**(5): p. 479-491.
63. Hoshino, A., et al., *Tumour exosome integrins determine organotropic metastasis*. Nature, 2015. **527**(7578): p. 329-35.
64. Keller, L. and K. Pantel, *Unravelling tumour heterogeneity by single-cell profiling of circulating tumour cells*. Nat Rev Cancer, 2019. **19**(10): p. 553-567.

65. Pantel, K. and R.H. Brakenhoff, *Dissecting the metastatic cascade*. Nat Rev Cancer, 2004. **4**(6): p. 448-56.
66. Husemann, Y., et al., *Systemic spread is an early step in breast cancer*. Cancer Cell, 2008. **13**(1): p. 58-68.
67. Sanger, N., et al., *Disseminated tumor cells in the bone marrow of patients with ductal carcinoma in situ*. Int J Cancer, 2011. **129**(10): p. 2522-6.
68. Morgan, T.M., et al., *Disseminated tumor cells in prostate cancer patients after radical prostatectomy and without evidence of disease predicts biochemical recurrence*. Clin Cancer Res, 2009. **15**(2): p. 677-83.
69. Rahman, M. and S. Mohammed, *Breast cancer metastasis and the lymphatic system*. Oncol Lett, 2015. **10**(3): p. 1233-1239.
70. Hanahan, D. and R.A. Weinberg, *The hallmarks of cancer*. Cell, 2000. **100**(1): p. 57-70.
71. Chambers, A.F., A.C. Groom, and I.C. MacDonald, *Dissemination and growth of cancer cells in metastatic sites*. Nat Rev Cancer, 2002. **2**(8): p. 563-72.
72. Nieto, M.A., et al., *Emt: 2016*. Cell, 2016. **166**(1): p. 21-45.
73. Chaffer, C.L., et al., *EMT, cell plasticity and metastasis*. Cancer Metastasis Rev, 2016. **35**(4): p. 645-654.
74. Scheel, C., et al., *Paracrine and autocrine signals induce and maintain mesenchymal and stem cell states in the breast*. Cell, 2011. **145**(6): p. 926-40.
75. Lamouille, S., J. Xu, and R. Derynck, *Molecular mechanisms of epithelial-mesenchymal transition*. Nat Rev Mol Cell Biol, 2014. **15**(3): p. 178-96.
76. Bhowmick, N.A., E.G. Neilson, and H.L. Moses, *Stromal fibroblasts in cancer initiation and progression*. Nature, 2004. **432**(7015): p. 332-7.
77. Guo, W., *Concise review: breast cancer stem cells: regulatory networks, stem cell niches, and disease relevance*. Stem Cells Transl Med, 2014. **3**(8): p. 942-8.
78. Smith, B.N. and N.A. Bhowmick, *Role of EMT in Metastasis and Therapy Resistance*. J Clin Med, 2016. **5**(2).
79. Peinado, H., D. Olmeda, and A. Cano, *Snail, Zeb and bHLH factors in tumour progression: an alliance against the epithelial phenotype?* Nat Rev Cancer, 2007. **7**(6): p. 415-28.
80. Tam, W.L. and R.A. Weinberg, *The epigenetics of epithelial-mesenchymal plasticity in cancer*. Nat Med, 2013. **19**(11): p. 1438-49.
81. Egeblad, M. and Z. Werb, *New functions for the matrix metalloproteinases in cancer progression*. Nat Rev Cancer, 2002. **2**(3): p. 161-74.
82. Wolf, K. and P. Friedl, *Extracellular matrix determinants of proteolytic and non-proteolytic cell migration*. Trends Cell Biol, 2011. **21**(12): p. 736-44.
83. Frisch, S.M. and H. Francis, *Disruption of epithelial cell-matrix interactions induces apoptosis*. J Cell Biol, 1994. **124**(4): p. 619-26.
84. Paoli, P., E. Giannoni, and P. Chiarugi, *Anoikis molecular pathways and its role in cancer progression*. Biochim Biophys Acta, 2013. **1833**(12): p. 3481-3498.
85. Pignatelli, J., et al., *Macrophage-dependent tumor cell transendothelial migration is mediated by Notch1/Mena(INV)-initiated invadopodium formation*. Sci Rep, 2016. **6**: p. 37874.
86. Hida, K., et al., *Contribution of Tumor Endothelial Cells in Cancer Progression*. Int J Mol Sci, 2018. **19**(5).
87. Nakamura, K. and M.J. Smyth, *Myeloid immunosuppression and immune checkpoints in the tumor microenvironment*. Cell Mol Immunol, 2020. **17**(1): p. 1-12.
88. Martinez-Outschoorn, U.E., et al., *Cancer metabolism: a therapeutic perspective*. Nat Rev Clin Oncol, 2017. **14**(1): p. 11-31.

89. Chang, S.F., et al., *Tumor cell cycle arrest induced by shear stress: Roles of integrins and Smad*. Proc Natl Acad Sci U S A, 2008. **105**(10): p. 3927-32.
90. Kienast, Y., et al., *Real-time imaging reveals the single steps of brain metastasis formation*. Nat Med, 2010. **16**(1): p. 116-22.
91. Meng, S., et al., *Circulating tumor cells in patients with breast cancer dormancy*. Clin Cancer Res, 2004. **10**(24): p. 8152-62.
92. Larson, C.J., et al., *Apoptosis of circulating tumor cells in prostate cancer patients*. Cytometry A, 2004. **62**(1): p. 46-53.
93. Labelle, M., S. Begum, and R.O. Hynes, *Direct signaling between platelets and cancer cells induces an epithelial-mesenchymal-like transition and promotes metastasis*. Cancer Cell, 2011. **20**(5): p. 576-90.
94. Menter, D.G., et al., *Platelets and cancer: a casual or causal relationship: revisited*. Cancer Metastasis Rev, 2014. **33**(1): p. 231-69.
95. Palumbo, J.S., et al., *Platelets and fibrin(ogen) increase metastatic potential by impeding natural killer cell-mediated elimination of tumor cells*. Blood, 2005. **105**(1): p. 178-85.
96. Malik, G., et al., *Plasma fibronectin promotes lung metastasis by contributions to fibrin clots and tumor cell invasion*. Cancer Res, 2010. **70**(11): p. 4327-34.
97. Haemmerle, M., et al., *Platelets reduce anoikis and promote metastasis by activating YAP1 signaling*. Nat Commun, 2017. **8**(1): p. 310.
98. Follain, G., et al., *Hemodynamic Forces Tune the Arrest, Adhesion, and Extravasation of Circulating Tumor Cells*. Dev Cell, 2018. **45**(1): p. 33-52 e12.
99. Im, J.H., et al., *Coagulation facilitates tumor cell spreading in the pulmonary vasculature during early metastatic colony formation*. Cancer Res, 2004. **64**(23): p. 8613-9.
100. Kang, Y. and K. Pantel, *Tumor cell dissemination: emerging biological insights from animal models and cancer patients*. Cancer Cell, 2013. **23**(5): p. 573-81.
101. Pei, D., et al., *Mesenchymal-epithelial transition in development and reprogramming*. Nat Cell Biol, 2019. **21**(1): p. 44-53.
102. Beerling, E., et al., *Plasticity between Epithelial and Mesenchymal States Unlinks EMT from Metastasis-Enhancing Stem Cell Capacity*. Cell Rep, 2016. **14**(10): p. 2281-8.
103. Alix-Panabieres, C., S. Mader, and K. Pantel, *Epithelial-mesenchymal plasticity in circulating tumor cells*. J Mol Med (Berl), 2017. **95**(2): p. 133-142.
104. Braun, S., et al., *A pooled analysis of bone marrow micrometastasis in breast cancer*. N Engl J Med, 2005. **353**(8): p. 793-802.
105. Freedland, S.J. and J.W. Moul, *Prostate specific antigen recurrence after definitive therapy*. J Urol, 2007. **177**(6): p. 1985-91.
106. Kennecke, H., et al., *Metastatic behavior of breast cancer subtypes*. J Clin Oncol, 2010. **28**(20): p. 3271-7.
107. Uhr, J.W. and K. Pantel, *Controversies in clinical cancer dormancy*. Proc Natl Acad Sci U S A, 2011. **108**(30): p. 12396-400.
108. Allard, W.J., et al., *Tumor cells circulate in the peripheral blood of all major carcinomas but not in healthy subjects or patients with nonmalignant diseases*. Clin Cancer Res, 2004. **10**(20): p. 6897-904.
109. Alix-Panabieres, C. and K. Pantel, *Challenges in circulating tumour cell research*. Nat Rev Cancer, 2014. **14**(9): p. 623-31.
110. Yap, T.A., et al., *Circulating tumor cells: a multifunctional biomarker*. Clin Cancer Res, 2014. **20**(10): p. 2553-68.

111. Brinkmann, F., et al., *A Versatile Microarray Platform for Capturing Rare Cells*. Sci Rep, 2015. **5**: p. 15342.
112. Keller, L., S. Werner, and K. Pantel, *Biology and clinical relevance of EpCAM*. Cell Stress, 2019. **3**(6): p. 165-180.
113. Riethdorf, S., et al., *Clinical applications of the CellSearch platform in cancer patients*. Adv Drug Deliv Rev, 2018. **125**: p. 102-121.
114. Fachin, F., et al., *Monolithic Chip for High-throughput Blood Cell Depletion to Sort Rare Circulating Tumor Cells*. Sci Rep, 2017. **7**(1): p. 10936.
115. Hanssen, A., et al., *Characterization of different CTC subpopulations in non-small cell lung cancer*. Sci Rep, 2016. **6**: p. 28010.
116. Hanssen, A., et al., *Detection of Circulating Tumor Cells in Non-Small Cell Lung Cancer*. Front Oncol, 2015. **5**: p. 207.
117. Went, P.T., et al., *Frequent EpCam protein expression in human carcinomas*. Hum Pathol, 2004. **35**(1): p. 122-8.
118. Schneegans, S., et al., *Pre-analytical factors affecting the establishment of a single tube assay for multiparameter liquid biopsy detection in melanoma patients*. Mol Oncol, 2020. **14**(5): p. 1001-1015.
119. Pantel, K. and C. Alix-Panabieres, *Liquid biopsy and minimal residual disease - latest advances and implications for cure*. Nat Rev Clin Oncol, 2019.
120. Ligthart, S.T., et al., *Unbiased and automated identification of a circulating tumour cell definition that associates with overall survival*. PLoS One, 2011. **6**(11): p. e27419.
121. Poruk, K.E., et al., *Circulating Tumor Cells Expressing Markers of Tumor-Initiating Cells Predict Poor Survival and Cancer Recurrence in Patients with Pancreatic Ductal Adenocarcinoma*. Clin Cancer Res, 2017. **23**(11): p. 2681-2690.
122. Yu, M., et al., *Circulating breast tumor cells exhibit dynamic changes in epithelial and mesenchymal composition*. Science, 2013. **339**(6119): p. 580-4.
123. Riethdorf, S., et al., *Detection and HER2 expression of circulating tumor cells: prospective monitoring in breast cancer patients treated in the neoadjuvant GeparQuattro trial*. Clin Cancer Res, 2010. **16**(9): p. 2634-45.
124. Muller, V., et al., *Prognostic impact of circulating tumor cells assessed with the CellSearch System and AdnaTest Breast in metastatic breast cancer patients: the DETECT study*. Breast Cancer Res, 2012. **14**(4): p. R118.
125. Gorges, T.M., et al., *Accession of Tumor Heterogeneity by Multiplex Transcriptome Profiling of Single Circulating Tumor Cells*. Clin Chem, 2016. **62**(11): p. 1504-1515.
126. Ntzifa, A., et al., *Gene expression in circulating tumor cells reveals a dynamic role of EMT and PD-L1 during osimertinib treatment in NSCLC patients*. Sci Rep, 2021. **11**(1): p. 2313.
127. Lee, C.H., et al., *Cancer panel analysis of circulating tumor cells in patients with breast cancer*. Oncol Lett, 2018. **16**(1): p. 612-618.
128. Polzer, B., et al., *Molecular profiling of single circulating tumor cells with diagnostic intention*. EMBO Mol Med, 2014. **6**(11): p. 1371-86.
129. Alix-Panabieres, C. and K. Pantel, *Liquid biopsy in cancer patients: advances in capturing viable CTCs for functional studies using the EPISPOT assay*. Expert Rev Mol Diagn, 2015. **15**(11): p. 1411-7.
130. Ramirez, J.M., et al., *Prognostic Relevance of Viable Circulating Tumor Cells Detected by EPISPOT in Metastatic Breast Cancer Patients*. Clinical Chemistry, 2014. **60**(1): p. 214-221.

131. Cortes-Hernandez, L.E., S.Z. Eslami, and C. Alix-Panabieres, *Circulating tumor cell as the functional aspect of liquid biopsy to understand the metastatic cascade in solid cancer*. Mol Aspects Med, 2020. **72**: p. 100816.
132. Kulasinghe, A., et al., *Short term ex-vivo expansion of circulating head and neck tumour cells*. Oncotarget, 2016. **7**(37): p. 60101-60109.
133. Yu, M., et al., *Cancer therapy. Ex vivo culture of circulating breast tumor cells for individualized testing of drug susceptibility*. Science, 2014. **345**(6193): p. 216-20.
134. Zhang, L., et al., *The identification and characterization of breast cancer CTCs competent for brain metastasis*. Sci Transl Med, 2013. **5**(180): p. 180ra48.
135. Cayrefourcq, L., et al., *Establishment and characterization of a cell line from human circulating colon cancer cells*. Cancer Res, 2015. **75**(5): p. 892-901.
136. Zhao, P., et al., *Establishment and Characterization of a CTC Cell Line from Peripheral Blood of Breast Cancer Patient*. J Cancer, 2019. **10**(24): p. 6095-6104.
137. Brungs, D., et al., *Establishment of novel long-term cultures from EpCAM positive and negative circulating tumour cells from patients with metastatic gastroesophageal cancer*. Sci Rep, 2020. **10**(1): p. 539.
138. Aceto, N., et al., *Circulating tumor cell clusters are oligoclonal precursors of breast cancer metastasis*. Cell, 2014. **158**(5): p. 1110-22.
139. Gkoutela, S., et al., *Circulating Tumor Cell Clustering Shapes DNA Methylation to Enable Metastasis Seeding*. Cell, 2019. **176**(1-2): p. 98-112 e14.
140. Khoo, B.L., et al., *Short-term expansion of breast circulating cancer cells predicts response to anti-cancer therapy*. Oncotarget, 2015. **6**(17): p. 15578-93.
141. Hodgkinson, C.L., et al., *Tumorigenicity and genetic profiling of circulating tumor cells in small-cell lung cancer*. Nat Med, 2014. **20**(8): p. 897-903.
142. Williamson, S.C., et al., *Vasculogenic mimicry in small cell lung cancer*. Nat Commun, 2016. **7**: p. 13322.
143. Baccelli, I., et al., *Identification of a population of blood circulating tumor cells from breast cancer patients that initiates metastasis in a xenograft assay*. Nat Biotechnol, 2013. **31**(6): p. 539-44.
144. Morrow, C.J., et al., *Tumourigenic non-small-cell lung cancer mesenchymal circulating tumour cells: a clinical case study*. Ann Oncol, 2016. **27**(6): p. 1155-1160.
145. Alix-Panabieres, C. and K. Pantel, *Liquid Biopsy: From Discovery to Clinical Application*. Cancer Discov, 2021. **11**(4): p. 858-873.
146. Cristofanilli, M., et al., *Circulating tumor cells, disease progression, and survival in metastatic breast cancer*. N Engl J Med, 2004. **351**(8): p. 781-91.
147. de Bono, J.S., et al., *Circulating tumor cells predict survival benefit from treatment in metastatic castration-resistant prostate cancer*. Clin Cancer Res, 2008. **14**(19): p. 6302-9.
148. Cohen, S.J., et al., *Relationship of circulating tumor cells to tumor response, progression-free survival, and overall survival in patients with metastatic colorectal cancer*. J Clin Oncol, 2008. **26**(19): p. 3213-21.
149. Dawood, S., et al., *Circulating tumor cells in metastatic breast cancer: from prognostic stratification to modification of the staging system? Cancer*, 2008. **113**(9): p. 2422-30.
150. Pierga, J.Y., et al., *High independent prognostic and predictive value of circulating tumor cells compared with serum tumor markers in a large prospective trial in first-line chemotherapy for metastatic breast cancer patients*. Ann Oncol, 2012. **23**(3): p. 618-624.

151. Scher, H.I., et al., *Circulating Tumor Cell Biomarker Panel As an Individual-Level Surrogate for Survival in Metastatic Castration-Resistant Prostate Cancer*. Journal of Clinical Oncology, 2015. **33**(12): p. 1348-+.
152. Chaudhuri, A.A., et al., *Early Detection of Molecular Residual Disease in Localized Lung Cancer by Circulating Tumor DNA Profiling*. Cancer Discov, 2017. **7**(12): p. 1394-1403.
153. Haselmann, V., et al., *Liquid Profiling of Circulating Tumor DNA in Plasma of Melanoma Patients for Companion Diagnostics and Monitoring of BRAF Inhibitor Therapy*. Clin Chem, 2018. **64**(5): p. 830-842.
154. Trapp, E., et al., *Presence of Circulating Tumor Cells in High-Risk Early Breast Cancer During Follow-Up and Prognosis*. J Natl Cancer Inst, 2019. **111**(4): p. 380-387.
155. Sparano, J., et al., *Association of Circulating Tumor Cells With Late Recurrence of Estrogen Receptor-Positive Breast Cancer: A Secondary Analysis of a Randomized Clinical Trial*. JAMA Oncol, 2018. **4**(12): p. 1700-1706.
156. Gebhardt, F., K.S. Zanker, and B. Brandt, *Differential expression of alternatively spliced c-erbB-2 mRNA in primary tumors, lymph node metastases, and bone marrow micrometastases from breast cancer patients*. Biochem Biophys Res Commun, 1998. **247**(2): p. 319-23.
157. Fehm, T., et al., *HER2 status of circulating tumor cells in patients with metastatic breast cancer: a prospective, multicenter trial*. Breast Cancer Res Treat, 2010. **124**(2): p. 403-12.
158. Heller, G., et al., *Circulating Tumor Cell Number as a Response Measure of Prolonged Survival for Metastatic Castration-Resistant Prostate Cancer: A Comparison With Prostate-Specific Antigen Across Five Randomized Phase III Clinical Trials*. J Clin Oncol, 2018. **36**(6): p. 572-580.
159. Cristofanilli, M., et al., *The clinical use of circulating tumor cells (CTCs) enumeration for staging of metastatic breast cancer (MBC): International expert consensus paper*. Crit Rev Oncol Hematol, 2019. **134**: p. 39-45.
160. Lorente, D., et al., *Decline in Circulating Tumor Cell Count and Treatment Outcome in Advanced Prostate Cancer*. Eur Urol, 2016. **70**(6): p. 985-992.
161. Bidard, F.C., et al., *Clinical validity of circulating tumour cells in patients with metastatic breast cancer: a pooled analysis of individual patient data*. Lancet Oncol, 2014. **15**(4): p. 406-14.
162. Okegawa, T., et al., *Circulating Tumor Cells as a Biomarker Predictive of Sensitivity to Docetaxel Chemotherapy in Patients with Castration-resistant Prostate Cancer*. Anticancer Research, 2014. **34**(11): p. 6705-6710.
163. Antonarakis, E.S., et al., *Clinical Significance of Androgen Receptor Splice Variant-7 mRNA Detection in Circulating Tumor Cells of Men With Metastatic Castration-Resistant Prostate Cancer Treated With First- and Second-Line Abiraterone and Enzalutamide*. J Clin Oncol, 2017. **35**(19): p. 2149-2156.
164. Nakazawa, M., et al., *Serial blood-based analysis of AR-V7 in men with advanced prostate cancer*. Ann Oncol, 2015. **26**(9): p. 1859-65.
165. Antonarakis, E.S., et al., *Androgen Receptor Splice Variant 7 and Efficacy of Taxane Chemotherapy in Patients With Metastatic Castration-Resistant Prostate Cancer*. JAMA Oncol, 2015. **1**(5): p. 582-91.
166. Buijs, J.T. and G. van der Pluijm, *Osteotropic cancers: from primary tumor to bone*. Cancer Lett, 2009. **273**(2): p. 177-93.
167. Koch, C., et al., *Pre-Analytical and Analytical Variables of Label-Independent Enrichment and Automated Detection of Circulating Tumor Cells in Cancer Patients*. Cancers (Basel), 2020. **12**(2).

168. Liu, H.Y., et al., *Evaluation of Microfluidic Ceiling Designs for the Capture of Circulating Tumor Cells on a Microarray Platform*. Adv Biosyst, 2020. **4**(2): p. e1900162.
169. Neves, R.P.L., et al., *Proficiency Testing to Assess Technical Performance for CTC-Processing and Detection Methods in CANCER-ID*. Clin Chem, 2021.
170. Hvichia, G.E., et al., *A novel microfluidic platform for size and deformability based separation and the subsequent molecular characterization of viable circulating tumor cells*. Int J Cancer, 2016. **138**(12): p. 2894-904.
171. El-Heliebi, A., et al., *In Situ Detection and Quantification of AR-V7, AR-FL, PSA, and KRAS Point Mutations in Circulating Tumor Cells*. Clin Chem, 2018.
172. Janning, M., et al., *Determination of PD-L1 Expression in Circulating Tumor Cells of NSCLC Patients and Correlation with Response to PD-1/PD-L1 Inhibitors*. Cancers (Basel), 2019. **11**(6).
173. Chudziak, J., et al., *Clinical evaluation of a novel microfluidic device for epitope-independent enrichment of circulating tumour cells in patients with small cell lung cancer*. Analyst, 2016. **141**(2): p. 669-78.
174. Franken, A., et al., *Label-Free Enrichment and Molecular Characterization of Viable Circulating Tumor Cells from Diagnostic Leukapheresis Products*. Clin Chem, 2019. **65**(4): p. 549-558.
175. Yoneda, K., et al., *Detection of circulating tumor cells with a novel microfluidic system in malignant pleural mesothelioma*. Cancer Sci, 2019. **110**(2): p. 726-733.
176. Jiang, J., et al., *An integrated microfluidic device for rapid and high-sensitivity analysis of circulating tumor cells*. Sci Rep, 2017. **7**: p. 42612.
177. Pecot, C.V., et al., *A novel platform for detection of CK+ and CK- CTCs*. Cancer Discov, 2011. **1**(7): p. 580-6.
178. Ozkumur, E., et al., *Inertial focusing for tumor antigen-dependent and -independent sorting of rare circulating tumor cells*. Sci Transl Med, 2013. **5**(179): p. 179ra47.
179. Gorges, K., et al., *Intra-Patient Heterogeneity of Circulating Tumor Cells and Circulating Tumor DNA in Blood of Melanoma Patients*. Cancers (Basel), 2019. **11**(11).
180. Donato, C., et al., *Hypoxia Triggers the Intravasation of Clustered Circulating Tumor Cells*. Cell Rep, 2020. **32**(10): p. 108105.
181. Mu, Z., et al., *Prospective assessment of the prognostic value of circulating tumor cells and their clusters in patients with advanced-stage breast cancer*. Breast Cancer Res Treat, 2015. **154**(3): p. 563-71.
182. Wang, C., et al., *Longitudinally collected CTCs and CTC-clusters and clinical outcomes of metastatic breast cancer*. Breast Cancer Res Treat, 2017. **161**(1): p. 83-94.
183. Thangavel, H., et al., *A CTC-Cluster-Specific Signature Derived from OMICS Analysis of Patient-Derived Xenograft Tumors Predicts Outcomes in Basal-Like Breast Cancer*. J Clin Med, 2019. **8**(11).
184. Project, E.-I. *CANCER-ID*. 2015 11.10.2021]; Available from: <https://www.cancer-id.eu/>.
185. Fehm, T.N., et al., *Diagnostic leukapheresis for CTC analysis in breast cancer patients: CTC frequency, clinical experiences and recommendations for standardized reporting*. Cytometry A, 2018. **93**(12): p. 1213-1219.
186. Stoecklein, N.H., et al., *Challenges for CTC-based liquid biopsies: low CTC frequency and diagnostic leukapheresis as a potential solution*. Expert Rev Mol Diagn, 2016. **16**(2): p. 147-64.
187. Hamburg-Eppendorf, U., *European Liquid Biopsy Society (ELBS)*. 2019.
188. Fidler, I.J., *The relationship of embolic homogeneity, number, size and viability to the incidence of experimental metastasis*. Eur J Cancer, 1973. **9**(3): p. 223-7.

189. Pantel, K., C. Hille, and H.I. Scher, *Circulating Tumor Cells in Prostate Cancer: From Discovery to Clinical Utility*. Clin Chem, 2019. **65**(1): p. 87-99.
190. Koch, C., et al., *Characterization of circulating breast cancer cells with tumorigenic and metastatic capacity*. EMBO Mol Med, 2020. **12**(9): p. e11908.
191. Sflomos, G., et al., *A Preclinical Model for ERalpha-Positive Breast Cancer Points to the Epithelial Microenvironment as Determinant of Luminal Phenotype and Hormone Response*. Cancer Cell, 2016. **29**(3): p. 407-22.
192. Bae, S.N., et al., *Molecular and cellular analysis of basement membrane invasion by human breast cancer cells in Matrigel-based in vitro assays*. Breast Cancer Res Treat, 1993. **24**(3): p. 241-55.
193. Dai, X., et al., *Breast Cancer Cell Line Classification and Its Relevance with Breast Tumor Subtyping*. J Cancer, 2017. **8**(16): p. 3131-3141.
194. Cancer Genome Atlas, N., *Comprehensive molecular portraits of human breast tumours*. Nature, 2012. **490**(7418): p. 61-70.
195. Parker, J.S., et al., *Supervised risk predictor of breast cancer based on intrinsic subtypes*. J Clin Oncol, 2009. **27**(8): p. 1160-7.
196. Ye, X. and R.A. Weinberg, *Epithelial-Mesenchymal Plasticity: A Central Regulator of Cancer Progression*. Trends Cell Biol, 2015. **25**(11): p. 675-86.
197. Mani, S.A., et al., *The epithelial-mesenchymal transition generates cells with properties of stem cells*. Cell, 2008. **133**(4): p. 704-15.
198. Fischer, K.R., et al., *Epithelial-to-mesenchymal transition is not required for lung metastasis but contributes to chemoresistance*. Nature, 2015. **527**(7579): p. 472-6.
199. Liu, X., et al., *Epithelial-type systemic breast carcinoma cells with a restricted mesenchymal transition are a major source of metastasis*. Sci Adv, 2019. **5**(6): p. eaav4275.
200. Bukholm, I.K., J.M. Nesland, and A.L. Borresen-Dale, *Re-expression of E-cadherin, alpha-catenin and beta-catenin, but not of gamma-catenin, in metastatic tissue from breast cancer patients [see comments]*. J Pathol, 2000. **190**(1): p. 15-9.
201. Jeschke, U., et al., *Expression of sialyl lewis X, sialyl Lewis A, E-cadherin and cathepsin-D in human breast cancer: immunohistochemical analysis in mammary carcinoma in situ, invasive carcinomas and their lymph node metastasis*. Anticancer Res, 2005. **25**(3A): p. 1615-22.
202. Kowalski, P.J., M.A. Rubin, and C.G. Kleer, *E-cadherin expression in primary carcinomas of the breast and its distant metastases*. Breast Cancer Res, 2003. **5**(6): p. R217-22.
203. Friedl, P. and D. Gilmour, *Collective cell migration in morphogenesis, regeneration and cancer*. Nat Rev Mol Cell Biol, 2009. **10**(7): p. 445-57.
204. Al-Hajj, M., et al., *Prospective identification of tumorigenic breast cancer cells*. Proc Natl Acad Sci U S A, 2003. **100**(7): p. 3983-8.
205. Dean, M., T. Fojo, and S. Bates, *Tumour stem cells and drug resistance*. Nat Rev Cancer, 2005. **5**(4): p. 275-84.
206. Balic, M., et al., *Most early disseminated cancer cells detected in bone marrow of breast cancer patients have a putative breast cancer stem cell phenotype*. Clin Cancer Res, 2006. **12**(19): p. 5615-21.
207. Ginestier, C., et al., *ALDH1 is a marker of normal and malignant human mammary stem cells and a predictor of poor clinical outcome*. Cell Stem Cell, 2007. **1**(5): p. 555-67.
208. Charafe-Jauffret, E., et al., *Aldehyde dehydrogenase 1-positive cancer stem cells mediate metastasis and poor clinical outcome in inflammatory breast cancer*. Clin Cancer Res, 2010. **16**(1): p. 45-55.

209. Liu, S.L., et al., *Breast Cancer Stem Cells Transition between Epithelial and Mesenchymal States Reflective of their Normal Counterparts*. Stem Cell Reports, 2014. **2**(1): p. 78-91.
210. Colacino, J.A., et al., *Heterogeneity of Human Breast Stem and Progenitor Cells as Revealed by Transcriptional Profiling*. Stem Cell Reports, 2018. **10**(5): p. 1596-1609.
211. Liu, Y., et al., *ALDH1A1 expression correlates with clinicopathologic features and poor prognosis of breast cancer patients: a systematic review and meta-analysis*. BMC Cancer, 2014. **14**: p. 444.
212. Kida, K., et al., *Effect of ALDH1 on prognosis and chemoresistance by breast cancer subtype*. Breast Cancer Res Treat, 2016. **156**(2): p. 261-9.
213. Zhong, Y., et al., *ALDH1 is a better clinical indicator for relapse of invasive ductal breast cancer than the CD44+/CD24- phenotype*. Med Oncol, 2014. **31**(3): p. 864.
214. Ricardo, S., et al., *Breast cancer stem cell markers CD44, CD24 and ALDH1: expression distribution within intrinsic molecular subtype*. J Clin Pathol, 2011. **64**(11): p. 937-46.
215. Rennstam, K., et al., *Numb protein expression correlates with a basal-like phenotype and cancer stem cell markers in primary breast cancer*. Breast Cancer Res Treat, 2010. **122**(2): p. 315-24.
216. Pece, S., et al., *NUMB-ing down cancer by more than just a NOTCH*. Biochim Biophys Acta, 2011. **1815**(1): p. 26-43.
217. Krishna, B.M., et al., *Notch signaling in breast cancer: From pathway analysis to therapy*. Cancer Lett, 2019. **461**: p. 123-131.
218. Lee, C.W., et al., *Molecular dependence of estrogen receptor-negative breast cancer on a notch-survivin signaling axis*. Cancer Res, 2008. **68**(13): p. 5273-81.
219. Reedijk, M., et al., *High-level coexpression of JAG1 and NOTCH1 is observed in human breast cancer and is associated with poor overall survival*. Cancer Res, 2005. **65**(18): p. 8530-7.
220. Colaluca, I.N., et al., *NUMB controls p53 tumour suppressor activity*. Nature, 2008. **451**(7174): p. 76-80.
221. Donehower, L.A., et al., *Integrated Analysis of TP53 Gene and Pathway Alterations in The Cancer Genome Atlas*. Cell Rep, 2019. **28**(11): p. 3010.
222. Osborne, R.J., et al., *Mutations in the p53 gene in primary human breast cancers*. Cancer Res, 1991. **51**(22): p. 6194-8.
223. Xian, J., et al., *Progress in the research of p53 tumour suppressor activity controlled by Numb in triple-negative breast cancer*. J Cell Mol Med, 2020. **24**(13): p. 7451-7459.
224. Frum, R.A. and S.R. Grossman, *Mechanisms of mutant p53 stabilization in cancer*. Subcell Biochem, 2014. **85**: p. 187-97.
225. Yue, X., et al., *Mutant p53 in Cancer: Accumulation, Gain-of-Function, and Therapy*. J Mol Biol, 2017. **429**(11): p. 1595-1606.
226. Mantovani, F., L. Collavin, and G. Del Sal, *Mutant p53 as a guardian of the cancer cell*. Cell Death Differ, 2019. **26**(2): p. 199-212.
227. Cope, L.M., et al., *Do breast cancer cell lines provide a relevant model of the patient tumor methylome?* PLoS One, 2014. **9**(8): p. e105545.
228. Hess, K.R., et al., *Metastatic patterns in adenocarcinoma*. Cancer, 2006. **106**(7): p. 1624-33.
229. Finn, R.S., et al., *The cyclin-dependent kinase 4/6 inhibitor palbociclib in combination with letrozole versus letrozole alone as first-line treatment of oestrogen receptor-positive, HER2-negative, advanced breast cancer (PALOMA-1/TRIO-18): a randomised phase 2 study*. Lancet Oncol, 2015. **16**(1): p. 25-35.
230. Finn, R.S., et al., *Palbociclib and Letrozole in Advanced Breast Cancer*. N Engl J Med, 2016. **375**(20): p. 1925-1936.

231. Finn, R.S., et al., *Efficacy and safety of palbociclib in combination with letrozole as first-line treatment of ER-positive, HER2-negative, advanced breast cancer: expanded analyses of subgroups from the randomized pivotal trial PALOMA-1/TRIO-18*. *Breast Cancer Res*, 2016. **18**(1): p. 67.
232. Lallo, A., et al., *Circulating tumor cells and CDX models as a tool for preclinical drug development*. *Transl Lung Cancer Res*, 2017. **6**(4): p. 397-408.
233. Sachs, N., et al., *A Living Biobank of Breast Cancer Organoids Captures Disease Heterogeneity*. *Cell*, 2018. **172**(1-2): p. 373-386 e10.
234. Litwin, M.S. and H.J. Tan, *The Diagnosis and Treatment of Prostate Cancer: A Review*. *JAMA*, 2017. **317**(24): p. 2532-2542.
235. Mostaghel, E.A., B. Montgomery, and P.S. Nelson, *Castration-resistant prostate cancer: targeting androgen metabolic pathways in recurrent disease*. *Urol Oncol*, 2009. **27**(3): p. 251-7.
236. Kirby, M., C. Hirst, and E.D. Crawford, *Characterising the castration-resistant prostate cancer population: a systematic review*. *Int J Clin Pract*, 2011. **65**(11): p. 1180-92.
237. Scher, H.I., et al., *Design and end points of clinical trials for patients with progressive prostate cancer and castrate levels of testosterone: recommendations of the Prostate Cancer Clinical Trials Working Group*. *J Clin Oncol*, 2008. **26**(7): p. 1148-59.
238. Luo, J., et al., *Role of Androgen Receptor Variants in Prostate Cancer: Report from the 2017 Mission Androgen Receptor Variants Meeting*. *Eur Urol*, 2018. **73**(5): p. 715-723.
239. Mateo, J., et al., *Managing Nonmetastatic Castration-resistant Prostate Cancer*. *Eur Urol*, 2019. **75**(2): p. 285-293.
240. Scher, H.I., et al., *Circulating tumor cell biomarker panel as an individual-level surrogate for survival in metastatic castration-resistant prostate cancer*. *J Clin Oncol*, 2015. **33**(12): p. 1348-55.
241. Joseph, J.D., et al., *A clinically relevant androgen receptor mutation confers resistance to second-generation antiandrogens enzalutamide and ARN-509*. *Cancer Discov*, 2013. **3**(9): p. 1020-9.
242. Korpai, M., et al., *An F876L mutation in androgen receptor confers genetic and phenotypic resistance to MDV3100 (enzalutamide)*. *Cancer Discov*, 2013. **3**(9): p. 1030-43.
243. Azad, A.A., et al., *Androgen Receptor Gene Aberrations in Circulating Cell-Free DNA: Biomarkers of Therapeutic Resistance in Castration-Resistant Prostate Cancer*. *Clin Cancer Res*, 2015. **21**(10): p. 2315-24.
244. Liu, L.L., et al., *Mechanisms of the androgen receptor splicing in prostate cancer cells*. *Oncogene*, 2014. **33**(24): p. 3140-50.
245. Watson, P.A., et al., *Constitutively active androgen receptor splice variants expressed in castration-resistant prostate cancer require full-length androgen receptor*. *Proc Natl Acad Sci U S A*, 2010. **107**(39): p. 16759-65.
246. De Laere, B., et al., *Comprehensive Profiling of the Androgen Receptor in Liquid Biopsies from Castration-resistant Prostate Cancer Reveals Novel Intra-AR Structural Variation and Splice Variant Expression Patterns*. *Eur Urol*, 2017. **72**(2): p. 192-200.
247. Sharp, A., et al., *Androgen receptor splice variant-7 expression emerges with castration resistance in prostate cancer*. *J Clin Invest*, 2019. **129**(1): p. 192-208.
248. Scher, H.I., et al., *Association of AR-V7 on Circulating Tumor Cells as a Treatment-Specific Biomarker With Outcomes and Survival in Castration-Resistant Prostate Cancer*. *JAMA Oncol*, 2016. **2**(11): p. 1441-1449.

249. Armstrong, A.J., et al., *Prospective Multicenter Study of Circulating Tumor Cell AR-V7 and Taxane Versus Hormonal Treatment Outcomes in Metastatic Castration-Resistant Prostate Cancer*. JCO Precis Oncol, 2020. **4**.
250. Onstenk, W., et al., *Efficacy of Cabazitaxel in Castration-resistant Prostate Cancer Is Independent of the Presence of AR-V7 in Circulating Tumor Cells*. Eur Urol, 2015. **68**(6): p. 939-45.
251. Hille, C., et al., *Detection of Androgen Receptor Variant 7 (ARV7) mRNA Levels in EpCAM-Enriched CTC Fractions for Monitoring Response to Androgen Targeting Therapies in Prostate Cancer*. Cells, 2019. **8**(9).
252. Xu, L., et al., *The Novel Association of Circulating Tumor Cells and Circulating Megakaryocytes with Prostate Cancer Prognosis*. Clin Cancer Res, 2017. **23**(17): p. 5112-5122.
253. Markou, A., et al., *Multiplex Gene Expression Profiling of In Vivo Isolated Circulating Tumor Cells in High-Risk Prostate Cancer Patients*. Clin Chem, 2018. **64**(2): p. 297-306.
254. de Wit, S., et al., *EpCAM(high) and EpCAM(low) circulating tumor cells in metastatic prostate and breast cancer patients*. Oncotarget, 2018. **9**(86): p. 35705-35716.
255. Yang, Y.J., et al., *Phenotypes of circulating tumour cells predict time to castration resistance in metastatic castration-sensitive prostate cancer*. BJU Int, 2019. **124**(2): p. 258-267.
256. Haslehurst, A.M., et al., *EMT transcription factors snail and slug directly contribute to cisplatin resistance in ovarian cancer*. BMC Cancer, 2012. **12**: p. 91.
257. To, S.Q., et al., *Expression of Androgen Receptor Splice Variant 7 or 9 in Whole Blood Does Not Predict Response to Androgen-Axis-targeting Agents in Metastatic Castration-resistant Prostate Cancer*. Eur Urol, 2018. **73**(6): p. 818-821.
258. Lu, D., et al., *Development of an immunofluorescent AR-V7 circulating tumor cell assay - A blood-based test for men with metastatic prostate cancer*. J Circ Biomark, 2020. **9**: p. 13-19.
259. Lovf, M., et al., *Multifocal Primary Prostate Cancer Exhibits High Degree of Genomic Heterogeneity*. Eur Urol, 2019. **75**(3): p. 498-505.
260. Graf, R.P., et al., *Clinical Utility of the Nuclear-localized AR-V7 Biomarker in Circulating Tumor Cells in Improving Physician Treatment Choice in Castration-resistant Prostate Cancer*. Eur Urol, 2020. **77**(2): p. 170-177.
261. Bidard, F.C., et al., *Efficacy of Circulating Tumor Cell Count-Driven vs Clinician-Driven First-line Therapy Choice in Hormone Receptor-Positive, ERBB2-Negative Metastatic Breast Cancer: The STIC CTC Randomized Clinical Trial*. JAMA Oncol, 2021. **7**(1): p. 34-41.

7. Declaration of Contribution

The publications listed below are arranged according to their order within this thesis, independent of the time point of release. The current impact factors (IF) of each journal are included in brackets.

7.1. Pre-Analytical and Analytical Variables of Label-Independent Enrichment and Automated Detection of Circulating Tumor Cells in Cancer Patients - *Cancers* (2020) [IF: 6.639]

The initial idea for this project was developed by Prof. Dr. Klaus Pantel and Dr. Tobias Gorges. In my PhD, I took over the planning of necessary experiments and their implementation independently. From culturing of the cell lines, determining the average cell size, performing spike-in experiments with healthy blood donors, staining the generated slides, to performing whole genome amplification of single cells and processing the cancer patient samples, the experiments were conducted by myself. The only steps in this project directly performed by others were the picking of single cells for whole genome amplification, which was done by Desiree Loreth, the statistical analyses, by Simon A. Jossee, and the evaluation of slides using the XCyto, which was performed by Svenja Schneegans and Okka J.W. Wilken.

Furthermore, the experiments of all result sections within this manuscript were planned by myself. As were the summary and evaluation of the generated data. The data was interpreted in consultation with Prof. Pantel who provided valuable guidance and support. Additionally, I wrote the first manuscript draft, designed all figures (with exception of Figure 1 and 2A) and generated all tables. I was also responsible for rewriting the manuscript to its final version and tasked with its submission as well as conducting the revision process prior to final publication.



Claudia Koch



Prof. Dr. med. Klaus Pantel

7.2. Evaluation of Microfluidic Ceiling Designs for the Capture of Circulating Tumor Cells on a Microarray Platform - *Advanced Biosystems (2019)* [IF: 3.536]

This project had been initiated by Prof. Dr. Klaus Pantel and Prof. Harald Fuchs and already resulted in a first publication [111]. It was a joint project between the University Medical Center Hamburg-Eppendorf (UKE) and the Karlsruhe Institute of Technology (KIT) supported by an ERC grant given to Prof. Pantel. The experiments were therefore divided to two different sites. While the KIT was mainly involved in technical and physical aspects (production of the chips, optimization of chip design), the UKE was involved in the biological and clinical testing. Together with Prof. Pantel, I planned the necessary experiments and aided in their conduction. These were the basis of sections 2.2 to 2.4. of the results section within this publication. I provided detailed experimental plans as well as practical laboratory aid for Hui Yu Liu and Ludwig J. Horst, who manually performed most experiments. I also performed whole genome amplification and subsequent visualization, demonstrating feasibility of our work-flow for downstream genomic analysis of single tumor cells. The evaluation, summary and analysis of the generated data were performed by myself. The data was interpreted in consultation with Prof. Pantel who provided valuable guidance and support. Additionally, I was substantially involved in writing the first manuscript draft, with a special focus on the biological aspects of the paper. I furthermore designed selected figures (3A, 5, Figure S2) and tables (Tables S1 and S2). I was also involved in fine-tuning the manuscript to its final version and substantially contributed to the revision process prior to final publication.



Claudia Koch



Prof. Dr. med. Klaus Pantel

7.3. Proficiency testing to assess technical performance for CTC-processing and detection methods in CANCER-ID – *Clinical Chemistry* (2021) [IF: 8.327]

CANCER-ID was a public-private partnership spearheaded by Prof. Dr. Klaus Pantel (academia) and Dr. Thomas Schlange (EFPIA industry) and supported by Europe's Innovative Medicines Initiative (IMI). It was a collaboration between 40 international partners from academia and industry, based predominantly in Europe, aiming at the establishment of standardized protocols for and clinical validation of blood-based biomarkers. In this publication, the performance of 5 different CTC enrichment technologies was directly compared in a large multi-national effort. In preparation for this manuscript, I intensively tested the Siemens and Parsortix® platforms and collaborated in the refinement of the protocols used within the ring trials through my results. Within this publication, I performed the ring-trial experiments for the Siemens and Parsortix devices at the UKE site. To this end, I processed the spike-in blood samples of both non-small lung cancer (NSCLC) cell lines, using the Siemens and Parsortix devices and performed the subsequent microscopic quantification of detected tumor cells. The results of this work are included in multiple figures (2B, 3A-D) and in result section "recovery of spiked cells using different technologies". As a co-author I did not write the first manuscript draft but contributed to fine-tuning the manuscript to its final version.



Claudia Koch



Prof. Dr. med. Klaus Pantel

7.4. Characterization of Circulating Breast Cancer Cells with Tumorigenic and Metastatic Capacity – *EMBO Molecular Medicine* (2020) [IF: 12.1]

This project was initiated by Prof. Dr. Klaus Pantel and Dr. Sabine Riethdorf. The CTC-ITB-01 cell line had been isolated by Dr. Andra Kuske and first morphological and phenotypical characterization had begun. My role in this project was to collect, evaluate, and structure the existing data as well as initiate the necessary analyses to complement and hone the knowledge collected. The contributing co-authors provided relevant data and performed experiments at their respective sites. Together with Prof. Pantel, I planned and executed the remaining necessary experiments. These were the basis of figure 5A,B, Figure EV2 A, Figure EV4 B, and Figure EV5 of the results section within this publication. The evaluation, summary and analysis of the generated data were performed by myself. The data was interpreted in consultation with Prof. Pantel and the respective co-authors, who provided valuable guidance and support. Additionally, I prepared the manuscript concept and wrote the first manuscript draft, finalized all figures and generated the table EV1. I was also significantly involved in rewriting the manuscript to its final version and tasked with its submission as well as conducting the revision process prior to final publication.



Claudia Koch



Prof. Dr. med. Klaus Pantel

7.5. In situ Detection and Quantification of AR-V7, AR-FL, PSA, and KRAS point mutations in circulating tumor cells – *Clinical Chemistry (2018)* [IF: 8.327]

This project was initiated by Prof. Dr. Klaus Pantel, Dr. Tobias Gorges and Dr. Amin El-Heliebi. The *in-situ* detection approach had been established in Dr. Amin El-Heliebi group and first experiments with *KRAS* detection in pancreatic cancer patients had begun. A collaboration was set up by Dr. Tobias Gorges and myself with Dr. Amin El-Heliebi to extend this promising method to the detection of *ARV7* transcripts in prostate cancer. For this, I performed Parsortix®-based enrichment of defined prostate cancer cell lines in whole blood to assess the performance of the in situ detection (Figure 1 A-F). Furthermore, our suggestion of combining *in-situ* *ARV7*, *PSA* and *AR-FL* detection with an immunocytochemical staining for keratin, CD45 and DAPI, provided added value to the existing assay. My role in this project was furthermore to collect clinical samples from prostate cancer patients, enrich the CTC fractions, store the corresponding sample slides and send these for evaluation to Dr. El-Heliebi's group (data for Figure 3, Figure 4). The generated data was interpreted in consultation with Dr. El-Heliebi and Prof. Pantel. As shared first author, I collaborated with the other co-authors in designing the manuscript concept and significantly contributed to writing the first manuscript draft. I was furthermore involved in rewriting the manuscript to its final version and aiding in the revision process prior to final publication.



Claudia Koch



Prof. Dr. med. Klaus Pantel

7.6. Detection of Androgen Receptor Variant (ARV7) mRNA Levels in EpCAM-enriched CTC Fractions for Monitoring Response to Androgen Targeting Therapies – *Cells* (2019) [IF: 6.600]

This project was initiated by Prof. Dr. Klaus Pantel and Dr. Tobias Gorges. The aim was to design a CellSearch® based method to detect *ARV7* in CTCs of prostate cancer patients and to have this method included into upcoming clinical trials. In my PhD, I took over the planning of necessary experiments and their implementation independently. From culturing of the cell lines, performing spike-in experiments with healthy blood donors, comparing RNA-isolation kits, designing adequate PCR primers, to performing qPCR runs the experiments were conducted by myself. My role was furthermore to collect and process the prostate cancer patient samples following technical validation of the developed *ARV7* detection assay. The only experiments in this project directly performed by others were the immunocytochemical stainings for *ARV7* and *AR-FL* protein, which were performed by the group of Catherine Alix-Panabières from the University of Montpellier. Furthermore, the experiments of all result sections within this manuscript were planned by myself, as were the summary and evaluation of the generated data. The data was interpreted in consultation with Prof. Pantel who provided valuable guidance and support. Additionally, I prepared the manuscript concept, wrote the first manuscript draft, designed and finalized all figures and generated all tables. I was also responsible for rewriting the manuscript to its final version and tasked with its submission as well as conducting the revision process prior to final publication.

The *ARV7* detection assay developed in this thesis was chosen for inclusion into a large multicenter clinical trial by a leading pharmaceutical company, which was unfortunately cancelled following slow initial patient enrollment and recruitment.



Claudia Koch



Prof. Dr. med. Klaus Pantel

8. Abbreviations

Abbreviation	Meaning
AB-serum	Human serum, type AB
ADT	Androgen deprivation therapy
ALDH	Aldehyde dehydrogenase 2
ANOVA	Analysis of variance
APC	Allophycocyanin
AR	Androgen receptor
AR-FL	Androgen receptor full length
ARV7	Androgen receptor variant 7
BC	Breast cancer
Bcl-2	B-cell lymphoma 2
BCT	Blood collection tube
BM	Bone metastasis
bp	Base pair
BSA	Bovine serum albumin
CD	Cluster of differentiation
CDH1	E-cadherin
CDK	Cyclin-dependent kinase
cDNA	Complementary DNA
CDX	CTC-derived explant
CK	Cytokeratin
CL	Cell line
CNA	Copy number aberration/alteration
Cq	Cycle of quantification
CRCa	Colorectal carcinoma
CRPC	Castration resistant prostate cancer
CS	CellSearch®
CSC	Cancer stem cell

Abbreviations

CSF	Cerebral spinal fluid
cT	Clinical tumor stage
CT	Computed tomography scan
CTC	Circulating tumor cell
ctDNA	Circulating tumor DNA
CYP17A1	Cytochrome-P450 family 17 A polypeptide 1
Da	Dalton
DAB	3,3-diaminobenzidine
DAPI	4',6-Diamidin-2-phenylindol
DEAB	Diethylaminobenzaldehyde
DFS	Disease-free survival
DHT	5 α -dihydroxytestosterone
DLA	Diagnostic leukapheresis
DMEM	Dulbecco's Modified Eagle Medium
DMSO	Dimethyl sulfoxide
DNA	Deoxyribonucleic acid
DTC	Disseminated tumor cell
ECM	Extracellular matrix
EDTA	Ethylenediaminetetraacetic acid
EGF	Epidermal growth factor
EGFR	Epidermal growth factor receptor
EMT	Epithelial-mesenchymal transition
EpCAM	Epithelial cell adhesion molecule
EPISPOT	Epithelial immune spot technology
ER	Estrogen receptor
ERBB2	Erb-b2 receptor tyrosine kinase 2 (alias HER2)
ET	Endocrine therapy
et al.	Et alii / et aliæ
E2	17- β -estradiol
FACS	Fluorescence-activated cell sorting
FCS	Fetal calf serum

Abbreviations

FDA	US Food and Drug Administration
FFPE	Formalin fixes paraffin embedded
FGF2	Fibroblast growth factor 2
FISH	Fluorescence <i>in situ</i> hybridisation
FITC	Fluorescein
gDNA	Genomic DNA
GFP	Green fluorescent protein
GIC	Gastrointestinal cancer
GLM	Generalized linear fixed-effects model
GnRH	Gonotropin-releasing hormone
h	hour
HD	Healthy donor
HER2	Human epidermal growth factor receptor 2 (alias ERBB2)
HR	Hormone receptor
IC50	Half maximal inhibitory concentration
ICC	Immunocytochemistry
IDC	Invasive ductal carcinoma
IF	Immunofluorescence
IgG	Immunglobulin G
IHC	Immunohistochemistry
ILC	Invasive lobular carcinoma
k	Kilo-
K	Keratin
k.d.	Knock down
Ki-67	Marker of proliferation Ki-67
L	Localized
LDH	Lactate dehydrogenase
LH	Luteinizing hormone
LOH	Loss of heterozygosity
luc	Luciferase
m	Milli-

Abbreviations

m	Metastatic
M	Molar
MAF	Minor allele frequency
MET	Mesenchymal-epithelial transition
min	Minute
MMP	Matrix metalloprotease
mo	Month
MRD	Minimal residual disease
MRI	Magnetic resonance imaging
mRNA	Messenger ribonucleic acid
mut	Mutant
M0	Without metastasis
M1	Metastasis diagnosed
n/N	Amount of experimental repetitions
n	Nano-
NHT	Novel hormonal therapy
NOTCH	Notch receptor 1
NSCLC	Non-small cell lung cancer
NSG	NOD scid gamma
NUMB	NUMB endocytic adaptor protein
OPG	Osteoprotegrin
OS	Overall survival
PAM50	50-gene signature classifier for breast cancer
PaCa	Pancreatic cancer
PBMC	Peripheral blood mononuclear cell
PBS	Phosphate buffered saline
PC / PCa	Prostate cancer
PCR	Polymerase chain reaction
PDMS	Polydimethylsiloxane
PDX	Patient-derived xenograft
Pen/Strep	Penicillin/Streptomycin

Abbreviations

PET	Positron emission tomography
PFA	Paraformaldehyde
PFS	Progression free survival
PIK3CA	Phosphoinositide-3-kinase, catalytic, alpha polypeptide
PR	Progesterone receptor
PSA	Prostate specific antigen
PSMA	Prostate specific membrane antigen
P53	Tumor protein 53
QC	Quality control
qPCR	Quantitative PCR
RCP	Rolling circle product
ROH	Runs of homozygosity
rpm	Rounds per minute
RPMI	Roswell Park Memorial Institute Medium
RT	Room temperature
SCLC	Small cell lung cancer
scr	Scramble
SHB	Staggered herringbone
shRNA	Short/small hairpin RNA
TBST	Tris-buffered saline
TGF β	Transforming growth factor beta
TME	Tumor microenvironment
TNM	Tumor, node, metastasis staging
TRUS	Transrectal ultrasound guided prostate biopsy
s	Second
s / SD	Standard deviation
SOP	Standard operating procedure
UICC	Union Internationale Contre le Cancer
VEGF	Vascular endothelial growth factor
WGA	Whole genome amplification
WES	Whole exome sequencing

Abbreviations

wt	Wild type
xg	Times gravitational acceleration
ZEB	Zinc finger E-box binding homebox
μ	Micro-

Gene abbreviation	Meaning
<i>ALDH</i>	Aldehyde dehydrogenase 1 family, member A1
<i>AKT1/2</i>	V-akt murine thymoma viral oncogene homolog 1/2
<i>AR</i>	Androgen receptor
<i>ARV7</i>	Androgen receptor variant 7
<i>ATM</i>	ATM serine/threonine kinase
<i>BRCA1/2</i>	Breast cancer 1/2, early onset
<i>CCDN1</i>	Homo sapiens cyclin D 1
<i>CDH1</i>	Cadherin 1, type 1, E-cadherin
<i>CDKN1A</i>	Cyclin dependent kinase inhibitor 1A
<i>CHEK2</i>	Checkpoint kinase 2
<i>EGFR</i>	Epidermal growth factor receptor
<i>EpCAM</i>	Epithelial cell adhesion molecule
<i>ERBB2/3</i>	V-erb-b2 erythroblastic leukemia viral oncogene homolog 2/3, neuro/glioblastoma derived oncogene homolog (avian), transcript variant 2/3
<i>ESR1/2</i>	Estrogen receptor 1/2
<i>FGFR1</i>	Fibroblast growth factor 1
<i>FOXA1</i>	Forkhead box 1A
<i>GAPDH</i>	Glyceraldehyde-3-phosphate dehydrogenase
<i>GATA3</i>	GATA binding protein 3
<i>HER2</i>	Homo sapiens v-erb-b2 erythroblastic leukemia viral oncogene homolog 2
<i>K19</i>	Keratin 19
<i>KRAS</i>	Homo sapiens v-Ki-ras2 Kirsten rat sarcoma viral oncogene homolog
<i>MAP3K1/6</i>	Mitogen-activated protein kinase kinase kinase 1/6
<i>MYC</i>	V-myc avian myelocytomatosis viral oncogene homolog

<i>NF1</i>	Neurofibromin
<i>PIK3CA</i>	Phosphoinositide-3-kinase, catalytic, alpha polypeptide
<i>PTEN</i>	Phosphatase and tensin homolog
<i>P27</i>	Endoplasmic reticulum protein 27
<i>RAD50</i>	RAD50 recombinase
<i>RAD51</i>	RAD51 recombinase
<i>RB1</i>	RB transcriptional co-repressor 1
<i>RNASEL</i>	Ribonuclease L
<i>SCRIB</i>	Scribble planar cell polarity protein
<i>STK11</i>	Serine/threonine kinase 11
<i>TBX3</i>	T-box transcription factor 3
<i>TP53</i>	Tumor protein 53
<i>TWIST1</i>	Twist homolog 1

9. Supplementary Data

All supplementary data, figures and tables are available online as supplementary information to the respective publications.

10. Acknowledgement

I would like to take this opportunity to sincerely thank the many people who contributed to the finalization of this PhD thesis to smaller or greater extent, directly or indirectly. This thesis has substantially benefited from your contributions and I am sincerely grateful to you all.

First and foremost I would like to thank my supervisor and mentor, Prof. Dr. Klaus Pantel. Thank you for giving me the opportunity to conduct my PhD thesis at the Institute of Tumor Biology (ITB), for the provided support, the valuable scientific contribution, the productive feedback, and the pleasant and open work environment. I have greatly benefitted from your wealth of knowledge and experience in the scientific realm but also in the everyday responsibilities and tasks of institute life. During my time as a PhD student I was given the opportunity to be involved in exciting scientific projects, to take part in scientific congresses, and collect experience in project coordination. Your confidence in my abilities and ongoing encouragement are highly appreciated and have supported me in taking over these new and at times challenging functions and responsibilities.

Further thanks goes out to my first supervisor, Dr. Tobias Gorges, who initially recruited me to the ITB. It was Tobias' competent and approachable demeanor that made me feel comfortable in my new position from the beginning. Tobias was always open and available to answer questions and very adept at fostering independence in parallel. His innovative ideas and motivation significantly shaped my thesis. Through his faith in my abilities he provided ample opportunity for me to make my projects my own. Together with Prof. Pantel he ensured that my thesis had a solid scientific base that I could rely on. In addition to his role as my scientific supervisor, I would like to thank him for the enjoyable atmosphere in his working group, the many helpful work and non-work related conversations, the provided advice, and the funny moments that brightened up long lab days.

I am grateful to Prof. Dr. Sigrun Reumann for agreeing to supervise my thesis, for her genuine interest in my work and for her patience and understanding for the extended duration of my PhD. This gratitude extends to the additional members of my examination commission, Prof. Dr. Julia Kehr and Prof. Dr. Gunhild von Amsberg for taking the time out of their busy schedules to support the successful conclusion of my PhD.

I would also like to thank PD Dr. Sabine Riethdorf and PD Dr. Harriet Wikman, who have always kept their doors open to discuss joint projects as well as more general questions/issues I encountered. I was lucky to work alongside both of them in exciting and fruitful projects and their substantial knowledge and experience have been a tremendous asset in many situations. A special thank you goes to Sabine for her valuable support in revising the CTC cell line paper during my maternity leave.

A massive thank you goes to all the valued collaborators and cooperation partners without whom this thesis would not have been possible. I would like to especially highlight the close and fruitful collaboration with Prof. Dr. Gunhild von Amsberg and Prof. Dr. Volkmar Müller, who always ensured that suitable cancer patient samples were accessible to attempt to answer our joint research questions. Further thanks goes to Dr. Amin El-Heliebi for the enjoyable and successful work on *ARV7* detection in prostate cancer and the interesting scientific discussions. Also, I would like to thank Dr. Michael Hirtz and Dr. Hui-Yu Liu from the Karlsruhe Institute of Technology for the pleasant collaboration on the CTCapture Chip. Last but not least, I am grateful to the members of the CANCER-ID consortium for the valuable experience of taking part in such a large undertaking, for their openness to welcoming new young researchers in their midst, their motivation, and the incredible joint scientific efforts.

I furthermore thank all employees of the Institute of Tumor Biology for the team spirit and the many great interactions. Special thanks goes out to Antje Andreas for all of her hands-on help and the heartfelt support. Dear Antje, without you this thesis would not have been possible. Similarly, I would like to thank Conny, who was a steady and helpful presence for the entirety of my time at the ITB. I thank Annkathrin Hanssen and Heather Scharpenseel for the great discussions about lab-life and life in general, for the many, many laughs and also the more serious conversations. I am grateful to Ludwig Horst and Okka Wilken for their interest and cleverness, their openness to learning and their amicability. I could not have wished for better or more suitable medical students to supervise.

Of the ITB team, two people require special mentioning at this point, Dr. Simon Joosse and Dr. Andra Kuske. Simon and Andra, I want to express how lucky I feel to not only have had great work experiences at the ITB but to have found close friends. Without you, my time at the ITB would not have been the same. I am thankful for the long conversations on work-related as well as personal matters. I am thankful for the lunches and dinners together, the laughs shared, and the sincere support during times in which the going got tough. I am truly grateful to call you both my friends.

Last but not least I want to extend heartfelt gratitude to my family, friends, and partner for their steady and ongoing support, for their belief in my capabilities, and for their encouragement. You have strengthened me during challenging moments and shared my joy over smaller and larger successes. I am tremendously thankful to my mother, Annegret Hille, and my mother in law, Margarete Koch, for gladly offering up their time to ensure I was able to put this thesis into writing in the knowledge that my son was lovingly cared for. Your efforts have resulted in the successful completion of this thesis and for this, I thank you.

11. Curriculum Vitae

Personal Information

Name: Claudia Koch (birth name: Claudia Hille)
Date of Birth: 11.04.1987
Nationality: German

Current Positions

04/2021 – today **Project manager** of the European Liquid Biopsy Society (ELBS)
Department of Tumor Biology, led by Prof. Dr. med. Klaus Pantel
University Medical Center Hamburg-Eppendorf (UKE), Hamburg

04/2015 – today **PhD student** at the University of Hamburg
PhD thesis:
"Molecular and functional characterization of pathways relevant to metastasis and cancer therapy in circulating tumor cells of breast and prostate cancer patients"
Department of Tumor Biology, led by Prof. Dr. med. Klaus Pantel
University Medical Center Hamburg-Eppendorf (UKE), Hamburg

Education

10/2011 – 04/2014 **Master of Science in Toxicology**
Charité University Medical Center, Berlin - Final grade: 1.6

Master's thesis:
"Functional characterisation of the cell specific and ligand dependent pro-apoptotic effects of the aryl hydrocarbon receptor"
Experimental Toxicology, Department of Chemical and Product Safety,
Federal Institute for Risk Assessment, Berlin

10/2006 – 08/2010 **Bachelor of Science in Biology** with a minor in Chemistry
Humboldt-University of Berlin, Berlin - Final grade: 2.3

Schooling

- 08/2003 – 06/2006 **Senior classes and school diploma**
German School Prague, Czech Republic - Final grade: 1.7
- 08/1993 – 07/2003 **Elementary and middle school**
German School London, UKE (4 years); Konrad Adenauer Gymnasium, Bonn
(3 years); German School Beijing, China (3 years)

Internships and placements

- 06/2014 – 12/2014 **Internship in CTC research**
Support of experimental design and practical implementation of projects
focused on isolation and characterization of circulating tumor cells
With Dr. Michael Drosh, Global Biomarker Research, Bayer Pharma AG,
Berlin
- 04/2011 – 03/2014 **Student research assistant**
With Dr. Marta Rosario, Institute of Cell- and Neurobiology, Center for
Anatomy, Charité University Medical Center, Berlin

12. Publications and presentations

12.1. Scientific publications and Review Articles

Rui P.L. Neves, Wim Ammerlaan, Kiki C. Andree, Sebastian Bender, Laure Cayrefourcq, Christiane Driemel, **Claudia Koch**, Elisabetta Rossi, Catherine Alix-Panabières, Fay Betsou, Klaus Pantel, Sabine Riethdorf, Thomas Schlange, Harriet Wikman, Rita Zamarchi, Leon W.M.M. Terstappen, and Nikolas H. Stoecklein for the CANCER-ID consortium – *Proficiency testing to assess technical performance for CTC-processing and detection methods in CANCER-ID*. Clinical Chemistry (2021); 67:4, 631-641

Claudia Koch*, Andra Kuske*, Simon A. Joosse, Goekhan Yigit, George Sflomos, Sonja Thaler, Daniel J. Smit, Stefan Werner, Kerstin Borgmann, Sebastian Gärtner, Parinaz Mossahebi Mohammadi, Laure Cayrefourcq, Janine Altmüller, Gabriela Salinas-Riester, Kaamini Raithatha, Arne Zibat, Yvonne Goy, Leonie Ott, Kai Bartkowiak, Tuan Zea Tan, Qing Zhou, Michael R. Speicher, Volkmar Müller, Tobias M. Gorges, Manfred Jücker, Jean-Paul Thiery, Cathrin Briskin, Sabine Riethdorf, Catherine Alix-Panabières, Klaus Pantel – *Characterization of Circulating Breast Cancer Cells with Tumorigenic and Metastatic Capacity*. EMBO Molecular Medicine (2020); 12(9):e11908.

Claudia Koch, Simon A. Joosse, Svenja Schneegans, Okka J. W. Wilken, Melanie Janning, Desiree Loreth, Volkmar Müller, Katharina Prieske, Malgorzata Banys-Paluchowski, Ludwig J. Horst, Sonja Loges, Sven Peine, Harriet Wikman, Tobias M. Gorges and Klaus Pantel – *Pre-Analytical and Analytical Variables of Label-Independent Enrichment and Automated Detection of Circulating Tumor Cells in Cancer Patients*. Cancers (2020); 12(2):442.

Simon A. Joosse, Burkhard Beyer, Christin Gasch, Paulina Nastały, Andra Kuske, Hendrik Isbarn, Ludwig J. Horst, **Claudia Hille**, Tobias M. Gorges, Laure Cayrefourcq, Catherine Alix-Panabières, Pierre Tennstedt, Sabine Riethdorf, Thorsten Schlomm, and Klaus Pantel – *Tumor- Associated Release of Prostatic Cells into the Blood after Transrectal Ultrasound-Guided Biopsy in Patients with Histologically Confirmed Prostate Cancer*. Clinical Chemistry (2020); 66(1):161-168

Hui-Yu Liu*, **Claudia Koch***, Anna Haller*, Simon A. Joosse, Ravi Kumar, Michael J. Vellekoop, Ludwig J. Horst, Laura Keller, Anna Babayan, Antonio Virgilio Failla, Jana Jensen, Sven Peine, Franz

Keplinger, Harald Fuchs, Klaus Pantel, and Michael Hirtz – *Evaluation of Microfluidic Ceiling Designs for the Capture of Circulating Tumor Cells on a Microarray Platform*. Advanced Biosystems (2019); 4, 1900162

Claudia Hille, Tobias M. Gorges, Sabine Riethdorf, Martine Mazel, Thomas Steuber, Gunhild von Amsberg, Frank König, Sven Peine, Catherine Alix-Panabières, Klaus Pantel - *Detection of Androgen Receptor Variant 7 (ARV7) mRNA Levels in EpCAM-Enriched CTC Fractions for Monitoring Response to Androgen Targeting Therapies in Prostate Cancer*. Cells (2019); 8(9):1067.

Melanie Janning, Franca Kobus, Anna Babayan, Harriet Wikman, Janna-Lisa Velthaus, Sonja Bergmann, Stefanie Schatz, Markus Falk, Lars-Arne Berger, Lisa-Marie Böttcher, Sarina Päsler, Tobias M. Gorges, Linda O’Flaherty, **Claudia Hille**, Simon A. Joosse, Ronald Simon, Markus Tiemann, Carsten Bokemeyer, Martin Reck, Sabine Riethdorf, Klaus Pantel and Sonja Loges - *Determination of PD-L1 Expression in Circulating Tumor Cells of NSCLC Patients and Correlation with Response to PD-1/PD-L1 Inhibitors*. Cancers (2019); 11(6): 835.

Franz L. Ricklefs, Cecile L. Maire, Rudolph Reimer, Lasse Dührsen, Katharina Kolbe, Mareike Holz, Enja Schneider, Anne Rissiek, Anna Babayan, **Claudia Hille**, Klaus Pantel, Susanne Krasemann, Markus Glatzel, Dieter Henrik Heiland, Jörg Flitsch, Tobias Martens, Nils Ole Schmidt, Sven Peine, Xandra O Breakefield, Sean Lawler, E Antonio Chiocca, Boris Fehse, Bernd Giebel, André Görgens, Manfred Westphal, Katrin Lamszus – *Imaging flow cytometry facilitates multiparametric characterization of extracellular vesicles in malignant brain tumors*. Journal of Extracellular Vesicles (2019); 8(1):1588555.

Klaus Pantel*, **Claudia Hille***, Howard Scher – *Circulating tumor cells in prostate cancer: from discovery to clinical utility*. Clinical Chemistry (2019); 65(1):87-99.

Claudia Hille, Klaus Pantel – *Circulating tumor cells in prostate cancer*. Nature Reviews Urology (2018); 15, pages265–266

Sabine Riethdorf, Linda Scarrott, **Claudia Hille**, Klaus Pantel - *EpCAM based detection of circulating tumor cells in carcinoma patients*. Advanced Drug Delivery Reviews (2018); 1;125:102-121

Amin El-Heliebi*, **Claudia Hille***, Navya Laxman*, Jessica Svedlund*, Christoph Haudum, Erkan Ercan, Thomas Kroneis, Shukun Chen, Maria Smolle, Christopher Rossmann, Tomasz Krzywkowski,

Annika Ahlford, Evangelia Darai, Gunhild von Amsberg, Winfried Alsdorf, Frank König, Matthias Löhr, Inge de Kruijff, Sabine Riethdorf, Tobias M. Gorges, Klaus Pantel, Thomas Bauernhofer, Mats Nilsson, Peter Sedlmayr - *In situ detection and quantification of AR-V7, AR-FL, PSA and KRAS point mutations in circulating tumor cells*. Clinical Chemistry (2018); 64(3):536-546.

Gautier Follain, Naël Osmani, Sofia Azevedo, Guillaume Allio, Luc Mercier, Matthia A. Karreman, Gergely Solecki, Maria Jesus Garcia-Leon, Olivier Lefebvre, Nina Fekonja, **Claudia Hille**, Vincent Chabannes, Guillaume Dollé, Thibaut Metivet, François Der Hovsepian, Christophe Prudhomme, Angélique Pichot, Nicodème Paul, Raphaël Carapito, Siamak Bahram, Bernhard Ruthensteiner, André Kemmling, Susanne Siemonsen, Tanja Schneider, Jens Fiehler, Markus Glatzel, Frank Winkler, Yannick Schwab, Klaus Pantel, Sébastien Harlepp, Jacky G. Goetz – *Hemodynamic forces tune the arrest, adhesion and extravasation of circulating tumor cells*. Cell (2018); 9;45(1):33-52.e12.

Nora Brychta*, Michael Drosch*, Christiane Driemel, Johannes C. Fischer, Rui P. Neves, Irene Exposito, Wolfram Knoefel, Birte Möhlendick, **Claudia Hille**, Antje Stresemann, Thomas Krahn, Matthias U. Kassack, Nikolas H. Stoecklein, and Oliver v. Ahsen – *Isolation of circulating tumor cells from pancreatic cancer by automated filtration*. Oncotarget (2017); 8:86143-86156

12.2. Oral congress presentations

Invited speaker: Liquid Biopsy Symposium; Bergen, Norway (2018) – *The role of CTCs as liquid biopsy in the management of cancer patients*

Selected oral presentation: Advances in Circulating Tumor Cells (ACTC); Rhodes, Greece (2017) – Comprehensive comparison and standardization of a label independent circulating tumor cell (CTC) enrichment platform

Invited speaker: CellSearch and DEP-Array User Meeting; Bologna, Italy (2017) - *Circulating Tumor Cells – the Hamburg Experience*

Invited speaker: KNMF-User Meeting; Karlsruhe Germany (2017) - *Circulating Tumor Cell Isolation Using the CTC-Capture Chip*

Invited speaker: World CDx; Boston MA, USA (2016) - *Epitope-Independent Capture and Harvest of CTCs from Blood*

12.3. Congress posters

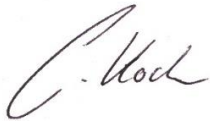
International Symposium on Minimal Residual Cancer (ISMRC); Hamburg, Germany (2016): **Claudia Hille**, Hui Yu Lui, Ludwig J. Horst, Anna Babayan, Tobias M. Gorges, Anna Haller, Michael Hirtz, Harrold Fuchs, Klaus Pantel - *Development of a novel microfluidic CTC detection platform*

International Symposium on Minimal Residual Cancer (ISMRC); Hamburg, Germany (2016): **Claudia Hille**, Frank König, Jörg Schröder, Cornelia Coith, Antje Andreas, Klaus Pantel, Tobias M. Gorges - *Detection of ARV7 positive CTCs in prostate cancer patients using CellSearch® in combination with qPCR*

13. Eidesstattliche Erklärung

Hiermit erkläre ich an Eides statt, dass ich die vorliegende Dissertationsschrift selbst verfasst und keine anderen als die angegebenen Quellen und Hilfsmittel verwendet habe.

Berlin, den 12.11.2021

A handwritten signature in black ink, appearing to read 'C. Koch', written in a cursive style.

Claudia Koch